Technische Universität München

Fakultät für Medizin

Design and characterization of a novel E3 ligase degrader targeting relevant cancer targets in gastrointestinal cancer

Svenja Lier

Vollständiger Abdruck, der von der Fakultät für Medizin der Technischen Universität München zur Erlangung des akademischen Grades einer

Doktorin der Naturwissenschaften

genehmigten Dissertation.

Vorsitzender: Prof. Dr. Markus Gerhard

Prüfer der Dissertation: 1. Prof. Dr. Günter Schneider
2. apl. Prof. Dr. Thomas Floss

Die Dissertation wurde am 02.02.2022 bei der Technischen Universität München eingereicht und durch die Fakultät für Medizin am 17.05.2022 angenommen.

1. Table of Content

2. LIST OF FIGURES

3. LIST OF TABLES

4. LIST OF ABBREVATIONS

3D/2D	three-dimensional/two-dimensional
5-FU	5-fluorouracil
AB	Antibody
AML	acute myeloid leukemia
APC	adenomatous-polyposis-coli
AR	androgen receptors
ARID2	AT-Rich Interaction Domain
ATP	adenosine triphosphate
AUC	Area under the curve
AURKA	Aurora Kinase A
bHLHZip	basic Helix Loop Helix leucin Zipper
BIR3	baculoviral IAP repeat
BRCA1/2	Breast cancer gene 1/2
BRD4	bromodomain containing 4
BSA	Bovine Serum Albumin
c-MYC	MYC
c-terminus	carboxy terminus
CCC	cholangiocarcinoma
CDK	cyclin-dependent kinases
CELMoD	Cereblon E3-ligase modulator
ChIP	chromatin immunoprecipitation
CI	chromosomal instability
CPA1	carboxypeptidase A1
CRBN	cereblon
CRC	Colorectal cancer
DMEM	Dulbecco's Modified Eagle's Medium
DMSO	Dimethylsulfoxid
DNA	deoxyribonucleic acid
EDTA	ethylenediaminetetraacetic acid
EGFR	epidermal growth factor/receptor
EMT	epithelial to mesenchymal transition
ER	endoplasmatic reticulum
eRF1	eukaryotic translation termination factor 1
eRF3	eukaryotic polypeptide chain release factor 3
ERRα	estrogen-related receptor alpha
ERα	estrogen receptor
FACS	Fluorescence activated cell sorting
FBS	Fetal bovine serum
Fbw7	F-box and WD repeat domain-containing 7
FC	Fold change
FDA	Food and Drug Administration
GSEA	gene set enrichment analysis
GSPT	GTP-binding protein for G to S phase transition
H3K4me3	tri-methylation of Lys 4 at the histone H3
HIF-1α	hypoxia-inducible factor 1α
hour	h
IAP	inhibitors of apoptosis proteins
KO	knockout

LOH	loss of heterozygosity
MAX	MYC associated factor X
MB	MYC box
MDM2	mouse double minute 2 homolog
min	minutes
MIZ-1	MYC interacting zinc-finger
MSI	microsatellite instability
mTOR	mechanistic target of rapamycin
MTT	Thiazolyl Blue Tetrazolium Bromide
n-terminus	amino terminus
nab-paclitaxel	albumin-bound paclitaxel
NES	nuclear export sequence
NF-κ B	nuclear factor kappa-light-chain-enhancer
NLS	nucleic localization sequence
o/n	overnight
Omomyc	dominant negative MYC variant
P/S	Penicillin/Streptomycin
PanIN	pancreatic intraepithelial neoplastic lesions
PBS	Phosphate buffered saline
PCR	polymerase chain reaction
PDAC	Pancreatic ductal adenocarcinoma
PDO	patient-derived-organoid
PEST	proline, glutamic acid and threonine
PFS	Progression free survival
PI	Propidium Iodide
PLK1	Polo-like-kinase 1
PROTAC	Proteolysis targeting chimera
qRT-PCR	Quantitative reverse ransricptase polymerase chain reaction
RBM39	RNA binding protein39
Rbx1	ring box protein 1
RIPK 1/3	receptor-interacting serine/threonine-protein kinase 1/3
RPMI	Roswell Park Memorial Institute
rRNA	ribosomal RNA
RspoI	R-spondin-I
RT	room temperature
SCID	severe combined immunodeficient
SDS	Sodium dodecylsulfate
sec	seconds
TAD	transactivation domain
TBS-T	Tris-Buffered saline buffer-Tween20
TMT	Tandem Mass Tag
TNF-α	tumor necrosis factor
TUM	Technical University Munich
UAE	ubiquitin activating enzyme
UV	ultra violet
VEGF/VEGFR	vascular endothelial growth factor/receptor
VHL	Von-Hippel-Lindau

5. ZUSAMMENFASSUNG

Mutationen, Amplifikationen oder Veränderungen in der Expression des Transkriptionsfaktors Myelocytomatose Onkogen (MYC) sind mit einem schlechteren Überleben in unterschiedlichsten Tumorentitäten assoziiert. MYC ist intrinsisch unstrukturiert, wodurch sich ein direktes „Targeting“ als äußerst schwierig erweist. Indirekte Inhibition und direkte genetische Inhibition von MYC führten in präklinischen Modellen von „pancreatic ductal adenocarcinoma“ (PDAC), sowie anderen Entitäten zu einer nahezu vollständigen Tumorregression. Deshalb ist es das Ziel dieser Arbeit, einen neuen MYC Inhibitor bzw. MYC DEGrader (MDEG) basierend auf der PROTAC Technologie zu entwickeln. Dafür wurden die MDEG Substanzen in Kooperation mit Prof. Dr. Siavosh Mahboobi entwickelt. 48 verschiedene chemische Substanzen wurden im Rahmen dieser Studie synthetisiert, indem ein Bindungsligand (10058-F4) des MYC/MAX Heterodimers mit dem Liganden (Thalidomid) der E3-ligase cereblon (CRBN) verknüpft wurde. Der Linker zwischen 10058-F4 und Thalidomid ist äußerst kritisch für die Funktionalität des PROTACs, daher wurden für den Linker verschiedene Längen und Elementzusammensetzungen eingesetzt. Die synthetisierten Substanzen wurden zunächst auf ihre Viabilität getestet, um deren Wirksamkeit in einem Panel aus unterschiedlichen PDAC Zelllinien zu ermitteln.

Die Substanz MDEG-541 zeigte in diesem Screen die höchste Effektivität. Eine Behandlung mit MDEG-541 führte zur Reduktion der Zellviabilität in gastrointestinalen Krebszellen. Der molekulare Mechanismus und der biologische Effekt der MDEG-541 Behandlung, wurde im Rahmen dieser Arbeit in der Kolonkarzinomzelllinie HCT116 und der PDAC Zelllinie PSN1 detailliert untersucht, da diese, beide über eine Amplifikation des *MYC* Gens verfügen. Die Behandlung mit MDEG-541 führte zu einer Degradation von GSPT1, GSPT2 und MYC, wobei die MYC Degradation verzögert stattgefunden hat. Analysen des Transkriptoms und Proteoms haben gezeigt, dass bekannte Krebs-assoziierte MYC-Signalwege wie E2F und Zellzyklus „HALLMARKs“ durch die MDEG-541 Behandlung inhibiert wurden und die Zellen dadurch in den Zelltod getrieben wurden. Außerdem konnte auch die Polo-like Kinase 1 (PLK1) als MDEG-541 „Target“ identifiziert werden. Die Inhibition der Proteinexpression von MYC, GSPT1, GSPT2 und PLK1 war abhängig von CRBN, dem Proteasom und der Ubiquitinierung. Zudem wurden präklinisch relevante, dreidimensionale Organoidmodelle zur Bestimmung der MDEG-541 Wirksamkeit hinzugezogen. Interessanterweise zeigte sich ein besonders gutes Ansprechen in Zellen und Organoiden mit geringer Expression von *GSPT1*.

Zusammenfassend wurde in dieser Arbeit ein neuer potenter PROTAC von GSPT1, GSPT2 und PLK1 entwickelt, der die Expression von MYC inhibiert. Die Degradation von MYC, GSPT1, GSPT2 und PLK1 stellt eine vielversprechende und neue Strategie dar, um verschiedene Krebsarten zu behandeln.

6. SUMMARY

Mutations, amplifications or alterations of the transcription factor Myelocytomatose Onkogen (MYC) are associated with poor survival in multiple cancers. Targeting oncogene MYC remains a challenge since it has an intrinsically disordered structure.

Indirect and direct genetic inhibition of MYC led to tumor regression in preclinical pancreatic ductal adenocarcinoma (PDAC) models and other tumor entities. Therefore, the aim of this work was to develop a novel MYC inhibitor or MYC DEGrader (MDEG) based on the PROTAC technology. For this purpose, the MDEG compounds were designed and produced in cooperation with Prof. Dr. Siavosh Mahboobi. 48 different chemical compounds were synthesized based on a binder (10058-F4) of the MYC/MAX heterodimer connected to the cereblon (CRBN) E3-ligase ligand (Thalidomide). The linker between 10058-F4 and Thalidomide is critical for the function of the PROTAC, and was therefore varying in length and element composition. All synthesized compounds were evaluated according to their effect on cell viability in multiple PDAC cell lines. MDEG-541 was identified as the most potent compound. Treatment with MDEG-541 led to reduced cell viability in gastrointestinal cancer cells. The molecular mechanisms and the biological effect of MDEG-541 treatment, was investigated in this work in detail in the *MYC* amplified colorectal cancer cell line HCT116 and PDAC cell line PSN1. Not only the degradation of MYC protein, but also a decrease of GSPT1 and GSPT2 protein was detected prior to MYC downregulation. Specifically, in transcriptome- and proteome-wide analysis, the involvement of prominent cancer related MYC-signaling pathways, E2F as well as cell cycle HALLMARKs, were observed after MDEG-541 treatment which resulted in cell death of the treated cell lines. Further, Polo-like kinase 1 (PLK1) was identified as MDEG-541 target. The degradation of MYC, GSPT1, GSPT2 and PLK1 in a dose- and time-dependent manner, was dependent on the CRBN, the proteasome and ubiquitination. Further, the efficiency of MDEG-541 was tested in preclinically relevant, three-dimensional (3D) organoid models. Interestingly, responsiveness of cancer cells and organoids correlated with low *GSPT1* gene expression.

Taken together, this work identified a novel potent PROTAC of GSPT1, GSPT2 and PLK1 resulting in the subsequent downregulation of MYC protein expression. The degradation of MYC, GSPT1, GSPT2 and PLK1 offers a promising and novel strategy to target multiple cancers.

7. INTRODUCTION

7.1 Pancreatic cancer

Compared to all cancer types, pancreatic cancer currently is the fourth leading cause of cancer-related death in the United States (Siegel et al., 2022; Siegel et al., 2020). Patients with pancreatic cancer have a particularly poor 5-year survival rate of about 9% (Rawla et al., 2019). Moreover, a GLOBOCAN abstraction analysis estimates a 77.7% increase of new pancreatic cancer cases from the year 2018 to 2040 (Bray et al., 2018).

7.1.1 Etiology of Pancreatic cancer

The development of pancreatic cancer can have different causes. About 5-10% of pancreatic cancers have a hereditary origin (Anand et al., 2008; Copur et al., 2020; Hruban et al., 1998; Klein, 2013; Thoma, 2018). These hereditary causes include specific syndromes which are associated with distinct gene alterations (Chen et al., 2017). For example, breast cancer gene 1 and 2 (BRCA1 and BRCA2) in hereditary breast cancer syndrome, Lynch syndrome connected to mismatch repair genes (Bujanda and Herreros-Villanueva, 2017; Grant et al., 2015; Kastrinos et al., 2009) as well as hereditary pancreatitis associated with gene alterations in carboxypeptidase A1 (CPA1), to mention only a few (Kujko et al., 2017; Lowenfels et al., 1993; Witt et al., 2013). In addition to hereditary factors, non-hereditary factors may also give rise to the development of pancreatic cancer. A meta-analysis from 2015 identified chronic pancreatitis, tobacco smoking, diabetes mellitus (Hemminki et al., 2010), obesity (high body mass index), hepatitis B virus infection, heavy alcohol intake and *Helicobacter pylori* infection (Raderer et al., 1998; Uemura et al., 2001) among the leading non-hereditary risk factors of pancreatic carcinogenesis (Maisonneuve and Lowenfels, 2015). The majority of non-hereditary risk factors can be positively influenced by behavioral and life-style changes (Maisonneuve and Lowenfels, 2015).

7.1.2 Tumorigenesis in PDAC

Approximately 90% of pancreatic ductal adenocarcinoma (PDAC) originate from pancreatic neoplasia by a multi-step process (Figure 1) (Adamska et al., 2017; Haeberle and Esposito, 2019).

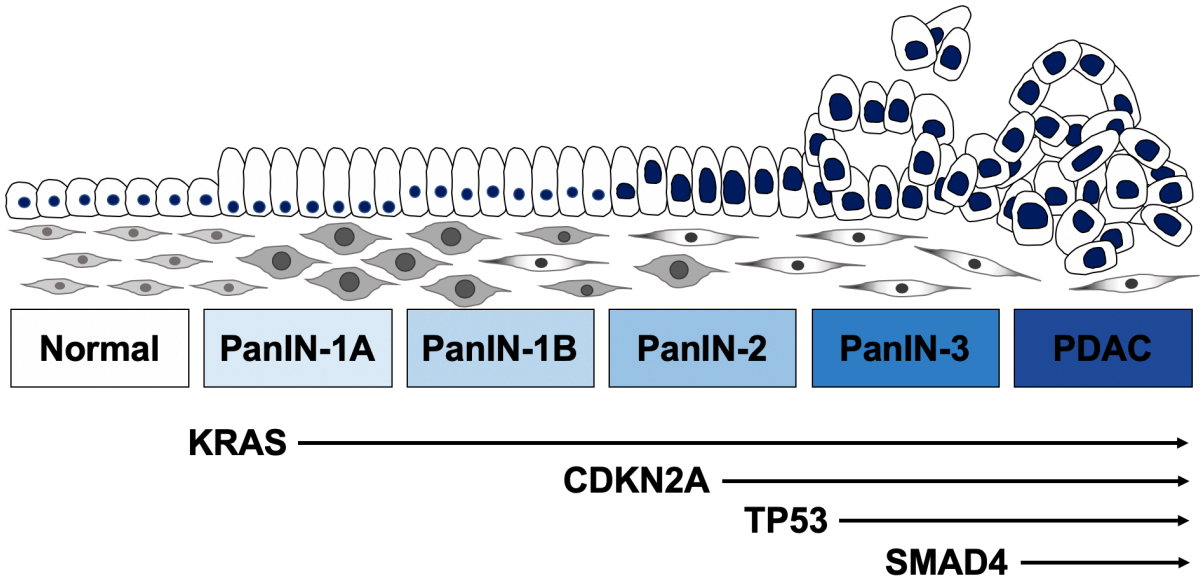

Figure 1: Tumorigenesis of pancreatic ductal adenocarcinoma (PDAC).
Healthy cells in the pancreas progress through a sequence of pancreatic intraepithelial lesions (PanIN-1A, -1B, -2 and -3) to develop PDAC. Specific molecular events including the mutation of KRAS in early lesions induce morphological changes in normal pancreas cells. Further developed lesions accumulate mutations of tumor suppressors CDKN2A, TP53 or SMAD4. Adapted from (Bhosale et al., 2018).

In classical PDAC, neoplasms originate from acinar cells which transdifferentiate to duct-like cells. These cells are characterized by embryonic progenitor properties, mostly induced by environmental stresses or genetic alterations, for instance the overexpression of TGFβ (Chuvin et al., 2017; Principe et al., 2016). This process is called acinar to ductal metaplasia and is considered the main origin of pancreatic intraepithelial neoplastic lesions (PanINs). In addition to acinar cells, pancreatic ductal cells can also give rise to PanINs (Lee et al., 2018). PanINs are classified into three grades according to their morphology (Figure 1). PanIN-1A are flat lesions while PanIN-1B are characterized by micropapillary lesions with altered cytoplasmic mucin. Both PanIN-1A and 1B are low grade lesions that can develop due to sustained stress signaling or oncogenic transformation. For example, an activating mutation of the oncogene KRAS can transform the cell to initiate PanIN-1 growth. Lesions may advance to PanIN-2 following additional nuclear alterations due to inactivated tumor suppressor genes, for instance CDNK2A, TP53 or SMAD4. The most advanced PanIN grade 3 develop through accumulation of alterations in tumor suppressors. At this grade the normal epithelial architecture is disrupted (Bhosale et al., 2018; Hruban et al., 2001; Hruban et al., 2004) and pancreatic lesions eventually progress to PDAC (Sausen et al., 2015).

7.1.3 Treatment of PDAC

Surgical resection of localized PDAC is currently known as the only curative approach in the clinic. However, due to advanced and disseminated carcinomas at the time of diagnosis, only 15-20% of PDACs qualify for resection (Klein, 2013). In addition to surgical resection, chemotherapy is also a potential strategy to treat pancreatic cancer. For over 20 years, gemcitabine was considered the standard chemotherapeutical treatment to target pancreatic cancer. In the clinic though, it only showed limited success in increasing patient´s life expectancy, pointing to the need for the development of improved therapy strategies (Adamska et al., 2017). As gemcitabine treatment was well tolerated in patients, it was considered for combination treatment to improve the survival benefit (Vincent et al., 2011).

Over the last two decades, numerous combination treatments were evaluated in clinical trials. In 2014, gemcitabine together with albumin-bound paclitaxel (nab-paclitaxel) was accepted as first-line treatment for PDAC in Europe, after it was shown to increase survival compared to gemcitabine monotreatment (Von Hoff et al., 2013). Another first-line treatment is the combination of the four FDA approved drugs leucovorin, 5-fluorouracil (5-FU), irinotecan and oxaliplatin - known under the designated name FOLFIRINOX – which significantly increased overall survival (Conroy et al., 2018). As of today, FOLFIRINOX remains the standard of care for locally advanced and metastatic PDAC (Sohal et al., 2021; Vega et al., 2020). However, severe side effects, namely grade 3 and 4 adverse events like tiredness, neutropenia and diarrhea, still occurred in 75.9% of the patients in the modified FOLFIRINOX group, compared to 52.9% in the gemcitabine group (Conroy et al., 2018). Therefore, only patients with good performance status are candidates for FOLFIRINOX treatment. In light of the severe side effects, moderate extension of life, and a low overall response rate of about 30%, the benefits of these first-line treatments remain questionable (Adamska et al., 2017), pointing out the urgent need to develop improved or new therapeutic strategies for pancreatic cancer treatment (Chllamma et al., 2016; Hua et al., 2018).

7.2 Colorectal Cancer (CRC)

According to the GLOBOCAN 2018 data, colorectal cancer (CRC) remains the third leading cause for cancer-related death worldwide, with approximately 10^6 expected deaths per year (Bray et al., 2018). In 2020, the estimated 5-year survival rate of bowel

cancer was 9% with an approximated incidence of 8-9%, making it the fourth most commonly diagnosed cancer in the US (Siegel et al., 2020).

7.2.1 Etiology of CRC

Colorectal carcinogenesis can have different causes. The risk of developing CRC is 2-4 times increased if a first-grade relative has the disease (De Rosa et al., 2015). About 5-10% of all CRCs are linked to high-risk gene mutations (Lorans et al., 2018). Classical tumor drivers in CRC include microsatellite instability, which can cause alterations in APC, KRAS/BRAF, DDC/SMAD4 and TP53, chromosomal instability, which in turn can cause alteration in β-catenin, BAX, TCF-4 IGF-IIR and TGF-β and CpG island methylation (Simon, 2016). These mutations can be induced by different syndromes. Lynch syndrome is the most common syndrome associated with hereditary CRC, increasing the risk of developing CRC by the age of 50 by 20% (Bonadona et al., 2011). Mutations in adenomatous-polyposis-coli (APC) were found to be associated with CRC carcinogenesis and are therefore one of the most common hereditary risk factors (Miyoshi et al., 1992). Non-hereditary risk factors include a diet of red and processed meats, commonly associated with a Western lifestyle (Chan et al., 2011; Kim et al., 2013; Zhao et al., 2017), obesity (Robsahm et al., 2013), smoking (Botteri et al., 2008; Limsui et al., 2010), alcohol consumption (Bagnardi et al., 2015; Fedirko et al., 2011) and diabetes mellitus (Jiang et al., 2011; Tsilidis et al., 2015). Similar to PDAC prevention, the majority of non-hereditary risk factors in CRC can be positively influenced by lifestyle changes. Additionally, regular colonoscopies after age 50 reduce the risk of developing precursor lesions with the potential to prevent occurrence of the disease.

7.2.2 Tumorigenesis of CRC

Onset of the disease is characterized by epithelial neoplasia in the colon or rectal mucosa. These precursor lesions are low grade dysplasia which eventually develop into high grade dysplasia (Fleming et al., 2012) and can also progress to a malignant adenocarcinoma stage with high potential to develop metastasis (Heitman et al., 2009). Patients with CRC metastasis have a median survival of ten months after diagnosis (Riihimaki et al., 2016).

The progression of colorectal tumorigenesis is driven by a series of genetic alterations in oncogenes and tumor suppressor genes which were first described by Fearon and Vogelstein (Figure 2) (Fearon and Vogelstein, 1990; Guruswamy and Rao, 2008).

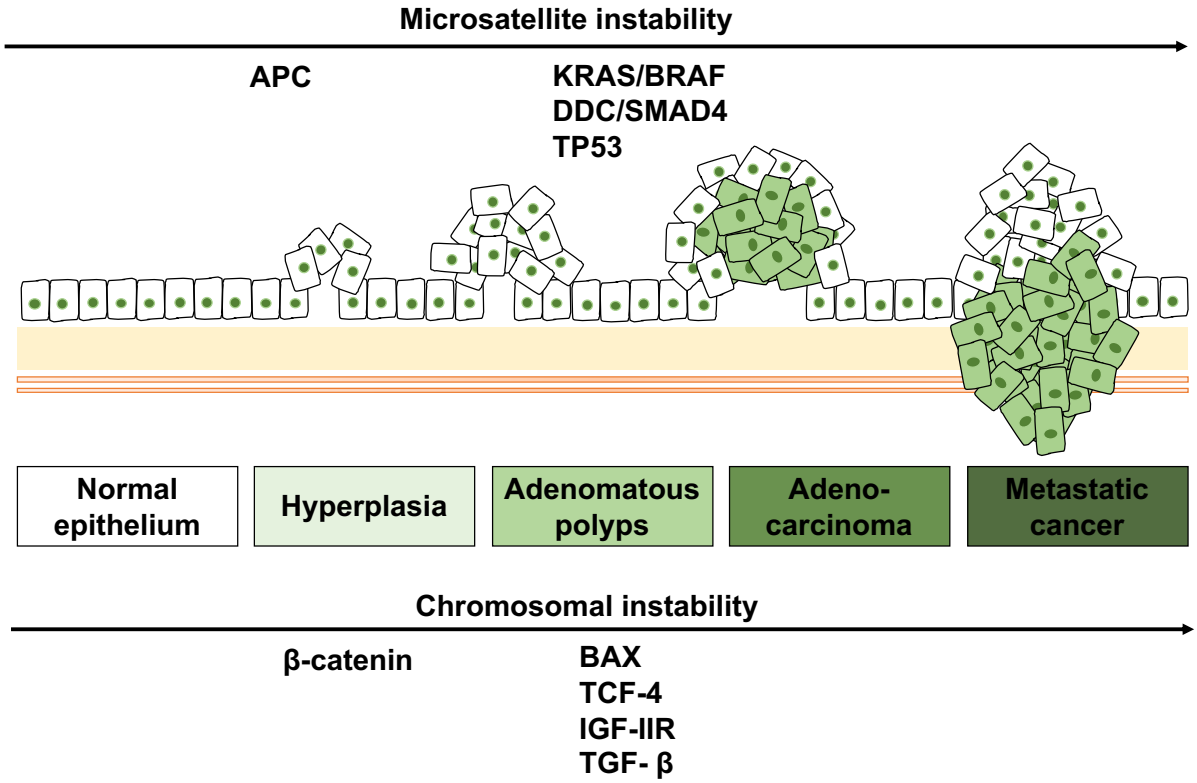

Figure 2: Tumorigenesis of colorectal cancer (CRC).
Normal epithelium in the colon or rectum progresses through a sequence of dysplastic lesions and polyps to develop colorectal adenocarcinoma. Genetic alterations are induced by instable microsatellites and chromosomal instability correlating with morphological changes of the healthy colon or rectal tissue. Events of microsatellite instability include mutation of APC occurring in early dysplasia of the colorectal tissue and KRAS/BRAF, DDC/SMAD4 or TP53 occurring in adenomatous polyps. Events of chromosomal instability include mutation of β-catenin occurring in early dysplasia of the colorectal tissue and BAX, TCF-4, IGF-IIR and TGF-β occurring in adenomatous polyps. Events of CpG island methylator also contribute to tumorigenesis in CRC but are not shown in the figure. Adapted from Guruswamy and Rao, 2008.

These genetic alterations are caused by three major pathways in CRC: Chromosomal instability (CIN) (Fodde et al., 2001), microsatellite instability (MSI) (Boland et al., 1998; Markowitz et al., 1995) and CpG island methylation (Nazemalhosseini Mojarad et al., 2013; Tejpar and Van Cutsem, 2002). Multiple genetic alterations accumulate during the progression of colorectal tumorigenesis, sometimes over multiple decades, although some mutations may be inherited such as the APC gene in familial adenomatous polyposis (Guruswamy and Rao, 2008).

7.2.3 Treatment of CRC

7.2.3.1 Endoscopic and surgical resection

The current standard treatment of low- and high-grade dysplasia is endoscopic polypectomy. Resection of dysplasia reduces the incidence of CRC and may prevent CRC-related death (Winawer et al., 1993; Zauber et al., 2012). In the case of failed

endoscopic resection of designated malignant polyps, partial surgical resection of the colon is necessary (Aarons et al., 2014).

Stage II colon cancer with invasion from the colon to nearby tissue is typically treated by colectomy. In this stage of colon cancer, chemotherapy might also be considered. Affected lymph nodes are usually resected after diagnosis and the patients are treated with an adjuvant chemotherapy. Advanced CRC is surgically resected if possible and treated with neo-adjuvant chemotherapy (McQuade et al., 2017).

7.2.3.2 Chemotherapy

Over six decades ago, the path for chemotherapy in CRC was paved following the development of 5-FU, a chemotherapy drug, that is now also routinely used for the treatment of additional cancer types such as PDAC (Heidelberger et al., 1957). In cultured leukemia cells, leucovorin could enhance the efficacy of 5-FU by approximately five times (Ullman et al., 1978). That said, it was also shown that patient suffered from severe side effects that could even lead to toxic death (Tsalic et al., 2003).

Life expectancy was further increased by 4.5 months when patients with advanced CRC were treated with combined regimes such as 5-FU, leucovorin and oxaliplatin (FOLFOX) compared to 5-FU, leucovorin and irinotecan treatment (Mini et al., 1990). FOLFOX treatment is under optimization considering distinct patients ages, tumor stages and conditions (André et al., 2020; André et al., 2018; Schmoll et al., 2015). However, multi-agent treatments often failed to increase patients' survival but showed increased toxicity instead (Goldberg et al., 2004). Therefore, targeted therapy is applied as alternative to conventional chemotherapy interventions (Xie et al., 2020). In 2004, cetuximab was approved by the FDA as the first targeted agent against epidermal growth factor receptor (EGFR) in CRC. In the same year, bevacizumab targeting vascular endothelial growth factor/receptor (VEGF/VEGFR) was approved, since then other targeting therapeutics followed. Current treatment guidelines for PDAC and CRC can be accessed via https://www.leitlinienprogramm-onkologie.de/home/.

In sum, the most promising therapy of CRC is the resection of dysplasia, which can lead to a complete cure in most patients. On the other hand, the reduced life expectancy of patients which are dependent on chemotherapeutical treatments, fails to satisfy expectations and points out the urgent need of modified or new therapeutic strategies.

7.3 The role of MYC in PDAC and CRC

Normal epithelium in the colon or rectum progresses through a sequence of dysplastic lesions and polyps to develop colorectal adenocarcinoma. Oncogene MYC is a well-known driver of CRC (Hu et al., 2021; Singh et al., 2021) and gene expression profiling demonstrated the crucial role of MYC in CRC-related signal transduction, cell-cycle and apoptosis pathways and anti-EGFR resistance (Strippoli et al., 2020). Therefore, the expression of MYC in CRC could represent a therapeutic target to treat the cancer. In the development of PDAC, healthy cells from the pancreas progress through a sequence of pancreatic intraepithelial lesions (PanIN-1A, -1B, -2 and -3) to a primary tumor. Specific molecular events including the mutation of KRAS in early lesions induce morphological changes in normal pancreas cells. Further developed lesions accumulate mutations of tumor suppressors CDKN2A, TP53 or SMAD4 (Bhosale et al., 2018). Besides these classical tumor drivers, an amplification of MYC gene was also associated with reduced overall survival in PDAC (Witkiewicz et al., 2015).

7.4 The structure of MYC

The transcription factor and oncogene MYC was first isolated in 1964 from a chicken as the transforming element v-myc of the avian leukemia virus MC29 (Duesberg and Vogt, 1979; Hu and Vogt, 1979; Payne et al., 1982; Sheiness and Bishop, 1979). V-myc is known to induce sarcoma as well as carcinoma and its ability to cause avian myelocytomatosis was eponymic. Vennstrom and colleagues isolated c-myc (further referred to as MYC) as cellular homolog of v-myc in avian and characterized it in rat, mouse, and human (Vennstrom et al., 1982).

Structurally, the MYC protein has four MYC boxes (Figure 3). MYC box I and II are located at the amino-terminal (n) end of the protein within a transactivation domain (TAD) (Kato et al., 1990). The central segment contains the MYC box III, MYC box IV and a nuclear localization sequence (NLS) (Dang and Lee, 1988) rich in proline, glutamic acid, threonine and residues (Cowling et al., 2006). MYC box III is important for transcriptional repression and inhibits MYC-mediated apoptotic activity (Herbst et al., 2005). MYC box IV is involved in MYC transcriptional activity (Cowling et al., 2006). The carboxy-terminal (c) region has a DNA binding motif and a basis-helix-loop-helix leucine zipper (bHLHZ) dimerization domain of about 100-amino-acids for heterodimerization with MYC associated factor X (MAX) (Blackwood and Eisenman, 1991).

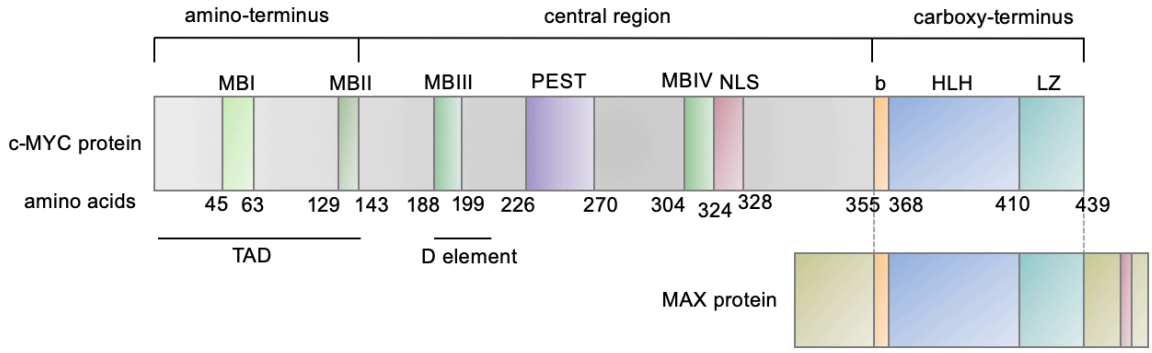

Figure 3: Structure of MYC protein
The MYC protein has 439 amino acids and is divided into three regions: The amino-terminus (n), the central region and the carboxy-terminus (c). The n-terminal domain of human MYC protein contains the MYC box I (MBI) and MYC box II (MBII). The central region with the MYC box III (MBIII), the proline, glutamic acid, and threonine rich (PEST) sequence, the nucleic localization sequence (NLS) and MYC box IV (MBIV). The carboxy-terminal domain includes a bHLH LZ (basic-helix-loop-helix leucin zipper) motif for heterodimerization with the MAX protein. Abbreviations: transactivation domain (TAD). Adapted from (Pelengaris et al., 2002) and (Farrell and Sears, 2014).

7.4.1 The function of the transcription factor MYC

Full-length MYC alone is incapable of binding to the DNA of target genes as MYC is a disordered protein (Amati et al., 1993; Amati et al., 1992; Fieber et al., 2001). That said, when MYC heterodimerizes with the MYC associated protein X (MAX) at the bHLHZ region, this complex can bind to E-box sequences and regulate their transcription (Amati et al., 1993; Amati et al., 1992; Blackwood and Eisenman, 1991; Kato et al., 1992; Park et al., 2004).

7.4.2 Transcriptional control by MYC

Numerous genome- and chromatin-wide studies described MYC as transcription factor by demonstrating that MYC is binding to a great number of promoters in eukaryotic cells (Cawley et al., 2004; Fernandez et al., 2003; Li et al., 2003; Zeller et al., 2006). Upon dimerization with MAX, MYC becomes a DNA binding protein with E-boxes in the promoters of these genes. Originally, MYC was considered a typical transcription factor recruited with a preference to the E-box 5′-CACGTG-3, but not with absolute specificity (Guo et al., 2014). MYC/MAX heterodimers were also shown to interact with non-canonical binding sites (Allevato et al., 2017). MYC was suggested as a global amplifier acting universally at active genes and increasing output at all active promoters thus affecting, for instance, cell cycle progression and cell growth signaling,

proliferation, pluripotency and ribosomal biogenesis (Figure 4) (Cowling et al., 2006; Dang, 2013; Nie et al., 2020; Nie et al., 2012).

In experiments by Sabò et al., it was concluded that MYC is not acting as a generic transcriptional amplifier but instead directly activates and represses distinct MYC gene sets, which results in an indirect amplification of global gene expression downstream of direct MYC targets (Sabò et al., 2014). Whether MYC is a specific or rather a general transcription factor is still discussed and facilitates the need of examination of MYC target genes in different contexts in the future (Nie et al., 2020).

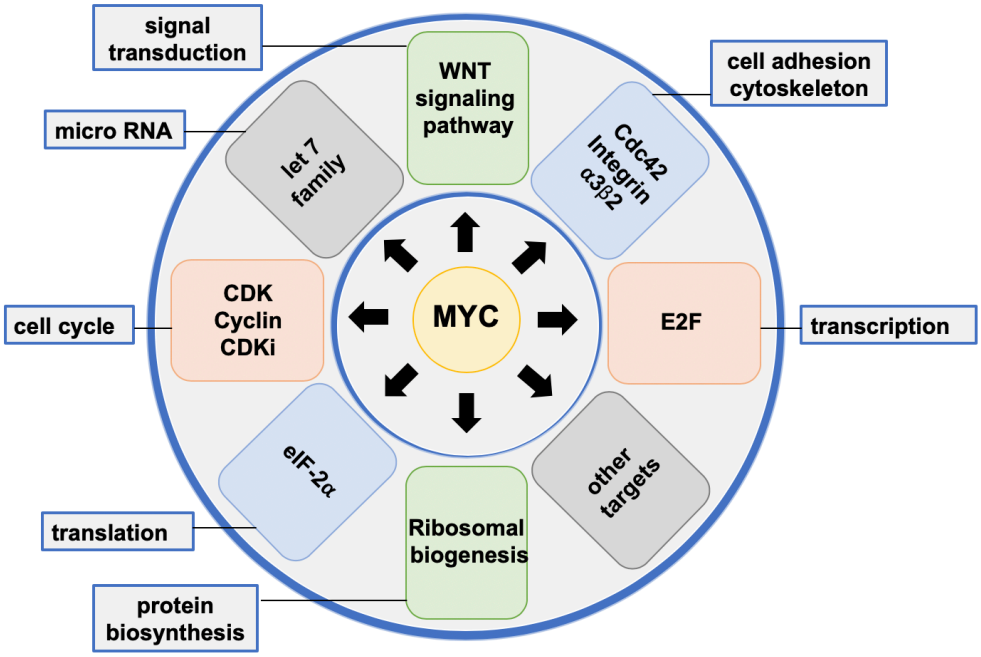

Figure 4: Function of MYC in eukaryotic human cells
MYC is regulating multiple cellular functions, for example, signal transduction, micro RNA, cell cycle, translation, protein biosynthesis, cell adhesion and cytoskeleton and transcription. MYC plays a role in these cellular functions by regulating a plethora of non-coding and protein-coding genes, for instance, E2F and WNT-signaling. Adapted from (Chen et al., 2018).

MYC also plays a role in regulating the anti-tumor immune response through the regulation of immune checkpoint proteins on the tumor cell surface, the innate immune regulator, cluster of differentiation 47 (CD47) and the adaptive immune checkpoint, programmed death-ligand 1 (PD-L1) (Casey et al., 2016). Since MYC directly binds CD47 and PD-L1, the inhibition of MYC led to the downregulation of their mRNA and protein which enhanced the anti-tumor immune response. Thus, the inhibition of MYC might also be a promising strategy to approach the anti-tumor immune response to

target cancer such as PDAC (Pan et al., 2019; Song et al., 2020; Wang et al., 2020a; Xi et al., 2020).

7.4.3 The role of MYC in cancer

7.4.3.1 Oncogenic transformation of MYC

MYC has the potential to malignantly transform cells and was shown to be the most frequently deregulated oncogene in human cancer (Beroukhim et al., 2010; Ciriello et al., 2013). MYC copy number alterations were identified for the first time in the human leukemia cell line HL60 in 1982 (Collins and Groudine, 1982). Two decades later, a hierarchical classification study of 'The Cancer Genome Atlas' showed amplification of MYC with a frequency of 14%, putting it into the top ten of all copy number alterations observed in ovarian, breast, and squamous cell lung cancers (Ciriello et al., 2013; Zack et al., 2013). The examination of over 500 PDAC samples revealed that MYC was specifically enriched in the squamous subtype (Bailey et al., 2016; Witkiewicz et al., 2015). Notably, PDAC patients had a reduced overall survival of less than 10 months when their tumors had a high MYC gene copy number. This indicates amplification of MYC as a potential marker of poor outcome in PDAC (Witkiewicz et al., 2015).

7.4.3.2 MYC in cancer development and maintenance

The association of MYC with tumor development could recently be confirmed in PanIN epithelial cells *in vitro,* where the acute activation of MYC induced stromal features comparable to spontaneously developed human PDAC. Furthermore, the inactivation of MYC in these cells reversed these stromal effects back to PanIN stage (Sodir et al., 2020). The association of MYC with tumor maintenance was confirmed in transgenic mouse models with inducible MYC. In these mice, established tumors regressed upon withdrawal of ectopic MYC expression, indicating that MYC plays a role in tumor maintenance *in vivo* (Arvanitis and Felsher, 2006).

MYC also plays a role in both invasive and metastatic behavior. An RNA interference-mediated MYC knockdown in metastatic human breast cancer cells prevented invasive behavior *in vitro* and inhibited cellular invasion, migration and distant metastasis *in vivo* (Wolfer et al., 2010). This suggests the oncogene MYC as a bona fide target not only in local primary tumors but also in advanced metastatic cancer (Soucek et al., 2008; Wolfer and Ramaswamy, 2011).

In line with these observations, as an integrator of numerous pathways, MYC plays a key role in tumorigenesis and maintenance and is therefore considered a promising pharmaceutical target to treat diverse types of cancer.

7.4.4 Concepts to target MYC

Until today, there is no efficient, direct small molecule inhibitor against MYC available in the clinic and therefore, MYC is considered as 'undruggable'. This may be due to the MYC monomer being a disordered protein and MYC having no effective binding pockets on its surface (Fieber et al., 2001; Michel and Cuchillo, 2012).

As mentioned before, when MYC heterodimerizes with MAX at the bHLHZ sequence, MYC becomes an ordered protein that can bind the E-box in the promoters of its target genes (Amati et al., 1993; Amati et al., 1992; Blackwood and Eisenman, 1991; Kato et al., 1992; Park et al., 2004). The heterodimerization domain of MYC and MAX provides a promising target sequence for a direct inhibitor that may prevent the interaction of MYC/MAX complex with the DNA of its target genes - and thereby disrupt the MYC-mediated transcriptional gene regulation (Fletcher and Prochownik, 2015).

7.4.4.1 Direct targeting of MYC

Inhibitors which directly target the heterodimerization domain of MYC and MAX include small molecules like Mycro3 (Kiessling et al., 2007), 10058-F4 (Guo et al., 2009), MYCMI-6 (Castell et al., 2018), KJ-Pyr-9 (Hart et al., 2014), Omomyc (Sodir et al., 2020) and EN4 (Boike et al., 2021).

Mycro3 was shown to inhibit MYC expression *in vitro* (Kiessling et al., 2007; Stellas et al., 2014). The small molecule inhibitor 10058-F4 inhibits dimerization of MYC and MAX, and decreased proliferation in leukemia cells and MYC protein expression. Although 10058-F4 induces apoptosis in human PDAC cells *in vitro*, the compound failed to induce cell death in Panc-1 xenograft mice *in vivo* (Zhang et al., 2015a). Also, compound MYCMI-6 inhibited MYC/MAX heterodimerization *in vitro* and induced apoptosis in breast cancer cell lines, but did not reduce MYC protein expression (AlSultan et al., 2021). In a mouse xenograft model, MYCMI-6 reduced tumor cell proliferation and induced apoptosis (Castell, 2018). KJ-Pyr-9 was isolated from a Kröhnke pyridine library as a MYC/MAX heterodimerization inhibitor. It blocked tumor growth in a human triple-negative breast cancer xenograft model (Hart et al., 2014). Further, Omomyc is a MYC dominant negative with a mutation in the bHLHLZ region. When MYC heterodimerizes with Omomyc, the binding of MYC to its target genes is prevented. In murine PDAC cell lines, inducible Omomyc diminished clonogenic

growth (Jung et al., 2017). Moreover, Omomyc inhibits transcriptional activation and repressed MYC target genes, leading to apoptosis and decreased tumor growth in mice (Massó-Vallés and Soucek, 2020; Soucek et al., 2002). Furthermore, EN4 directly targets MYC and its transcriptional activity *in vitro* by reducing MYC and MAX thermal stability, downregulating transcriptional MYC targets and impairing tumorigenesis (Boike et al., 2021). *In vivo* experiments still need to be performed with EN4.

7.4.4.2 Indirect targeting of MYC

Indirect targeting of MYC oncogene either reduces MYC protein expression or interferes with genes necessary for the activation of MYC (Wirth et al., 2016). In the last decade, bromodomain (BRD) and extra terminal domain (BET) family members were identified as the main regulators of MYC. It was shown that indirect targeting of transcriptional coactivator BRD-containing 4 (BRD4) regulates the protein expression of MYC tightly. This inspired the development of several BET small-molecule inhibitors (BET-I, JQ1). For example, JQ1 was identified as a potent BRD4 inhibitor (Filippakopoulos et al., 2010) that induces transcriptional repression of MYC, thus exhibiting antitumor effects *in vitro* and *in vivo* (Zuber et al., 2011).

7.5 The polypeptide chain release factor 3 (eRF3)

Polypeptide chain release factor 3 (eRF3) exists of two homologous genes, namely, eRF3a located on the human chromosome 16 encoding for GSPT1 protein and eRF3b mapped on the human X chromosome encoding for GSPT2 protein (Hansen et al., 1999; Jakobsen et al., 2001; Ozawa et al., 1992).

7.5.1 The role of eRF3 in cancer

eRF3 encodes the GTP-binding protein for G to S phase transition (GSPT) protein and its overexpression was widely detected in gastrointestinal cancer - from aberrant crypt foci to advanced carcinomas as well as in the CRC cell line HCT116 (Dang et al., 2005) - used in this work. In a study from 2005, an eRF3b gene overexpression was found in 66% of tested intestinal type carcinomas (N=12) (Malta-Vacas et al., 2005). The first exon of eRF3a contains a (GGC)n expansion coding for proteins with different n-terminal variants (Malta-Vacas et al., 2009a; Malta-Vacas et al., 2009b). Malta-Vacas et al. suggested that the presence of a 12-GGC allele in eRF3b provides a potential novel risk marker for various types of cancer.

In HCT116 cells, the depletion of eRF3a induced the inhibition of the mTOR pathway, arrested the cells at G1 cell cycle phase and impaired clonogenic survival and

proliferation (Chauvin et al., 2007). Under growth-limiting conditions *in vitro,* the eRF3a depletion was associated with apoptosis. *In vivo*, a depletion of eRF3a in HCT116 tumor xenografts prevented tumor growth (Dang et al., 2005).

7.5.2 The role of eRF3 in translational termination

eRF3 is a small GTPase protein which has no significant intrinsic GTPase activity (Zhouravleva et al., 1995). Efficient and fast termination of translation in eukaryotes depends on the sequential ribosomal entry of eRF3 and eRF1 (Beißel et al., 2019). eRF1 is a key player in translational termination and recognizes all three stop codons (UAA, UAG and UGA) in the mRNA. When eRF3a or eRF3b bind to eRF1, the GTPase activity of eRF3 at the A site of ribosomes, which functions as binding site for t-RNAs, is enhanced (Salas-Marco and Bedwell, 2004). Together with GTP and Mg^{2+}, this quaternary complex facilitates the initiation of translational termination (Mitkevich et al., 2006).

7.5.3 Targeting eRF3

The protein eRF3 can be targeted with the CRBN E3-ligase modulator (CELMoD) CC-885. CC-885 was identified to target GSPT1 and GSPT2 by binding to the cullin4 (CRL4) CRBN-DDB1-E3-ligase complex. GSPT1 was then ubiquitinated and degraded by the proteasome. Similar to genetic depletion of eRF3a, chemical degradation of GSPT1 and GSPT2 with CC-885 induced apoptosis in various tumors with potent antitumor activity (Matyskiela et al., 2016a; Matyskiela et al., 2016b; Sperling et al., 2019). Furthermore, the CELMoD CC-90009, a derivative of CC-885, was shown to target GSPT1 by inducing apoptosis and growth inhibition in AML cells (Lopez-Girona et al., 2019)

7.6 Polo-like kinase 1 (PLK1)

The polo-like kinases (PLK) are serine/threonine protein kinases and include five members (Golsteyn et al., 1996; Lens et al., 2010). PLK1 is involved in multiple cell proliferative processes, for instance, entry in mitosis and G2/M checkpoint, coordination of the centrosome, the spindle assembly, chromosome segregation and DNA replication.

7.6.1 The role of PLK1 in cancer

An overexpression of PLK1 was detected in most of human cancers and was associated with poor overall survival of these patients (Ramani et al., 2015; Tut et al., 2015; Zhang et al., 2015b). The inhibition of PLK1 with RNAi or kinase inhibitors was

potently preventing proliferation of cancer cell and induced apoptosis (Bu et al., 2008; de Oliveira et al., 2012). Specifically, in the early development of pancreatic cancer an overexpression of PLK1 was detected (Weichert et al., 2005). Further, in colorectal cancer the overexpression of PLK1 was associated with migration and invasion of these cells (Han et al., 2012). Interestingly, PLK1 not only shows oncogenic characteristics, but also has tumor-suppressive potential as shown in APC-truncated colon cancer cells (de Cárcer, 2019; Raab et al., 2018).

7.6.2 MYC and PLK1

In 2016, it was published that the expression of PLK1 is essential for stabilizing oncoprotein MYC. Specifically, PLK1 was shown to antagonize the degradation of N-Myc by destabilizing the ubiquitin E3-ligase, F-box and WD repeat domain-containing 7 (Fbw7) and was shown to stabilize MYC by promoting its phosphorylation. Therefore, inhibition of PLK1 and indirect inhibition of MYC via BCL2 was proposed as a promising strategy to disrupt the positive feed-forward circuit between MYC and PLK1 and to target MYC overexpressing cancers (Xiao et al., 2016).

7.6.3 Targeting PLK1

PLK1 can be inhibited via two functionally different drug targets in the structure of PLK1. On the one hand, the N-terminal catalytic domain and on the other hand the C-terminal polo-box domain (Murugan et al., 2011). Multiple promising small-molecule kinase inhibitors were developed, for example Onvansertib, which was recently tested in a combinational phase I/II clinical trial to treat metastatic colorectal cancer (NCT03829410). Further, volasertib, competing with ATP at the catalytic binding site of PLK1, was shown to be a potent inhibitor of PLK1 in preclinical studies and clinical trials in solid tumors, as well as AML (Murugan et al., 2011). In HCT116 xenograft tumor models, volasertib treatment induced growth inhibition and reduced tumor growth, which led to tumor regression (Rudolph et al., 2009). In tumor-bearing mice the treatment with volasertib resulted in cell cycle arrest and apoptosis (Barr et al., 2004).

7.7 Proteolysis targeting chimeras (PROTACs)

The PROTAC technology was first published 19 years ago as a promising novel approach to target proteins considered ’undruggable’, but for which a small molecule ligand can still be provided (Deshaies, 2015a; Sakamoto et al., 2001). After 15 years of optimizing and improving the chemical compounds, the first potent PROTACs were

finally published by Bondeson et al. and Winter et al. (Bondeson et al., 2015; Winter et al., 2015).

PROTACs take advantage of the intracellular ubiquitin-depended proteolysis that regulates protein levels in the cell (Alabi and Crews, 2021). The technology is based on a heterobifunctional PROTAC compound consisting of three components - a recruiter for an E3-ligase, a binder of the protein of interest, and a linker that connects them (Figure 5) (Sakamoto et al., 2001).

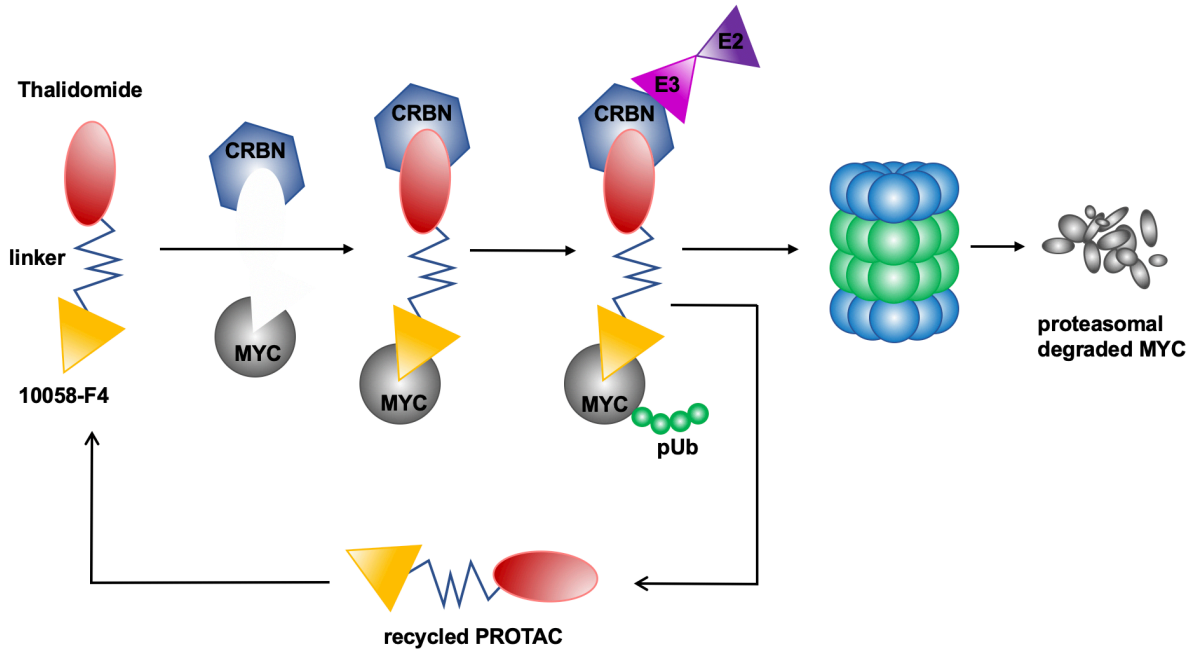

Figure 5: Mechanism of PROTACs
The PROTAC has three components. A binder (Thalidomide) of cereblon (CRBN) as part of the DDB1-CUL4-X-box protein ligase complex that is linked to the binder (10058-F4) of the target protein (MYC). Through close spatial relationship the E3-ligase poly-ubiquitinates the protein of interest which is detected by the 26S proteasome. Subsequently, the proteasome degrades MYC. The PROTAC is then free for following rounds of degradation.

PROTACs hijack the E3-ligase and consequently position proteins in a spatially favorable presentation to facilitate substrate poly-ubiquitination, thereby selectively knocking down levels of the targeted protein (Burslem et al., 2018). This shift from inhibition of a target protein to its removal by degradation allows irreversible targeting of proteins (Lai and Crews, 2017). Thus, a polyubiquitinated target protein can dissociate from the PROTAC which can once again bind to another target protein, which can prolong its function (Lai and Crews, 2017).

E3-ligases orchestrate protein ubiquitination and degradation in eukaryotic cells (Zheng and Shabek, 2017). So far, about 600 E3-ubiquitin-ligases have been identified in the human genome which are all potentially able to poly-ubiquitinate proteins of interest targeted by a specific PROTAC (Zheng and Shabek, 2017). The ubiquitously expressed E3-ligase CRBN is part of the DDB1-CUL4-X-box protein ligase complex and known to initiate the proteasomal degradation of proteins, for instance, MEIS2 (Fischer et al., 2014). Binding of Thalidomide or its analogues to CRBN prevents ubiquitination and proteasomal degradation of this E3-ligase. In human myeloma cells, the treatment with Thalidomide led to the stabilization and accumulation of the CRBN protein. This resulted in an increased cullin-4 RING E3-ligase-mediated degradation of PROTAC target proteins (Liu et al., 2015). Therefore, Thalidomide was chosen as ligand of the CRBN E3-ligase in this work.

The PROTAC technology can potentially be used for any protein for which a small molecule ligand can be developed, regardless of whether the target is classically ’druggable’ or not (Deshaies, 2015b). In this work, the MYC inhibitor 10058-F4 was used as the binder for the protein of interest (Huang et al., 2006).

7.8 Aim of the project

The aim of this study was to examine a novel targeting strategy for cancer therapy. Therefore, a potent degrader of MYC and its network was designed and validated.

Targeting of the MYC oncogene still remains a challenge. Hence, it was the aim of this work to inhibit MYC signaling by utilizing the PROTAC technology. This novel approach provides several advantages, including the targeting of proteins considered as ‘undruggable’.

Specifically, in this work it was aimed to establish and validate a novel MYC DEGrader, MDEG-541, in the MYC amplified cell lines PDAC and CRC cell lines. The dose-and time-dependent degradation of MYC protein and off-targets after MDEG-541 treatment was examined. Specifically, in transcriptome- and proteome-wide analysis, the involvement of prominent cancer related MYC-signaling pathways, E2F and cell cycle HALLMARKs, were observed after MDEG-541 treatment. Further, the dependency of the degradation of MYC and MDEG-541 off-targets on the CRBN, the proteasome and ubiquitination were examined. The efficiency of MDEG-541 was tested in preclinically relevant, three-dimensional (3D) organoid models and the specific mode of cell death was determined after MDEG-541 treatment.

8. Material

Table 1: List of technical equipment

Instrument	Company
AS2000 Maxwell® 16 instrument	Promega, Walldorf, Germany
Clariostar 4300741	BMG Labtech, Ortenberg, Germany
FC Multiskan	Thermo Fisher Scientific, Munich, Germany
FLUOstar® OPTIMA	BMG Labtech, Champigny-sur-Marne, France
Gallios™ Flow Cytometer, RRID:SCR_019639	Beckman Coulter, Brea, CA, USA
MIKRO 220 R table centrifuge	Hettich, Kirchlengern, Germany
Mini-PROTEAN® Tetra Vertical, 1.5 mm	Bio-Rad, Munich, Germany
NB-203XL CO_2 Incubator	N-BIOTEK Co., Ltd., Gyeonggi-Do, Korea
Odyssey® Fc, RRID:SCR_015795	Li-cor Biosciences GmbH, Bad Homburg vor der Höhe, Germany
PERFECTION V370 PHOTO DIN A4 Photoscanner	Epson, Suwa, Japan
Rotina 380 R	Hettich, Kirchlengern, Germany
SP8 LIGHTENING Confocal microscope	Leica, Wetzlar, Germany
StepOnePlus Real-Time PCR System (4376357), RRID:SCR_015805	Applied Biosystems, Munich, Germany
T100 Thermal Cycler	Bio-Rad, Munich, Germany
ThermoMixer® C	Eppendorf, Munich, Germany
Wet/Tank blotting system	Bio-Rad, Munich, Germany

Table 2: List of Kits used for the experiments

Kit	Catalogue Number	Company
AllPrep DNA/RNA Kits	80284	Qiagen, Venlo, Netherlands
CellTiter-Glo® Luminescent Cell Viability Assay	G7570	Promega, Walldorf, Germany
FITC Annexin V Apoptosis Detection Kit I (RUO), RRID:AB_2869082	556547	Becton Dickinson, Franklin Heights, NJ, USA
GoTaq® qPCR Master Mix	A6001	Promega, Walldorf, Germany
Maxwell® 16 LEV simplyRNA Purification Kits	AS1280	Promega, Walldorf, Germany
NucleoSpin Plasmid Transfection-grade	740490.10	Macherey-Naggel GmbH, Düren, Germany

Table 3: List of compounds/reagents

Compounds/Reagents	Catalogue Number	Company
(±)-Thalidomide	T144	Sigma-Aldrich, Munich, Germany
(R)-MG132	M8699	Sigma-Aldrich, Munich, Germany
10058-F4	S7153	Selleckchem, Munich, Germany
24-well Polypropylene Microplates, clear, Corning®	142475	Thermo Fisher Scientific, Munich, Germany
384-well White/Clear Bottom Polystyrene Microplates, Corning®	3765	Thermo Fisher Scientific, Munich, Germany
80% Ethanol	N-33635	Brüggemann Alcohol, Heilbronn, Germany
96-well Polypropylene Microplates, clear, Corning®	3343	Thermo Fisher Scientific, Munich, Germany
ABgene™ EasyStrip™	15596619	Thermo Fisher Scientific, Munich, Germany
Bortezomib	5043140001	Sigma-Aldrich, Munich, Germany
BsmBI-v2 restriction enzyme	R0739	New England Biolabs., Frankfurt a. Main, Germany

Cell Recovery Solution, 100 mL Corning®	354253	Thermo Fisher Scientific, Munich, Germany
Cell Scraper	83.1830	Starstedt, Nümbrecht, Germany
Cellstar Cell culture bottle	660175	Greiner BIO-ONE, Kremsmünster, Austria
CELLSTAR® Polypropylen Röhrchen	227261	Greiner BIO-ONE, Kremsmünster, Austria
Costar® TC-Treated Multiple Well Plates 24-well, Corning®	CLS3527	Sigma-Aldrich, Munich, Germany
Costar® TC-Treated Multiple Well Plates 6-well, Corning®	CLS3516	Thermo Fisher Scientific, Munich, Germany
Crystal violet	C6158	Sigma-Aldrich, Munich, Germany
DMSO	A3672	AppliChem, Darmstadt, Germany
Dulbecco´s Modified Eagle´s Medium	D5030	Sigma-Aldrich, Munich, Germany
Dulbecco´s PBS	D8537-500 mL	Sigma-Aldrich, Munich, Germany
EDTA (Versen) 1% (w/v) in PBS w/o CA^{2+}	L 2113	Biochrom GmbH, Berlin, Germany
Eppendorf Safe-Lock Tubes, 1.5 mL	0030120086	Eppendorf, Munich, Germany
Eppendorf Safe-Lock Tubes, 2mL	0030120094	Eppendorf, Munich, Germany
Ethidium promide solution	E1510	Sigma-Aldrich, Munich, Germany
Falcon® Round-Bottom Polystyrene Tubes	38055	STEMCELL Technologies, Cologne, Germany
Falcon™ Chambered Cell Culture Slides	10364551	Thermo Fisher Scientific, Munich, Germany
FBS Superior	S 0615	Merck, Darmstadt, Munich
Filtropur	20003477	Starstedt, Nümbrecht, Germany
Gel Saver-Tip II	GSII054R	Kisker Biotech GmbH & Co. KG, Steinfurt, Germany
lentiCRISPRv2 puro	98290	Addgene, Watertown, MA USA
Lipofectamine 2000 Transfection Reagent	11668030	Thermo Fisher Scientific, Munich, Germany
Matrigel®, Growth Factor Reduced (GFR) Basement Membrane Matrix, LDEV-free, Corning®	354230	Thermo Fisher Scientific, Munich, Germany
MTT	M5655	Sigma-Aldrich, Munich, Germany
Neubauer counting chamber	10490171	Thermo Fisher Scientific, Munich, Germany
One Shot™ Stbl3™ Chemically Competent *E. coli*	C737303	Thermo Fisher Scientific, Munich, Germany
Opti-MEM with GlutaMAX, Gibco	12559099	Thermo Fisher Scientific, Munich, Germany
PCR® MICROPLATE, Axygen	PCR-96-LP-AP-C	Thermo Fisher Scientific, Munich, Germany
Platemax CyclerSeal Sealing Film, Axygen	PCR-TS	Thermo Fisher Scientific, Munich, Germany
pMD2.G	12259	Addgene, Watertown, MA USA
Polybrene Infection / Transfection Reagent	TR-1003	Sigma-Aldrich, Munich, Germany
Propidium Iodide	P4170	Sigma-Aldrich, Munich, Germany
psPAX2	12260	Addgene, Watertown, MA USA
PureLink™ RNase A, 10 mL, Invitrogen	1772940	Thermo Fisher Scientific, Munich, Germany
Q5® High-Fidelity DNA Polymerase	M0491S	New England Biolab, Frankfurt, Germany

REDTaq® ReadyMix™ PCR Reaction Mix	R2523	Sigma-Aldrich, Munich, Germany
RPMI 1640 Medium, GlutaMAX™ Supplement	61870044	Thermo Fisher Scientific, Munich, Germany
Safe seal tube, 1.5 mL	72.706	Starstedt, Nümbrecht, Germany
SDS NA-salt in Pellets	20765.03	Serva, Rosenheim, Germany
T4 DNA Ligase	M0202S	New England Biolabs., Frankfurt a. Main, Germany
T4 DNA Ligase Reaction Buffer	B0202S	New England Biolabs., Frankfurt a. Main, Germany
TAK-243	S8341	Selleckchem, Munich, Germany
tissue-culture treated culture dishes, Corning®	CLS430599	Thermo Fisher Scientific, Munich, Germany
TrypLE™ Express Enzyme (1x), 100 mL	12604013	Thermo Fisher Scientific, Munich, Germany
Volasertib	A10135	Adooq Bioscience, Ivrine, CA, USA
Zeocin Selection Reagent	R25005	Thermo Fisher Scientific, Munich, Germany

Table 4: Ingredients for medium for organoid primary culture

Product	Catalogue Number	Final conc.	Company
3,3,5-Triiodo-L- thyronine	T2877	5 nM	Sigma-Aldrich, Munich, Germany
A83-01	72022	0,5 µM	STEMCELL Technologies, Cologne, Germany
Bovine Pituitary Extract	P1476	25 µg/ml	Sigma-Aldrich, Munich, Germany
Cholera toxin	C8052	100 ng/ml	Sigma-Aldrich, Munich, Germany
D-Glucose	G8270	5 mg/mL	Sigma-Aldrich, Munich, Germany
Dexamethasone	D1756	1 µM	Sigma-Aldrich, Munich, Germany
DMEM/F12-500 mL	11330032	-	Thermo Fisher Scientific, Munich, Germany
ITS + premix, Corning®	10070791	0.5% (w/v)	Thermo Fisher Scientific, Munich, Germany
Neuregulin	100-03	100 ng/ml	Pepro Tech, Hamburg, Germany
Nicotinamide	N3376	10 mM	Sigma-Aldrich, Munich, Germany
Nu-Serum IV, Corning®	355100	5% (v/v)	Thermo Fisher Scientific, Munich, Germany
Penicillin/Streptomycin	15140-122	1% (v/v)	Thermo Fisher Scientific, Munich, Germany
Primocin	Ant-pm-1	100 µg/ml	Invivogen, San Diego, CA, USA
Rock inhibitor Y-27632	72304	10 µM	STEMCELL Technologies, Cologne, Germany

Table 5: Ingredients for medium for human cancer associated fibroblasts

Product	Catalogue Number	Final conc.	Company
DMEM (1X) low glucose (1g/l)	31885023	41.25%(v/v)	Thermo Fisher Scientific, Munich, Germany
DMEM F12 (1X)	31330038	41.25%(v/v)	Thermo Fisher Scientific, Munich, Germany
FBS	10270106	3.67%(v/v)	Thermo Fisher Scientific, Munich, Germany
Penicillin/Streptomycin	15140-122	1% (v/v)	Thermo Fisher Scientific, Munich, Germany
Primocin	Ant-pm-1	0.165% (v/v)	Invivogen, San Diego, CA, USA

Table 6: Products used for western blot

Product Name	Catalogue Number	Description	Company
Albumin	11930.03	lyophilized powder, ≥96%	Serva, Rosenheim, Germany
Bradford Reagent	39222.01	5x concentrate	Serva, Rosenheim, Germany
cOmplete™, Mini, EDTA-free Protease Inhibitor Cocktail	11836170001	Dissolved in 1.5 mL H_2O (7x conc. stock solution)	Roche Diagnostics GmbH, Basel, Swiss
Mini-PROTEAN Comb	1653365	10-well with 66 µL Volume, 15-well with 40 µL Volume	Bio-Rad, Munich, Germany
Nitrocellulose Blotting Membrane	10600001	0.2 µM	GE Healthcare Life Science, Freiburg im Breisgau, Germany
Nonfat-Dried Milk Bovine	M7409	Powder, 5% (w/v) PBS-T	Sigma-Aldrich, Munich, Germany
Page RulerTM Prestained	26616	Protein Ladder	Thermo Fisher Scientific, Munich, Germany
Phosphatase-Inhibitor-mix I, powder	39050.03	1 mg/mL	Serva, Rosenheim, Germany

Table 7: List of antibodies used for western blot 2nd AB

Antibody	Catalogue Number	Dilution	Source	Molecular Weights (kDa)	Company
β-ACTIN	4967, RRID:AB_1607797	1:10,000	mouse, monoclonal	45	Cell Signaling, Danvers, MA, USA
α-TUBULIN	T5168, RRID:AB_922700	1:10,000	mouse, monoclonal	50	Sigma-Aldrich, Munich, Germany
Anti-mouse IgG (H+L) (DyLight™ 680 Conjugate)	5470	1:10,000	mouse	-	Cell Signaling, Danvers, MA, USA
Anti-mouse IgG (H+L) (DyLight™ 800 4X PEG Conjugate)	5257	1:10,000	mouse	-	Cell Signaling, Danvers, MA, USA
Anti-rabbit IgG (H+L) (DyLight™ 680 Conjugate)	5366	1:10,000	rabbit	-	Cell Signaling, Danvers, MA, USA
Anti-rabbit IgG (H+L) (DyLight™ 800 4X PEG Conjugate)	5151	1:10,000	rabbit	-	Cell Signaling, Danvers, MA, USA
ATF2 (C-19),	sc-187, RRID:AB_630885	1:100	rabbit, polyclonal	70	Santa Cruz Biotechnology Inc., TX, USA
ATF4 (D4B8)	11815 RRID:AB_2616025	1:1,000	rabbit, polyclonal	49	Cell Signaling, Danvers, USA

c-MYC	9402, RRID:AB_2151827	1:1,000	rabbit, polyclonal	62/64	Cell Signaling, Danvers, USA
CDK2	558896, RRID:AB_397149	1:1,000	rabbit, polyclonal	33	Becton Dickinson, Franklin Heights, NJ, USA
CDK4 (C-22)	sc-260, RRID:AB_631219	1:1,00	rabbit, polyclonal	30	Santa Cruz Biotechnology Inc., TX, USA
CRBN	immunized rabbits,	1:2,000	rabbit, polyclonal	55	Innovagen
Cyclin D1 (HD11)	sc-246, RRID:AB_627348	1:1,000	mouse, monoclonal	37	Santa Cruz Biotechnology Inc., TX, USA
E2F-1(C-20)	sc-193, RRID:AB_631394	1:100	rabbit, polyclonal	60	Santa Cruz Biotechnology Inc., TX, USA
eIF2α,	9722, RRID:AB_2230924	1:1,000	rabbit, polyclonal	38	Cell Signaling, Danvers, MA, USA
GSPT1	ab49878, RRID:AB_2115507	1:1,000	rabbit, polyclonal	84	Abcam, Cambridge, England
GSPT2	PA5-44324, RRID:AB_2606798	1:1,000	rabbit, polyclonal	69	Invitrogen, Thermo Fisher Scientific, Munich, Germany
HSP90 α/β	sc-13119, RRID:AB_675659	1:100	mouse, monoclonal	90	Santa Cruz Biotechnology Inc., TX, USA
MLKL (D2I6N)	14993, RRID:AB_2721822	1:1,000	rabbit, monoclonal	54	Cell Signaling, Danvers, MA, USA
p-eIF2α (Ser51)	3398, RRID:AB_2096481	1:1,000	rabbit, monoclonal	38	Cell Signaling, Danvers, MA, USA
p-MLKL (Ser358)	91689, RRID:AB_2732034	1:1,000	rabbit, monoclonal	45	Cell Signaling, Danvers, MA, USA
p-PERK (T982)	ab192591, RRID:AB_2728666	1:1,000	rabbit, polyclonal	170	Abcam, Cambridge, England
PERK	sc-13073, RRID:AB_2230863	1:100	rabbit, monoclonal	125	Santa Cruz Biotechnology Inc., TX, USA
PLK1	sc-17783, RRID:AB_628157	1:250	mouse, monoclonal	66	Santa Cruz Biotechnology Inc., TX, USA
pRB (Ser807/811)	8516, RRID:AB_11178658	1:1,000	rabbit, monoclonal	110	Cell Signaling, Danvers, USA

Table 8: List of Buffers, Gels and Solutions

Name	Ingredients	Application
ACK Buffer	150 mM NH_4Cl 10 mM $KHCO_3$ 0.1 mM Na_2EDTA, pH 7.4	Lysis of red blood cells
Freezing Medium	Dulbecco´s Modified Eagles Medium, high glucose 10% (v/v) FCS 10% (v/v) DMSO	Storage of cell lines at -80°C/in nitrogen

KCM Buffer (5x)	0.5 M KCl 0.15 M $MCaCl_2$ 0.25 mL $MgCl_2$	Transformation of bacteria
Laemmli Buffer (5x)	250 mM Tris-HCl (pH 6.8) 4% (w/v) SDS 40% (v/v) Glycerol 0.05% (w/v) Bromphenolblue add 5% (v/v) β-Mercaptoethanol before usage	Denaturation of proteins and charching negative
LB-Agar	4% (w/v) LB-Agar powder, (Luria/Miller) X.969.2, Carl Roth, Karlsruhe, Germany 100 µM (v/v) Ampicillin	Growth of bacteria
LB-Medium	2.5% (v/v) LB-Medium powder, (Luria/Miller) X968.1, Carl Roth, Karlsruhe, Germany 50 µM Ampicillin	growth of bacteria
PBS (1x)	137 mM Sodium chloride 270 µM Kalium chloride 4.0 mM Disodium phosphate	Washing buffer
Proteomics Buffer	2% (w/v) SDS 40 mM Tris-HCl, pH 7.6	Harvesting of Proteins
Resolving gel (10%)	390 mM Tris-HCl, pH 8.8 10% (v/v) Acrylamide 0.1% (v/v) SDS 0.05% (v/v) APS 0.05% (v/v) Temed	Separation of proteins
Resolving gel (15%)	300 mM Tris-HCl, pH 8.8 15% (v/v) Acrylamide 0.1% (v/v) SDS 0.05% (v/v) APS 0.05% (v/v) Temed	Separation of proteins
Resolving gel (7.5%)	390 mM Tris-HCl, pH 8.8 7.5% (v/v) Acrylamide 0.1% (v/v) SDS 0.05% (v/v) APS 0.05% (v/v) Temed	Separation of proteins
RIPA Buffer	150 mM $NaCl_2$ 1% (w/v) NP40 0.5% (w/v) Sodium Deoxychlorate (DOC) 0.1% (w/v) SDS 50 mM Tris-HCl, pH 8	Harvesting of hole cell protein lysates
Running Buffer (1x)	192 mM Glycine 25 mM TRIS 3.47 mM SDS	Separation of proteins
Stacking gel (4.4%)	125 mM Tris-HCl, pH 6.8 4.4% (v/v) Acrylamide 0.1% (v/v) SDS 0.05% (v/v) APS 0.2% (v/v) Temed	Collection of proteins
TE Buffer	1 mM Tris-HCl (pH 8.0) 0.5 M EDTA	Resuspension and storage of nucleic acids
Transfer Buffer (1x)	192 mM Glycine 25 mM TRIS 20% (v/v) Methanol	Blotting of separated proteins from the gel to a nitrocellulose membrane

Table 9: Cell lines

Cell line	Source	Disease	Medium	Characteristics
HEK293, RRID:CVCL_0045	human	embryonic kidney	DMEM	epithelial, adherent

BxPC-3, RRID:CVCL_0186	human	Pancreatic adenocarcinoma	RMPI	epithelial, adherent
DANG, RRID:CVCL_0243	human	Pancreatic adenocarcinoma	RMPI	epithelial, adherent
HPAC, RRID:CVCL_3517	human	Pancreatic adenocarcinoma	DMEM	epithelial, adherent
HUPT3, RRID:CVCL_1299	human	Pancreatic adenocarcinoma	DMEM	epithelial, adherent
KP4, RRID:CVCL_8727	human	Pancreatic adenocarcinoma	DMEM	epithelial, adherent
MIA PaCa-2, RRID:CVCL_0428	human	Pancreatic adenocarcinoma	DMEM	epithelial, adherent
Panc-1, RRID:CVCL_0480	human	Ducts, epithelioid carcinoma	DMEM	epithelial, adherent
PATU8988S, RRID:CVCL_1846	human	Pancreatic adenocarcinoma	DMEM	epithelial, adherent
PATU8988T, RRID:CVCL_1847	human	Pancreatic adenocarcinoma	DMEM	epithelial, adherent
PSN1, RRID:CVCL_1644	human	Pancreatic adenocarcinoma	RMPI,	epithelial, adherent
NCI-H716, RRID:CVCL_1581	human	Colorectal adenocarcinoma, cecum	RMPI	epithelial, adherent
SW480, RRID:CVCL_0546	human	Dukes' type B, colorectal adenocarcinoma	DMEM	epithelial, adherent
SW707, RRID:CVCL_6230	human	Rectal adenocarcinoma	DMEM	epithelial, adherent
T84, RRID:CVCL_0555	human	Colorectal cancer, derived from metastatic site lung	DMEM	epithelial, adherent
COLO320, RRID:CVCL_1989	human	Dukes' type C, colorectal adenocarcinoma	RMPI	rounded and refractile
HCT116, RRID:CVCL_0291	human	Colorectal carcinoma	DMEM	epithelial, adherent
HT-29, RRID:CVCL_0320	human	Colorectal adenocarcinoma	RMPI	epithelial, adherent

Table 10: Softwares and programs

Software	**Company**
Adobe Illustrator CC 2018, RRID:SCR_010279	Adobe Inc., San José, CA, USA
FlowJo 8.8.6, RRID:SCR_008520	FlowJo, Becton Dickinson, Franklin Heights, NJ, USA
GraphPad Prism Software v5, RRID:SCR_002798	GraphPad Software, San Diego, CA, USA
ImageJ, RRID:SCR_003070	NIH, Bethesda, MD, USA
Microsoft Office 2010, RID:SCR_016137	Microsoft, Redmond, WA, USA
NanoDrop ND-1000 3.1	NanoDrop, Informer Technlologies, Inc.,
R software	R Core Team, GNU GPL
StepOne Software V2.3, RRID:SCR_014281	Thermo Fisher Scientific, Munich, Germany

9. Methods

9.1.1 Two-dimensional cell culture

9.1.1.1 Cell culture maintenance

For maintenance, the cells were cultured in either Dulbecco's Modified Eagle's Medium (DMEM) or Roswell Park Memorial Institute (RPMI) medium supplemented with 10% (v/v) Fetal bovine serum (FBS) and 1% (v/v) Penicillin/Streptomycin (P/S). 80% confluent cells were detached with 0.05% (v/v) ethylenediaminetetraacetic acid (EDTA), diluted in phosphate buffered saline (PBS) and re-cultured in fresh medium. For experiments the cancer cell lines were cultured in medium supplemented with 10% FBS without antibiotics. Cells were incubated at 37°C with 5% (v/v) CO_2 and counted with a Neubauer chamber. Authentication of all cell lines was performed in 2020 by short tandem repeat (STR) profiling (Mycrosynth, Balgach, Switzerland) or single Nucleotide Polymorphism (SNP)-Profiling by Multiplexion (Multiplexion GmbH, Heidelberg, Germany).

9.1.1.2 Mycoplasma test

Cells were tested for mycoplasma contamination by cultivating in P/S-free medium. After two weeks 2 mL of the supernatant medium were harvested and centrifuged for two min at 250 g to remove cell debris. The supernatant was collected and centrifuged for ten min at 24,000 g. The supernatant was discarded, and the pellet containing the mycoplasma was resuspended in 50 µL of TE Buffer to solubilize the DNA and protect it from degradation. The solubilized pellet was heated at 95°C for three min to reverse the hydrogen bond and obtain two single DNA strands. A polymerase chain reaction (PCR) with included positive and negative control was performed to amplify the DNA sample with following primers:

Table 11: Primer pairs for mycoplasma testing

forward primers (5´→3`)	reverse primer (3´→5´)
CGC CTG AGT AGT ACG TTC GC	GCG GTG TGT ACA AGA CCC GA
CGC CTG AGT AGT ACG TAC GC	GCG GTG TGT ACA AAA CCC GA
TGC CTG GGT AT ACA TTC GC	GCG GTG TGT ACA AAC CCC GA
TGC CTG AGT AGT ACA TTC GC	
CGC CTG AGT AGT ATG CTC GC	
CAC CTG AGT AGT ATG CTC GC	
CGC CTG GGT AGGT ACA TTC GC	

The forward- and reverse-primer mix was prepared with 10 µL of the respective primer. Both mixes were filled up with H_2O to a final volume of 100 µL and were used to pipet the PCR mix.

Table 12: Preparation of primer mix for mycoplasma testing

Reagent	Volume per reaction (µL)
DNA	2
RedTaq Premix	15
forward primer mix	2
reverse primer mix	2
H2O	9

The DNA sample was amplified by terminal cycling starting with an initial activation step for 15 min at 95°C. 40 cycles were performed specifically starting with denaturation for 1 min at 94°C, primer annealing for 1 min at 53°C and elongation for 1 min at 74°C. The PCR was terminated at 12°C. The amplified DNA was separated on a 1.5% (w/v) agarose gel prepared with 0.5 µg/mL ethidiumpromide. The PCR products were visualized by exposing the gel to UV light.

9.1.1.3 Drug Screen

To evaluate the cell metabolism of several cell lines a viability assay was performed, quantifying the reduction of Thiazolyl Blue Tetrazolium Bromide 3 (MTT) reagent to insoluble, purple colored formazan via the NAD(P)H-dependent oxireductase enzymes. 2500 cells per well were seeded in 96-well plates in triplicates and left to attach o/n. The following day cells were treated with MDEG-541 using a 7-point or 12-point dilution ranging from 50 µM to 0.78 µM or 48 nM. Ten PDAC cell lines (BxPC-3, DANG, HPAC, HUPT3, KP4, MIA PaCa-2, Panc-1, PATU8988S, PATU8988T, PSN1 and seven CRC cell lines (COLO320 HCT116, HT-29, NCI-H716, SW480, SW707, T84) were tested in at least three independent biological replicates.
Matching vehicle controls were included and all compounds were incubated for 72 h under culturing conditions. In order to determine viability, 10 µM MTT reagent was added to each well and incubated for 4 h at 37°C. Subsequently, the supernatant was removed, 200 µL DMSO:EtOH (1:1, Dimethylsulfoxid:Ethanol) were added to dissolve the MTT reagent in each well. The plate was shaken for five min before absorbance was measured at 595 nm using a Multiskan plate reader. Individual readings for each

treatment were normalized to its respective vehicle control to calculate drug sensitivity and half-maximal growth inhibitory concentration determined as GI_{50} values.

9.1.1.4 Calculation of GI_{50} values and their correlation with gene expression

The MDEG-541 drug sensitivity of the PDAC and CRC cell lines was determined via GI_{50} values. The GI_{50} was calculated with GraphPad Prism 5 by non-linear regression and log transformation (log(inhibitor) vs. normalized response-variable slope) of the data. The GI_{50} values were correlated to the gene expression from the RNA seq data in the Cancer Cell Line Encyclopedia (CCLE, CCLE_expression_full.csv, February 2020, Depmap portal: https://depmap.org/portal/download) using R. Following the GTEx pipeline of the Broad Institute the gene expression was quantified as log2 transcripts per million and correlated with the GI_{50} values using Spearman statistics using R. The correlation coefficient of the GI_{50} values and CRBN single-gene expression from CCLE was calculated with Spearman statistics using GraphPad Prism.

9.1.2 Organoid cell culture

9.1.2.1 Production of Rspol conditioned medium

The proliferation of patient-derived organoids requires the activation of the LGR5 receptor by its ligand R-spondin-1. The R-spondin-1 overexpressing cell line HEK293T, provided by the Hubrecht Institute (Uppsalalaan 8, 3584 CT Utrecht, Netherlands) was grown in selection medium by adding 300 µg/µl Zeocin to DMEM with 10% (v/v) FBS and 1% (v/v) P/S in a 175 cm flask. The 80% confluent flask was split into six 175 cm flasks without Zeocin. When the cells were 80% confluent, the medium was removed and conditioning medium containing DMEM-F12 without supplements was added. After one week in the incubator at 37°C, the medium was harvested, centrifuged for five min at 250 g, cleared through a 0.22 µM filter and 10% (v/v) of R-spondin-1 conditioned medium was added to the medium of the organoids.

9.1.2.2 Isolation of patient-derived organoids

Organoid isolation, passaging and drug-screen were performed by Felix Orben and Aylin Aydemir. Tissue-derived cells can be placed in Matrigel matrix to mimic the growth conditions and tissue architecture of the extra cellular matrix (ECM). In the presence of suitable exogenous factors, the tissue-derived cells can grow in 3D clusters displaying a model of complex growth conditions. 3D models were established and evaluated according to the declaration of Helsinki and approved by the local ethical

committee (Project 207/15). A written informed consent from the patients was obtained for research use prior to the investigation.

The samples were collected by endoscopy punctures or surgical resection in the Klinikum rechts der Isar, Munich. Patient biopsies were kept in cold DMEM-F12 on ice in a 15 mL falcon and processed quickly. The sample was centrifuged at 250 g at 4°C for five min and the supernatant was discarded. Large samples were mechanically precut with a scalpel and washed with cold PBS. The sample was centrifuged again at 250 g and 4°C for five min and the supernatant was discarded. 3 mL of ACK Buffer were added and incubated at room temperature (RT) by inverting the 15 mL falcon until all red blood cells were lysed. 8 mL cold PBS were supplemented and the falcon was centrifuged at 250 g and 4°C for five min. 3 mL of TrypLE were added and incubated for five min at 37°C to dissociate organoids to a single cell suspension. The organoids were then counted with a Neubauer chamber for follow up experiments, seeded to expand the organoid line by adding 8 mL PBS to the falcon and centrifuged at 250 g at 4°C for five min. The supernatant was removed carefully, and the pellet was dissolved in 50 µL Matrigel on ice. The mix was placed in the middle of a well of a 24-well plate to form a Matrigel dome and the plate was incubated for ten min at 37°C for polymerization. 500 µL of pre-warmed medium was supplemented with 10 µM Rock inhibitor on the Matrigel dome, enhancing the survival of the dissociated single cells and inhibiting apoptosis.

Organoids were screened for mutated KRAS to ensure the cancerous potential of the organoids. KRAS mutations were determined by Sanger Sequencing by isolating the organoid DNA with the DNA/RNA Micro Kit (Qiagen, Germany). DNA was amplified with a PCR using the Q5® High-Fidelity DNA Polymerase (New England Biolab) with the following primers hKRAS_ex2_flank_Fw: 5`G G T A C T G G T G G A G T A T T T G A T A G T G 3` and hKRAS_ex2_flank_Rv 5`G G T C C T G C A C C A G T A A T A T G C A 3`. Sanger sequencing was conducted by Eurofins (Ebersberg, Germany).

9.1.2.3 Passaging of patient-derived organoids growing cells

Patient derived organoids were passaged by washing them with PBS and covering the Matrigel with 200-300 µL of cold Cell Recovery Solution. 1 mL of ice-cold PBS was added to the Cell Recovery Solution and the Matrigel was scrapped off using a pipet tip. Subsequently, the Matrigel was resuspended to dissolve the extracellular matrix with the cells. The Matrigel-Cell Recovery Solution-PBS-mixture was transferred into a 15 ml falcon tube to incubate for 30 min on ice. The sample was centrifuged at 250 g

and 4°C for five min before the supernatant was discarded carefully. Organoids were expanded (1:2 or 1:3), dependent on the pellet size by dissolving the pellet properly in Matrigel (50 µL/well) on ice. The Matrigel was placed in the middle of a well of a prewarmed 24-well plate. After ten min of incubation, 500 µL of prewarmed medium with 10 µM Rock inhibitor was added to each dome.

9.1.2.4 Drug screen of patient-derived organoids

To test for cell viability of organoids, the CellTiter-Glo® Luminescent Cell Viability Assay was used to quantifiy the presence of ATP (Adenosintriphosphate). The amount of ATP is an indication of the metabolic activity of the tested cells. Only organoids which re-grew after a freeze thaw cycle were analyzed and drug screens of organoids were performed in between passage 5-17.

The medium on the 24-well plate was aspirated and the Matrigel was washed with PBS once. 200-300 µL of cold Cell Recovery Solution and 1000 µL PSB were added to each well to scrape off and mechanically dissolve the Matrigel. The mix was transferred into a 15 mL falcon. The falcon tube was incubated for 30 min on ice and then centrifuged at 250 g and 4°C for five min. PBS was discarded, and 2 mL were kept to resuspend the cells. The falcon was filled up to 8 mL with cold PBS and centrifuged for 250 g at 4°C for five min. 1 mL TrypLE were supplemented to the falcon and incubated for one min at 37°C. The falcon was filled up with 8 mL of warm DMEM and centrifuged at 250 g and 4°C for five min. The supernatant was discarded and the cell pellet was resuspended in 1 ml of medium with Rock inhibitor. The cells were counted and 500 cells/well in 20 µL drug screen solution (2 µL Matrigel + 18 µL medium growth medium + 10 µM Rock-Inhibitor) were transferred to a 384-well plate. To prevent evaporation 50 µL of PBS were filled to empty wells on the 384-well plate. The plate was centrifuged for 10 seconds at 500 rpm. Cells were treated in triplicates the following day by adding 4 µL MDEG in a nine-point dilution starting with 50 µM to 0.78 µM and a vehicle control. The experiment was analyzed after 72 h of treatment by pipetting 5 µL of Cell Titer Glo Reagent into the wells. The plates were shaken for ten min followed by 20 min incubation at RT protected from light. Luminescence was measured with the FluoStar Optima in triplicates and three biological replicates were normalized to the DMSO vehicle control.

9.1.3 Human cancer-associated fibroblasts

Fibroblast were provided by Arlett Schäfer, AG Reichert, and established according to the following protocol. Frist, a fresh biopsy from the PDAC of a patient was placed on the lid of a 10 cm cell culture dish and the fibrotic area was cut into small pieces. Two to three pieces of cut fibrotic area were placed in a 6-well plate and 3 mL CAF medium were added. After 24 h, the medium was replaced and after further 48 h the tissue pieces were transferred to a new 6-well plate. 1.5 mL of CAF medium were added carefully per well without detaching the tissue. When the grown fibroblasts were confluent, they were splitted and the tissue was reused to generate more fibroblasts. Sequenced trypsinization was used to minimize epithelial cells. For MTT, 3,000 fibroblasts were seeded in DMEM medium with 10 % FBS per well in a 96-well plate. The fibroblasts were treated the next day for 72 h with seven 1:2 dilutions of MDEG-541 ranging from 50 µM-0.78µM.

9.1.4 Clonogenic assay

The colony formation of the cell lines PSN1 (250 cells/well) and HCT116 (200 cells/well) were performed in a 24-well tissue culture plate. The cells were treated in triplicates with 5 µM, 10 µM or, 20 µM MDEG-541 and the respective vehicle controls for twelve days (PSN1) and ten days (HCT116). After the long-term treatment, the supernatant was gently removed and cells were washed twice with PBS. The colonies were fixed and stained with a 0.4% (w/v) crystal violet solution for 30 min followed by gently washing the stained colonies under running tab water. The 24-well tissue culture plates were airdried and scanned. To quantify the colonies, 200 µl 1% (w/v) sodium dodecyl sulfate (SDS) were added to each well dissolving the crystal violet and plates were incubated o/n under shaking before absorbance was measured at 565 nm using a microplate reader.

9.1.5 Fluorescence activated cell sorting (FACS)-Cell death analysis with Annexin V/PI

To determine the number of cells undergoing cell death after treatment with MDEG-541 or control compounds 10058-F4 and Thalidomide respectively, the cellular DNA of the treated cells was stained with Propidium Iodide (PI) and Annexin V and quantified. In cells that undergo cell death, phosphatidylserine is translocated from the inner plasma membrane to the surface where it binds to fluorochrome-labeled Annexin

V. Here, a FITC labeled Annexin V was used for the detection of exposed phosphatidylserine due to loss of membrane integrity. Simultaneous staining with PI allows to distinguish between the mode of cell death by flow cytometry. PI were added to each sample to dye the double stranded DNA.

The FITC Annexin V Apoptosis Detection Kit I (RUO) from Becton Dickinson was used according to manufacturer's guidelines to detect cell death. In brief, 106 cells of the cell line PSN1 and HCT116 were seeded in a 10 cm cell culture dish. The cells were treated the following day with 10 µM MDEG-541 or the respective control compounds 10058-F4 and Thalidomide. The experiment was finished after 48 h treatment with MDEG-541 by collecting the medium and washing the cells with 5 mL PBS, which was also transferred to the falcon tube. Cells were detached with 0.05% (v/v) EDTA as previously described and also transferred to the falcon. The cells were washed twice with PBS, centrifuged for five min at 1000 rpm at RT before the cell pellet was resuspended in 1 mL of 1x Binding Buffer. 500 µL of the solution was transferred to a 5 mL reaction tube and 5 µL of FITC Annexin V and 5 µL of PI were added. The cells were vortexed gently and incubated for 15 min at RT in the dark. Finally, 500 µL of 1x Binding Buffer were added to each reaction tube and the samples were analyzed by flow cytometry on a Gallios™ Flow Cytometer. Data was analyzed with FlowJo 8.8.6.

9.1.6 RNA sequencing

RNA sequencing was performed to determine the global effect of MDEG-541 treatment on the transcriptome of cancer cells. Therefore, 106 cells of PSN1 and HCT116 cells were seeded on a 10 cm cell culture dish. The following day the cells were treated for 24 h with 20 µM MDEG-541. The samples were harvested following the Maxwell® 16 LEV simplyRNA Purification Kit according to manufacturer's instructions.

9.1.6.1 NextSeq 500 (Illumina)

RNA seq was performed by Dr. Rupert Öllinger in the lab of Prof. Dr. Roland Rad, TranslaTUM, Technical University Munich (TUM) as previously described (Parekh et al., 2016). In brief, the concentration of the RNA was measured with Qubit. For 3´-sequencing, a poly(A)-RNA barcoded cDNA of each sample was generated. The library was prepared with unique molecular identifiers, Maxima RT polymerase using oligo-dT primer containing barcodes and an adapter. A template switch oligo was used to extend the 5`ends of the cDNAs. The full-length cDNA samples were pooled and amplified with primers binding to the template switch oligo-site and the adapter. After

cDNA fragmentation the Tru-Seq-Adapters were ligated with the NEBNext® Ultra™ II FS DNA Library Prep Kit from Illumina®. 3`-end-fragments were amplified with the Illumina P5 and P7 overhangs. To archive a better cluster recognition the P5 and P7 sites were exchanged to allow sequencing of the cDNA in read1 and barcodes/unique molecular identifiers in read2. Read1 was sequenced with 65 cycles for the cDNA and 16 cycles for the barcodes/unique molecular identifiers. The library was sequenced on a NextSeq 500 (Illumina). The puplished Drop-seq pipeline (v.1.0) was used to process the data and generate sample-wise and gene-wise unique molecular identifier tables (Macosko et al., 2015). The genome GRCh38 was used as reference to align the samples. Hence, the definition of transcripts and genes were used according to the ENSEMBL annotation release 75.

9.1.6.2 RNA seq data analysis

Data was further analyzed with the help of Dr. Andrea Coluccio and Lukas Krauβ, M. Sc. (AG Schneider, Technical University Munich). Data was further analyzed using RStudio Version 1.2.5033 and DEseq2 (Love et al., 2014). Genes with sum (read counts) < 1 were removed and remaining counts were normalized and transformed using regularized log transformation (rlog) implemented in the DEseq2 package. Further gene set enrichment analysis (GSEA) or Genetrail Analysis were performed using the rlog transformed matrix.

RNA-sequencing data of PSN1 and HCT116 cells treated for 24 h with MDEG-541 compared to DMSO vehicle control were analyzed using the GSEA App 4.0.3. Enrichment Scores of HALLMARK signatures were downloaded from the MSigDB for both cell lines.

9.1.7 Proteomics

The cell line PSN1 was seeded and treated the next day with 10 µM MDEG-541 for 1, 2, 4, 6, 8, 10, 12, 16, 20 and, 24 h. Untreated cells were used as control and designated as timepoint 0. Following treatment, cells were washed twice with PBS and harvested after five min of incubation with 0.5 mL of 40 mM Proteomics Buffer on ice. The samples were flash frozen in liquid nitrogen and stored at -80°C. One replicate was performed in this experiment.

The proteomics experiment was performed by Dr. Stephanie Heinzlmeir in the lab of Prof. Dr. Bernhard Küster, Chair of Proteomics and Bioanalytics, at TUM according the following protocol.

9.1.7.1 Proteomics, LC-MS^3 analysis, Peptide and protein identification and quantification, and Proteome data analysis

To reduce viscosity, the sample was boiled at 95ºC for ten minutes and trifluoroacetic acid was added to a final concentration of 1%. To neutralize the sample (final pH 7.6-8.0), 300 mM N-methylmorpholin was added to a final concentration of 2%. The protein concentration in cell lysate was determined using the BCA assay (Thermo Fisher Scientific) according to the protocol of the manufacturer. The beads suspension for sp3 sample workup was prepared by mixing magnetic SeraMag-A and SeraMag-B beads (10 µl per sample of each type; Cytiva) in a ratio of 1:1, washing them three times with ddH2O and resuspending them in 10 µl ddH2O per sample. A total of 100 µg per sample was mixed with 10 µl beads suspension. Acetonitrile (ACN) was added to a final concentration of 70% and incubated at room temperature, 18 min, 800 rpm. After discarding the supernatant, beads were washed twice using 200 µl ethanol, 30 sec incubation, and once using 180 µl ACN, 15 sec incubation. The supernatant was discarded and the beads air-dried for 30 sec, before 50 µl of 16 mM (4-(2-hydroxyethyl)-1-piperazineethanesulfonic acid (HEPES) pH 8.5 was added. Proteins were reduced with 10 mM dithiothreitol (DTT) for 45 min at 37°C and 800 rpm, and alkylated with 55 mM chloroacetamide (CAA) at RT in the dark for 30 min. Proteins were digested in a 1:100 trypsin/substrate weight ratio overnight at 37°C and 800 rpm. On the next day, the samples were sonicated to resuspend the beads and another round of digestion (1:100 trypsin/substrate weight ratio) was performed for 6 h at 37°C and 800 rpm. Samples were sonicated three times for 30 sec and supernatant was collected. Beads were washed once with 20 µl ddH2O, sonicated three times for 30 sec, and supernatants were combined with previous supernatants. Samples were frozen at -80°C and dried in a SpeedVac. Afterwards, labeling of the desalted peptides was performed with tandem mass tags 11 (TMT11)-plex (Thermo Fisher Scientific) as previously described (Zecha et al., 2019).

One TMT channel was used for each treatment time and peptides were pooled after labeling (126 = 0 h, 127N = 1 h, 127C = 2 h, 128N = 4 h, 128C = 6 h, 129N = 8 h, 129C = 10 h, 130N = 12 h, 130C = 16 h, 131N = 20 h, 131C = 24 h). A Dionex Ultra 3000 HPLC system operating a Waters XBridge BEH130 C18 3.5 µm 2.1 × 250 mm column was used to fractionate 500 µg of pooled peptides at a flow rate of 200 µl/min. Buffer A was 25 mM ammonium bicarbonate (pH = 8.0), buffer B was 100% ultrapure water (ELGA), buffer C was 100% ACN. The proportion of buffer A was kept at 10% during

separation. 500 µg pooled peptides were separated by a linear gradient from 9-42% C in 86 min, followed by a linear gradient from 42-80% C in 12 min. Fractions were collected every minute into a 96-well plate and one third of each fraction was subsequently pooled into 46 fractions by adding fraction 49 to fraction 1, fraction 50 to fraction 2, and so forth. Peptide fractions were frozen at −80°C freezer, dried in a SpeedVac without prior desalting, and stored at -20°C until LC-MSn analysis.

9.1.7.2 LC-MS^3 analysis of the time-resolved MDEG-541 treatment

For microflow LC-MSMS, a Dionex UltiMate 3000 RSLCnano System was coupled online to an Orbitrap Fusion Lumos mass spectrometer (Thermo Fisher Scientific) as described in detail in a previous publication (Bian et al., 2020). Peptides were dissolved in solvent A (0.1% FA in 3% DMSO, Hahne et al., 2013) and one third (app. 3 µg) was directly injected onto the microflow LC system.

Online chromatography was performed using a commercially available Thermo Fisher Scientific Acclaim PepMap 100 C18 LC column (2 µm particle size, 1 mm ID × 150 mm; catalog number 164711). Column temperature was maintained at 55°C using the integrated column oven. Peptides were delivered at a flow rate of 50 µl/min and separated using a 27 min linear gradient from 6% to 33% LC solvent B (0.1% FA, 3% DMSO in ACN) in LC solvent A. The Orbitrap Fusion Lumos was operated as follows: positive polarity; spray voltage 3.5 kV, capillary temperature 325°C; vaporizer temperature 125°C. The flow rates of sheath gas, aux gas and sweep gas were set to 32, 5, and 0, respectively. For TMT labeled peptides, the cycle time was set to 1.2 s. Full MS resolution was set to 60,000 at m/z 200 and the mass range was set to 360–1560. Full MS AGC target value was 4E5 with a maximum IT of 50 ms and RF lens value was set to 50. The MIPS properties were set to peptide. Default charges were set to state 2–6. The dynamic exclusion duration was set to 50 s, exclude after one time. For readout of MS2 spectra, the ion trap was used applying the rapid scan function. The isolation width was set to 0.6 m/z, the first mass was fixed at 100 m/z, activation type was HCD, HCD collision energy [%] was 32. The AGC target value was set to 1.2E4 at a maximum IT of 40 ms. The precursor selection range was set to 400–2000, exclusion mass widths were set to 20 m/z for low and 5 m/z for high. For MS3 spectra readout, the orbitrap was used spectra at 50,000 resolution and over a scan range of 100–1000. Synchronous precursor selection (SPS) was enabled, the number of SPS precursors was set to 8. MS isolation window was 1.2 m/z, activation type was

HCD, and HCD collision energy was 55%. The AGC target was 1E5 with a maximum IT of 86 ms.

9.1.7.3 Peptide and protein identification and quantification

Protein and peptide identification and quantification was performed using MaxQuant (Cox et al., 2008, version 1.6.2.10, RRID:SCR_014485) by searching the tandem MS data against all canonical protein sequences as annotated in the UniProt reference database (human proteins only, 88,391 entries, downloaded 22.07.2013, internally annotated with PFAM domains, two MYC isoforms were separately listed) using the search engine Andromeda (Cox et al., 2011). The results have been deposited to the ProteomeXchange Consortium (http://www.proteomexchange.org/) (RRID: SCR_004055) via the PRIDE partner repository (RRID:SCR_003411) with the data set identifier: PXD018674. Carbamidomethylated cysteine was set as fixed modification and oxidation of methionine and N-terminal protein acetylation as variable modification. Trypsin/P was specified as the proteolytic enzyme and up to two missed cleavage sites were allowed. The minimum peptide length was set to seven and all data was adjusted to 1% peptide-spectrum match (PSM) and 1% protein false discovery rate (FDR). MS3-based TMT quantification was enabled, taking TMT correction factors as supplied by the manufacturer into account.

9.1.7.4 Proteome data analysis

Data analysis was performed using the Perseus software suite (Tyanova et al., 2016, version 1.5.8.5) and Microsoft Excel with identified and quantified protein groups. Protein groups were filtered for contaminants and reverse hits, and total sum normalization and log2 transformation were performed. The 24 h timepoint showed high differences to the other timepoints and was not considered for the analysis of regulated proteins. Data was filtered for at least 1 valid value and the log2 ratio of 0 h versus 20 h treatment was calculated. A cutoff of log2 ratio of 1 (corresponding to a factor of 2) was used to identify proteins showing a time-dependent effect (downregulation log2 ratio < -1, upregulation log2 ratio >1). Resulting proteins were Z-scored and a hierarchical clustering (pearson correlation, number of clusters: 300, maximal number of iterations: 10, number of restarts: 1) was performed. Of the five identified clusters, two clusters showed upregulation with time, one cluster showed downregulation with time and two clusters showed mixed response. Data quality and temporal effects of individual proteins were analyzed on PSM level.

9.1.7.5 Proteome GSEA data processing

The proteome analysis of MDEG-541 treated PSN1 cells was used to calculate the log2FC of proteins at the indicate time points compared to untreated controls (timepoint 0). The log2FC was used as a rank to run a pre-ranked GSEA analysis via the GSEA App 4.0.3. Enrichment scores for the genesets HALLMARK and KEGG were downloaded from the MSigDB homepage for the timepoints 1, 2, 4, 6, 8, 10, 12, 16, and 20 h after 10 µM MDEG-541 treatment (Lukas Krauß, M. Sc.). Normalized enrichment scores were demonstrated for all timepoints. In addition, enrichments Scores of the distinct gensets were shown in detail after 20 h treatment with MDEG-541.

9.1.8 Western blot

Western blot is an established method to detect proteins with specific antibodies. In a first step, proteins from a cell lysate are separated by size with gel-electrophoresis. An SDS-gel with a distinct pore size is generating protein bands, which are then transferred onto a nitrocellulose membrane.

9.1.8.1 Protein extraction and BCA Assay

10^6 cells were seeded per 10 cm cell culture dish and treated the following day with MDEG-541 or respective controls. Following the incubation period, the protein was harvested on ice. In detail, the 10 cm cell culture dishes were washed with cold PBS twice and the supernatant was completely removed, before 80 µL of RIPA Buffer supplemented with 1% (v/v) protease inhibitor and phosphatase inhibitor were pipetted onto the cells. The harvested cells were incubated for 30 min on ice to release the proteins and disrupt protein interactions. The lysate was centrifuged for ten min at 4°C and 16,000 rpm to remove cell debris. 1:5 of 5x Laemmli Buffer was added to the supernatant to charge the proteins negatively. The samples were incubated for five min at 95°C while shaking and immediately cooled down on ice to denaturate proteins. A Bradford Assay was performed in technical triplicates using 300 µL 1x Bradford Reagent and 1 µL protein sample added to each well of a 96-well plate. A standard curve with known concentrations of BSA (8 µg/ml, 4 µg/ml, 2 µg/ml, 1 µg/ml, 0.5 µg/µL and 0 µg/µl) was created. The 96-plate was shaken for 5 min at RT and absorption was measured at 595 nm with a luminometer. Finally, the sample protein concentration was estimated based on the standard curve and used to load the same amount of protein on the SDS-gel.

9.1.8.2 SDS-PAGE and western blot

To separate the proteins depending on their size, an SDS-gel with a distinct polyacrylamide concentration was prepared. To detect proteins of interest with high molecular weight an SDS-gel with large pores was prepared by using 7.5% polyacrylamide. Smaller proteins were best detected with a smaller pored SDS-gel with 15% polyacrylamide. All SDS-gels were prepared with a thickness of 1.5 mm. Each gel was composed of a resolving gel (7.5%, 10% or 15%) and stacking gel (4.4%). The SDS gel was submerged in running buffer and 1.2 µL of Page RulerTM Prestained Protein Ladder as well as 40 µL (10-pocket combs)/25 µL (15-pocket comb) of protein sample with 1x Laemmli Buffer were gently added to the wells. Proteins were separated for 3 h at 80 V. Smaller proteins migrate more rapidly to the positively charged anode than larger proteins due to the pore size of the polyacrylamide gel. Proteins were transferred from the gel onto the membrane following the wet blot method. Therefore, 1 L of cold Transfer Buffer was filled into a blotting chamber with a cooling unit. The gel sandwich and fiber pads were briefly equilibrated in cold 1x Transfer Buffer and layered in the following order: one fiber pad, two whatman papers, the nitrocellulose membrane, the gel, two whatman papers and a fiber pad. The sandwich was then placed into the electrode module with the membrane pointed to the anode and the blot was run at 0.4 A for two hours at 4°C.

9.1.8.3 Blocking and incubation with antibodies (ABs)

The blotted membrane was blocked for 30 min in 5% (w/v) milk in PBS. Membranes were incubated with primary AB at 4°C o/n under constant agitation. After washing with PBS-T (3x for five min), the membrane was incubated for one h with a fluorescence secondary AB raised against the species of the primary AB at RT under constant agitation. Respective AB concentrations are described in Table 7. After washing with PBS-T (3x for five min), antigen bands were visualized with the Odyssey Fc Imaging System.

The protein bands were quantified using Image J software and relative protein levels were calculated as a percentage of the loading control. A minimum of three biological replicates were used for the statistical analysis.

9.1.9 Protein Experiments

For dose-responses PSN1 and HCT116 cells were then treated with MDEG-541 for 24 h and control compounds 10058-F4 and Thalidomide at different concentrations

(5 µM, 10 µM or, 20 µM). For time-kinetics the cells were treated in biological triplicates with 10 µM MDEG-541 for 1, 2, 4, 6, 8, 10, 12, 24, 48 and 72 h.
For rescue experiments the cells were pre-treated with either 100 nM Bortezomib, 5 µM MG-132 proteasome inhibitor or 200 nM of the ubiquitin inhibitor TAK-243. After 4 h of inhibition, 10 µM MDEG-541 were added for another 20 h as single agent or to the pre-treated cells in a combination treatment. DMSO vehicle control was also performed.

9.1.10 Statistical analysis

Data was analyzed using Microsoft Excel. Graphs were generated and statistical analysis was performed. Data was analyzed with unpaired two-sided student's t-test, one-way ANOVA, two-way ANOVA, Spearman correlation using the Graph Pad Prism 5 software. Data is shown as mean values ± SD. A p-value < 0.05 was considered statistically significant. Significant data are explained in detail in the according figure description if relevant for the meaning and purpose of the experiment.

9.1.11 Generation of CRBN deficient cell lines

To test the dependency of MDEG-541 on CRBN, genetically CRBN deficient cell clones (PSN1 and HCT cells) were generated using the CRISPR/Cas system (Ishino et al., 1987). The technology is based on a specific sgRNA (single guide ribonucleic acid) guiding the molecular scissor protein Cas9 to a distinct target region in the genome of CRBN. Specifically, Cas9 cuts the DNA double strand, which in turn starts the cell's own DNA repair machinery. By non-homologous end-joining, an altered DNA sequence can be inserted into the original DNA double strand, which can lead to either insertions or deletions (indels), resulting in a disruption of the CRBN genome.

9.1.12 Plasmid cloning

Two favorable sgRNAs (sgRNA 1 or sgRNA 2) were designed with the Zhang Lab tool (https://zlab.bio/guide-design-resources), targeting the CRBN gene and cloned into a vector (Figure 6).

Figure 6: Annotation of sgRNA 1 and sgRNA 2 into the CRBN genome
Upper panel: Annotation of sgRNA 1 into the beginning of Exon 1 in the CRBN genome. Lower panel: Annotation of sgRNA 2 into the middle region of Exon 1 in the CRBN genome.

The human CRBN gene consists of 12 exons. sgRNA 1 was located at the beginning of exon 1, while sgRNA 2 was located in the middle of exon 1. The sgRNAs was annealed by mixing 1 µL of the forward/reverse oligo (100 µM), 1µL T4 DNA Ligase Buffer and 7µL H_2O.

The mixture was incubated at 95°C for five min and then slowly cooled down at RT for 30 min before 490 µL H_2O were added (1:50 dilution). Each sgRNAs was cloned into a lentiCRISPR v2 puro plasmid by Golden Gate Assembly. In brief, 1 µL lentiCRISPR v2 puro plasmid (90 ng/µL), 1 µL annealed and diluted oligos, 2 µL T4 DNA Ligase Buffer, 1 µL T4 DNA Ligase, 1 µL BsmBI and 14 µL H_2O were combined. The reaction was initiated by warming the PCR stripes at 37°C for five min to activate the restriction enzymes and then at 16°C for ten min to activate the ligase. This was repeated for ten cycles, followed by the inactivation of the enzymes for 5 min at 55°C, and the inactivation of the ligase for 5 min at 80°C. The reaction was terminated at 10°C. The plasmids were sequenced with Eurofins and published on Addgene (166240, 166241).

Table 13: Sequence of sgRNA 1 and sgRNA 2
Two single guide RNAs are shown with their respective forward/reverse oligo used for cloning into a lentiCRISPR v2 puro plasmid.

	Guide	forward oligo	reverse oligo
sgRNA 1	GGCCGGCGAAGGAGATCAGC	CACCGGCCGGCGAAGGAGATCAGC	AAACGCTGATCTCCTTCGCCGGCC
sgRNA 2	GCAGGACGCTGCGCACAACA	CACCGCAGGACGCTGCGCACAACA	AAACTGTTGTGCGCAGCGTCCTGC

9.1.12.1 Bacteria transformation

2 µL of the product containing the successfully cloned sgRNAs were transformed into bacteria adding 20 µL 5x KCM Buffer and 75 µL H2O. 100 µL of Stbl3 E.coli bacteria were added and incubated for 20 min on ice. After incubation of an additional ten min at RT, 1 mL LB medium was added. The sample was shaken at 37°C for one h and the mix was centrifuged for two min at 370 rcf. The supernatant was removed and 200 µL of LB medium was added and plated on LB agar plates. Bacteria that were successfully transformed with sgRNA contained an ampicillin resistance and continued to grow on the LB agar plates supplemented with ampicillin (100 µg/µL). The plates were incubated at 30°C o/n and a clone was randomly picked the next day and incubated in 5 mL LB medium. The bacteria were grown at 30°C o/n in LB medium containing ampicillin (100 µg/µL) at 200 rpm before the plasmids were isolated from the bacteria the following day according to the NucleoSpin Kit from Macherey-Nagel. Purified plasmids were sequenced to test for insertion of the desirable sgRNA. Two sgRNAs targeting two regions in exon 1 of the CRBN gene were successfully cloned generating two separate plasmids.

9.1.12.2 Lentivirus production and transfection

$2x10^6$ HEK293 cells were seeded in 10 cm cell culture dishes in DMEM supplemented with 10% (v/v) FBS. On the second day, a master mix with 1.1 µg/µl psPAX2, 0.46 µg/µl pMD2.G, 2 µg of the lentiCRISPR v2 plasmid with sgRNA 1 or 2, respectively, was prepared with 10 µL H_2O. 18 µL Lipofectamine were prepared in 270 µL Opti-MEM and incubated at RT for five min before the master mix was added and incubated an additional 20 to 30 min at RT. The solution was added dropwise on the HEK cells and incubated at 37°C o/n, before the medium of the transfected HEK cells was changed to 4 mL DMEM with 30% (v/v) FBS. The following day, the viral virus containing supernatant was taken removed and stored at 4°C. Another 4 mL of DMEM containing 30% (v/v) FBS was added to the HEKs in the 10 cm culture dish. The following day, the supernatant was collected similar to the previous day and centrifuged at 500 g for five min to pellet the HEK cells. The supernatant was filtered and stored at -80°C.

The cell lines PSN1 and HCT116 were transduced with the lentivirus. 50,000 cells were counted and seeded in a well of a 6-well plate. The following day, the supernatant was removed and replaced with 1 mL of the lentivirus containing supernatant. 5 µg/mL of

polybrene were added. After 6 h of incubation, 1 mL of medium was added to the cells. The following day, the medium was removed and replaced with fresh medium. Transduced cells were selected with puromycin by adding 5µg/mL in fresh medium on the cells and a control cell was treated in parallel. After two rounds of selection with fresh 5µg/mL puromycin supplied medium, the untransfected control cells were dead and the selection was finished. Selected cells were seeded at a dilution of 0.5 cells/well in a 96-well plate to select single clones. Single clones were expanded in 48-, 24- and 6-well plates, successively, frozen and tested with western blot for CRBN knockout (KO). In brief, cells were cultured in a 6-well plate and protein was prepared according the western blot protocol from a 6-well plate. The CRBN protein level was determined with a primary rabbit AB, a kind gift from AG Bassermann (TUM). Single cell clones without CRBN protein expression were picked for sanger sequencing. Clone 6 of sgRNA 1 and clone 2 of sgRNA 2 were picked from the transduced cell line PSN1 for further experiments. Clone 4 from sgRNA 2 was picked from the transduced cell line HCT116 for further experiments.

10. RESULTS

10.1 Determining a potent MYC PROTAC

This work describes the design and validation of a novel CRBN-dependent MYC DEGrader (MDEG) targeting the proliferative MYC network. Therefore, 47 different chemical variants of the degrader were designed and modified in the laboratory of the cooperation partner Prof. Dr. S. Mahboobi by linking 10058-F4 to Thalidomide. A linker of 8 C atoms was found to be favorable to ubiquitinate and proteasomal degrade MYC and was used as connection between Thalidomide and 10058-F4.

MDEG-541 was determined most potent via an MTT assay in the PDAC cell lines PSN1, Panc-1, MIA PaCa-2, BxPC-3 and ImimPC1 (Figure 7).

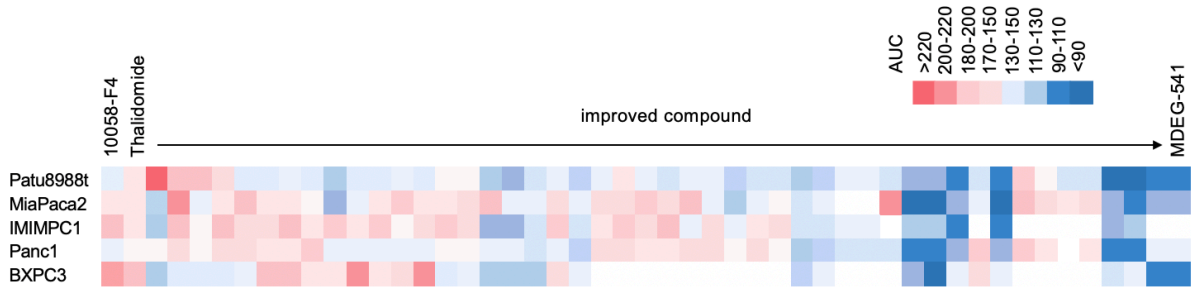

Figure 7: Heatmap of the Area under the curve (AUC) of all tested compounds
Area under the curve (AUC) obtained from MTT assays in the PDAC cell lines PSN1, Panc-1, MIA PaCa-2, BxPC-3 and ImimPC1, testing 48 potential MYC degraders and the control 10058-F4 and Thalidomide. The most potent compound to reduce cell viability and MYC protein level - MDEG-541 - is indicated.

In the following, the effect of MDEG-541 was examined in detail in the MYC amplified cell lines PSN1 and HCT116 (Figure 8).

10.2 Structure of the MYC degrader MDEG-541 and degradation of MYC protein in a dose-dependent manner

Treatment with MDEG-541 significantly reduced MYC protein level in a dose-dependent manner in PSN1 and HCT116 cells after 24 h (Figure 8 B, C). The treatment controls 10058-F4 and Thalidomide had no effect on MYC protein expression compared to treatment with MDEG-541 (Figure 8 B, C).

The treatment of the cell line PSN1 with 5 µM MDEG-541 reduced MYC protein level by 51.24%. 10 µM MDEG-541 treatment reduced MYC protein level by 36.45% and treatment with 20 µM MDEG-541 downregulated MYC protein by 74.25% compared to the DMSO vehicle control (set as 100%, Figure 8 B). The treatment of HCT116 cells with 10 µM and 20 µM MDEG-541 decreased MYC protein levels (Figure 8 C).

Treatment with 10 µM MDEG-541 decreased MYC protein by 63.82% and 20 µM MDEG-541 reduced MYC protein levels to under 1% compared to the DMSO control (set as 100%).

Together, this data indicates that 24 h after treatment with 5 µM, 10 µM and 20 µM MDEG-541, MYC protein expression was decreased in a dose-dependent manner.

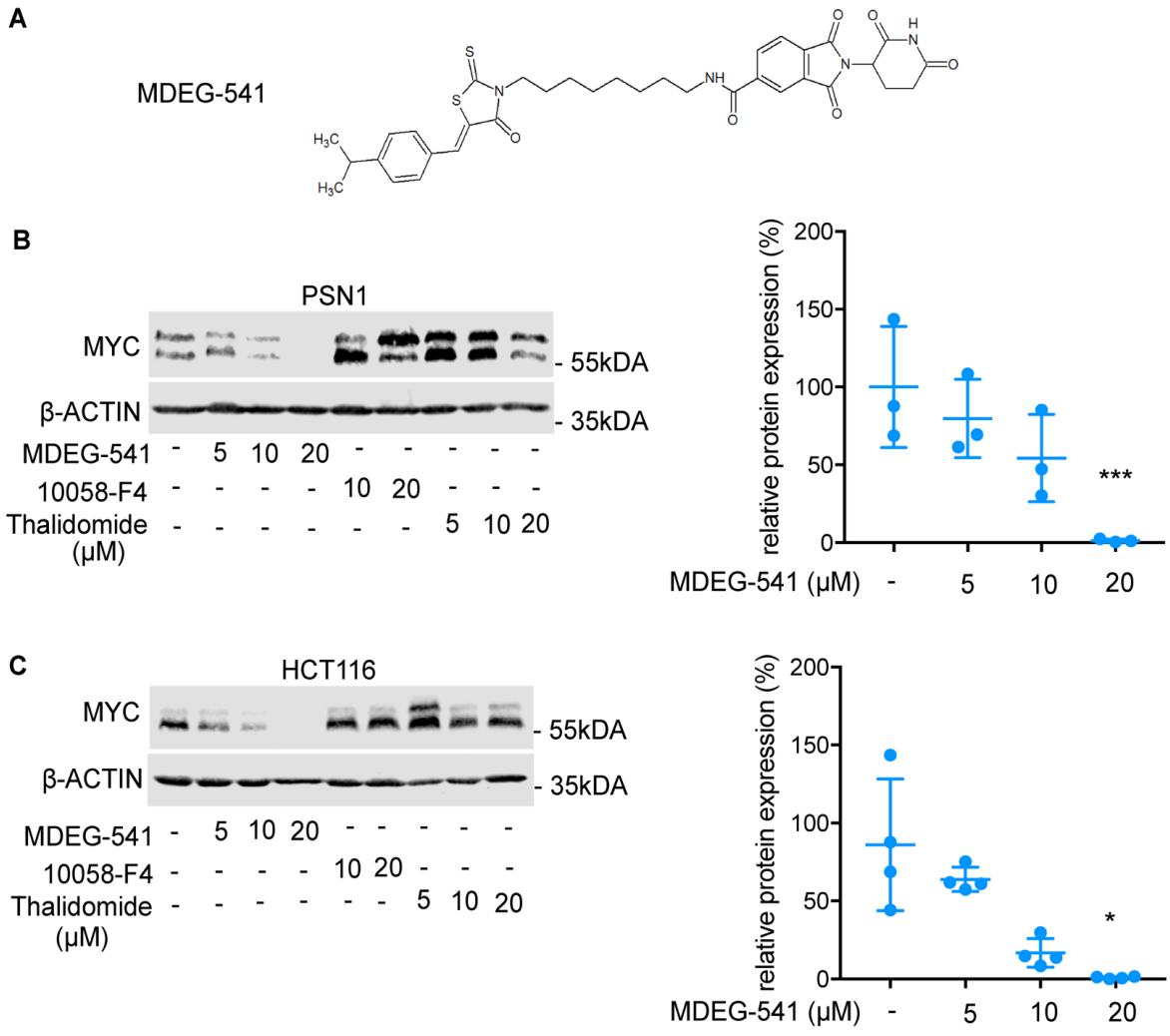

Figure 8: Structure of MDEG-541 and degradation of MYC protein in a dose-dependent manner

(A) Chemical structure of MDEG-541. (B) Western blot of MYC protein and quantification after treatment with MDEG-541, vehicle control (DMSO), treatment control 10058-F4 and Thalidomide for 24 h in the cell line PSN1 and (C) HCT116. Shown is one representative western blot of three biological replicates. Cells were treated with MDEG-541 (5 µM, 10 µM or, 20 µM) or treatment control Thalidomide (5 µM, 10 µM or, 20 µM) and treatment control 10058-F4 (10 µM and 20 µM). β-ACTIN/α-TUBULIN: loading control. Data was normalized to DMSO vehicle control. Statistics: Two-way ANOVA and Bonferroni´s multiple comparisons test: *p<0.01, **p<0.001, ***p<0.0001.

10.3 Degradation of MYC, GSPT1 and GSPT2 protein in a time-dependent manner and global proteasome-wide regulation after of MDEG-541 treatment

To determine the effect of MDEG-541 treatment on the proteome, Tandem Mass Tag (TMT) mass spectrometry was performed (in collaboration with Dr. Stephanie Heinzlmeir in the lab of Prof. Dr. Bernhard Küster (TUM), Chair of Proteomics and Bioanalytics). The proteome analysis of PSN1 cells treated with 10 µM MDEG-541 was used to calculate the log fold change (FC) of proteins at the indicated time points compared to untreated control (Figure 9 A and B). GSPT2 is not expressed in cell line HCT116.

In addition to MYC, a further 110 proteins were detected in the global proteomics analysis in a downregulated cluster (Supplementary Table 1, Figure 9 A) and 46 proteins were found in an upregulated cluster (Supplementary Table 2, Figure 9 B) after 20 h MDEG-541 treatment. This data indicates that other proteins in addition to the targeted MYC protein were up- and downregulated after MDEG-541 treatment, suggesting possible off-targets of MDEG-541. Specifically, seven proteins including GSPT1 (red), GSPT2 (orange) were strongly reduced in a cluster after 20 h of MDEG-541 treatment in cell line PSN1 prior to MYC downregulation (Figure 9 A).

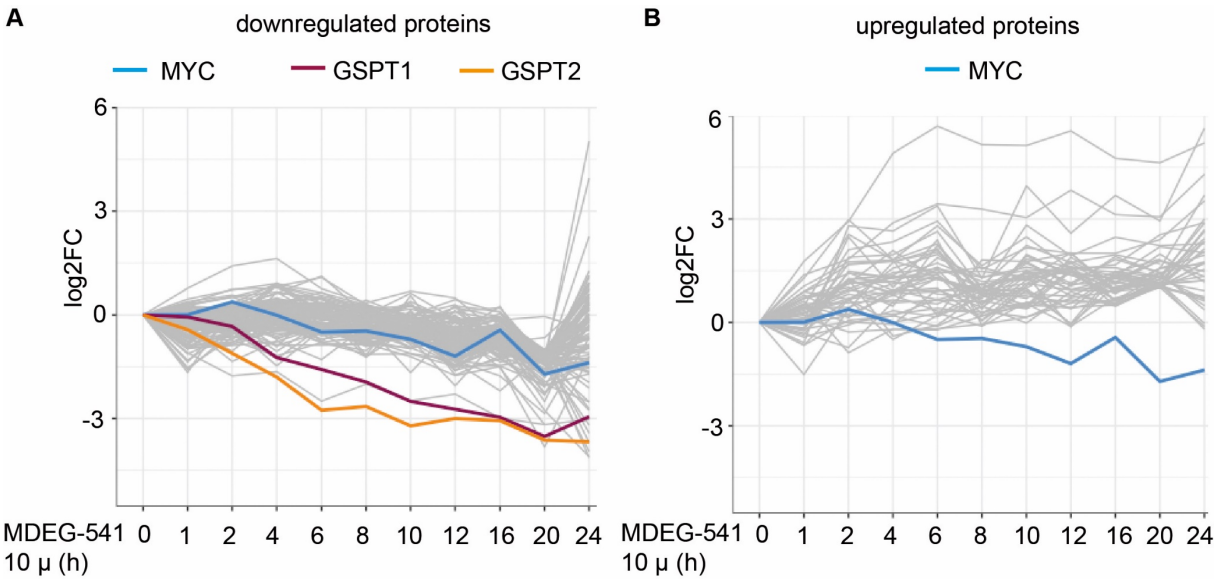

Figure 9: Degradation of MYC, GSPT1, GSPT2 and PLK1 protein in a time-dependent manner and global proteasome-wide regulation after of MDEG-541 treatment
(A) Mass spectrometry measurement of protein expression in response to MDEG-541 treatment (10 µM) over the indicated time points and untreated control. Shown is the expression change over all time points of 110 proteins (grey), including MYC protein (blue), GSPT1 (red) and GSPT2 (orange) downregulated and (B) 46 upregulated proteins (grey) as well as MYC protein (blue) with a significant FC at 20 hours after 10 µM MDEG-541 treatment.

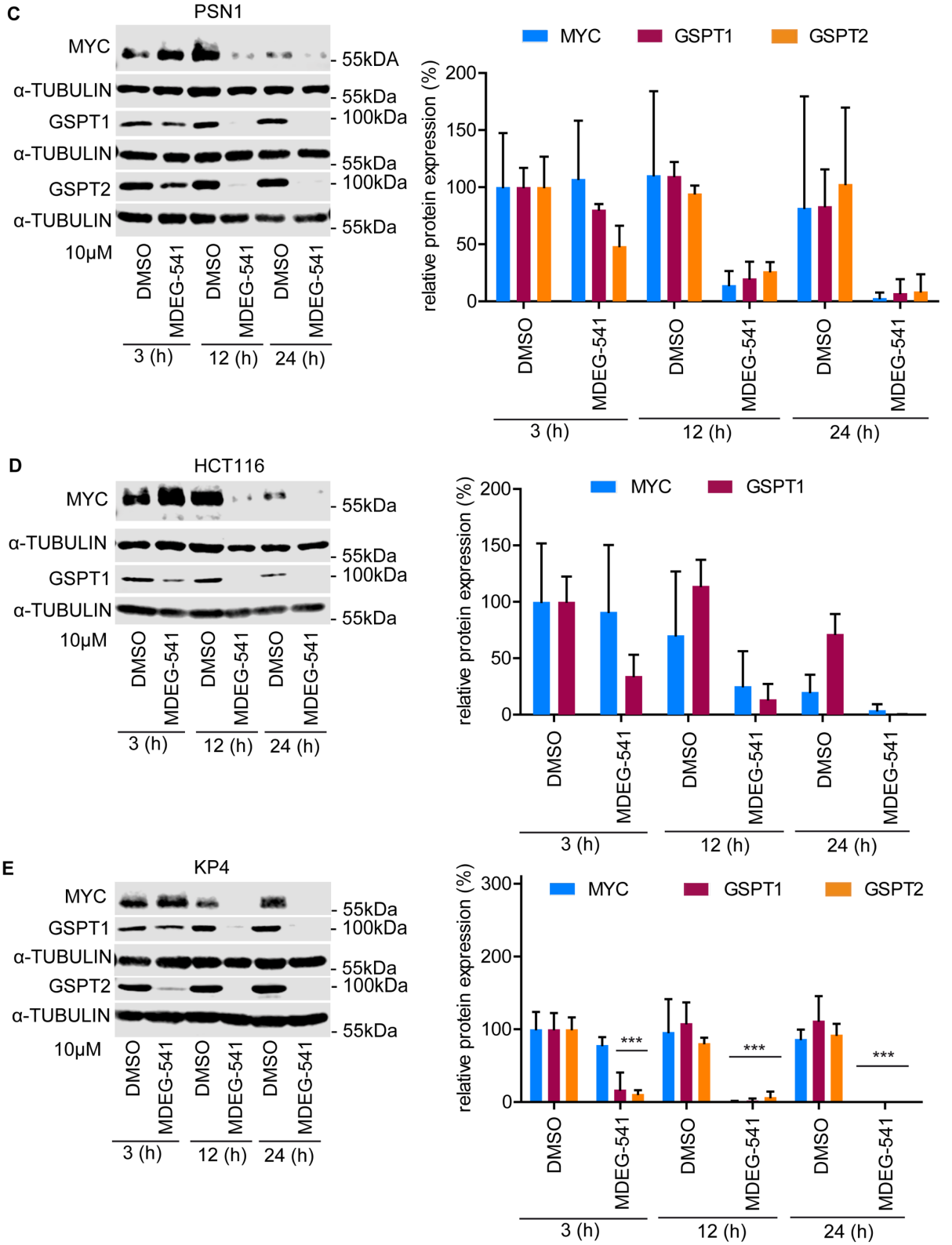

Figure 9: Degradation of MYC, GSPT1, GSPT2 and PLK1 protein in a time-dependent manner and global proteasome-wide regulation after of MDEG-541 treatment

(C) Western blot of MYC, GSPT1 and GSPT2 and quantification after 10 μM MDEG-541 treatment for 3 h, 12 h and 24 h in the cell line PSN1, (D) HCT116 and (E) KP4. One representative western blot of three biological replicates. Treatment with DMSO vehicle control for 3 h, 12 h and 24 h. α-TUBULIN: loading control. Data was normalized to DMSO vehicle control. Statistics: Two-way ANOVA and Bonferroni´s multiple comparisons test: *p<0.01, **p<0.001, ***p<0.0001.

This downregulation of GSPT1 and GSPT2 was confirmed on western blot in PSN1, HCT116 and KP4 cells after MDEG-541 treatment (Figure 8 C-E). Expression of GSPT2 was not detected in the cell line HCT116.

These results indicate downregulation of GSPT1 and GSPT2 proteins prior to MYC protein degradation in the cell line PSN1 after MDEG-541 treatment. To further examine the interaction of MDEG-541 with off-targets and their effect on MYC protein expression, the cell lines PSN1, HCT116 and KP4 were treated with inhibitors and degraders of GSPT1.

10.4 Dose-dependent downregulation of MYC after treatment with CRBN E3-ligase modulator (CELMoD) CC-885

The cell lines PSN1 and HCT116 were treated with the allosteric GSPT1 inhibitor CC-885 for 24h and the protein expression of MYC, GSPT1 and GSPT2 was observed with western blot (Figure 10 C and D). The protein expression of MYC was decreased by 77.77 % in PSN1 in a dose-dependent manner after 0.25 µM CC-885 treatment, by 64.71 % after 0.5 µM CC-885 treatment and by 96.56 % after 1 µM CC-885 treatment compared to DMSO vehicle control (set as 100%, Figure 10 C). In HCT116 cells, MYC protein expression was downregulated by 70.12% after 0.25 µM CC-885 treatment, by 87.37% after 0.5 µM CC-885 and by 100% after 1 µM CC-885 compared to DMSO vehicle control (set as 100%, Figure 10 D). The protein expression of GSPT1 and GSPT2 was decreased by 100% after 0.25 µM, 0.5 µM and 1 µM treatment with CC-885 compared to DMSO vehicle control (Figure 10 C and D). In addition, treatment with MDEG-541 for 24 h reduced GSPT1 and GSPT2 protein expression in PSN1 and HCT116 cells in a dose-dependent manner (Figure 10 A and B).

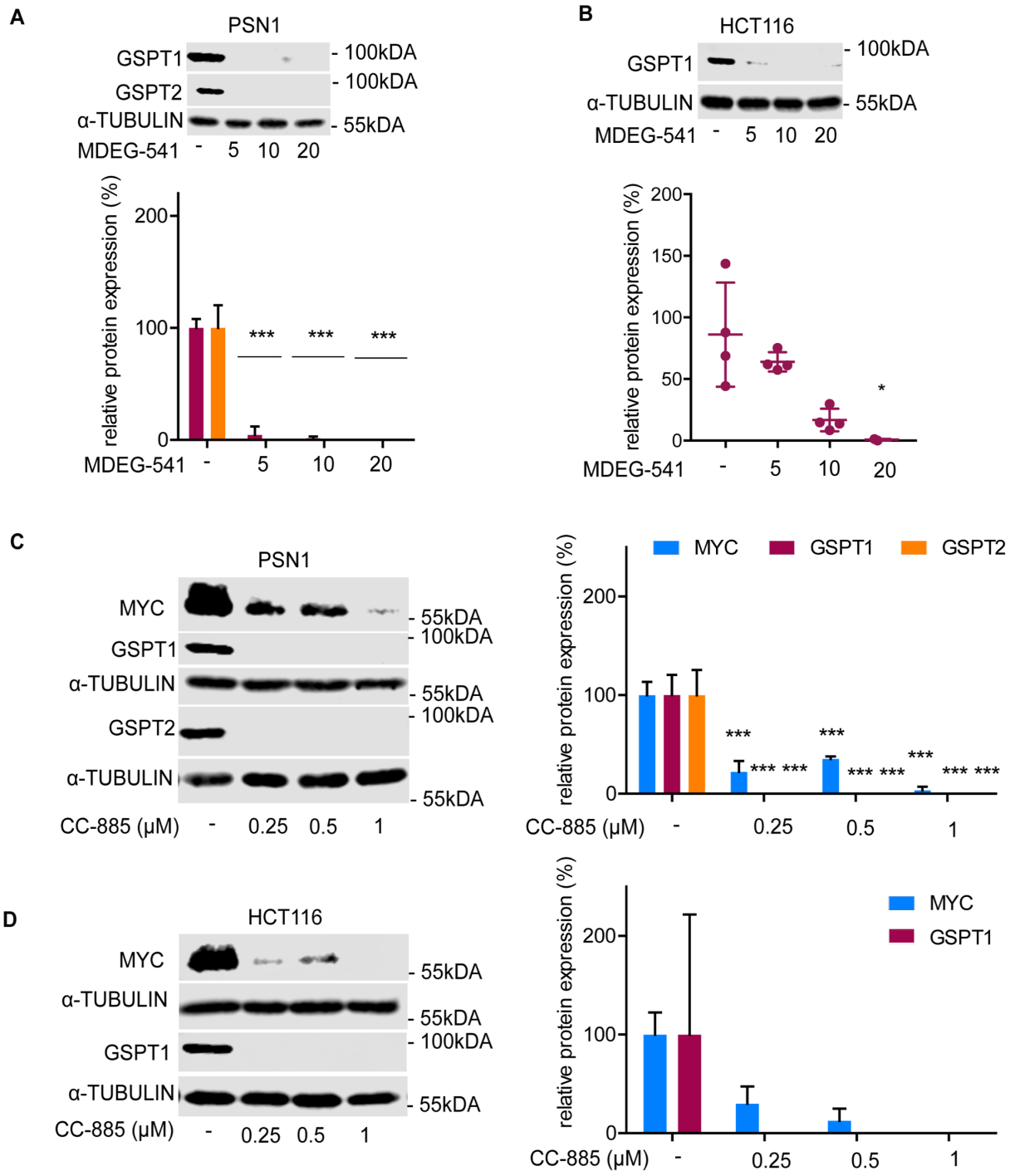

Figure 10: Dose-dependent downregulation of MYC, GSPT1 and GSPT2 after treatment with CC-885

(A) Western blot of MYC, GSPT1 and GSPT2 protein and quantification after treatment with 0.25 μM, 0.5 μM and 1 μM CC-885 and vehicle control (DMSO) for 24 h in the cell line PSN1. (B) Western blot of MYC and GSPT1 protein and quantification after treatment with 0.25 μM, 0.5 μM and 1 μM CC-885 and vehicle control (DMSO) for 24 h in the cell line HCT116. (C) Western blot of MYC protein and quantification after treatment with 5 μM, 10 μM and 20 μM CC-90009 and vehicle control (DMSO) for 24 h in the cell line PSN1 (left panel), HCT116 (middle panel) and KP4 (right panel). Shown is one representative western blot of three biological replicates. α-TUBULIN: loading control. Data was normalized to DMSO vehicle control. Statistics: Two-way ANOVA and Bonferroni´s multiple comparisons test: *p<0.01, **p<0.001, ***p<0.0001.

10.5 CRBN E3-ligase modulator (CELMoD) CC-90009 showed no effect on MYC protein expression

Treatment with CC-90009 downregulated GSPT1 and GSPT2 protein expression in a dose-dependent manner, but did not regulate MYC protein expression 24 h after treatment in PSN1, HCT116 or, KP4 cells (Figure 11).

These results indicate that specific targeting and downregulation of GSPT1 was not regulating MYC protein expression. However, targeting GSPT1 and GSPT2 via CRBN E3-ligase modulator (CELMoD) CC-885 was downregulating MYC protein expression in a dose-dependent manner.

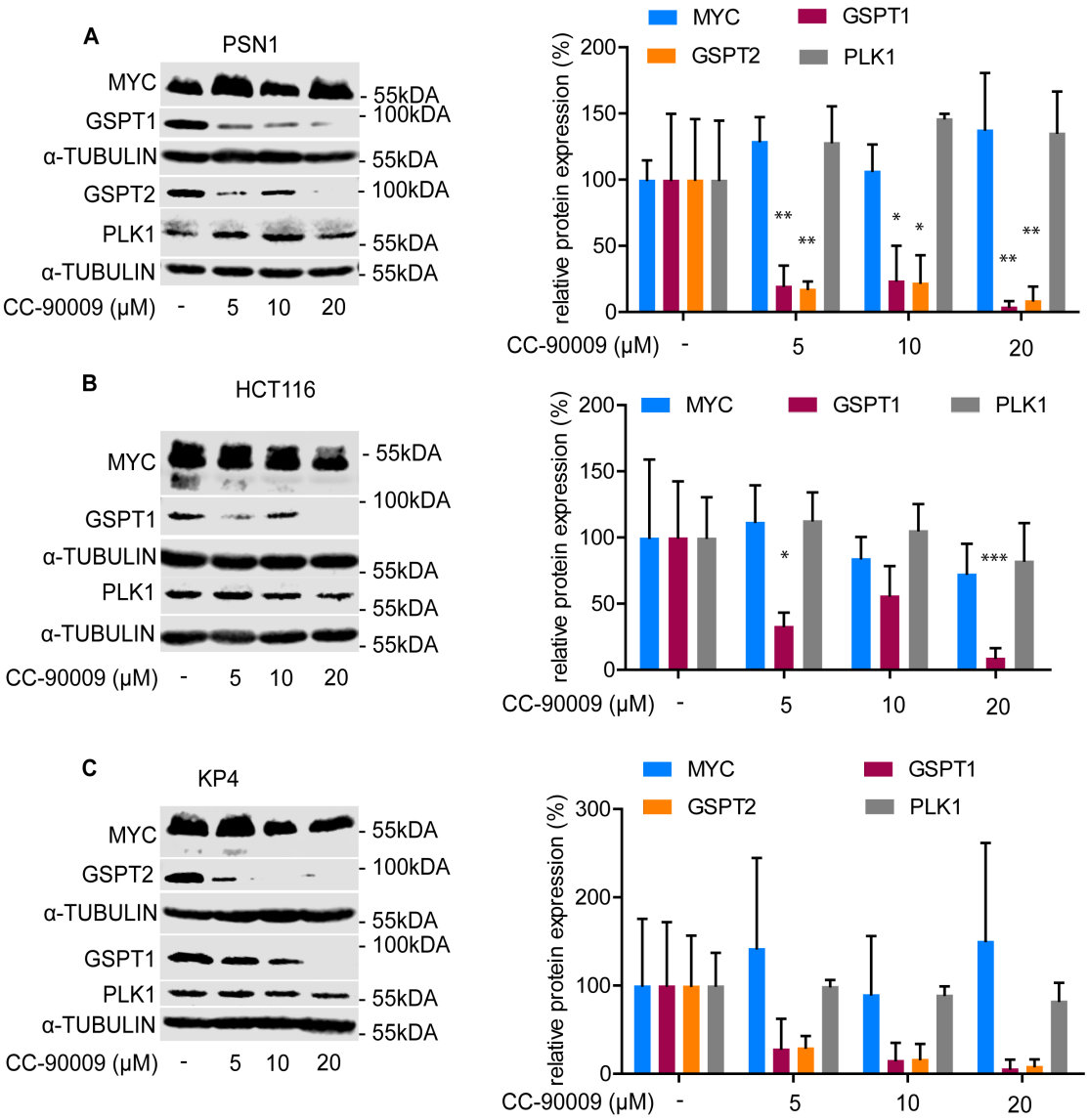

Figure 11: Dose-dependent downregulation of MYC after treatment with CC-90009
(A) Western blot of MYC, GSPT1, GSPT2 and PLK1 protein and quantification after treatment with 5 μM, 10 μM and 20 μM CC-90009 and vehicle control (DMSO) for 24 h in the cell line PSN1, (B) HCT116 and (C) KP4. Shown is one representative western blot of three biological replicates. α-TUBULIN: loading control. Data was normalized to DMSO vehicle control. Statistics: Two-way ANOVA and Bonferroni´s multiple comparisons test: *p<0.01, **p<0.001, ***p<0.0001.

10.6 Dose-dependent downregulation of PLK1 after treatment with MDEG-541

To validate if PLK1 might play a role in MYC protein expression after MDEG-541 treatment, the cell lines PSN1 and HCT116 were treated for 24 h with MDEG-541 in a dose-dependent manner and with 10 µM MDEG-541 in a time-dependent manner (Figure 12 A and B). In both cell lines, a dose-and time-dependent downregulation of PLK1 protein expression was observed after MDEG-541 treatment.

To validate if PLK1 might play a role in MYC protein expression the cell lines PSN1, HCT116 and KP4 were treated for 24 h with PLK1 inhibitor Volasertib in a dose-dependent manner (Figure 12 C). Treatment with 0.25 µM, 0.5µM and with 1µM Volasertib reduced MYC protein expression in a dose-dependent manner compared to DMSO vehicle control in all tested cell lines (set to 100%, Figure 12 C).

These results suggest that PLK1 is an additional off-target of MDEG-541 treatment. Further, MDEG-541-mediated inhibition of PLK1 might induce the downregulation of MYC protein expression.

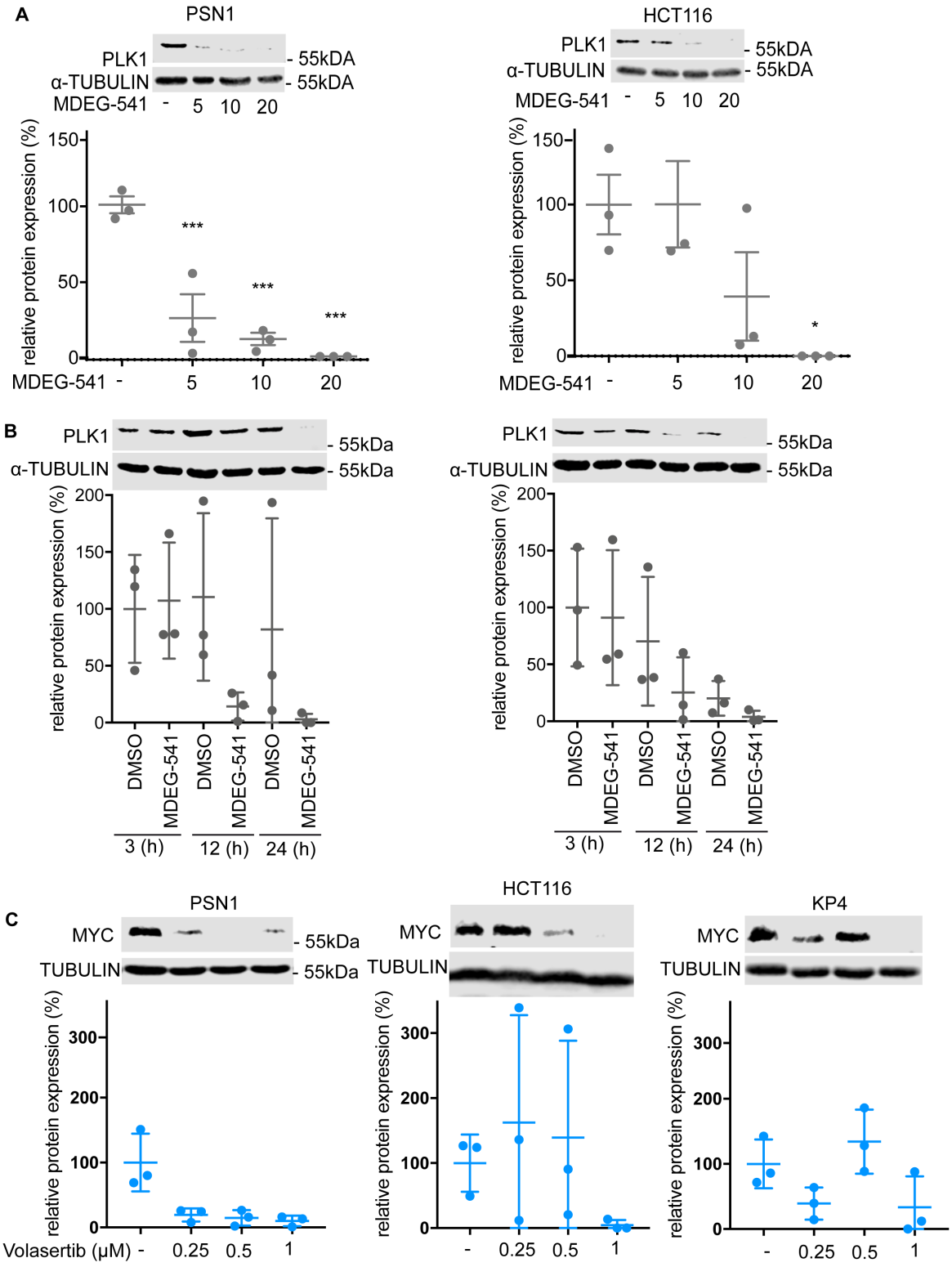

Figure 12: Dose-dependent downregulation of MYC after treatment with Volasertib
Western blot of PLK1 protein and quantification after treatment with (A) 5 μM, 10 μM and 20 μM MDEG-541 and vehicle control (DMSO) for 24 h in the cell line PSN1 (left panel) and HCT116 (right panel) and (B) with 10 μM, MDEG-541 and vehicle control (DMSO) for 3 h, 12 h and 24 h in the cell line PSN1 (left panel) and HCT116 (right panel). (C) Western blot of MYC protein and quantification after treatment with 0.25 μM, 0.5 μM and 1 μM Volasertib and vehicle control (DMSO) for 24 h in the cell line PSN1 (left panel), HCT116 (middle panel) and KP4 (right panel). Shown is one representative western blot of three biological replicates. α-TUBULIN: loading control. Data was normalized to DMSO vehicle control. Statistics: Two-way ANOVA and Bonferroni´s multiple comparisons test: *p<0.01, **p<0.001, ***p<0.0001.

10.7 Dose-dependent downregulation of GSPT2 after treatment with modified MDEG-541 substance 619

To determine if Thalidomide and the linker can cause the same effects as MDEG-541 or, if the 10058-F4 moiety also plays a role in the regulation of proteins 24 h after MDEG-541 treatment, the modified compound 619 (Figure 13 A) without a 10058-F4 moiety was tested on PSN1, HCT116 and KP4 cells. Neither MYC, nor GSPT1 or PLK1 protein expression was affected by the treatment of 619 in any of the tested cell lines (Figure 13 B-D). However, GSPT2 protein expression was downregulated in cell line PSN1 and KP4 in a dose-dependent manner. Specifically, in the cell line PSN1, GSPT2 protein was decreased by 62.72 % after 5 µM of 619 treatment, by 83.34 % after 10 µM and by 94.26 % after 20 µM of treatment compared to DMSO vehicle control (set to 100%, Figure 13 B). In the KP4 cells, GSPT2 protein was reduced by 53.95 % after 5 µM of 619 treatment, by 61.58 % after 10 µM and by 99.13 % after 20 µM of treatment compared to DMSO vehicle control (set to 100%, Figure 13 D).
Together, these results show that a modified MDEG-541, namely 619, was not downregulating MYC protein expression, but GSPT2 protein level.

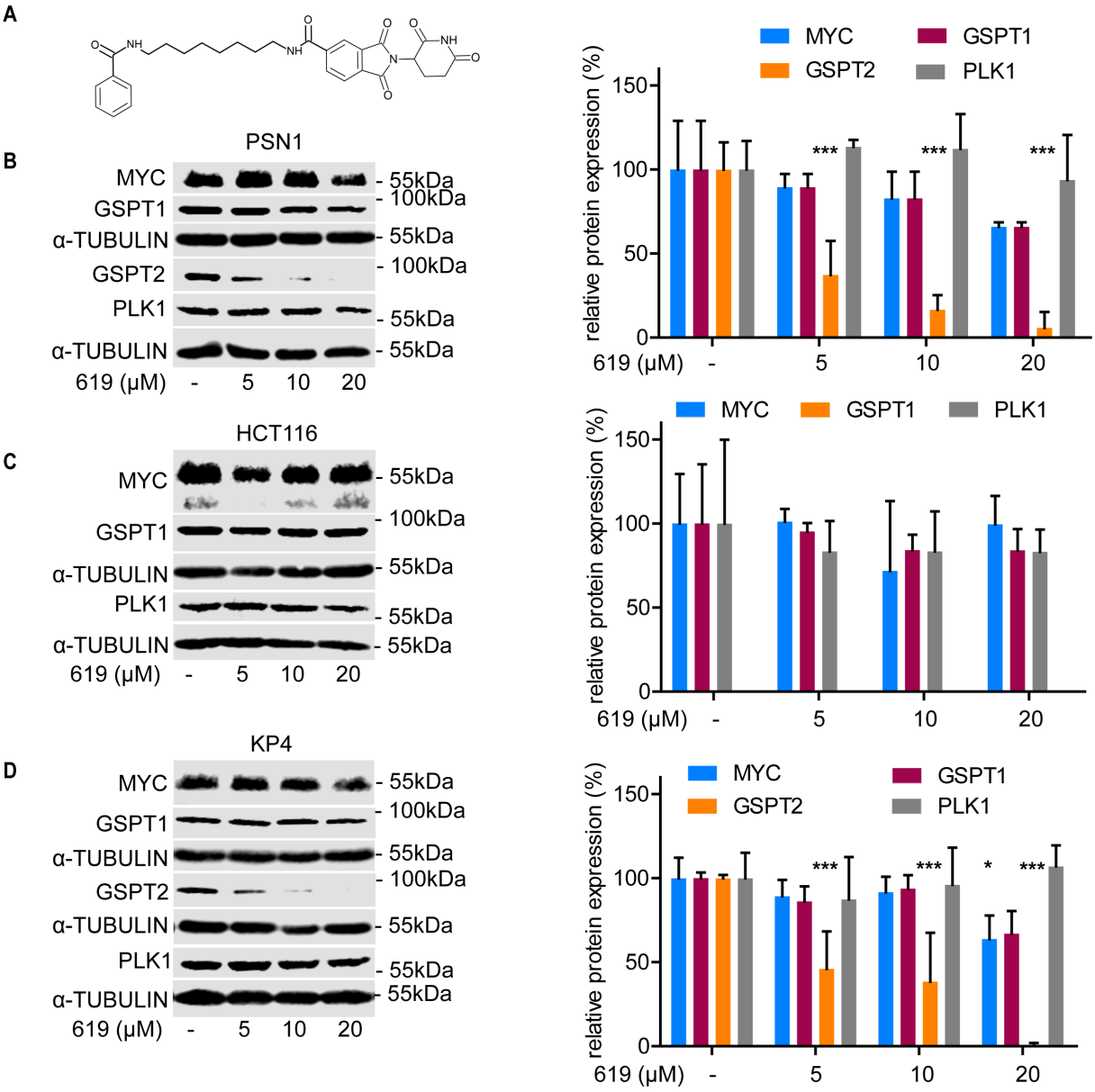

Figure 13: Dose-dependent downregulation of GSPT2 after treatment with modified MDEG-541 treatment control 619

(A) Chemical structure of MDEG-541. (B) Western blot of MYC, GSPT1, GSPT2 and PLK1 protein and quantification after treatment with 5 µM, 10 µM and 20 µM 619 and vehicle control (DMSO) for 24 h in the cell line PSN1. (C) Western blot of MYC, GSPT1 and PLK1 protein and quantification after treatment with 5 µM, 10 µM and 20 µM 619 and vehicle control (DMSO) for 24 h in the cell line HCT116. (D) Western blot of MYC, GSPT1, GSPT2 and PLK1 protein and quantification after treatment with 5 µM, 10 µM and 20 µM 619 and vehicle control (DMSO) for 24 h in the cell line KP4. Shown is one representative western blot of three biological replicates. α-TUBULIN: loading control. Data was normalized to DMSO vehicle control. Statistics: Two-way ANOVA and Bonferroni´s multiple comparisons test: *p<0.01, **p<0.001, ***p<0.0001.

10.8 Inhibition of the proteasome prevented MDEG-541-mediated degradation of MYC, GSPT1, GSPT2 and PLK1

This experiment aims to examine whether the action of MDEG-541 to degrade MYC, GSPT1, GSPT2 and PLK1 is dependent on the proteasomal degradation step. Therefore, the proteasome was inhibited by Bortezomib and MG-132. PSN1 and HCT116 cells were treated for 4 h with either 100 nM of Bortezomib or 5 µM of MG-132 prior to treatment with 10 µM MDEG-541 for an additional 20 h.

As previously shown (Figure 8 B and C), single agent MDEG-541 treatment in cell line PSN1 decreased MYC protein level by 98.1%, GSPT1 protein level was decreased by 91.82% and GSPT2 protein level by 97.97% compared to DMSO vehicle control (set as 100%, Figure 14 A). Prior inhibition of proteasomal degradation with the proteasome inhibitor Bortezomib prevented the degradation of MYC, GSPT1, GSPT2 and PLK1 in the cell line PSN1 after MDEG-541 treatment (Figure 14 A). Likewise, the proteasome inhibitor MDEG-132 increased MYC, GSPT1, GSPT2 and PLK1 protein in the cell line PSN1 following MDEG-541 treatment.

Similar to the results observed in PSN1 cells, MDEG-541 treatment in the cell line HCT116 decreased MYC protein level by 99.6% and GSPT1 protein level to 99.1% compared to DMSO vehicle control (set as 100%, Figure 14 B). The prior inhibition of proteasomal degradation with proteasome inhibitor Bortezomib completely prevented the degradation of MYC, GSPT1 and PLK1 protein in the cell line HCT116 after MDEG-541 treatment (Figure 14 B). Similarly, the proteasome inhibitor MDEG-132 rescued MYC, GSPT1 and PLK1 protein level in the cell line HCT116 after MDEG-541 treatment.

Also, the downregulation of MYC, GSPT1 and GSPT2 protein expression after CC-885 treatment was rescued after the inhibition of the proteasome in PSN1 and HCT116 cells (Supplementary Figure 1).

In sum, these experiments indicate that the proteasome is essential for MDEG-541 to mediate the degradation of MYC, GSPT1, GSPT2 and PLK1.

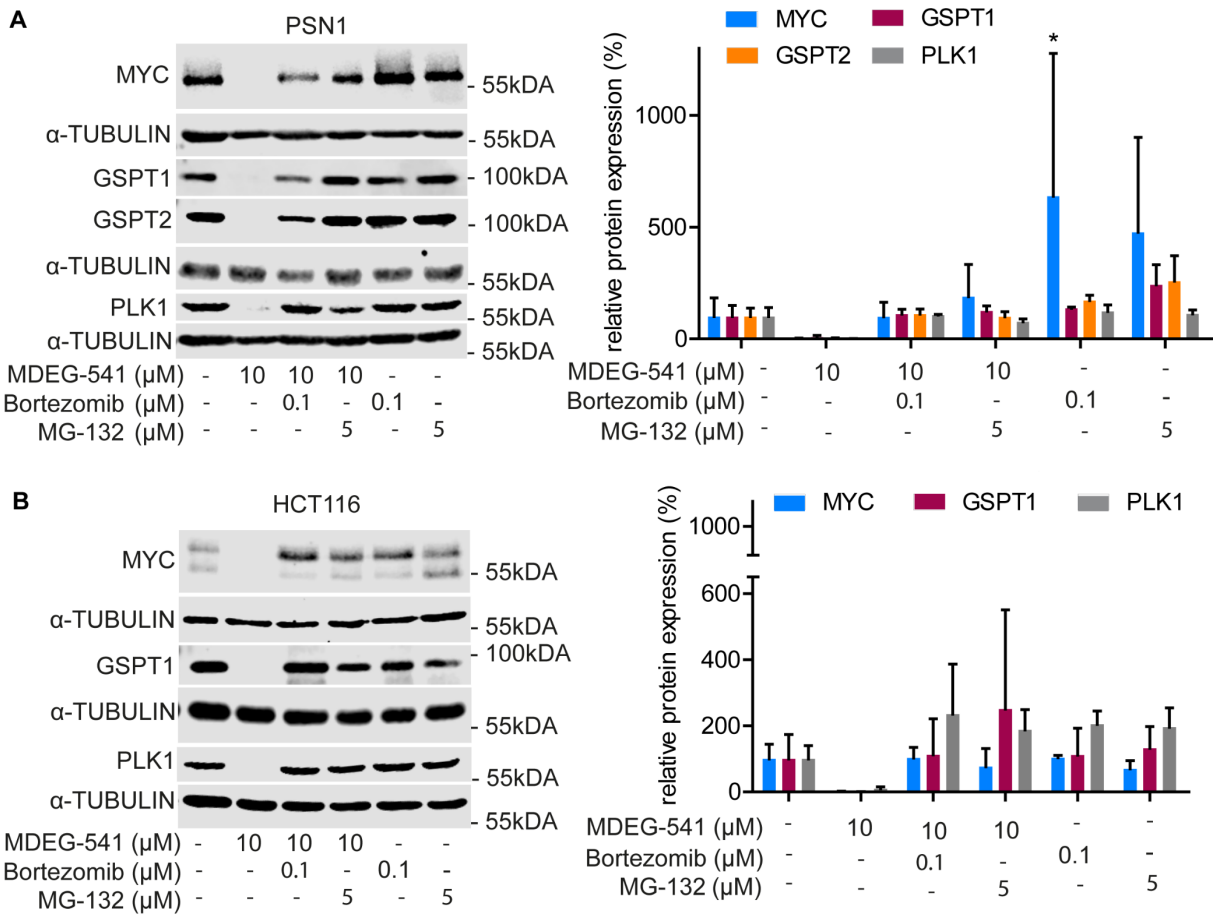

Figure 14: Inhibition of the proteasome prevented MDEG-541-mediated degradation of MYC, GSPT1, GSPT2 and PLK1
Western blot of MYC, GSPT1, GSPT2 and PLK1 and quantification of cell lines (A) PSN1 and western blot of MYC, GSPT1 and PLK1 and quantification of cell line (B) HCT116 pre-treated for 4 h with proteasome inhibitors Bortezomib (0.1 μM) or MG-132 (5 μM) followed by 20 h treatment with 10 μM MDEG-541 treatment. Shown is one representative western blot of three biological replicates. Cells were treated for 24 h with DMSO vehicle control. Loading control: β-ACTIN/α-TUBULIN. Data was normalized to DMSO vehicle control. Statistics: Two-way ANOVA and Bonferroni´s multiple comparisons test: *p<0.01, **p<0.001, ***p<0.0001.

10.9 Inhibition of ubiquitination prevented MDEG-541-mediated MYC, GSPT1, GSPT2 and PLK1 degradation

To examine whether degradation of MYC, GSPT1, GSPT2 and PLK1 protein after MDEG-541 treatment is dependent on ubiquitination in PSN1 and HCT116 cells, the ubiquitin activating enzyme (UAE) was inhibited with 200 nM TAK-243 for 4 h.

Treatment with 10 μM MDEG-541 for 20 h degraded MYC, GSPT1, GSPT2 and PLK1 protein in cell line PSN1 and HCT116 compared to DMSO vehicle control (set to 100%, Figure 15 A). Prior inhibition of the UAE completely rescued the degradation of MYC, GSPT1, GSPT2 and PLK1 protein in PSN1 cells after MDEG-541 treatment. Prior

treatment with TAK-243 rescued the degradation of MYC and partially rescued the degradation of GSPT1 and PLK1 after MDEG-541 treatment (Figure 15 B).

The downregulation of MYC, GSPT1 and GSPT2 protein expression after CC-885 treatment was rescued after the inhibition of the UAE in PSN1 and HCT116 cells (Supplementary Figure 2).

This data confirms the dependency of MDEG-541-mediated degradation of GSPT1, GSPT2, MYC and PLK1 on ubiquitination.

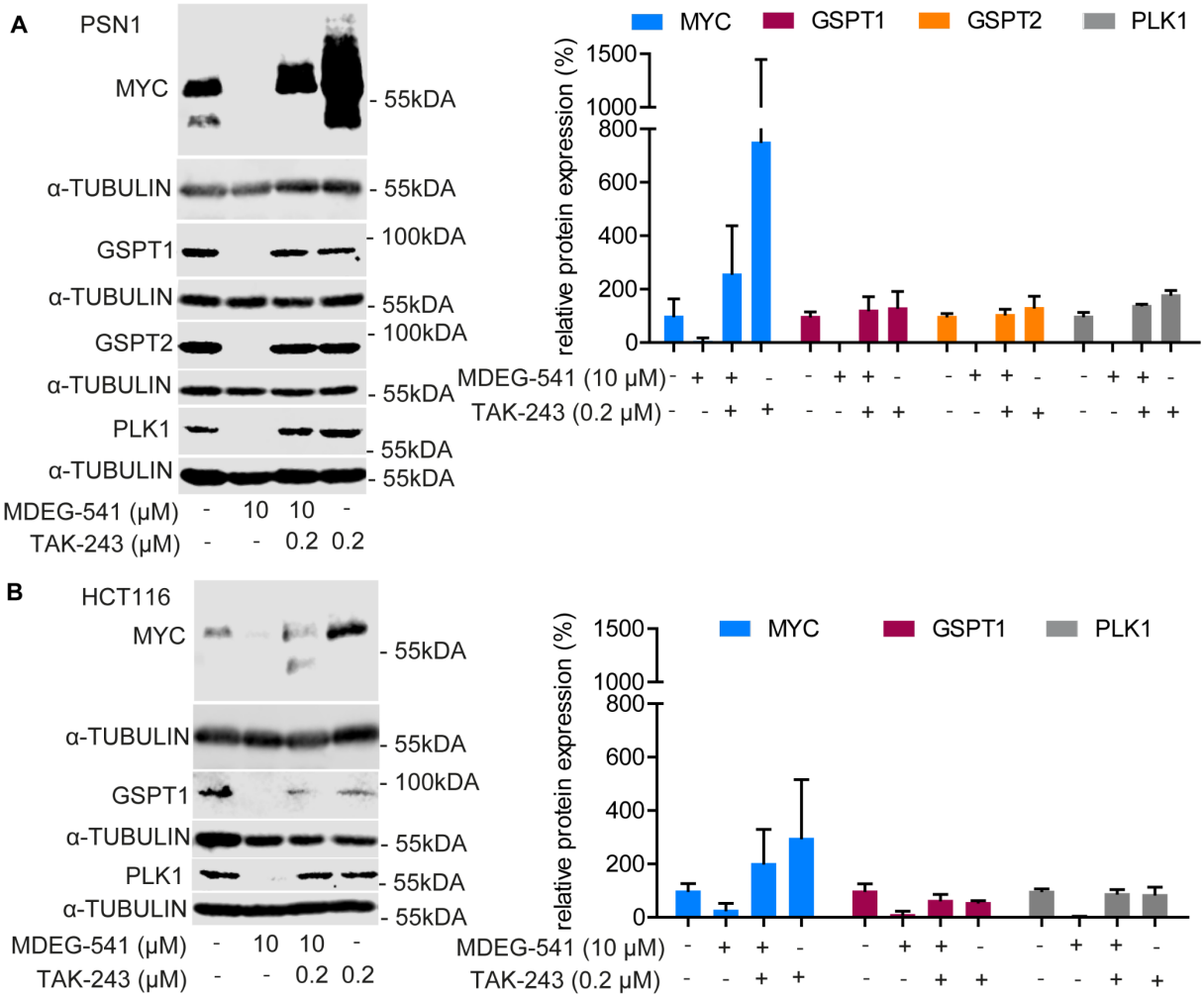

Figure 15: Inhibition of ubiquitination prevented MDEG-541-mediated MYC, GSPT1, GSPT2 and PLK1 degradation

Western blot of MYC, GSPT1, GSPT2 and PLK1 and quantification of cell line (A) PSN1 and western blot of MYC, GSPT1 PLK1 and quantification of cell line (B) HCT116 pre-treated for 4 h with 0.2 μM of the UAE inhibitor TAK-243 followed by 20 h treatment with 10 μM MDEG-541. Shown is one representative western blot of three biological replicates. Cells were treated for 24 h with vehicle control. Loading control: α-TUBULIN. Data was normalized to DMSO vehicle control. Statistics: Two-way ANOVA and Bonferroni´s multiple comparisons test: *p<0.01, **p<0.001, ***p<0.0001.

10.10 Knockout of the CRBN E3-ligase prevented MDEG-541-mediated degradation of MYC, GSPT1, GSPT2 and PLK1 protein

To evaluate whether the mechanism of MDEG-541 relies on the recruitment of CRBN, the E3-ligase was genetically deleted in cell lines PSN1 and HCT116 and CRBN knockout (KO) cells were subsequently treated with MDEG-541 for 24 h. KO of CRBN was confirmed by western blots (Figure 16 A-D). MDEG-541 treatment of CRBN proficient parental cells and CRBN deficient cells was compared.

MDEG-541 treatment of the CRBN proficient parental PSN1 cells degraded MYC (10 µM: 50.78%, 20 µM: 100%), GSPT1 (5 µM: 95.66%, 10 µM: 96.39%, 20µM: 99.84%), GSPT2 (5 µM: 45.67%, 10µM: 64.39%, 20 µM: 72.18%) and PLK1 (20 µM: 64.98%) protein level (Figure 16 A). In both CRBN deficient PSN1 cell clones, MYC and PLK1 protein expression was completely rescued after MDEG-541 treatment compared to DMSO vehicle control of the CRBN proficient parental cells (set to 100%, Figure 16 A). MDEG-541 treatment of the CRBN deficient PSN1 cells downregulated GSPT1 protein level in clone 6 sgRNA1 (5 µM: 2.56%%, 10 µM: 4.57%, 20 µM: 64.66%) and clone 4 sgRNA2 (5 µM: 44.91%, 10 µM: 42.05%, 20 µM: 42.61%) compared to DMSO vehicle control (set to 100%). GSPT2 protein level was reduced in clone 6 sgRNA1 (5 µM: 3.68%, 10 µM: 18.12%, 20 µM: 28%) and clone 4 sgRNA2 (5 µM: 25.63%, 10 µM: 39.63%, 20 µM: 38.76%) after MDEG-541 treatment compared to DMSO vehicle control (set to 100%).

MDEG-541 treatment of CRBN proficient parental HCT116 cells decreased MYC protein level (5 µM: 54.41%, 10 µM: 99.35%, 20 µM: 99.6%), GSPT1 (5 µM: 66.1%, 10 µM: 86.22%, 20 µM: 98.66%) and PLK1 protein level (10 µM: 33.46%, 20 µM: 73.71%) in a dose-dependent manner compared to DMSO vehicle control (set to 100%, Figure 16 B). In the CRBN KO cell lines PSN1 clone 6 sgRNA1 and PSN1 clone 2 sgRNA2, no degradation of GSPT1, MYC and PLK1 protein level following 5 µM, 10 µM or 20 µM MDEG-541 treatment was observed in comparison to parental CRBN proficient PSN1 cells.

Also, treatment of CRBN KO cell lines PSN1 and HCT116 with CC-885 rescued the inhibition of MYC, GSPT1 and GSPT2 (Supplementary Figure 3).

In sum, this data indicates that the degradation of MYC and PLK1 after MDEG-541 treatment is dependent on the CRBN in PSN1 and HCT116 cells. MDEG-541-mediated downregulation of GSPT1 and GSPT2 was partially rescued in CRBN deficient clones.

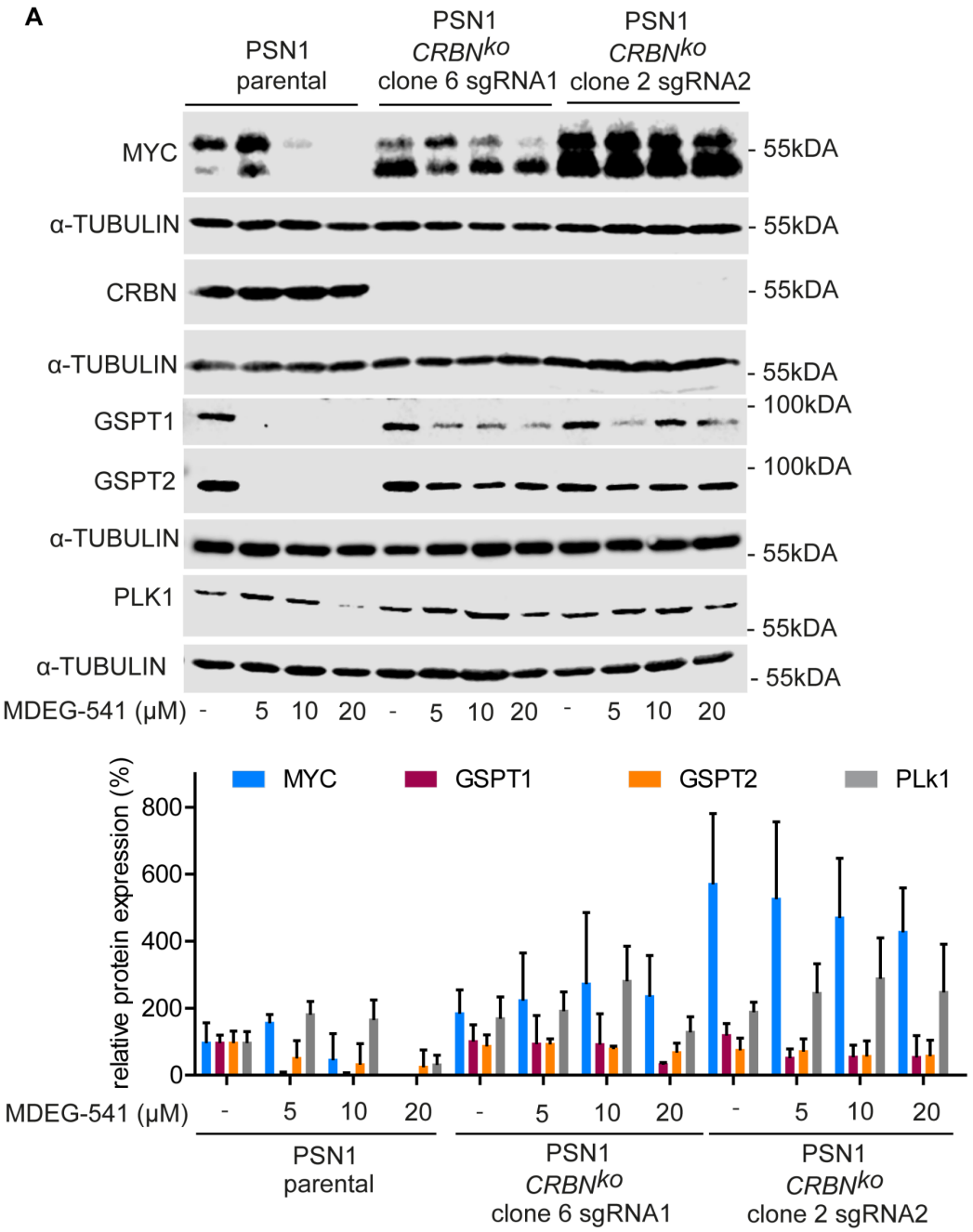

Figure 16: Knockout of CRBN E3-ligase prevented MDEG-541-mediated degradation of MYC, GSPT1, GSPT2 and PLK1

(A) Western blots and quantification of MYC, GSPT1, GSPT2, PLK1 and CRBN protein of the CRBN-proficient parental cell line PSN1 and the CRBN-deficient PSN1 clone 6 sgRNA1 and PSN1 clone 4 sgRNA2 cells treated with 5 μM, 10 μM or, 20 μM of MDEG-541 for 24 h. Shown is one representative western blot of three biological replicates. Cells were treated with MDEG-541 and DMSO vehicle control for 24 h. Loading control: α-TUBULIN. Data was normalized to DMSO vehicle control. Statistics: Two-way ANOVA, ns.

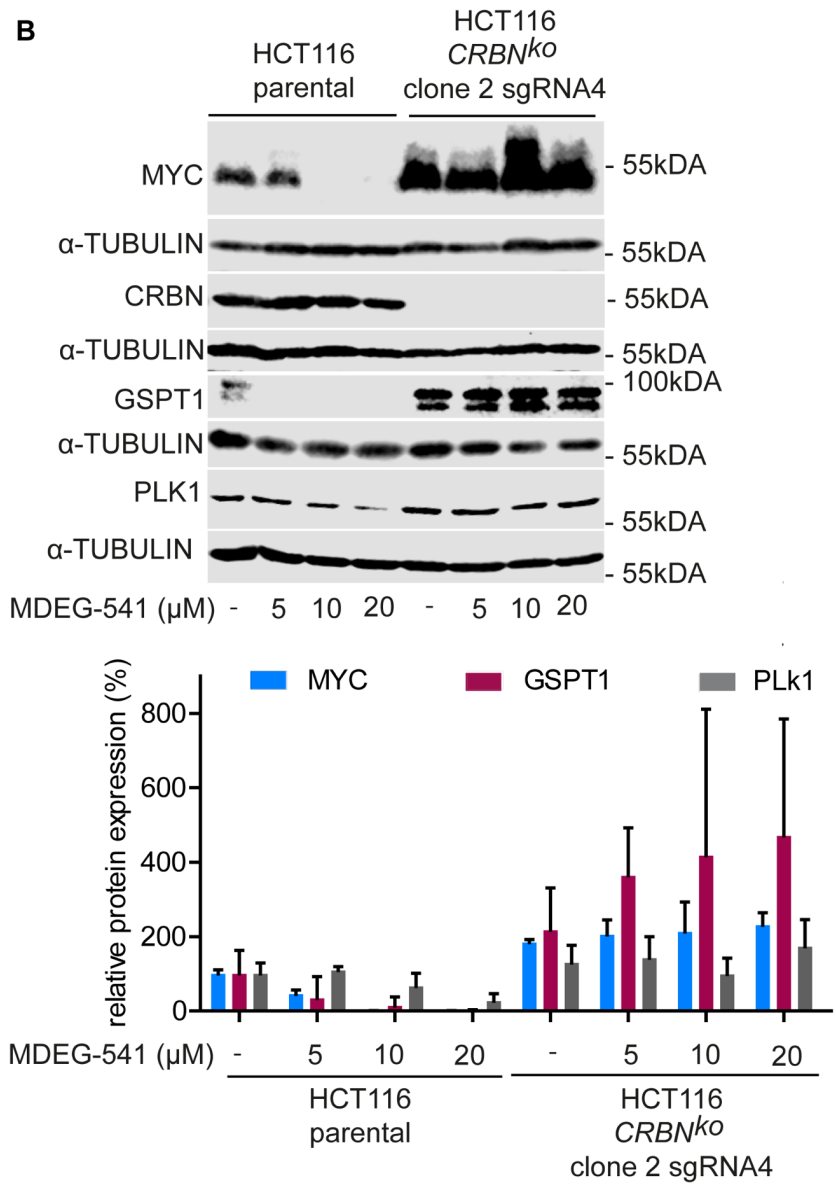

Figure 16: Knockout of CRBN E3-ligase prevented MDEG-541-mediated degradation of MYC, GSPT1, GSPT2 and PLK1

(B) Western blots and quantification of MYC, GSPT1, PLK1 and CRBN protein in the CRBN-proficient parental cell line HCT116 and the CRBN-deficient HCT116 cell clone 2 sgRNA2 treated with 5 μM, 10 μM or, 20 μM of MDEG-541 for 24 h. Shown is one representative western blot of three biological replicates. Cells were treated with MDEG-541 and DMSO vehicle control for 24 h. Loading control: α-TUBULIN. Data was normalized to DMSO vehicle control. Statistics: Two-way ANOVA, ns.

10.11 Reduced cell viability as result of MDEG-541, CC-885 and Volasertib treatment in PDAC and CRC cell lines

To determine the ability of MDEG-541, 619, CC-885, CC-90009 and Volasertib to reduce the viability of cell lines PSN1, HCT116 and KP4, an MTT assay was performed. Both cell lines were treated for 72 h with either twelve different concentrations (1:2 dilution) of MDEG-541, 619, CC-90009 and the treatment controls 10058-F4 or Thalidomide ranging from 50 µM to 24 nM, with CC-885, or Volasertib ranging from 1 µM to 0.2 nM and the vehicle control DMSO.

Treatment with MDEG-541 reduced the viability in dose-dependent manner with a half-maximal growth inhibitory concentration (GI_{50}) of 10.7 µM in PSN1 cells, GI_{50} of 14.3 µM in HCT116 cells and a GI_{50} of 1.22 µM in KP4 cells (Figure 17 A). Vice versa, Thalidomide did not affect cell viability of PSN1 and HCT116 cells significantly compared to MDEG-541 treatment. 10058-F4 had a weak effect on reducing cell viability in cell line HCT116 compared to Thalidomide control treatment.

Treatment with 619 for 72 h decreased cell viability in cell line PSN1 with a GI_{50} value of 76.76 µM (Figure 17 B), in cell line HCT116 with a GI_{50} value of 50.04 µM and in cell line KP4 with a GI_{50} value of 36.62 µM. 72 h of CC-885 treatment reduced cell viability in cell line PSN1 with a GI_{50} value of 0.039 µM (Figure 17 B) and in cell line HCT116 with a GI_{50} value of 0.074 µM. Treatment with CC-90009 for 72 h decreased cell viability in cell line KP4 with a GI_{50} value of 74.27 µM, however, in cell lines PSN1 and HCT116, CC-90009 treatment had no cell viability reducing effect. Treatment with Volasertib for 72 h decreased cell viability in cell line PSN1 with a GI_{50} value of 0.26 µM (Figure 17 B).

The cell line KP4 was the most sensitive cell line after treatment with all tested compounds. Based on these results, MDEG-541 decreased cell viability in PSN1, HCT116 and KP4 cells compared to the single moieties 10058-F4 and Thalidomide. Further, MDEG-541 outperformed 619 to reduce cell viability in all tested cell lines.

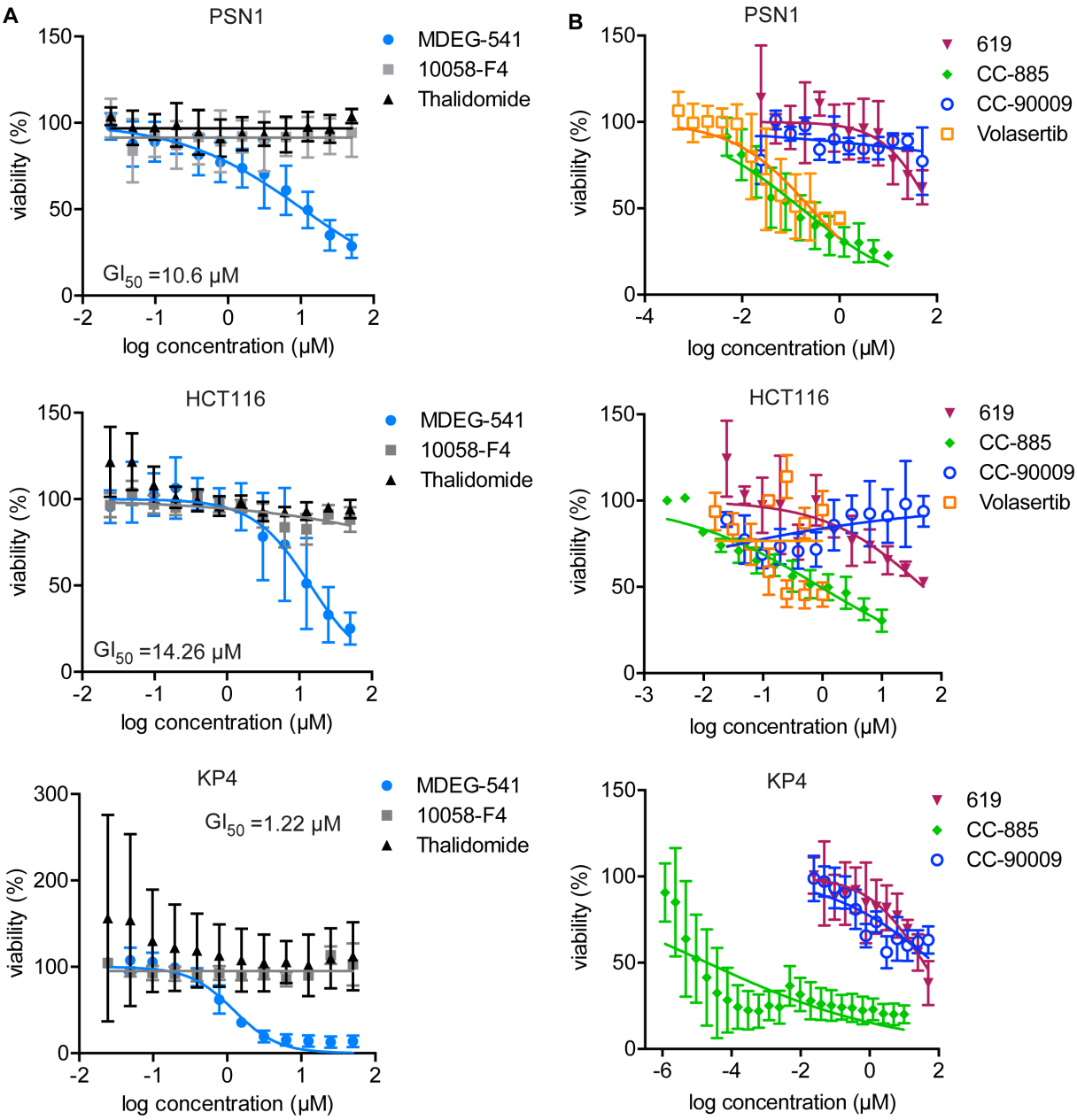

Figure 17: Reduced cell viability as result of MDEG-541, CC-885 and Volasertib treatment in PDAC and CRC cell lines

(A) Determination of cell viability (%) and GI_{50} values by MTT assay in cell lines PSN1 (upper panel, one representative western blot of five biological replicates), HCT116 (middle panel, one representative western blot of five biological replicates) and KP4 (lower panel, one representative western blot of three biological replicates) after MDEG-541, 10058-F4 and Thalidomide treatment. (B) Evaluation of cell viability (%) and GI_{50} values by MTT assay in cell lines PSN1 (upper panel), HCT116 (middle panel) and KP4 (lower panel) after CC-885, CC-90009, Volasertib and 619 treatment. Shown is one representative western blot of three biological replicates. Cells were treated for 72 h with 12 dilutions of MDEG-541, 619, CC-90009, 10058-F4 and Thalidomide in a 1:2 dilution (50 µM-24.41 nM), CC-885 in PSN1 and HCT116: 1 µM-15.6 nM and KP4: 1 µM-0.488 nM or Volasertib (1 µM to 0.2 nM). Data was normalized to DMSO vehicle control. Shown is the mean ± SD.

10.12 Long-term treatment of cancer cell lines with MDEG-541 and CC-885 inhibited colony formation

The MTT assay (Figure 17) showed that cell viability was reduced after 72 h of MDEG-541 or CC-885 treatment. To examine the effect of long-term treatment, colony formation was tested in cell lines PSN1 and HCT116 after treatment with MDEG-541 (5 µM, 10 µM or, 20 µM; PSN1 for 12 days, HCT117 for 10 days) or CC-885 (0.25µM, 0.5µM or, 1µM, PSN1 and HCT116 for 10 days). MDEG-541 decreased formation of colonies in both cell lines in a dose-dependent manner compared to treatment controls 10058-F4, Thalidomide and DMSO vehicle control (Figure 18 A). Specifically, 10µM MDEG-541 treatment reduced formation of PSN1 cell colonies by 56.47% and 20 µM MDEG-541 treatment reduced the formation of PSN1 cell colonies by 74.9% after 12 days of treatment (Figure 18 C). In HCT116 cells colony formation was decreased after 10 days of treatment with 5 µM MDEG-541 by 34.58%, with 10 µM MDEG-541 by 79.02% and with 20 µM MDEG-541 by 90.9% compared to treatment controls 10058-F4 or Thalidomide and DMSO vehicle control (set to 100%, Figure 18 D).

Similarly, CC-885 reduced colony formation in cell lines PSN1 and HCT116 compared to and DMSO vehicle control (Figure 18 B). Quantification of the stained colonies showed a significant reduction of PSN1 cell colonies after treatment with 0.25 µM CC-885 by 72.11%, with 0.5 µM CC-885 by 84.07% and with 1 µM by 90.56% compared to DMSO vehicle control (set so 100%, Figure 18 E).

In HCT116 cells, treatment with 0.25 µM, 0.5 µM or, 1 µM CC-885 inhibited colony formation. Specifically, treatment with 0.25 µM CC-885 led to a 1.97% reduction of absorbance in clonogenic assays compared to DMSO vehicle control (set to 100%). Quantification of absorbance after treatment with 0.5 µM CC-885 demonstrated decreased colony formation by 14.68% and 1 µM treatment by 53.55%, compared to DMSO vehicle control (set to 100%, Figure 18 D).

In conclusion, the long-term treatment with MDEG-541 and CC-885 reduced the ability to form of cell colonies in PSN1 and HCT116 compared to the treatment controls 10058-F4 and Thalidomide or DMSO vehicle control.

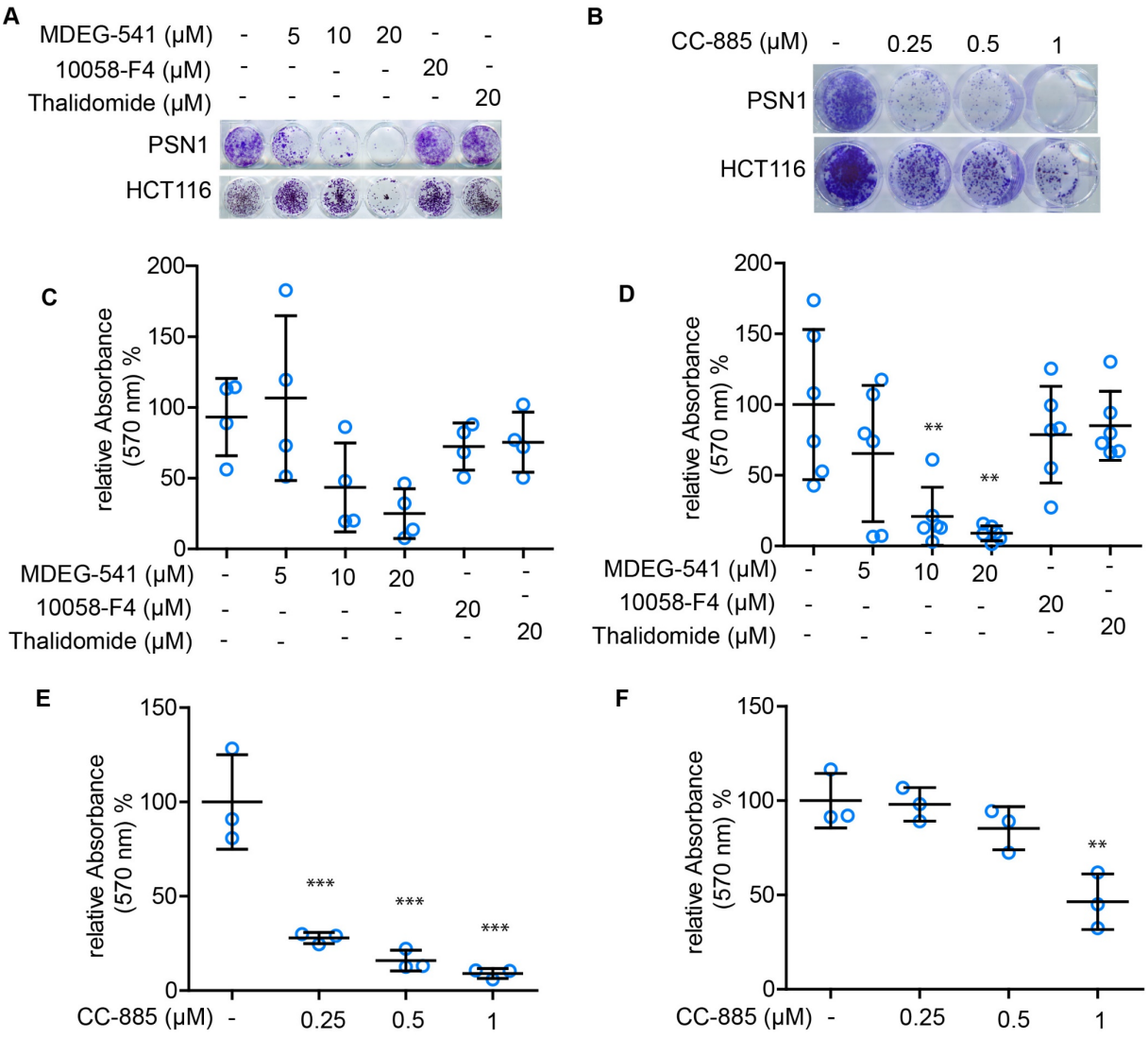

Figure 18: Long-term treatment of cancer cell lines with MDEG-541 and CC-885 inhibited colony formation

(A, upper panel) PSN1 cell colony formation after treatment with 5 µM, 10 µM or, 20 µM MDEG-541, treatment control 10058-F4 or Thalidomide and vehicle control DMSO (one representative clonogenic assay of four biological replicates) for 12 days. (A, lower panel) HCT116 cell colony formation after treatment with 5 µM, 10 µM or, 20 µM MDEG-541, treatment control 10058-F4 or Thalidomide and vehicle control DMSO (one representative clonogenic assay of six biological replicates) cells for 10 days. (B, upper panel) PSN1 cell colony formation and (B, lower panel) HCT116 cell colony formation after treatment with 0.25 µM, 0.5 µM or, 1 µM CC-885 and vehicle control DMSO (one representative clonogenic assay of three biological replicates) for 10 days. Quantification of (C) PSN1 and (D) HCT116 cell colony formation after treatment with MDEG-541, treatment control 10058-F4 or Thalidomide and vehicle control DMSO. (E) Quantification of PSN1 and (F) HCT116 cell colony formation after treatment with CC-885, treatment control 10058-F4 or Thalidomide and vehicle control DMSO. Data was normalized to DMSO vehicle control. Statistics: One-way ANOVA and Bonferroni´s multiple comparisons test: *p<0.01, **p<0.001, ***p<0.0001.

10.13 MDEG-541 treatment showed an overlap in mRNA expression with GSPT1 KD HCT116 cells

To determine the effect of GSPT1/2 and MYC withdrawal on the transcriptome due to MDEG-541 treatment RNA seq was performed to calculate the log FC of regulated genes.

To examine the regulation of the MYC network by GSPT1, RNA seq data of HCT116 cells with an RNAi induced GSPT1-depletion were compared to HCT116 cells treated with 20 µM MDEG-541 for 24 h. In total, six enriched and five depleted HALLMARKs overlapped after MDEG-541 treatment and the RNAi approach (Figure 19 A and B). Specifically, HALLMARK_TNFA_SIGNALING_VIA_NFKB was detected as most significantly enriched in both approaches (Figure 19 C). Moreover, a significant depletion of the pro-proliferative HALLMARKs MYC target V1/V2, E2F signatures and G2M checkpoint was observed (Figure 19 D).

This data suggests that the downregulation of GSPT1/2 and MYC by MDEG-541 treatment as well as RNAi induced GSPT1-depletion on HCT116 genome strongly overlap. The overlapping HALLMARKs indicate a downregulation of pro-proliferative signaling and an involvement of tumor necrosis factor – nuclear factor kappa-light-chain-enhancer (TNF-α -NF-κ B) signaling in these cells after MDEG-541 treatment. Therefore, the pro-proliferative pathways and cell fate signaling were evaluated in the next steps.

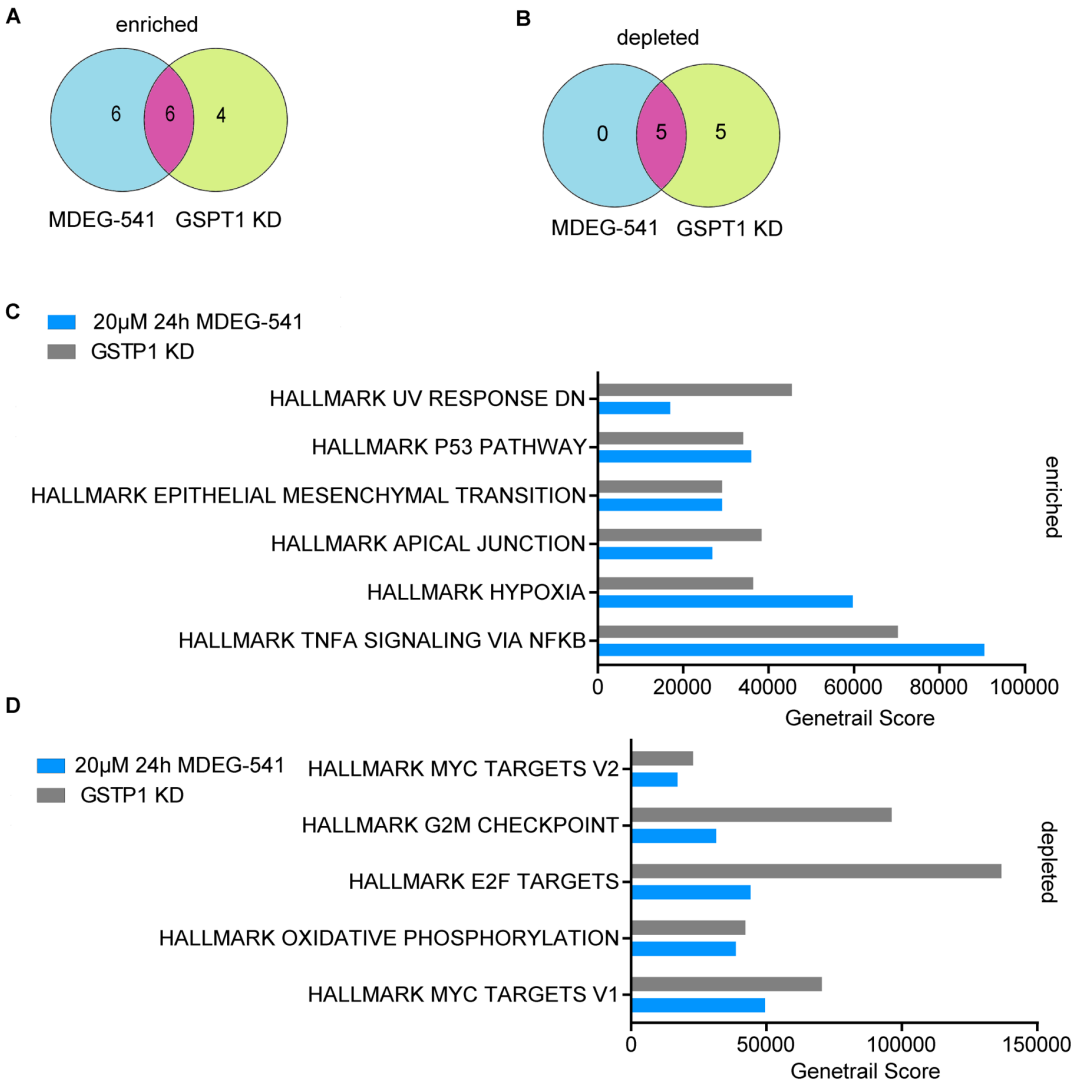

Figure 19: MDEG-541 treatment showed an overlap in mRNA expression with GSPT1 KD HCT116 cells
To examine the regulation of the MYC network by GSPT1, RNA seq data of HCT116 cells with an RNAi induced GSPT1-depletion were compared to HCT116 cells treated with 20 µM MDEG-541 for 24 h. A Genetrail analysis was performed with HALLMARK signature and compared between both HCT116 RNA seq data. Shown are overlapping (A) enriched and (B) depleted Genetrail HALLMARKs. Detailed analysis and Genetrail score of overlapping (C) enriched and overlapping (D) depleted HALLMARKs observed after MDEG-541 treatment and the RNAi approach.

10.14 MDEG-541 treatment reduced the expression of proteins playing a role in cell cycle control

To determine the regulation of pro-proliferative pathways observed in RNA seq after MDEG-541 treatment (Figure 20 E), E2F signaling and the cell cycle pathway was examined on protein level. Therefore, a global proteomics analysis of PSN1 cells treated with 10 µM MDEG-541 for indicated timepoints was performed by Dr. Stephanie Heinzlmeir in the lab of Prof. Dr. Bernhard Küster, Chair of Proteomics and Bioanalytics, at TUM. Analysis of the proteomics data demonstrated a downregulation

of the GSEA HALLMARK_E2F TARGETS in a time-dependent manner (Figure 20 A). Furthermore, a downregulation of the KEGG_CELL_CYCLE signature in a time-dependent manner was observed (Figure 20 B).

To verify this data, the proteins playing a role in cell cycle control and E2F signaling, were further investigated on western blot. The treatment with 10 µM MDEG-541 for 24 h reduced protein expression of CDK2, CDK4, cyclin D1 and E2F1 in PSN1 and HCT116 cells compared to DMSO vehicle control (Figure 20 D-E).

Specifically, in PSN1 cells the protein expression of CDK2 was reduced by 66.27% and in HCT116 cells by 90.56% after 24 h treatment with 10 µM MDEG-541 compared to DMSO vehicle control (set as 100%). CDK4 protein expression was significantly decreased by 98.4% in PSN1 cells 24 h after treatment with 10 µM MDEG-541 and in HCT116 cells after 3 h by 24.5%, after 12 h by 30.68% and after 24 h by 97.51% compared to DMSO vehicle control (set as 100%). Cyclin D1 was significantly reduced in PSN1 cells after 12 h and 24 h MDEG-541 treatment by 76.79% and 94.11%, respectively, compared to DMSO vehicle control (set as 100%). Likewise, Cyclin D1 was significantly downregulated in HCT116 cells after 12 h and 24 h MDEG-541 treatment by 92.7% and 85.4%, respectively, compared to DMSO vehicle control (set as 100%).

In the cell line PSN1, E2F1 protein expression was significantly decreased after 12 h and 24 h MDEG-541 treatment by 81.79% and 99.13%, respectively, compared to DMSO vehicle control (set as 100%). In the cell line HCT116, E2F1 was significantly reduced by 64.7% after 24 h of treatment with 10 µM MDEG-541, compared to DMSO vehicle control (set as 100%).

Furthermore, in the cell line PSN1 phosphorylation of RB at Ser807/811 was downregulated by 56.54% after 3 h treatment with 10 µM MDED-541, by 58.86% after 12 h of treatment and no phosphorylated RB was detected on western blot after 24 h compared to DMSO vehicle control (set as 100%). Similarly, in HCT116 cells phosphorylation of RB was reduced by 25.15% after 3 h treatment with 10 µM MDEG-541, by 65.2% after 12 h of treatment and by 91.29% after 24 h compared to DMSO vehicle control (set as 100%).

In sum, MDEG-541 treatment reduced E2F1 protein and HALLMARK_E2F_targets. Moreover, expression of investigated proteins associated with the cell cycle were downregulated.

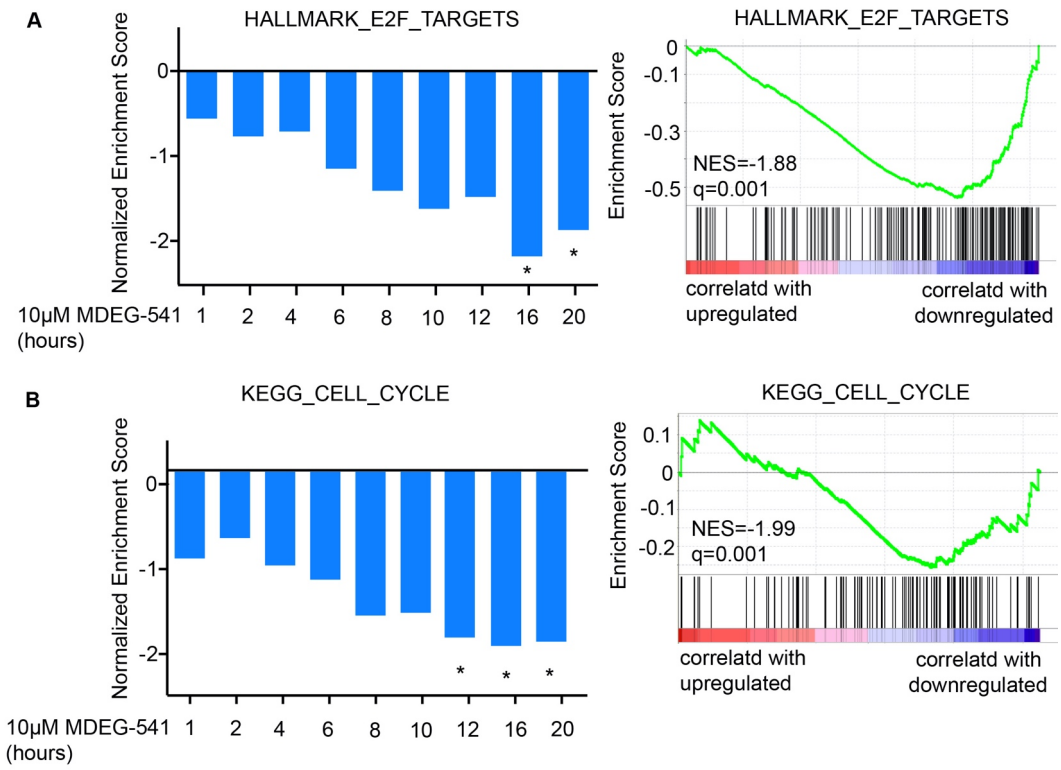

Figure 20: MDEG-541 treatment reduced the expression of proteins playing a role in cell cycle control

(A) Proteome analysis of MDEG-541 treated PSN1 cells at the indicate time points was used to calculate the log FC of proteins compared to untreated control. The log FC was used as a rank to run a pre-ranked HALLMARK Signatures GSEA analysis (GSEA App 4.0.3). Shown is the normalized enrichment score of HALLMARK_E2F_TARGETS over the indicated time points (left panel). Detailed regulation of the GSEA HALLMARK_E2F_TARGETS signature was shown after 20 h treatment with MDEG-541 (right panel). (B) Shown is the normalized enrichment score of KEGG_CELL_CYCLE over the indicated time points (left panel). Detailed regulation of the GSEA KEGG_CELL_CYCLE signature was shown after 20 h treatment with MDEG-541 (right panel). * FDR q value <0.05.

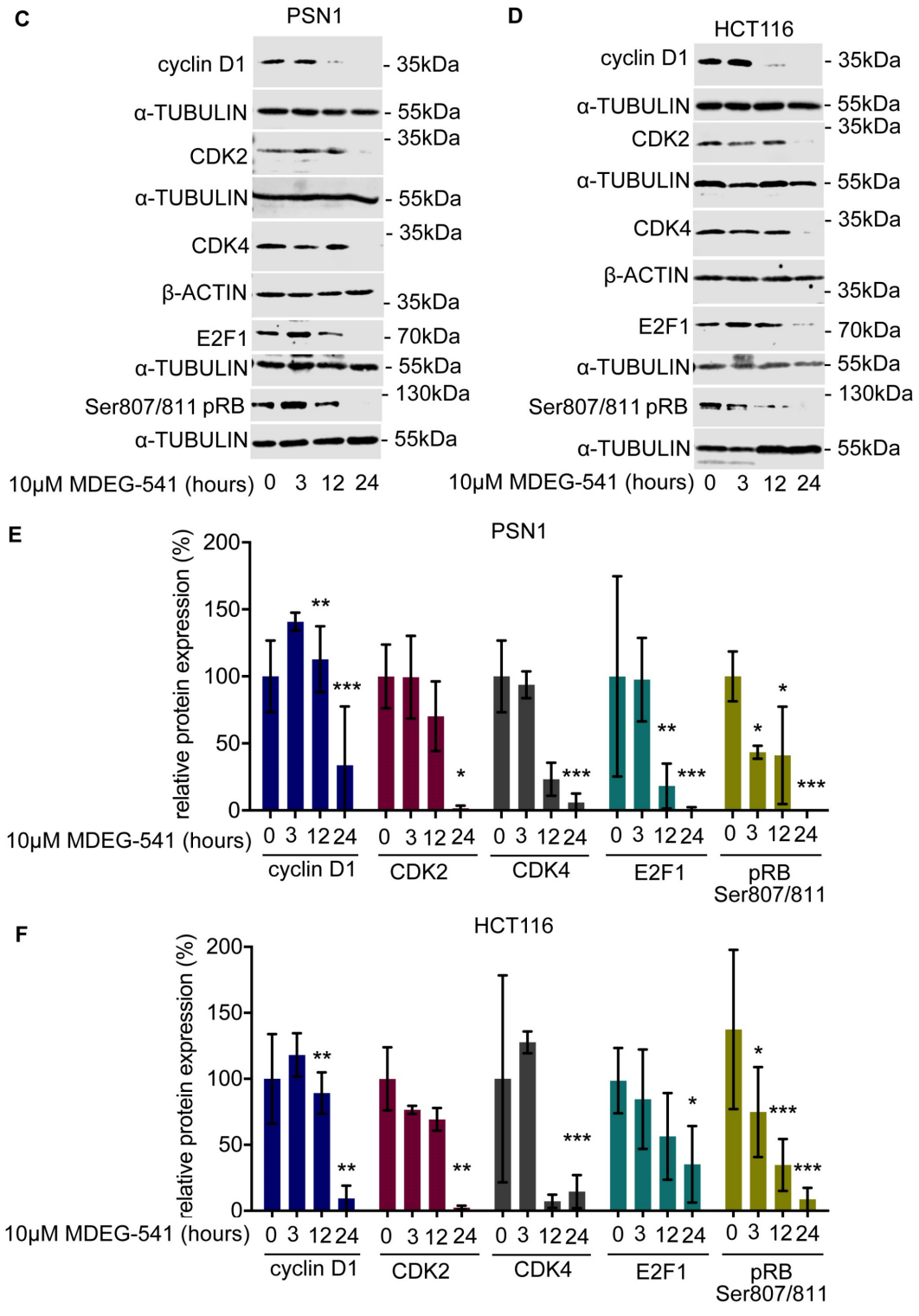

Figure 20: MDEG-541 treatment reduced the expression of proteins playing a role in cell cycle control

Western blots of CDK2, CDK4, cyclin D1, E2F1 and pRB (Ser807/811) in cell line (C) PSN1 (one representative western blot of three biological replicates) and in cell line (D) HCT116 (one representative western blot of three biological replicates) after 3 h, 12 h, and 24 h of treatment with 10 μM MDEG-541. α-TUBULIN or β-ACTIN were used as loading control. Data was normalized to DMSO vehicle control. Statistics: Two-way ANOVA and Bonferroni´s multiple comparisons test: *p<0.01, **p<0.001, ***p<0.0001.

10.15 MDEG-541 treatment induced unfolded protein response

Contrary to the downregulation of proteins playing a role in cell cycle control, an upregulation of proteins associated with unfolded protein response (UPR) was observed via RNA seq after MDEG-541 treatment. RNA seq was performed by Dr. Rupert Öllinger in the lab of Prof. Dr. Roland Rad, TranslaTUM, Klinikum rechts der Isar, TUM. A GSEA analysis was run with log2FC gene expression of PSN1 and HCT116 cells treated for 24 h with 20 µM MDEG-541 compared to DMSO vehicle control. The HALLMARK_UNFOLDED_PROTEIN_RESPONSE was upregulated in both cell lines (Figure 21 E and F).

To verify the RNA seq results, proteins playing a role in UPR, were examined on western blot. Therefore, the protein expression of ATF2, ATF4, the phosphorylation of PERK at T982 and the phosphorylation of EIF2α at Ser51 protein were determined after 10 µM MDEG-541 treatment for 3 h, 12 h and 24 h. MDEG-541 treatment induced ATF2 and ATF4 protein expression with increasing treatment times in PSN1 (Figure 21 A and C) and HCT116 (Figure 21 B and D) cells. The phosphorylation of EIF2α and PERK are associated with UPR and were increased in PSN1 cells after 24 h treatment with 10 µM MDEG-541 by 98.05% and 215%, respectively, compared to 24 h DMSO vehicle control (set to 100%, Figure 21 A and C). This upregulation of EIF2α and PERK phosphorylation was also observed in HCT116 cells leading to a 27.21% increase of pEIF2α after 12 h of 10 µM MDEG-541 treatment and a 179.54% increase of pPERK after 24 h treatment with 10 µM MDEG-541 compared to DMSO vehicle control (set to 100%). Treatment of cell lines PSN1 and HCT116 with 10 µM MDEG-541 for 3 h, 12 h or 24 h did not upregulate the expression of pan EIF2α and PERK. In PSN1 cells the expression of pan PERK protein was downregulated in a time-dependent manner after 3 h, 12 h and 24 h treatment with MDEG-541 compared to DMSO vehicle control (set to 100%).

In summary, RNA seq analysis showed an upregulation of UPR in PSN1 cells after 24h MDEG-541 treatment verified on western blot by the upregulation of pPERK, pEIF2α, ATF2 and ATF4.

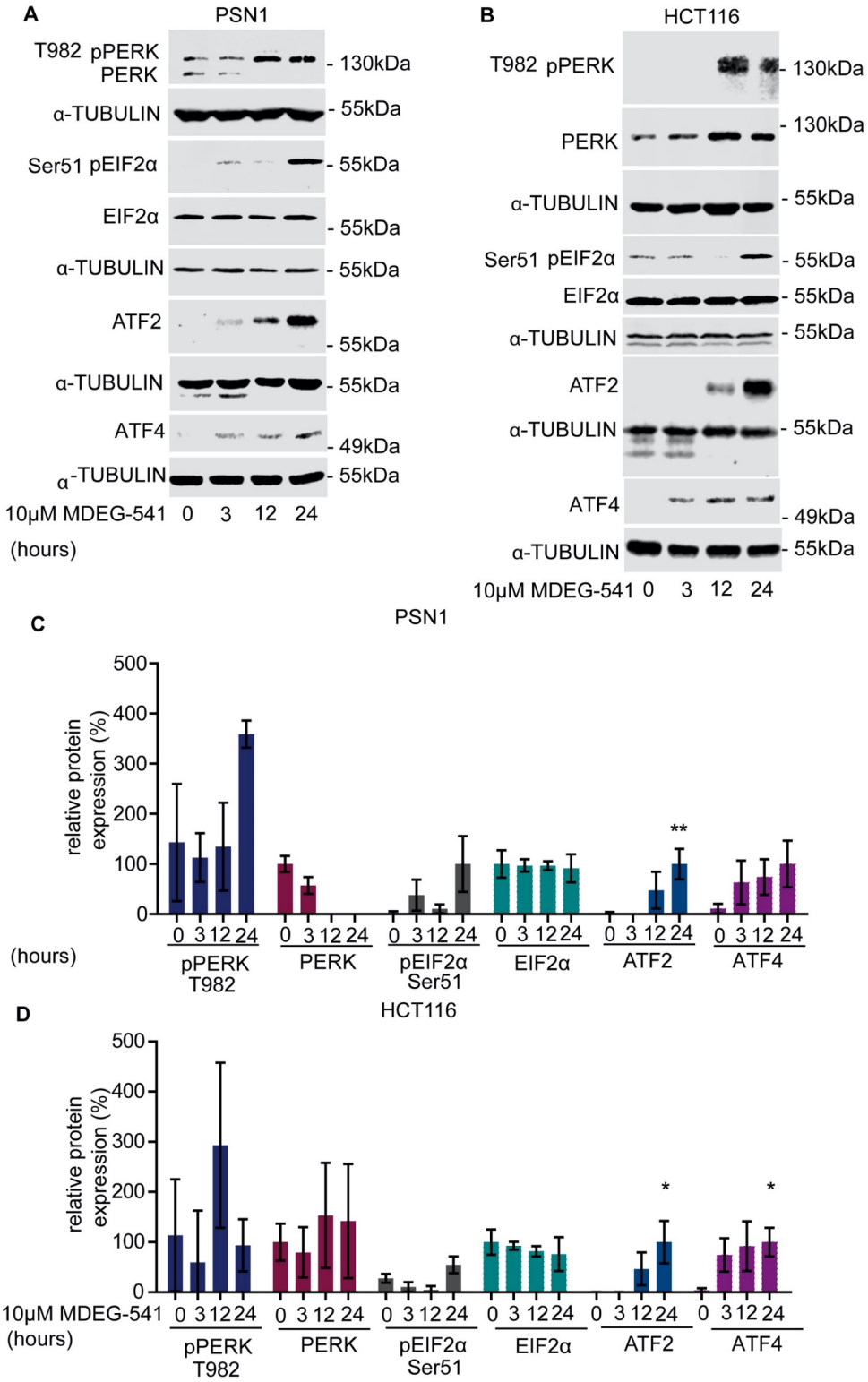

Figure 21: MDEG-541 treatment induced unfolded protein response
(A) Western blots of UPR associated proteins ATF2, ATF4 Ser51 pEIF2α/EIF2α and T982 pPERK/PERK in the cell line PSN1 (one representative western blot of three biological replicates) and in the cell line (B) HCT116 (one representative western blot of three biological replicates) after 3 h, 12 h and 24 h of 10 μM MDEG-541 treatment. Loading control: α-TUBULIN. (C) Quantification of western blots of the proteins ATF2, ATF4 Ser51 pEIF2α/EIF2α and T982 pPERK/PERK in the cell line PSN1 and (D) HCT116. Loading control: α-TUBULIN. Data was normalized to DMSO vehicle control.

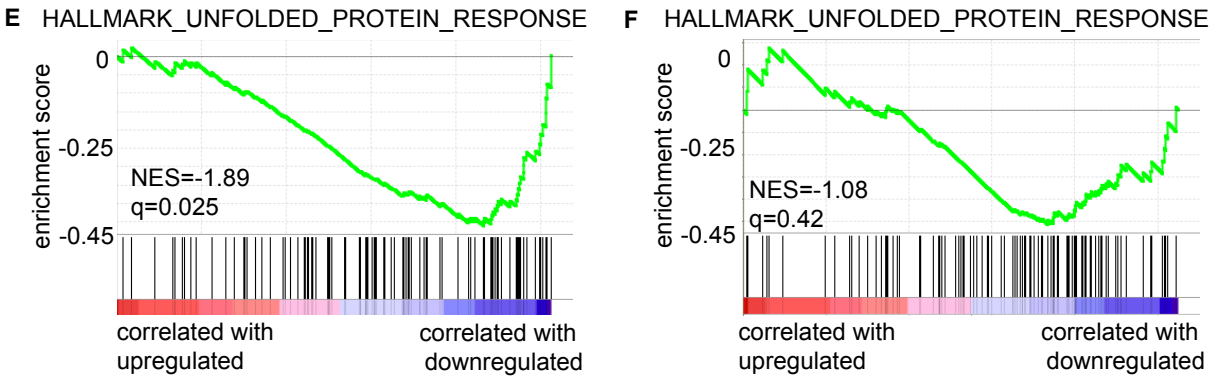

Figure 21: MDEG-541 treatment induces unfolded protein response
RNA seq of MDEG-541 treated (E) HCT116 and (F) PSN1 cells treated for 24 h with 20 µM MDEG-541 were used to calculate the log FC of genes compared to DMSO vehicle control. The log FC was used to run HALLMARK Signatures GSEA analysis (GSEA App 4.0.3). Shown is the normalized enrichment score of the HALLMARK_UNFOLDED_ PROTEIN_RESPONSE. * FDR q value <0.05.
Statistics: One-way ANOVA and Bonferroni´s multiple comparisons test: *p<0.01, **p<0.001, ***p<0.0001.

10.16 MDEG-541 treatment induced cell death

To determine the effect of MDEG-541 treatment on the cell fate of the cell lines PSN1 and HCT116, the cells were stained with PI and Annexin V prior to FACS analysis. Therefore, both cell lines were treated with DMSO, 10 µM MDEG-541, 10058-F4 or, Thalidomide for 48 h. The number of viable cells (characterized by no staining for Annexin V and PI) decreased significantly to 46.47% in PSN1 cells after MDEG-541 treatment compared to DMSO control where 80.57 % viable cell were observed (Figure 22 A and C). In the cell line HCT116, viable cells were reduced to 21.89% after MDEG-541 treatment compared to DMSO vehicle control where 78.05% of viable cell were observed (Figure 22 B and D). The number of dead cells by necrosis or necroptosis characterized by cells stained with PI (and no staining with Annexin V) increased significantly to 62.1% in PSN1 cells after MDEG-541 treatment compared to DMSO vehicle control where 18.13% of cells were stained with PI (Figure 22 C). In HCT116 cells treatment with MDEG-541 induced necrosis or necroptosis in 77.13% of the cells compared to DMSO vehicle control where 21.85% of the cell were stained positive with PI (Figure 22 A-D).

No significant increase of cells undergoing early (stained positive for Annexin V, no PI staining detected), or late apoptosis (stained positive for both, Annexin V and PI) were detected in PSN1 or HCT116 cells. Moreover, there was no effect detected after 10058-F4 and Thalidomide treatment on the cells compared to DMSO vehicle control.

These results indicate a significant increase in the number of dead cells due to necrosis or necroptosis after 48 h MDEG-541 treatment characterized by PI positive (Annexin V negative) cells.

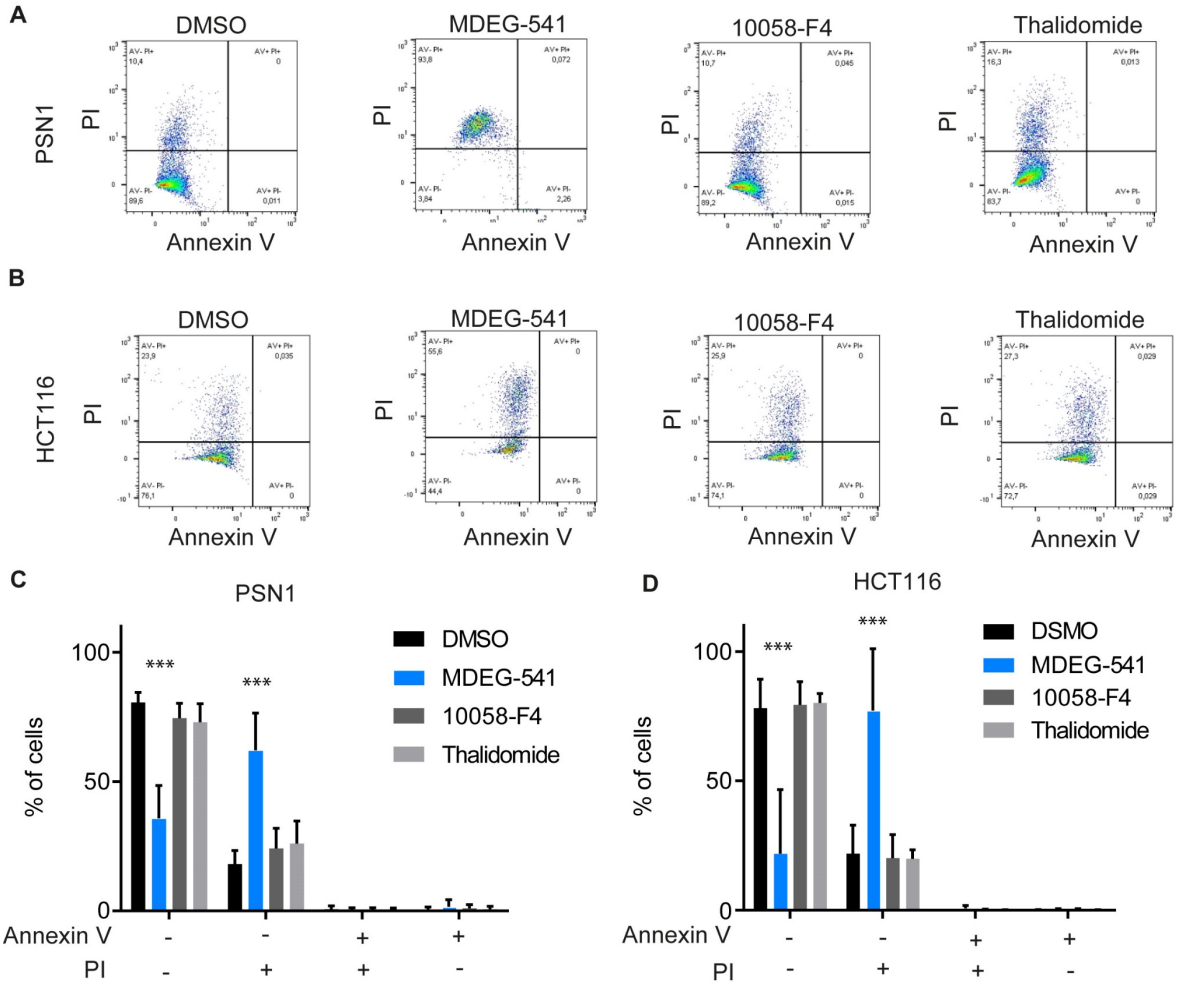

Figure 22: MDEG-541 treatment induced cell death
(A) Treatment of cell lines PSN1 (one representative FACS analysis of three biological replicates) and (B) HCT116 (one representative FACS analysis of three biological replicates) after 48h treatment with DMSO vehicle control, 10 µM MDEG-541, 10 µM 10058-F4 or, 10 µM Thalidomide staining with PI and Annexin V and subsequent FACS analysis. (C) Quantification of PSN1 and (D) HCT116 cells (values as percentage of total cell number) stained with PI and/or Annexin V. Data was normalized to DMSO vehicle control.
Statistics: Two-way ANOVA and Bonferroni´s multiple comparisons test: *p<0.01, **p<0.001, ***p<0.0001.

10.17 MDEG-541 treatment induced necroptosis and CC-885 treatment induced apoptosis

The PI positive staining of cell lines PSN1 and HCT116 treated with 10 µM MDEG-541 for 48 h indicated that the cells might die due to necrosis or necroptosis (Figure 23 A-D). To examine cell fate after MDEG-541 treatment, cleavage of PARP was used as indicator of apoptosis and phosphorylation of MLKL at Ser358 was used as indicator of necroptosis. PSN1 and HCT116 cells were treated for 12 h, 24 h, 48 h and 72 h, respectively, with 10 µM MDEG-541, for 24 h with the apoptosis inducing compound Bortezomib (0.1 nM, positive control) and for 24 h with the DMSO vehicle control. Cleavage of PARP was induced in both cell lines after Bortezomib treatment compared to DMSO vehicle control (Figure 23 A and B). Treatment with 10 µM MDEG-541 did not upregulate cleavage of PARP protein in PSN1 and HCT116 cells compared to DMSO vehicle control. However, the treatment with MDEG-541 resulted in the phosphorylation of necroptosis marker MLKL in PSN1 and HCT116 cells compared to DMSO vehicle control (Figure 23 A-B). Specifically, in PSN1 cells phosphorylation of MLKL was upregulated by 107.65% after 24 h MDEG-541 treatment, by 136.96% after 48 h of treatment and by 133.67% after 72 h of treatment compared to DMSO vehicle control. Likewise, in HCT116 cells the phosphorylation of MLKL was increased by 62.89% after 24 h MDEG-541 treatment, by 135.22% after 48 h of treatment and by 380.43% after 72 h of treatment compared to DMSO vehicle control.

In conclusion, the western blots show an increase in phosphorylation of necroptosis marker MLKL after MDEG-541 treatment, but no induction in cleavage of apoptosis marker PARP. These results, together with the data from the FACS analysis (Figure 22), indicate that cells treated with MDEG-541 might undergo necroptosis.

While MDEG-541 treatment did not induce apoptosis, treatment of 0.5 µM with GSPT1 degrader CC-885 increased protein cleavage of PARP (Figure 23 C and D). Specifically, in PSN1 cells cleavage of PARP was upregulated after 12 h of CC-885 treatment by 20.79%, after 24 h by 26.82%, after 48 h of treatment by 3.61% and after 72 h by 20.21% compared to DMSO vehicle control (Figure 23 C). In cell line HCT116 PARP cleavage was increased after 12 h of CC-885 treatment by 11.37%, after 24 h by 32.23% and after 48 h of treatment by 25.54% compared to DMSO vehicle control (Figure 23 D).

This data indicates, that CC-885 treatment might induce apoptosis in PSN1 and HCT116 cells.

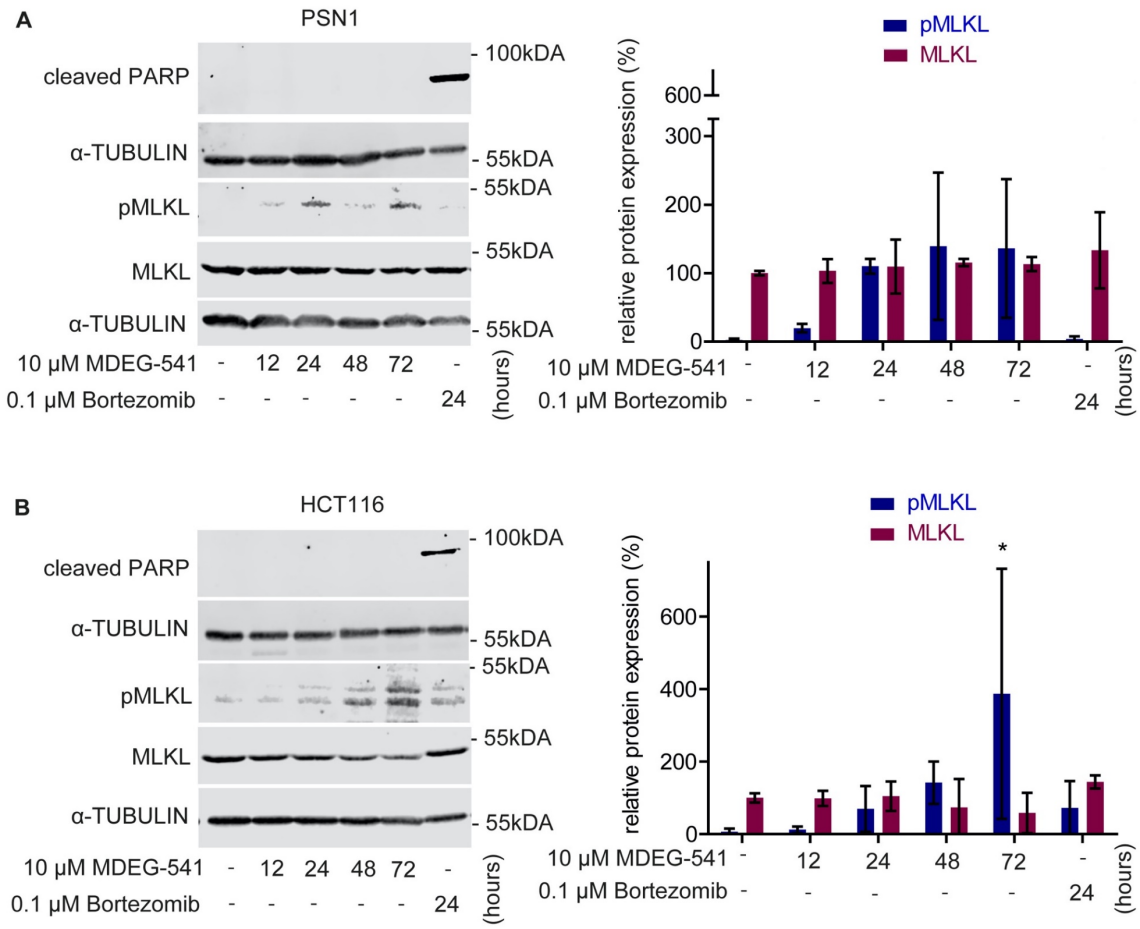

Figure 23: MDEG-541 treatment induced Necroptosis and CC-885 treatment induces Apoptosis

(A) Western blots (Ser358 pMLKL, MLKL and cleaved PARP) and quantification (Ser358 pMLKL, MLKL) after treatment with 10 μM MDEG-541 in the cell line PSN1 (one representative western blot of three biological replicates with exception of cleaved PARP, were one biological replicate was performed) and in the cell line (B) HCT116 (one representative western blot of three biological replicates). Loading control: α-TUBULIN. Data was normalized to DMSO vehicle control. Statistics: One-way ANOVA and Bonferroni´s multiple comparisons test: *p<0.01, **p<0.001, ***p<0.0001.

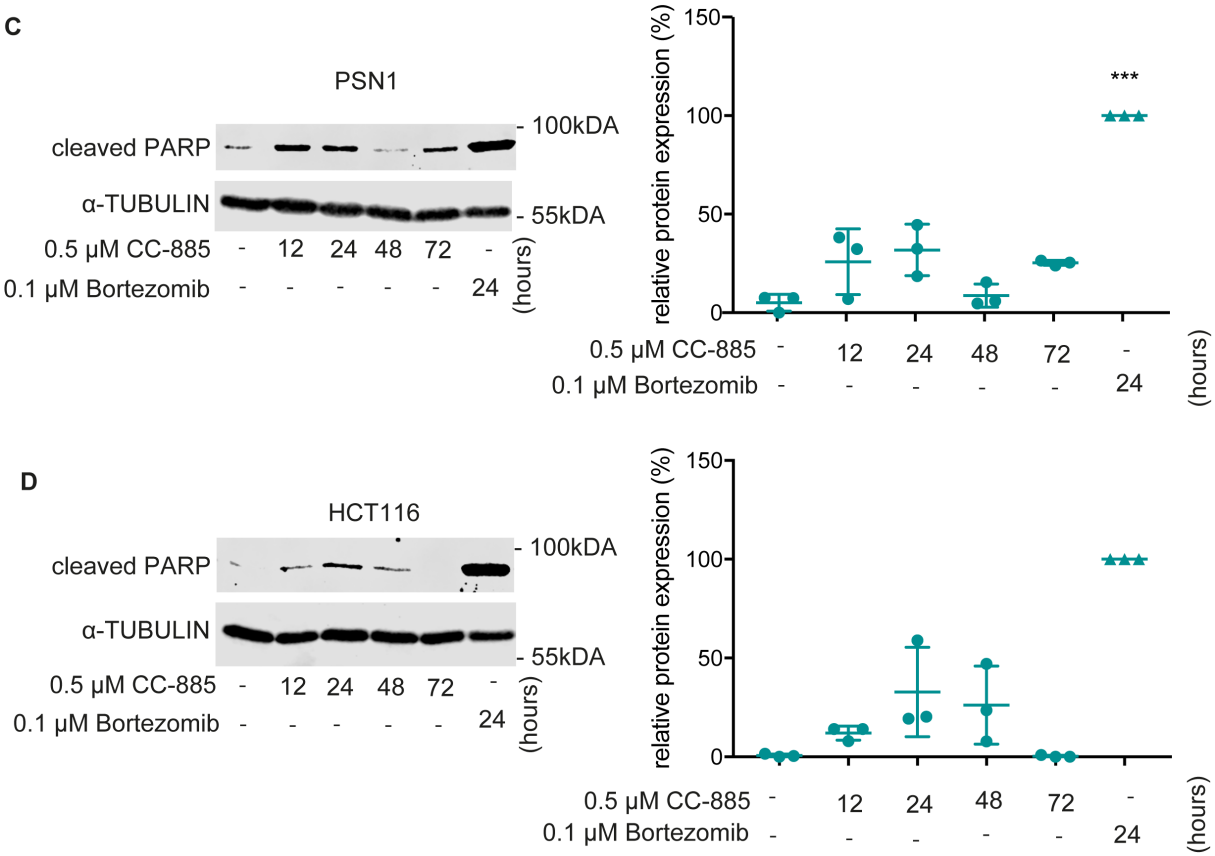

Figure 23: MDEG-541 treatment induces Necroptosis and CC-885 treatment induces Apoptosis

(C) Western blots and quantification of cleaved PARP after treatment with 0.5 µM CC-885 in the cell line PSN1(one representative western blot of three biological replicates) and (D) HCT116 (one representative western blot of three biological replicates). Cells were treated with 10 µM MDEG-541 or 0.5 µM CC-885 for 12 h, 24 h, 48 h and 72 h, with the apoptosis inducing Bortezomib (positive control) for 24 h and DMSO vehicle control. Loading control: α-TUBULIN. Data was normalized to DMSO vehicle control. Statistics: One-way ANOVA and Bonferroni´s multiple comparisons test: *p<0.01, **p<0.001, ***p<0.0001.

10.18 Reduced cell viability in human CRCs and PDAC cell lines as results of MDEG-541 treatment and correlation of cell viability with GSPT1 and CRBN mRNA expression

To examine the reduction of cell viability in the cell lines PSN1 and HCT116 after 72 h of treatment with MDEG-541 in a larger sample size, ten PDAC cell lines (BxPC-3, DANG, HPAC, HUPT3, KP4, MIA PaCa-2, Panc-1, PATU8988S, PATU8988T, PSN1) and seven CRC cell lines (COLO320, HCT116, HT-29, NCI-H716, SW480, SW707, T84) were treated with twelve dilutions of MDEG-541 in a 1:2 dilution ranging from 50 µM to 24 nM.

The GI_{50} of all 17 cell lines was calculated after 72 h MDEG-541 treatment and showed a heterogeneous responsiveness with mean GI_{50} of 15.86 µM ± 13.6 µM (Figure 24 A).

Further comparison of the GI_{50} values of the cells showed a significantly stronger effect of MDEG-541 on PDAC cells lines than on CRC cell lines (Figure 24 C). With a mean GI_{50} of 9.55 µM ± 8.4 µM PDAC cell lines were almost twice as responsive to MDEG-541 *in vitro* than to CRC cell lines with a mean GI_{50} of 22.16 µM ± 13.42 µM.

To find possible explanations for the heterogeneous responsiveness of the cell lines to the treatment with MDEG-541, the GI_{50} were correlated with the gene expression reported in the CCLE database (RRID:SCR_007073).

Gene expression of MYC and GSPT2 CCLE mRNA were not associated with the GI_{50} values of the cell lines (Figure 24 D). That said, the gene expression of GSPT1 was correlated positively with the GI_{50} values after 72 h MDEG-541 treatment in 16 CRC and PDAC cell lines (cell line SW707 was excluded, as no CCLE data was available, Figure 24 F). GSPT1 expression was positively correlated with GI_{50} values, suggesting that a high GSPT1 gene expression is an indicator of a reduced response to MDEG-541 treatment as well as a high GI_{50} value in these cell lines.

Interestingly, the CRBN gene expression was found to be negatively correlated with the responsiveness of the MDEG-541 treated cell lines (Figure 24 D, Supplementary Table 3). Specifically, high CRBN gene expression serves as an indicator of high responsiveness in the cell lines treated with MDEG-541 (Figure 24 E).

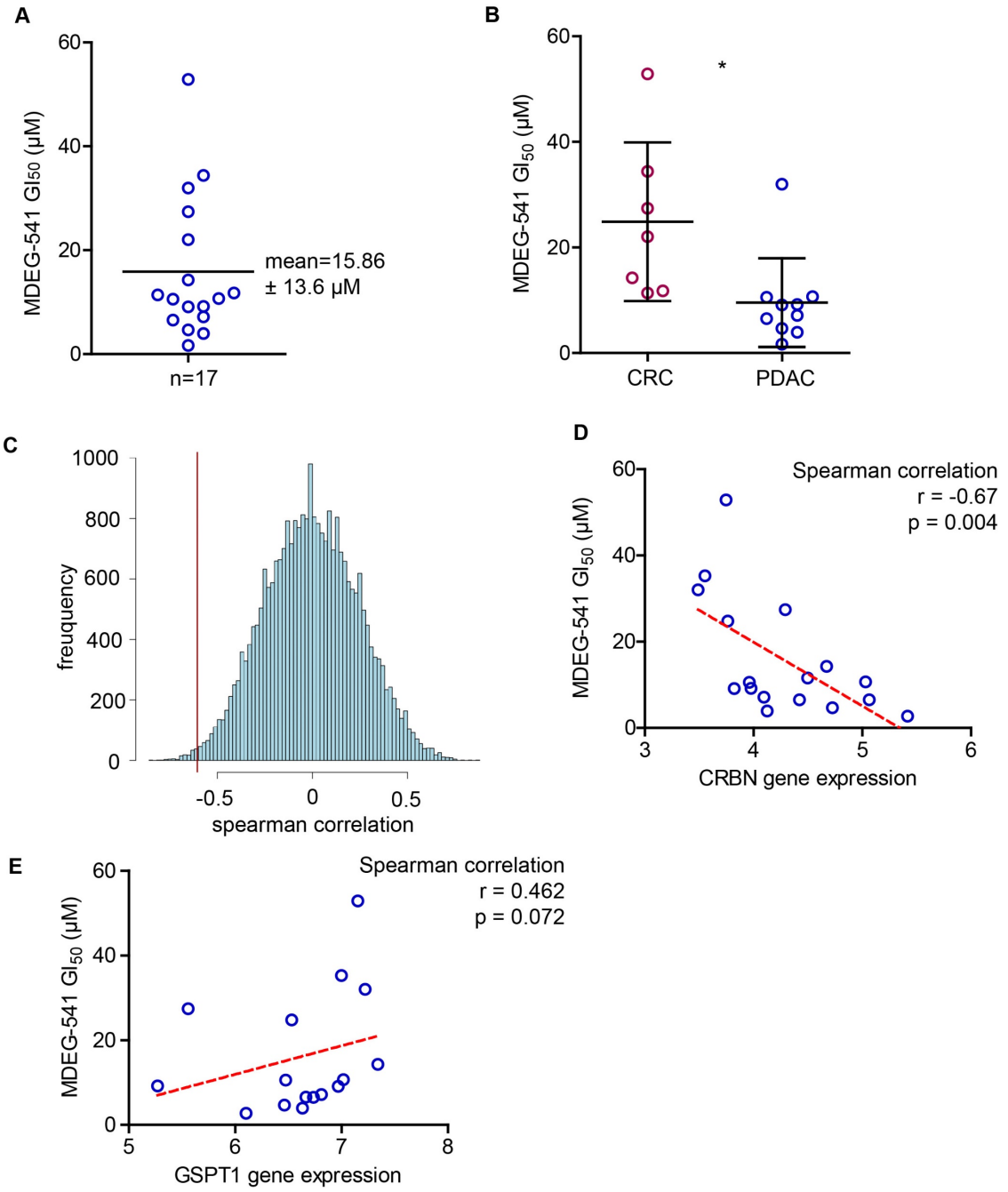

Figure 24: Reduced cell viability in human CRCs and PDAC cell lines as results of MDEG-541 treatment and correlation of cell viability with GSPT1 and CRBN mRNA expression
Cells were treated in a twelve-point two-fold dilution with (A) MDEG-541 (17 cell lines: PDAC cell lines: BxPC-3, DANG, HPAC, HUPT3, KP4, MIA PaCa-2, Panc-1, PATU8988S, PATU8988T, PSN1, Colon cancer cell lines: COLO320, HCT116, HT-29, NCI-H716, SW480, SW707, T84) to calculate the mean 50% growth inhibitory concentration (GI_{50}). GI_{50} values were based on a minimum of three biological replicates. (B) Responsiveness (GI_{50}) of cell lines of the two tumor types CRC and PDAC to MDEG-541 treatment for 72 h. Unpaired two-tailed t-test t(15)=2.547, p=0.0223 *. (C) Distribution frequency of Spearman correlation coefficient of CCLE mRNA expression dataset to the MDEG-541 GI_{50} from 16 cell lines. Cell line SW707 was excluded as no CCLE data was available. CRBN gene expression is indicated as a red bar. (D) Correlation of CRBN mRNA expression and (E) GSPT1 gene expression with the GI_{50} values in 16 human colon and pancreatic cancer cell lines. The Spearman r and the p-value are indicated. Three biological experiments and three technical replicates were analyzed in MTT. Shown is the mean ± SD.

10.19 Reduced cell viability in human organoids as result of MDEG-541 treatment

To verify the results obtained from PDAC cell lines grown in 2D culture (Figure 25) and to further examine the reduction of cell viability after 72 h of treatment with MDEG-541, its effect on patient-derived organoids (3D culture) was determined. Therefore, seven organoids originating from PDAC, namely B140, B169, B188, B203, B211, B250, B226 and one organoid isolated from a cholangiocarcinoma, namely B178, were generated in collaboration with Felix Orben (TUM) as described in the Methods chapter 7.2.2.2. The organoids were compared according to the reduction of cell viability after 72 h MDEG-541 treatment in a 1:2 dilution ranging from 50 µM to 78 nM. The sensitivity of MDEG-541 in organoids was heterogenous and spreads from 1.66 µM (GI_{50}) in the most sensitive organoid B211 to 15.19 µM (GI_{50}) in the organoid B203 (Figure 25 A). MDEG-541 had no effect on the cell viability of organoid B140, thus this organoid was determined to be resistant towards MDEG-541 (Figure 25 C). The responsiveness of organoids after MDEG-541 treatment correlated positively with GSPT1 gene expression (Figure 25 E).

The MYC inhibitor 10058-F4 (treatment control) also reduced the cell viability of organoids while Thalidomide (treatment control) had no effect on the cell viability of organoids. A comparison of the GI_{50} means calculated from all organoids showed a significantly stronger decrease of the cell viability in organoids after MDEG-541 treatment compared to 10058-F4 control treatment (GI_{50} mean MDEG-541: 6.05 µM ± 4.79 µM compared to GI_{50} mean 10058-F4: 18.83 µM ± 10.9 µM, Figure 25 A). Out of two PDAC patient biopsies, cancer-associated fibroblasts were isolated and treated with MDEG-541 to determine a potential therapeutic window. Fibroblasts B336 had a GI_{50} of 66.15vµM, B339 showed a GI_{50} of 72.29 µM.

In summary, the treatment of organoids with MDEG-541 is comparable to the 2D-grown cell lines. Specifically, cells and organoids with low GSPT1 gene expression were sensitive to MDEG-541 treatment.

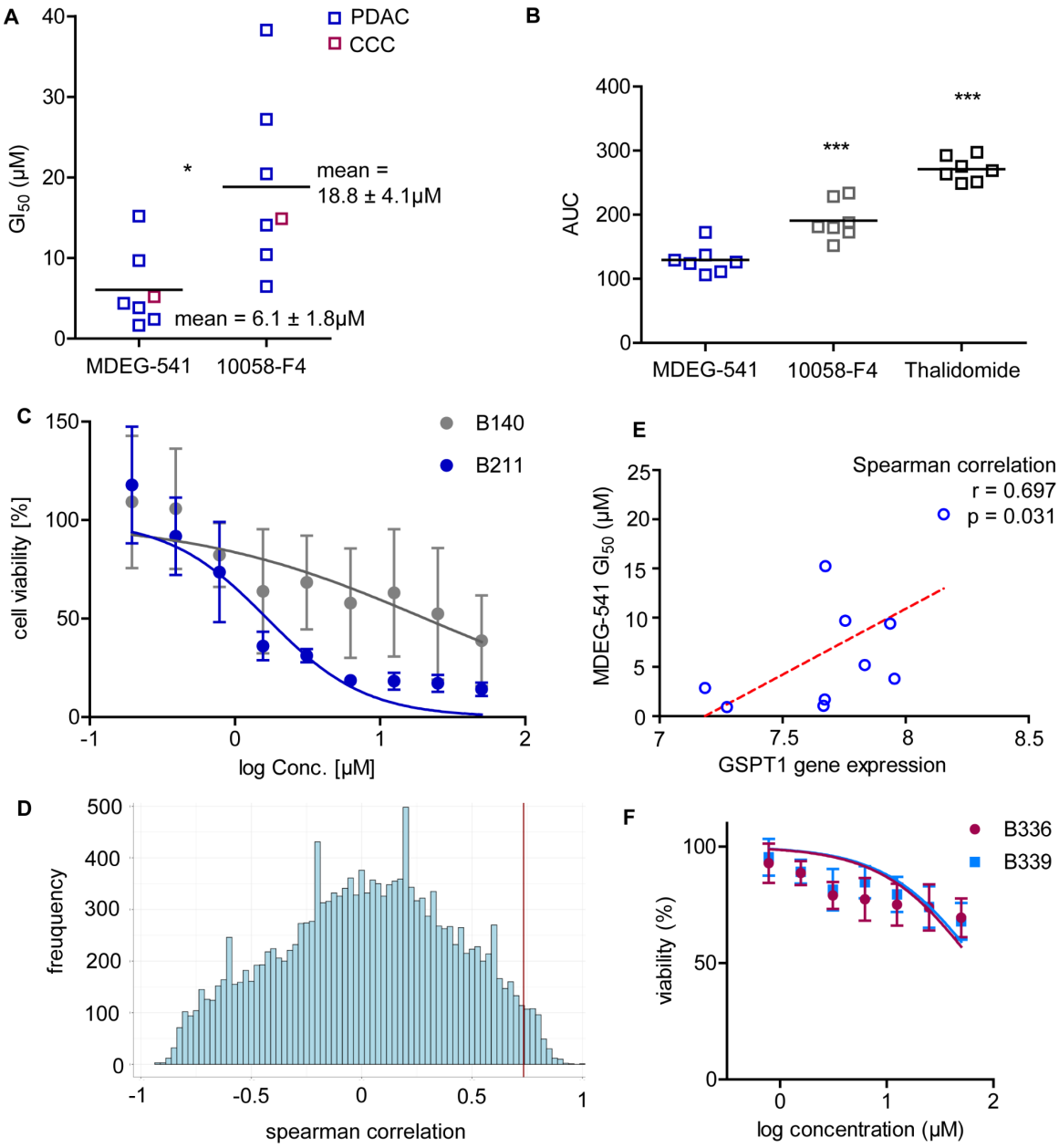

Figure 25: Reduced cell viability in human CRCs and PDAC cell lines as results of MDEG-541 treatment and correlation of cell viability with GSPT1 and CRBN mRNA expression
(A) Growth inhibitory concentration 50% (GI_{50}) of seven gastrointestinal cancer organoids (PDAC: B169, B188, B203, B211, B226, B250, CCC: B178). Organoids were treated in a seven-point 1:2 dilution (range: 50 µM - 78 nM) with MDEG-541 or 10058-F4. The mean GI_{50} is indicated by a line. Statistics: unpaired two-tailed t-test, t(12)=2.841, p=0.0149 *. (B) AUC of gastrointestinal cancer organoids treated in a seven-point 1:2 dilution (range: 50 µM - 0.78 µM) with MDEG-541, 10058-F4 or Thalidomide. (C) Representative dose-response after 72 h of MDEG-541 treatment in the resistant organoid B140 and the sensitive organoid B211. Three biological experiments and three technical replicates were analyzed. Shown is the mean ± SD. (D) Distribution frequency of Spearman correlation coefficient of mRNA expression correlated to the MDEG-541 GI_{50} from nine organoids. GSPT1 gene expression is indicated as a red bar. (E) GSPT1 gene expression correlated with the GI_{50} values in nine organoids. The Spearman r and the p-value are indicated. (F) GI_{50} of two human cancer associated fibroblasts treated in a seven-point 1:2 dilution (range: 50 µM - 0.78 µM) with MDEG-541. Statistics: The GI_{50} mean was compared by an unpaired t-test, the Spearman r and the p-value are indicated.

11. DISCUSSION

Targeting the transcription factor MYC has been a scientific challenge for decades. Due to its intrinsically disordered structure, MYC is still considered as ‘undruggable’ (Chen et al., 2018), although there are novel promising approaches, which seem to overcome this ‘undruggability’ (Puvvula and Moon, 2021). Therefore, it was the aim of this work to use the PROTAC technology to target oncogene MYC in cancer.
This thesis provides a detailed characterization of a novel PROTAC called MDEG-541, which is based on the E3-ligase-binder Thalidomide and a small molecule MYC/MAX-binder 10058-F4, in CRC and PDAC cells. MDEG-541 was shown to target MYC protein and MYC signaling as well as GSPT1/2 and PLK1, which leads to the induction of necroptosis.

11.1 The CRBN recruiter Thalidomide

The E3-ligase CRBN was chosen from the pool of over 300 E3-ligases in human cells, since CRBN is ubiquitously expressed in human tissue making it a promising approach for tumors occurring in all human tissues (Higgins et al., 2004; Xin et al., 2008). Moreover, CRBN expression was upregulated in multiple cancer types, for instance, lymphoma and multiple myeloma, which might result in an increased efficiency of the PROTAC in cancer tissue with elevated CRBN expression (Safran et al., 2010). The immunomodulatory drug Thalidomide from the phthalimide family was shown not to inhibit but to recruit and stabilize CRBN and was therefore chosen as E3-ligase binding moiety in the PROTAC design (Winter et al., 2015).

Seven proteins were observed to be strongly downregulated in a proteome analysis after 4 hours of MDEG-541 treatment (Figure 9 A). Two of these proteins, GSPT1 and GSPT2, are phenotypically relevant off-target of phthalimide-based heterobifunctional degraders (Gao et al., 2020). This restriction to specificity might be caused by the individual structure of the PROTAC (Figure 8 A) and can be considered as one of the greatest limits of the MDEG-541 investigated in this work. Also, other groups observed off-target activity with PROTACs which were supposed to target, for example, receptor tyrosine kinases (RTKs) (Ishoey et al., 2018) or MDM2 (Yang et al., 2019).

A comparison of the Thalidomide-binder showed that in MDEG-541, the Thalidomide-binder differs in one oxygen double bond compared to the promiscuous receptor

kinase inhibitors (Ishoey et al., 2018). Both variants resulted in the degradation of GSPT1 (Figure 8-13). Conversely, proteomics analysis of the phthalimide-based PROTAC showed, that dBET1 did not degrade GSPT1 or GSPT2 (Winter et al., 2015). A closer look at the structure of this PROTAC indicated that in MDEG-541, the Thalidomide-moiety is linked at the 4th position of the phenol-ring to the octylene linker with an oxygen-double bond. In contrast to these observations with MDEG-541, the dBET1 PROTAC presented in Winter et al. (2015) was connected at the 2nd position of the phenol-ring to a single- and double-oxygen bond. This data suggests that the position of the linker at the phenol-ring of Thalidomide might influence the mode of action of the degrader rather than the derivatives attached to the Thalidomide ligand (Wang et al., 2020b).

Moreover, other heterobifunctional degraders based on Pomalidomide did not degrade GSPT1 or GSPT2. Instead, Yamamoto et al. (2020) could show a degradation of the AT-Rich Interaction Domain (ARID2) by using a PROTAC with a Pomalidomide-binder (Yamamoto et al., 2020). Interestingly, ARID2 also plays a role in transcriptional regulation of target genes including MYC. Consequently, Pomalidomide-treatment inhibited the expression and proliferation of MYC. A recent publication showed that depletion of ARID2 impairs DNA repair, thereby facilitating the proliferative and metastatic potential of the cells and that suggested ARID2 as a tumor suppressor in lung cancer (Moreno et al., 2020). This data suggests a Pomalidomide-moiety for PROTACs as promising approach to expand the spectrum of PROTACs indirectly targeting MYC. Consequently, both compounds, the Pomalidomide-PROTAC and the Thalidomide- degrader MDEG-541, might have off-targets which result in the downregulation of MYC protein in treated cells.

Recently, it was demonstrated that the CELMoD CC-885 ubiquitinates and degrades the cell cycle promoting kinase PLK1 (Li et al., 2020). Therefore, the effect of MDEG-541 on PLK1 protein expression was examined. Indeed, MDEG-541 treatment decreased PLK1 protein expression in a dose-dependent manner in this thesis (Figure 8). Since PLK1 was shown to regulate protein expression of MYC family members, we investigated if the inhibition of PLK1 via Volasertib could downregulate MYC protein expression in PSN1 and HCT116 cells (Ren et al., 2018; Tan et al., 2013; Wang et al., 2021; Xiao et al., 2016). Indeed, the results indicated a downregulated of MYC upon treatment with Volasertib. Since, MDEG-541 was also shown to decrease PLK1 protein

expression these data might give a hint that PLK1 could act as a neo-substrate of CRBN which also effects MYC protein expression. However, it must still be examined in the future if MDEG-541 is directly degrading MYC as a PROTAC or if PLK1 or other targets of MDEG-541 are affecting the molecular and cellular outcome of these treated cells.

We observed a wide-spread distribution of GI_{50} values after MDEG-541 treatment in all 17 tested PDAC and CRC cancer cell lines indicating a heterogeneity in their responsiveness (Figure 24). Sensitivity after MDEG-541 treatment varied from a GI_{50} of 2.72 µM in the most sensitive cell line KP4, to reduced sensitivity in cell line SW480 with a GI_{50} of 27.43 µM and the most resistant tested cell line NCI-H716 with a GI_{50} of 52.87 µM. This high grade of heterogeneity indicated that under specific genetic context, cell lines show different responses towards MDEG541 treatment. Indeed, it was shown in this work that increased *CRBN* gene expression correlated with increased sensitivity of 17 PDAC and CRC cell lines after MDEG-541 treatment (Figure 24). A similar observation was made by Otto et al. (2019) with CRC cell lines treated with the dBET1 PROTAC, where they showed that the cell line SW480, which was resistant to dBET1 treatment, had low CRBN mRNA levels (Otto et al., 2019). This data supports our results that CRBN is required for the activity of Thalidomide-based bifunctional degraders and low levels of *CRBN* might associated with resistance to these PROTACs.

To verify our results in a preclinically relevant model, we tested several patient-derived organoids with MDEG-541. Again, differences in the efficacy of MDEG were observed. Interestingly, the correlation with CRBN expression could not be confirmed here. Further analysis with similar model systems and an expansion of the cohort number would be required to analyze this result in a more robust way. Also, specific mutations or expression levels of other genes in patient-derived-organoids (PDOs) might diminish a correlation of CRBN expression with responsiveness after MDEG-541 treatment. Actually, it was shown in this thesis that the gene expression level of GSPT1 correlated positively with responsiveness after MDEG-541 treatment of PDOs. These results were also reproduced with the 17 tested PDAC and CRC cell lines, demonstrating a significant correlation of GI_{50} values with GSPT1 gene expression (Figure 24 E) underlining the possibility of other factors than CRBN expression level influencing the cellular and molecular effects of MDEG-541 on the treated cells.

Using MDEG-541 to degrade MYC together with the well-known neo-targets of phthalimide-binders, GSPT1/2, and oncogene PLK1, offers a novel targeting strategy and might provide an additional advantage compared to degrading MYC alone. Increased GSPT1 expression has been repeatedly reported to be associated with multidrug resistance and a worse clinical prognosis. Recently, a chemo-resistance to cisplatin in lung cancer stem cells was observed together with transcriptional activation of GSPT1 (Li et al., 2020) while in breast cancer the expression of GSPT1 was associated with resistance against docetaxel and paclitaxel (Arai et al., 2008). Furthermore, GSPT1 is associated with gastrointestinal cancer (Brito et al., 2005). Therefore, targeting GSPT1, GSPT2, PLK1 and, oncogene MYC might provide an improved degrader to treat cancer and specifically PDAC, a cancer with a dismal prognosis and a lack of promising targeting options (Orth et al., 2019).
To design a PROTAC not targeting GSPT1 and GSPT2 or other potential off-targets, a chemical modification of the E3-ligase-binder or a replacement of Thalidomide with another E3-ligase-binder might be considered to increase selectivity, reduce the effect on potential off-targets, and the risk of side effects and toxicity. Promising E3-ligases include Von-Hippel-Lindau (VHL), mouse double minute 2 homolog (MDM2) or other inhibitors of apoptosis proteins (IAPs). VHL is the most popular E3-ligase recruited by PROTACs (Girardini et al., 2019) and was found to be more selective than CRBN-based PROTACs (Bondeson et al., 2018).

In conclusion, it was shown that a subgroup of gastrointestinal cancer characterized by higher GSPT1 gene expression levels was more sensitive towards MDEG-541 treatment then cancer cells and PDOs with lower GSPT1 gene expression. Moreover, MDEG-541 is limited regarding its selectivity towards MYC which might be explained by off-target effects caused by the E3-ligase recruiter Thalidomide or the linker positioning.

11.2 The 10058-F4 moiety

As the transcription factor, MYC is dependent on heterodimerization with MAX to bind its targets and inhibiting the MYC/MAX heterodimerization domain is a conceivable approach to directly target MYC. In this thesis, 10058-F4 was chosen as binding moiety of MDEG-541, since it was shown to reduce MYC protein expression, inhibit MYC/MAX interaction and induce apoptosis in the MYC amplified acute myeloid leukemia (AML) cell line HL-60 (Xu et al., 2001).

To test if the 10058-F4 binding moiety is necessary for the cellular activity of MDEG-541, the compound 619 was synthesized, containing Thalidomide and the linker, but lacking the 10058-F4 binding moiety. Compound 619 failed to reduce MYC and GSPT1 protein expression compared to MDEG-541. However, the downregulation of GSPT2 protein after 619 treatment indicates an increase of specificity compared to MDEG-541. The compound MDEG-541 outperformed compound 619 in reducing cell viability, indicating that cellular activity and MYC regulation might be dependent on an additional neo-substrate of the E3-ligase CRBN. Further, it could be tested in the future if a different linker length or design coupled to Thalidomide could induce similar molecular activity as MDEG-541 with the 100058-F4 binding moiety.

In addition, another MYC/MAX heterodimerization inhibitor active at lower concentrations could be chosen as MYC binding moiety in prospective works to increase the efficiency of MDEG-541. In the near future PROTACs with the MYC inhibitor EN4 are under design and are going to be tested.

11.3 The linker between 10058-F4 and Thalidomide

A linker with eight alkyl groups connects 10058-F4 with Thalidomide in MDEG-541 (Figure 8 A). Measurement of the cell viability showed that MDEG-541 is more potent to reduce cell viability in PSN1 and HCT116 cells compared to 10058-F4, Thalidomide and DMSO vehicle control (Figure 17). Potential MDEG candidates with other linker lengths between 10058-F4 and Thalidomide failed to reduce cell viability and MYC protein level with a comparable potency as MDEG-541 and were consequently not considered as promising MDEGs (Figure 7).

In 2011, a PROTAC was published targeting estrogen receptor α (ERα), indicating a significant effect of the linker length on the efficacy of the PROTAC (Cyrus et al., 2011). The work group of Craig Crews pointed out the importance of the PROTAC linker length and distinct linker attachments, since their VHL-based PROTAC recruited the E3-ligase differentially, resulting in the degradation of different subunits of the POI (Smith et al., 2019). Specifically, they could show that the formation of a ternary complex and the protein-protein interaction between the PROTAC, the POI and the E3-ligase was driving the selectivity of the PROTAC (Bondeson et al., 2018). Therefore, it could be examined in the future if other linker designs than the once tested for the PROTAC in this work, could increase its selectivity.

11.4 Cell fate of MDEG-541-treated cells

The data in this work indicated, that treatment with MDEG-541 might inhibit the cell cycle in cells (Figure 20). Since MYC, GSPT1/2 and PLK1 are associated with cell cycle progression, their downregulation due to MDEG-541 treatment could also contribute to the growth arrest of these treated cells (García-Gutiérrez et al., 2019). Together, the general knowledge of cell cycle regulation by PLK1, MYC and GSPT1/2 emphasize the observed MDEG-541-mediated regulation of cell cycle.

The transcription factor MYC does not only play a key role in cell proliferation, but also in cell death. Both, the inhibition of MYC with 10058-F4 as well as the degradation of GSPT1 with CC-885 were shown to induced apoptosis before and in this work (Figure 23, Dang et al., 2005; Matyskiela et al., 2016). Moreover, the treatment with MDEG-541 was shown to induce unfolded protein response (UPR, Figure 21) and cell death in the cell lines PSN1 and HCT116 tested in this thesis (Figure 22 and 23). Usually, UPR is induced upon endoplasmatic reticulum (ER) stress in the cell to restore homeostasis. Due to prolonged exposure to stress, the cell is insufficient to restore homeostasis inducing cell death (Saveljeva et al., 2015). However, it needs to be determined in future experiments, if MDEG-541-mediated cell death might actually be induced by an UPR.

Specifically, the treatment with MDEG-541 suggests that cell death might be induced via necroptosis in PSN1 and HCT116 cells (Figure 22 and 23). Similar to apoptosis, necroptosis is a mode of programmed cell death which is often encouraged when caspase-8 induced extrinsic apoptotic cell death is inhibited (Sun et al., 1999). Once necroptosis is induced by TNF-α, death receptor or interferon, receptor-interacting serine/threonine-protein kinase 1 and 3 (RIPK1 and RIPK3) heterodimerize and promote the oligomerization of MLKL by phosphorylation. GSEA analysis of RNA seq data after MDEG-541 treatment showed a significant enrichment of TNF-α Hallmark gene set signaling in HCT116 cells (Figure 19). Furthermore, an upregulation of phosphorylated MLKL was observed after treatment with MDEG-541 in PSN1 and HCT116 cells (Figure 23). Both results underline the suggestions that MDEG-541 treated cells might undergo necroptosis.

GSPT1 is associated with apoptosis when a normal cell undergoes stress. The calpain protease was shown to mediate the proteolytic cleavage of GSPT1 at Ala73 into p-eRF3 upon exposure to ER stressors (Hashimoto et al., 2015). This processed isoform

with a specific IAP-binding motif inhibits IAPs such as cIAP1, cIAP2 and XIAP, to release active caspases and promote apoptosis (Hashimoto et al., 2014). Here, the MDEG-541-mediated degradation of GSPT1 might prevent the calpain-induced degradation of GSPT1 into p-eRF3 with a functional IAP-binding motif and instead favors its proteolysis into an overall dysfunctional protein. Consequently, this could prevent the binding and inhibition of IAPs by p-eRF3 and blocks caspase-induced programmed apoptosis. Since apoptosis might be blocked and the treatment with MDEG-541 induces stress to the cells, this could pressure the MDEG-541 treated cells to undergo necroptosis. To validate this hypothesis p-eRF3 expression after MDEG-541 treatment should be examined in future experiments.

Little is known so far about an involvement of MYC or GSPT1 in necroptosis. In 2020, Seong and colleagues detected a direct interaction of MYC and RIPK3 that prevents heterodimerization with RIPK1 (Seong et al., 2020). The work group could show that depletion of MYC induced the expression of key players in necroptosis, which enhanced antitumor activity *in vivo*. Furthermore, TNF-α–dependent induction of necroptosis degraded MYC dependent on the proteasome (Seong et al., 2020). This data might give a hint that MDEG-541, which induces necroptosis after 12 h of treatment, could further facilitate the degradation of MYC.

In addition, the inhibition of PLK1 is not only associated with apoptosis but also with necroptosis. The PLK1 inhibitor BI2536 was shown to induce mitotic catastrophe, leading to necroptotic cell death in androgen-insensitive prostate cancer cells emphasizing the observed effect of MDEG-541 on cell fate (Deeraksa et al., 2013).

In conclusion, this data underlines the previously described observation of MDEG-541 treatment on the cell cycle (Figure 20), which might be driven by the degradation of GSTP1/2, the reduction of PLK1 protein level and/or the downregulation of MYC, which subsequently may have effects on MYC downstream signaling.

11.5 Potential risks of targeting GSPT1/2, PLK1 and MYC with MDEG-541

Downregulating MYC should be examined critically as MYC plays a central role in cell physiology (Stefan and Bister, 2017). Thus, the inhibition or degradation of MYC can potentially cause serious side effect in patients by interfering with proliferation and cell growth, not only in cancerous cells but also in healthy tissue. Soucek and colleagues

(2008) assessed in a preclinical mouse model of Ras-induced, non-small-cell lung cancer that systemic MYC inhibition by the inducible dominant negative MYC variant Omomyc led to serious alterations in highly proliferative tissue. Interestingly, these serious effects were well tolerated over extended periods of time and completely reversible (Soucek et al., 2008). The results were later confirmed in gliomas and pancreatic islet tumors (Annibali et al., 2014; Sodir et al., 2011). This *in vivo* data suggests that targeting oncogene MYC in cancer tissue with MDEG-541 might also affect MYC in healthy tissues resulting in side effects. However, these side effects might be reversible when MDEG-541 is withdrawn as demonstrated with Omomyc. Moreover, the metronomic inhibition of MYC in mice with a genomically instable TP53-deficient background, led to a complete tumor regression. Even after one year those mice were alive without any tumor recurrence or resistance (Soucek et al., 2013). This data indicates that the MDEG-541 approach might not be limited *in vivo* by resistance mechanisms. Nevertheless, MDEG-541 was not only shown to decrease MYC protein but also PLK1, GSPT1/2 and 107 other proteins (Figure 9 A).

The GSPT1 degrader CC-885 showed significant toxicities associated with various off-targets, limiting its clinical development (Hao et al., 2020; Li et al., 2020). Therefore, *in vivo* experiments should be performed with MDEG-541 to examine possible side effects and resistance mechanisms, especially as GSPT1/2 depletion has not been examined *in vivo* at all. The examination of all downregulated proteins in the proteome analysis was out of the scope of this work, but should be examined in future experiments.

11.6 Future perspective

In 2019, the first PROTAC (ARV-110 by ARVINAS) targeting the androgen receptor went into phase I/II clinical trials to treat prostate cancer (Mullard, 2019). The same company is currently testing the ER+/HER2-targeting PROTAC ARV-471 in a clinical trial to treat breast cancer. First results from these clinical trials are expected to be published in 2022/2023 (NCT04072952, NCT03888612).

Furthermore, Laura Soucek, who founded peptomyc and worked on Omomyc since the 90ies, started to treat the first patient with Omo-103 in a clinical phase I/II trial (NCT04808362) in 2021 (Massó-Vallés and Soucek, 2020). If clinical trials fulfill expectations, the first direct MYC inhibitor could be available to patients to treat multiple cancer types in the near future.

Through new technologies, such as PROTAC and further development of synthetic peptides, a new generation of inhibitors is being developed that will make the ‘undruggable’ status for MYC obsolete and may find entry into clinical use in the next few years.

12. APPENDIX

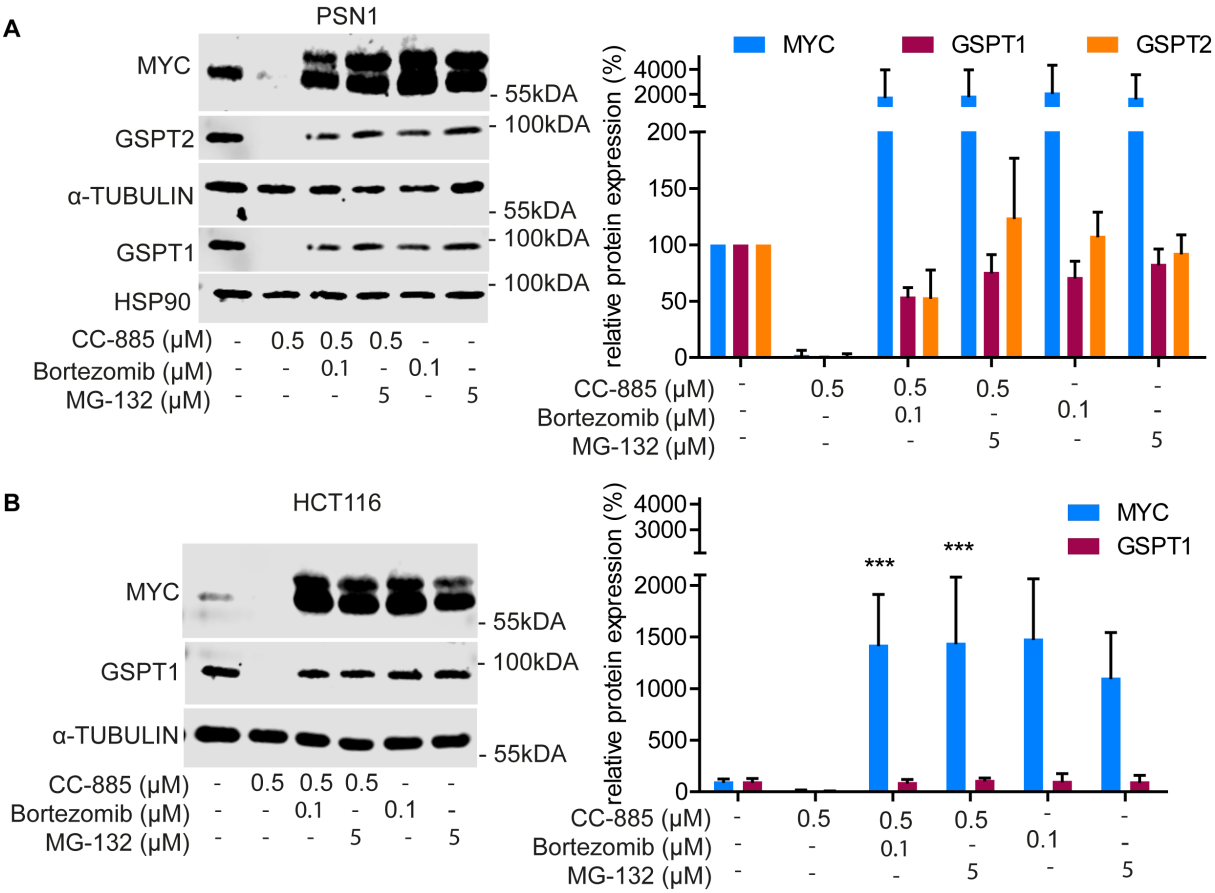

Supplementary Figure 1: Inhibition of the proteasome prevented MDEG-541-mediated degradation of MYC, GSPT1 and GSPT2

Western blot of MYC, GSPT1 and GSPT2 and quantification of cell lines (A) PSN1 and Western blot of MYC and GSPT1 and quantification of cell line (B) HCT116 pre-treated for 4 h with proteasome inhibitors Bortezomib (0.1 μM) or MG-132 (5 μM) followed by 20 h treatment with 0.5 μM CC-885 treatment. Shown is one representative western blot of three biological replicates. Cells were treated for 24 h with DMSO vehicle control. Loading control: α-TUBULIN/HSP90. Data was normalized to DMSO vehicle control. Statistics: Two-way ANOVA and Bonferroni´s multiple comparisons test: *p<0.01, **p<0.001, ***p<0.0001.

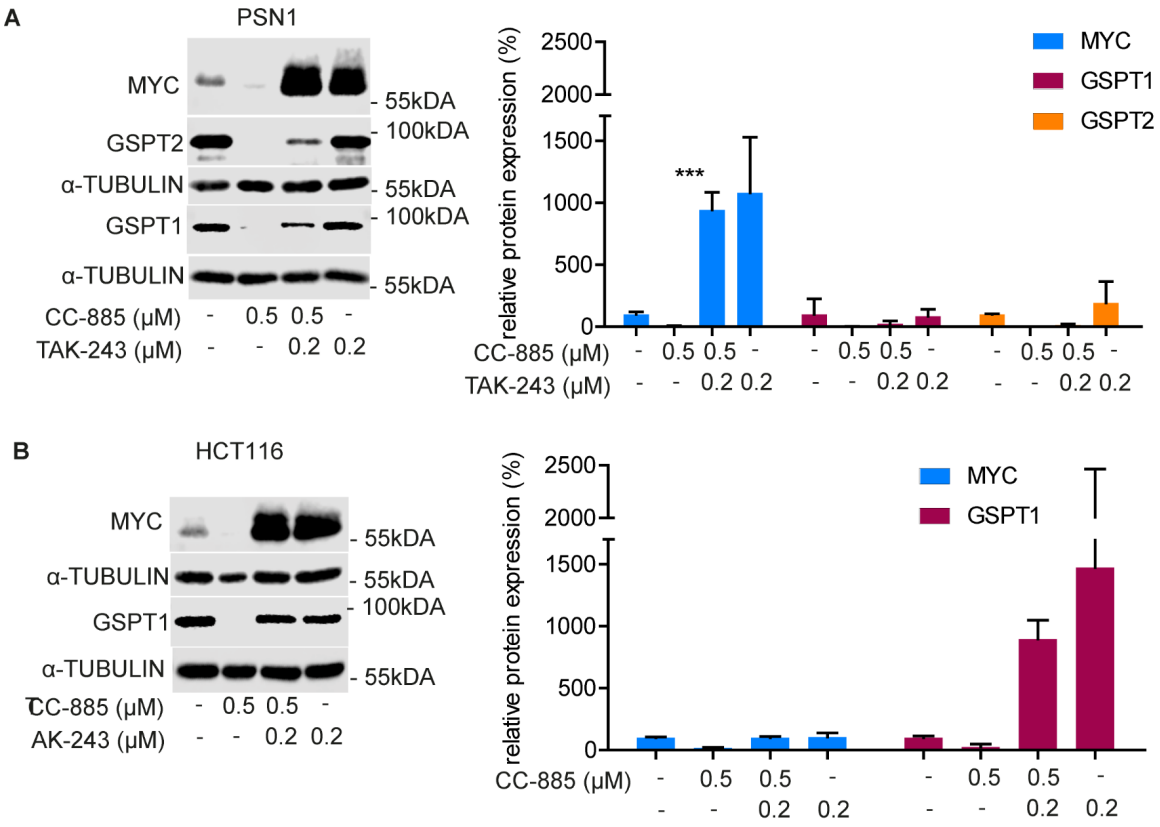

Supplementary Figure 2: Inhibition of ubiquitination prevented CC-885-mediated MYC, GSPT1 and GSPT2 degradation

Western blot of MYC, GSPT1 and GSPT2 and quantification of cell line (A) PSN1 and Western blot of MYC and GSPT1 and quantification of cell line (B) HCT116 pre-treated for 4 h with 0.2 μM of the UAE inhibitor TAK-243 followed by 20 h treatment with 0.5 μM CC-885. Shown is one representative western blot of three biological replicates. Cells were treated for 24 h with vehicle control. Loading control: α-TUBULIN. Data was normalized to DMSO vehicle control. Statistics: Two-way ANOVA and Bonferroni´s multiple comparisons test: *p<0.01, **p<0.001, ***p<0.0001.

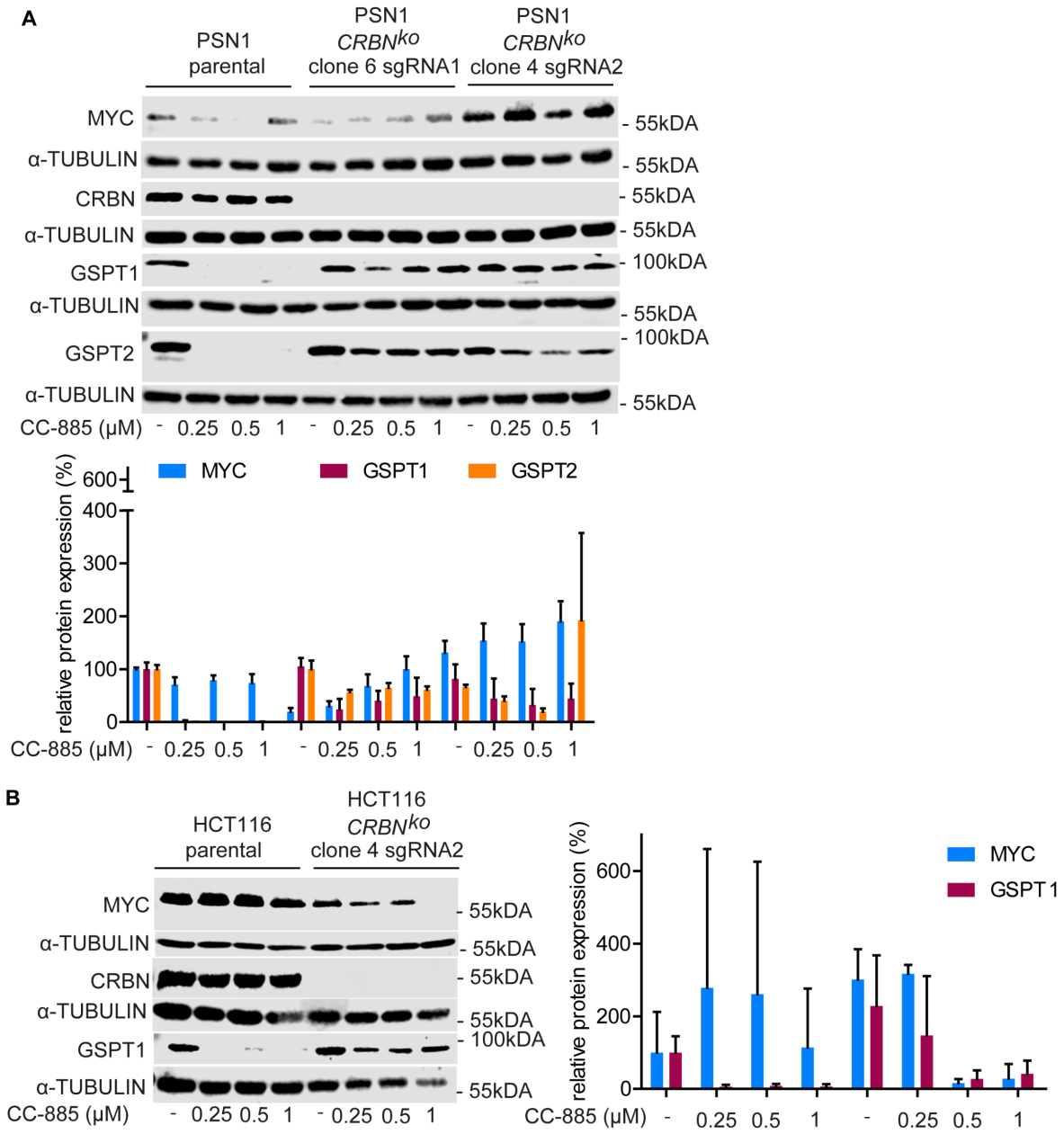

Supplementary Figure 3: Knockout of CRBN E3-ligase prevented CC-885-mediated degradation of MYC, GSPT1 and GSPT2

(A) Western blots and quantification of MYC, GSPT1, GSPT2 and CRBN protein of the CRBN-proficient parental cell line PSN1 and the CRBN-deficient PSN1 clone 6 sgRNA1 and PSN1 clone 4 sgRNA2 cells treated with 0.25 μM, 0.5 μM or, 1 μM of CC-885 for 24 h.

(B) Western blots and quantification of MYC, GSPT1, PLK1 and CRBN protein in the CRBN-proficient parental cell line HCT116 and the CRBN-deficient HCT116 cell clone 2 sgRNA2 treated with 0.25 μM, 0.5 μM or, 1 μM of CC-885 for 24 h. Shown is one representative western blot of three biological replicates. Cells were treated with vehicle control for 24 h. Loading control: α-TUBULIN. Data was normalized to DMSO vehicle control. Statistics: Two-way ANOVA, ns.

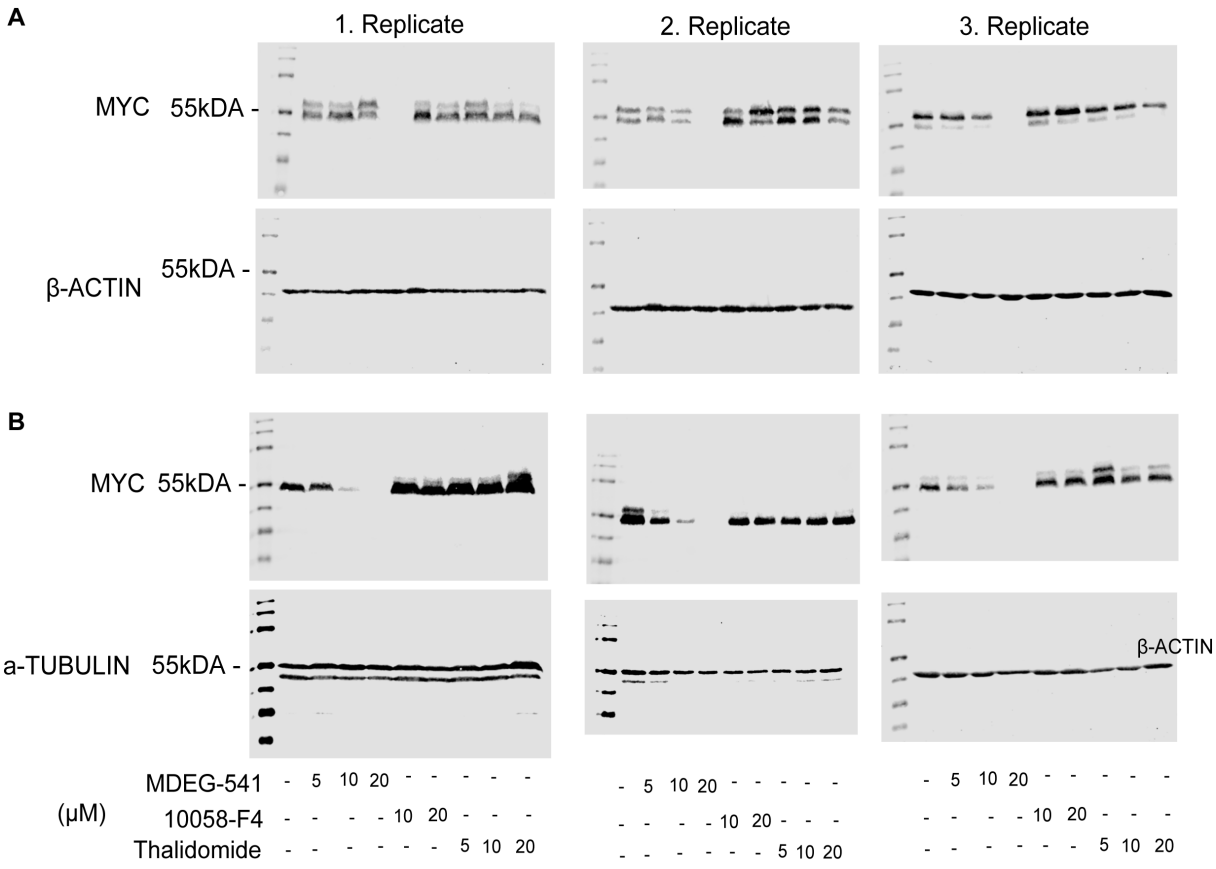

Supplementary Figure 4: Rawdata of western blots according to Figure 8
(A) PSN1 (B) HCT116. For experimental conditions, quantification and statistics, refer to Figure 8.

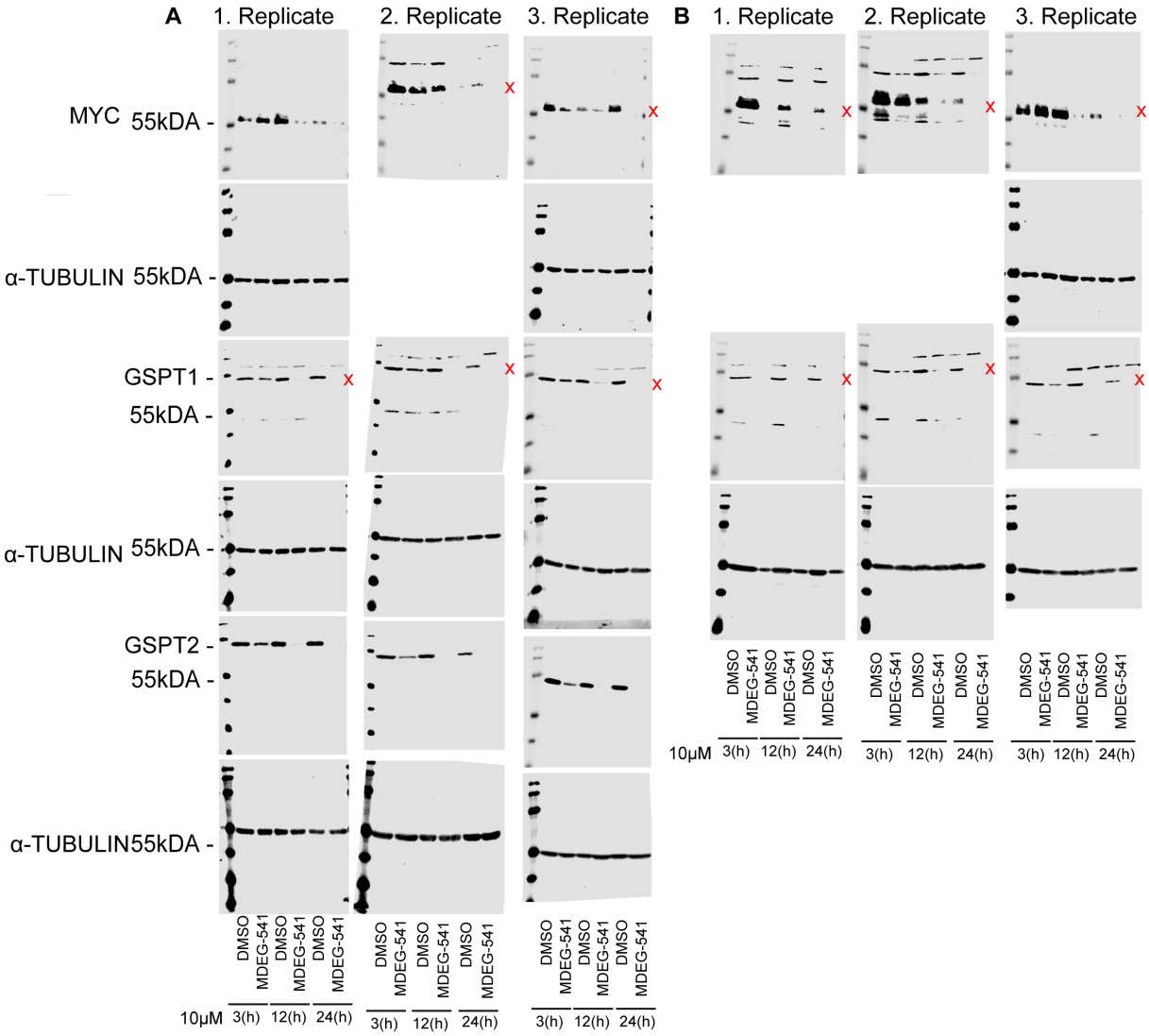

Supplementary Figure 5: Rawdata for western blots according to Figure 9
(A) PSN1 (B) HCT116. The red cross marks the respective protein band. For experimental conditions, quantification and statistics, refer to Figure 9.

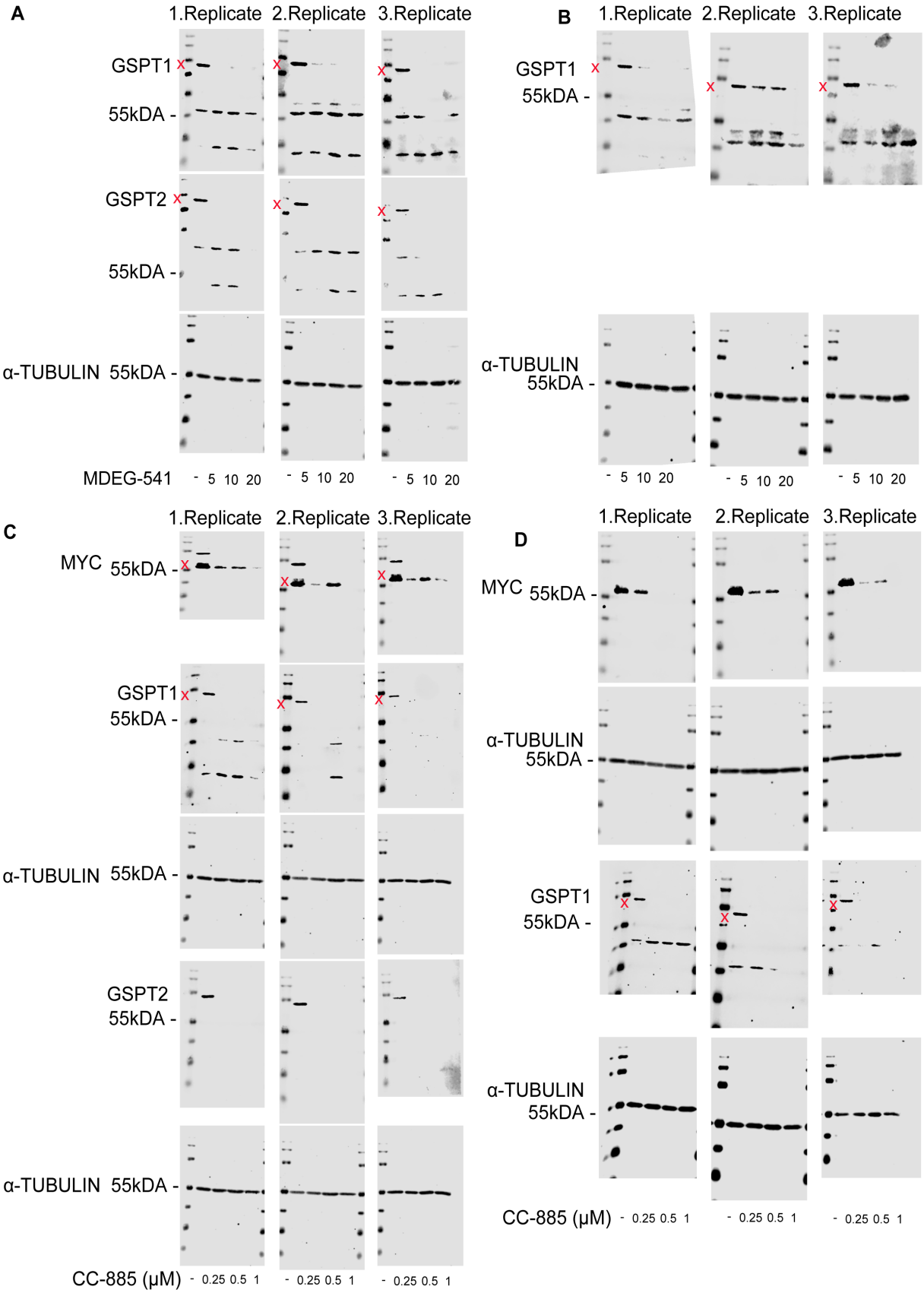

Supplementary Figure 6: Rawdata of western blots according to Figure 10
(A) PSN1 (B) HCT116 (C) PSN1 (D) HCT116. The red cross marks the respective protein band. For experimental conditions, quantification and statistics, refer to Figure 10.

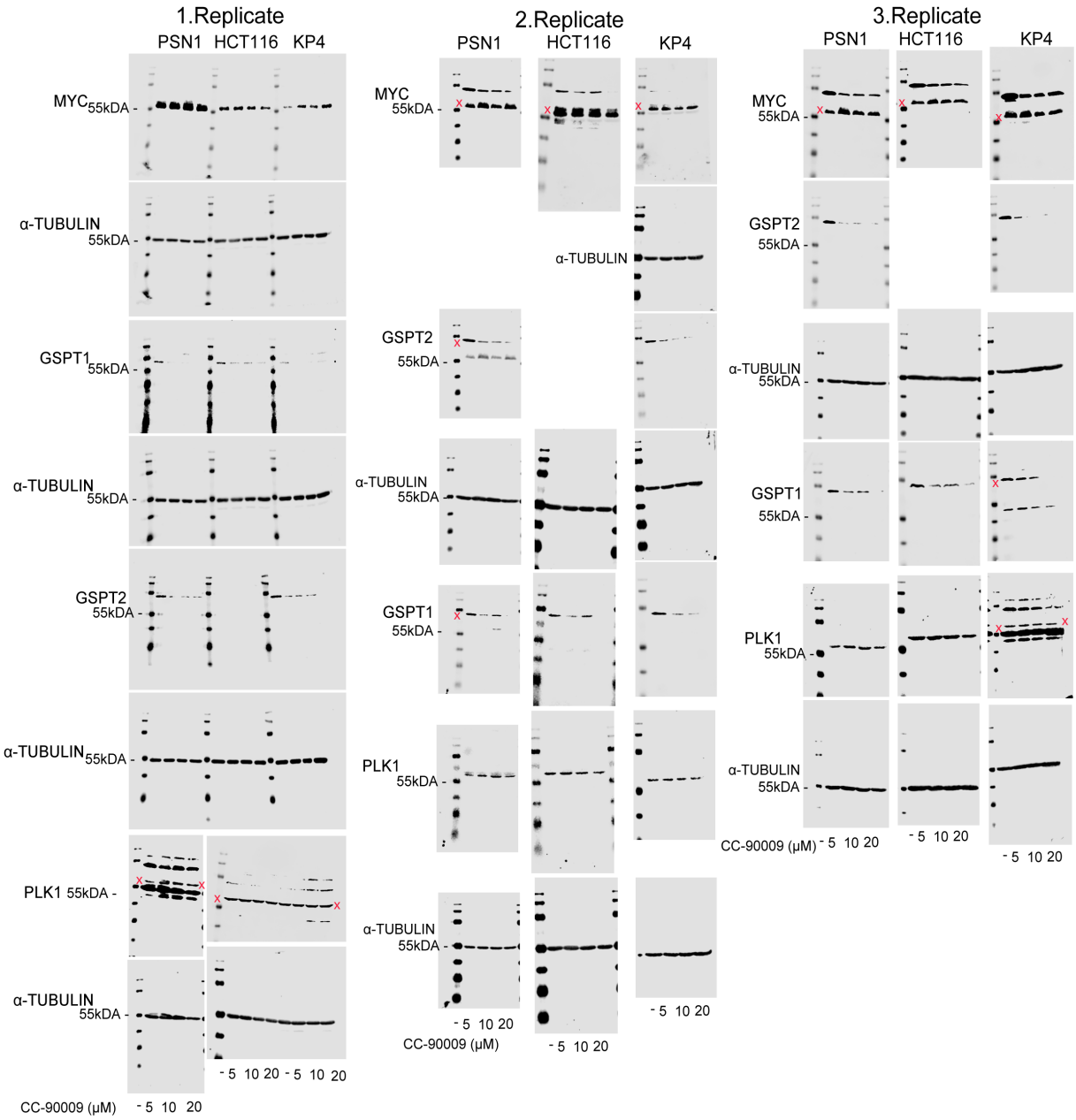

Supplementary Figure 7: Rawdata of western blots according to Figure 11
The red cross marks the respective protein band. For experimental conditions, quantification and statistics, refer to Figure 11.

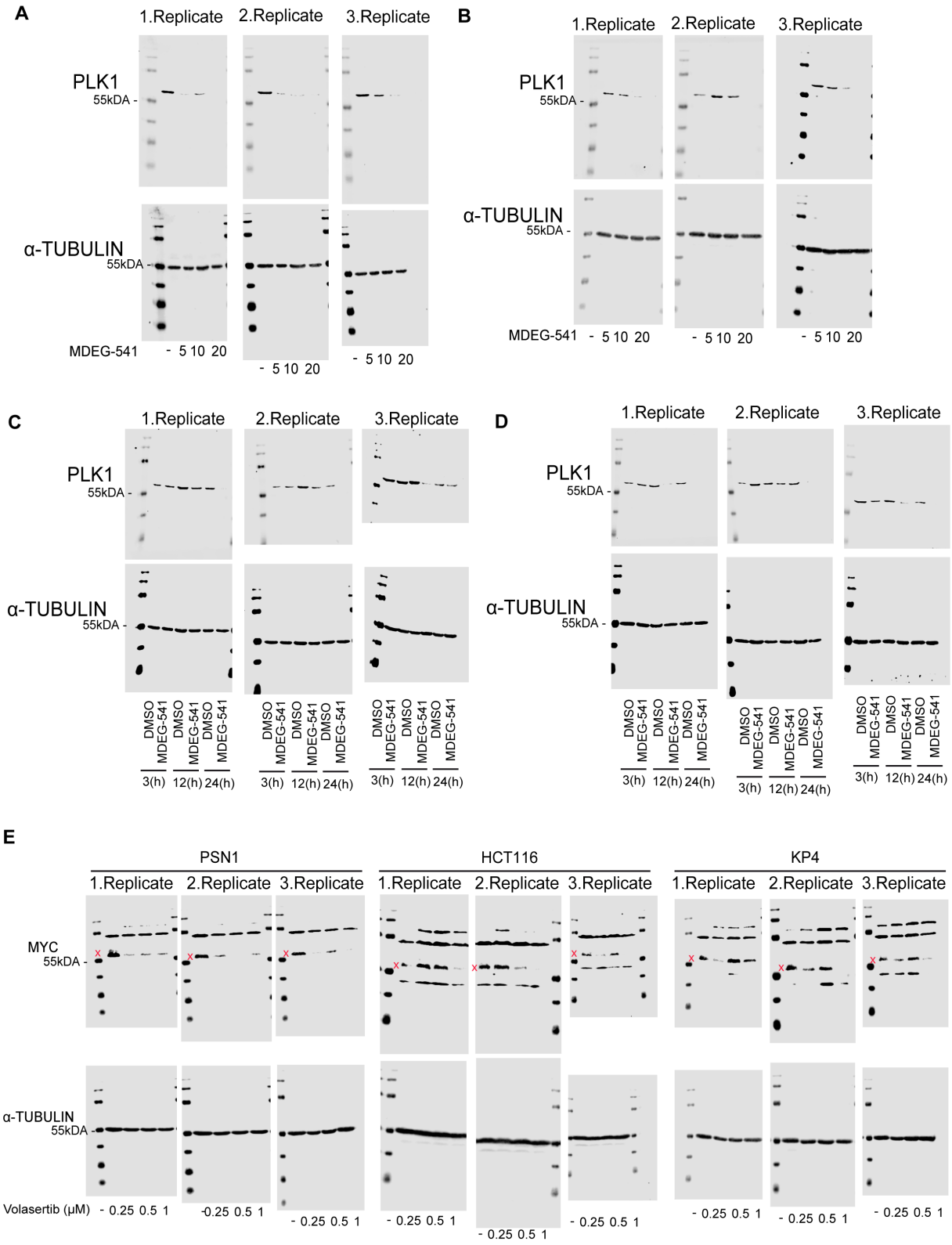

Supplementary Figure 8: Rawdata of western blots according to Figure 12
(A) PSN1 (B) HCT116 C) PSN1 (D) HCT116 (E) PSN1, HCT116 and KP4. The red cross marks the respective protein band. For experimental conditions, quantification and statistics, refer to Figure 12.

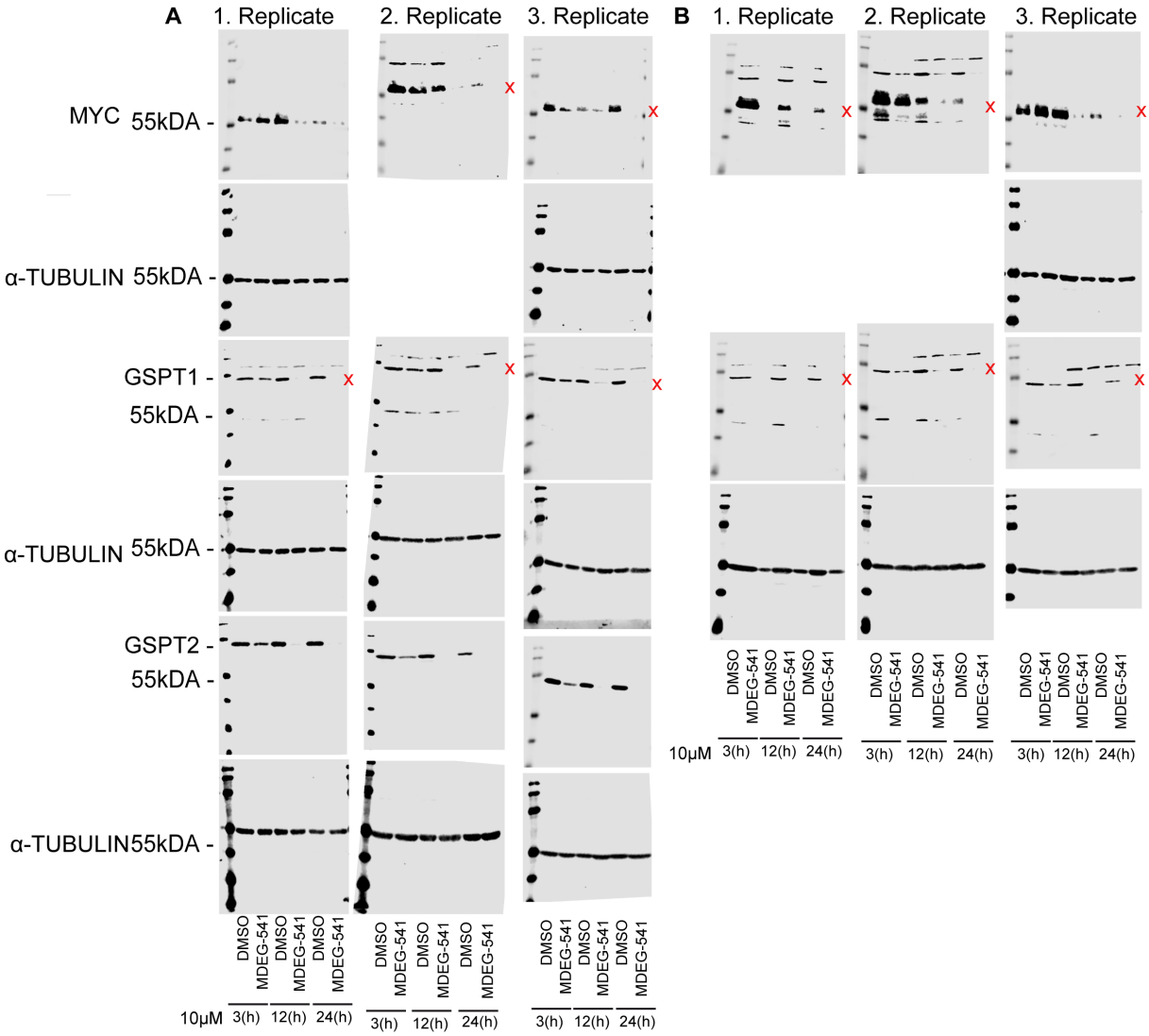

Supplementary Figure 9: Rawdata of western blots according to Figure 13
(A) PSN1 (B) HCT116. The red cross marks the respective protein band. For experimental conditions, quantification and statistics, refer to Figure 13.

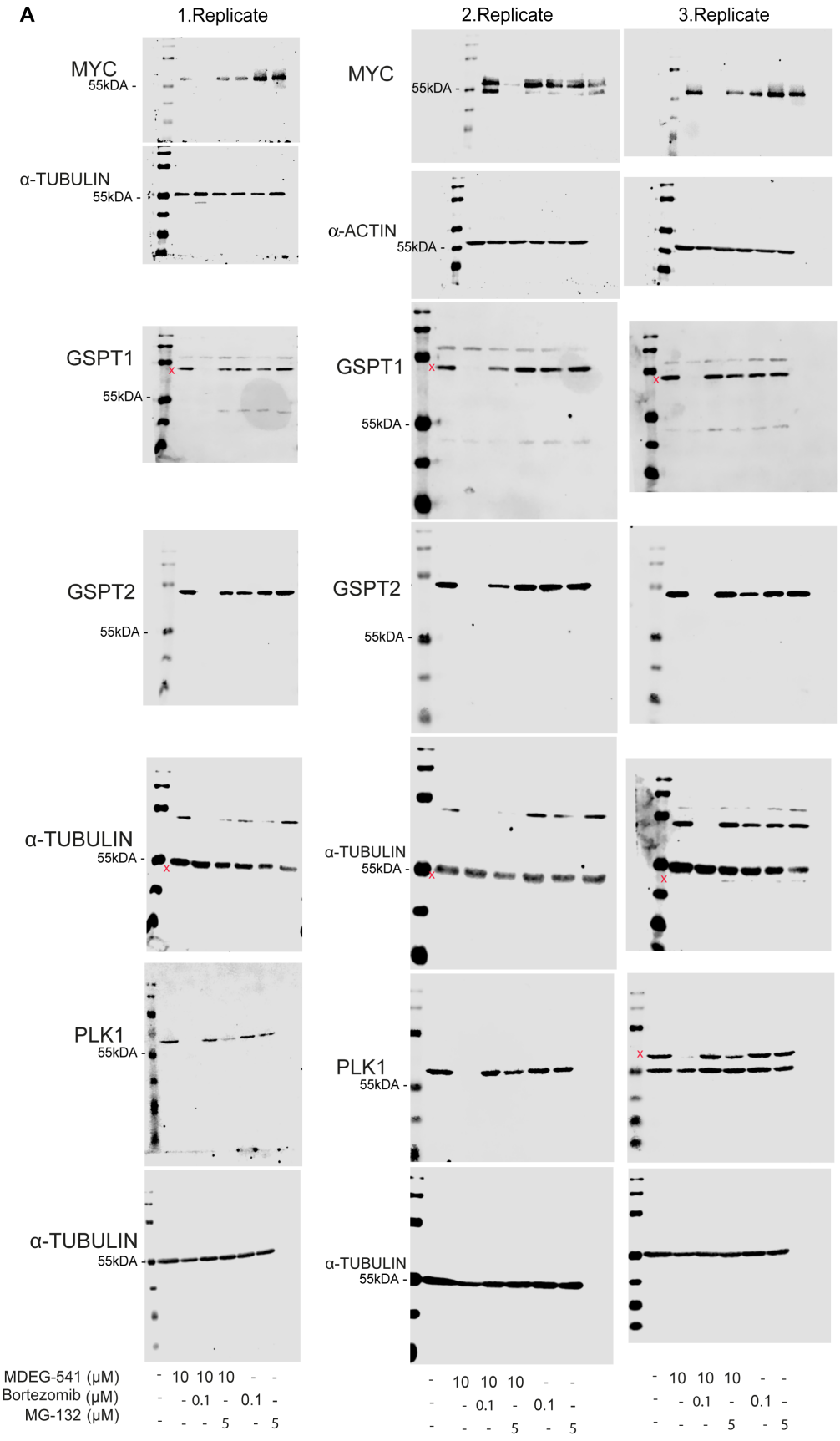

Supplementary Figure 10: Rawdata of western blots according to Figure 14 (A) PSN1 (B) HCT116. The red cross marks the respective protein band. For experimental conditions, quantification and statistics, refer to Figure 14.

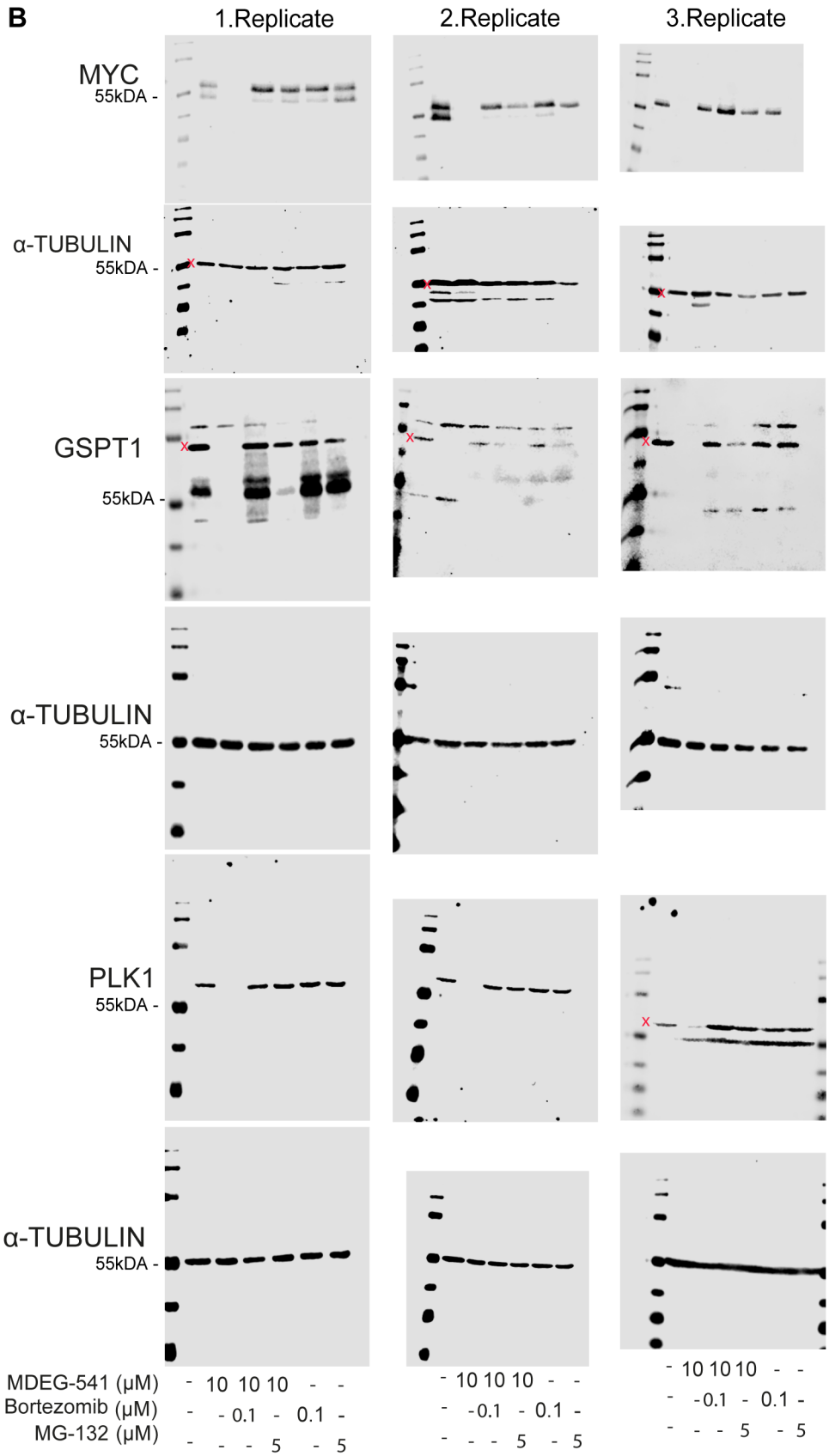

Supplementary Figure 10: Rawdata of western blots according to Figure 14 (A) PSN1 (B) HCT116. The red cross marks the respective protein band. For experimental conditions, quantification and statistics, refer to Figure 14.

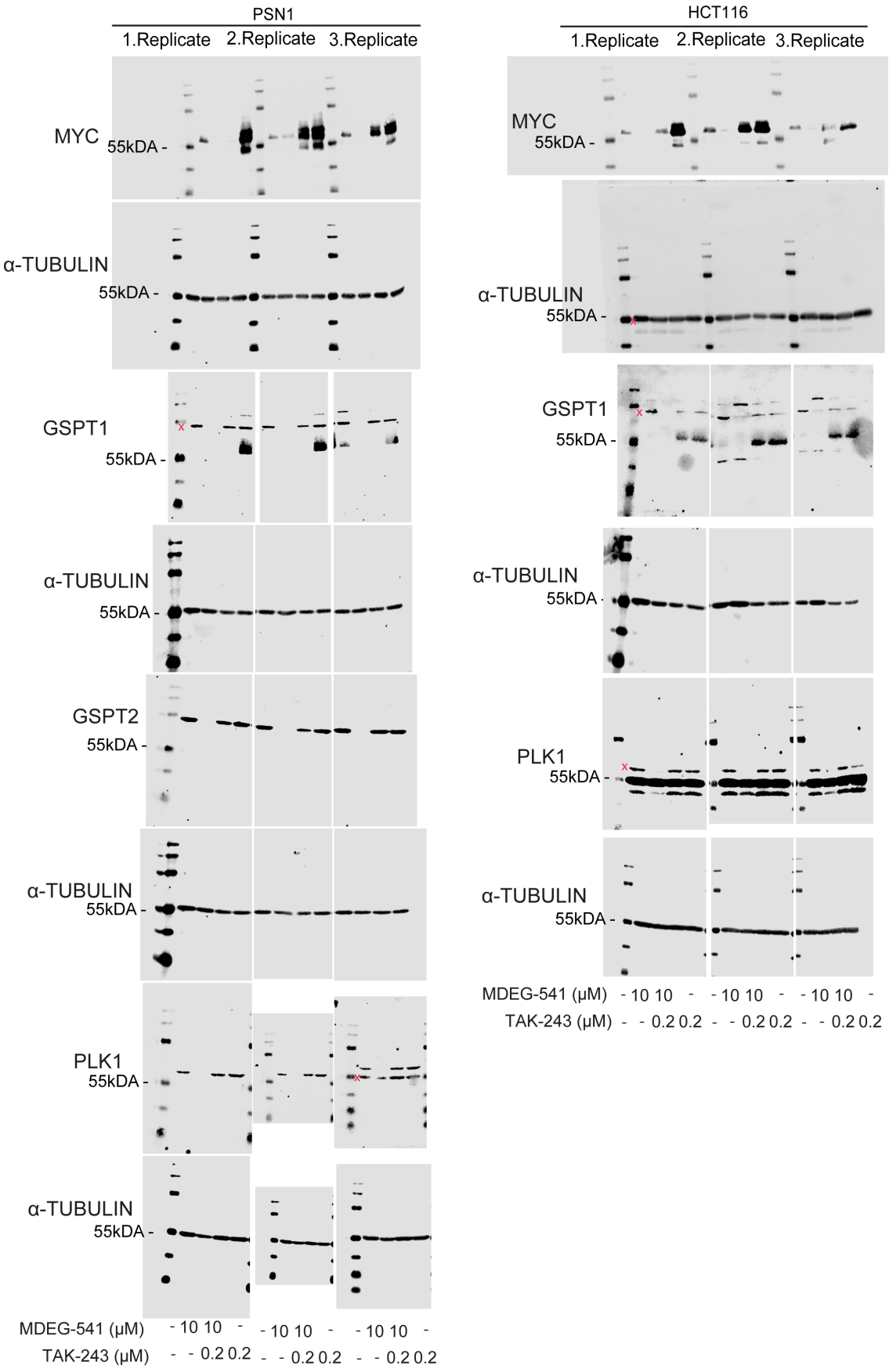

Supplementary Figure 11: Rawdata of western blots according to Figure 15
The red cross marks the respective protein band. For experimental conditions, quantification and statistics, refer to Figure 15.

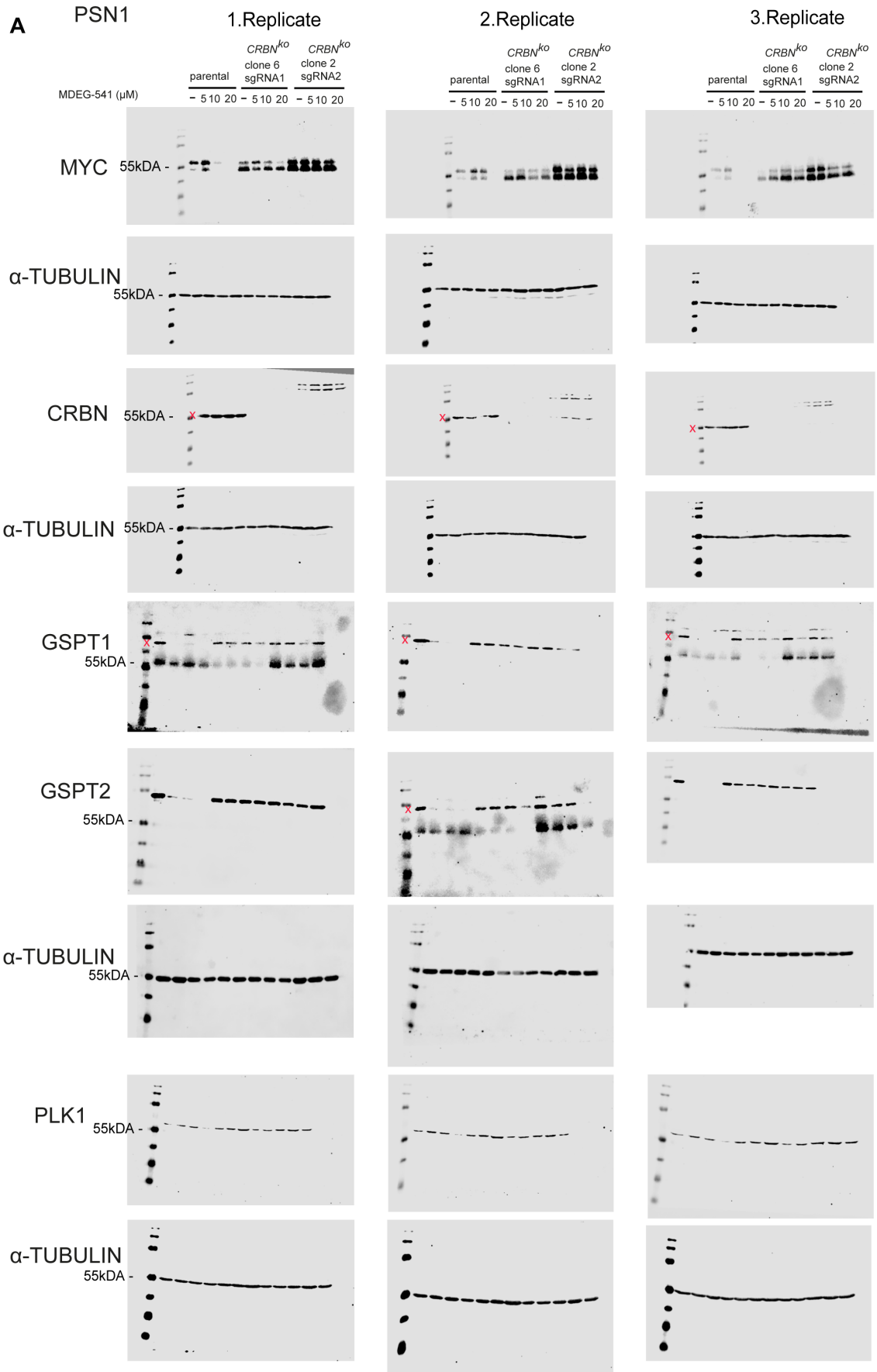

Supplementary Figure 12: Rawdata of western blots according to Figure 16 (A) PSN1 (B) HCT116. The red cross marks the respective protein band. For experimental conditions, quantification and statistics, refer to Figure 16.

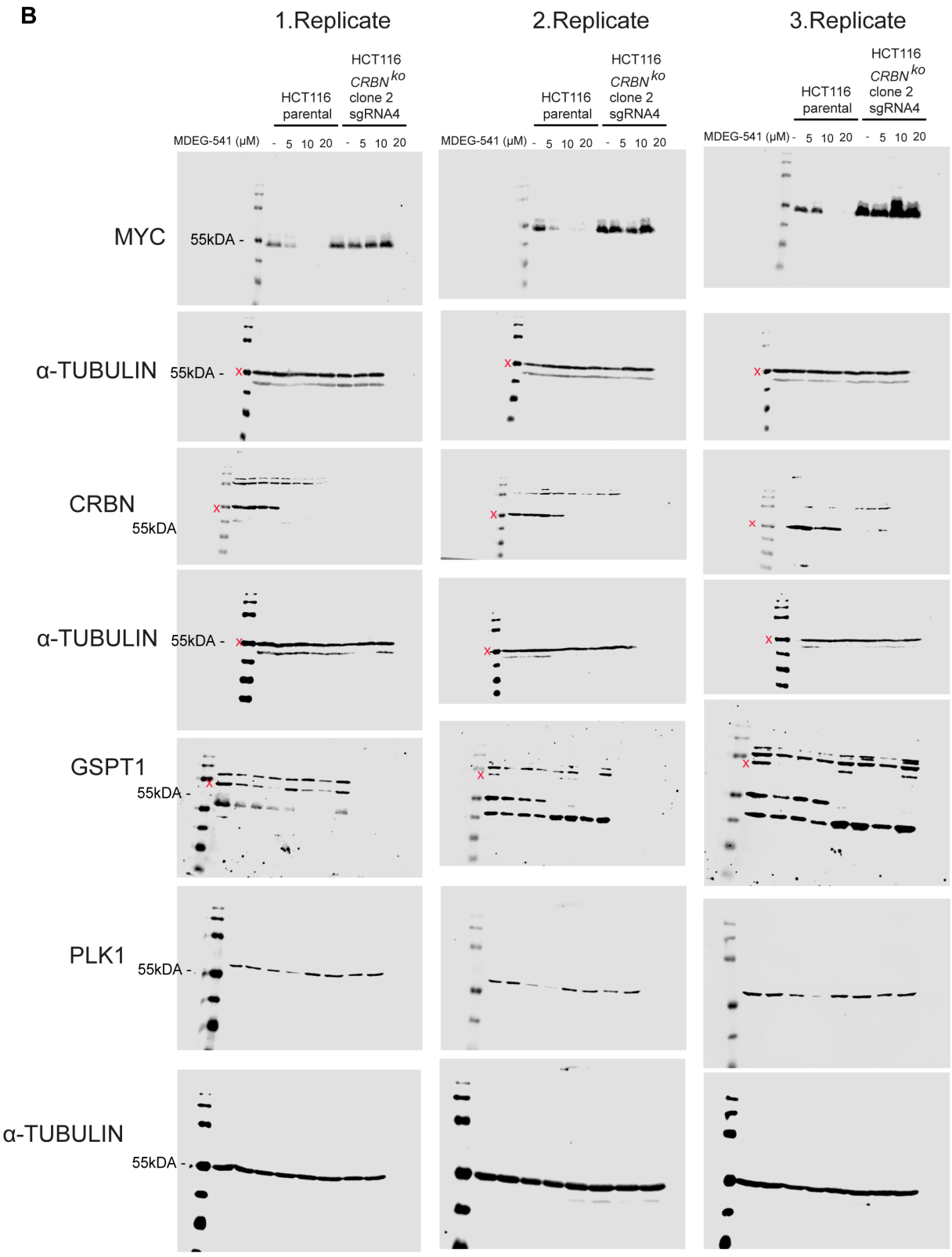

Supplementary Figure 12: Rawdata of western blots according to Figure 16 (A) PSN1 (B) HCT116. The red cross marks the respective protein band. For experimental conditions, quantification and statistics, refer to Figure 16.

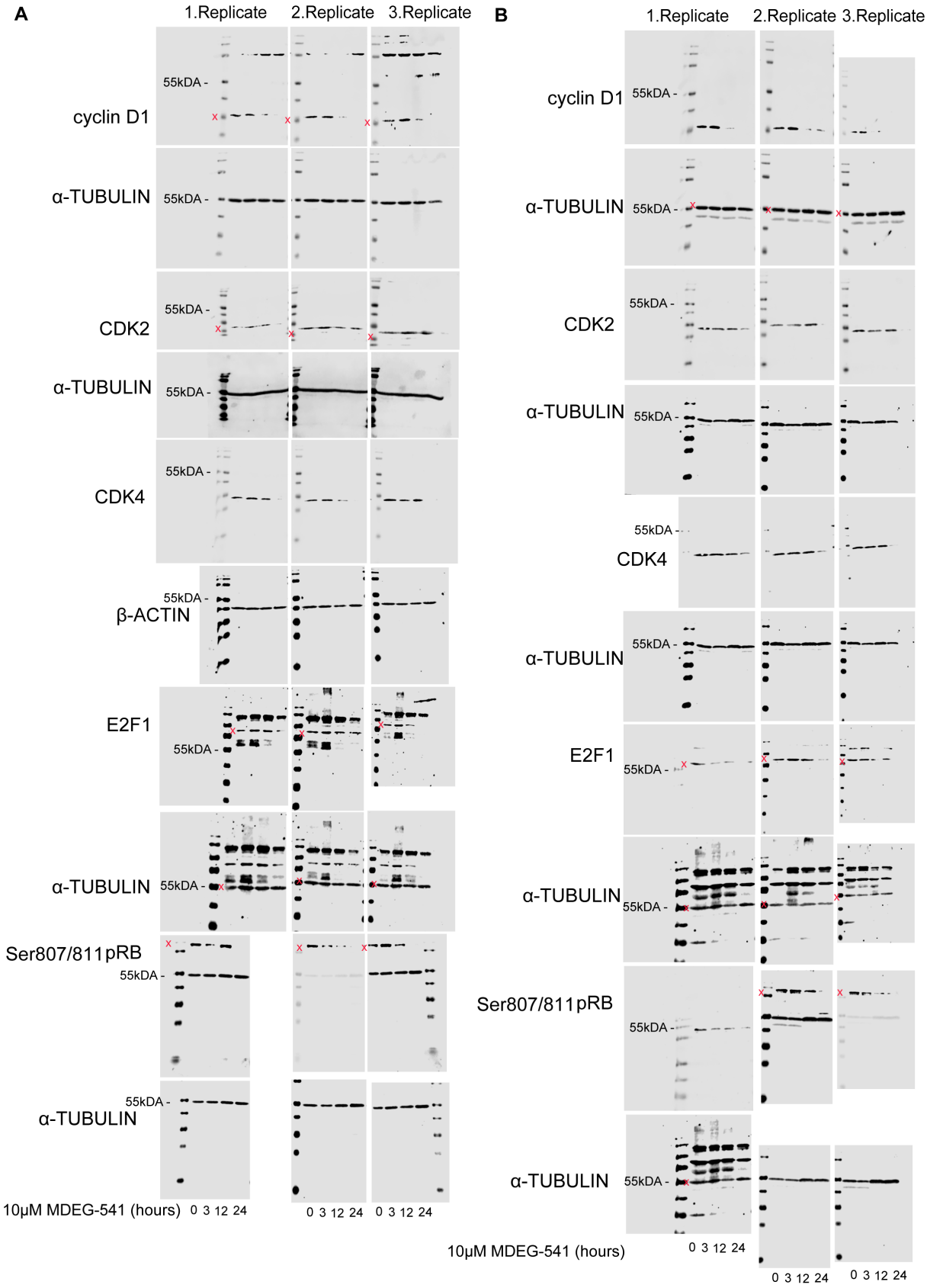

Supplementary Figure 13: Rawdata of western blots according to Figure 20 (A) PSN1 (B) HCT116. The red cross marks the respective protein band. For experimental conditions, quantification and statistics, refer to Figure 20.

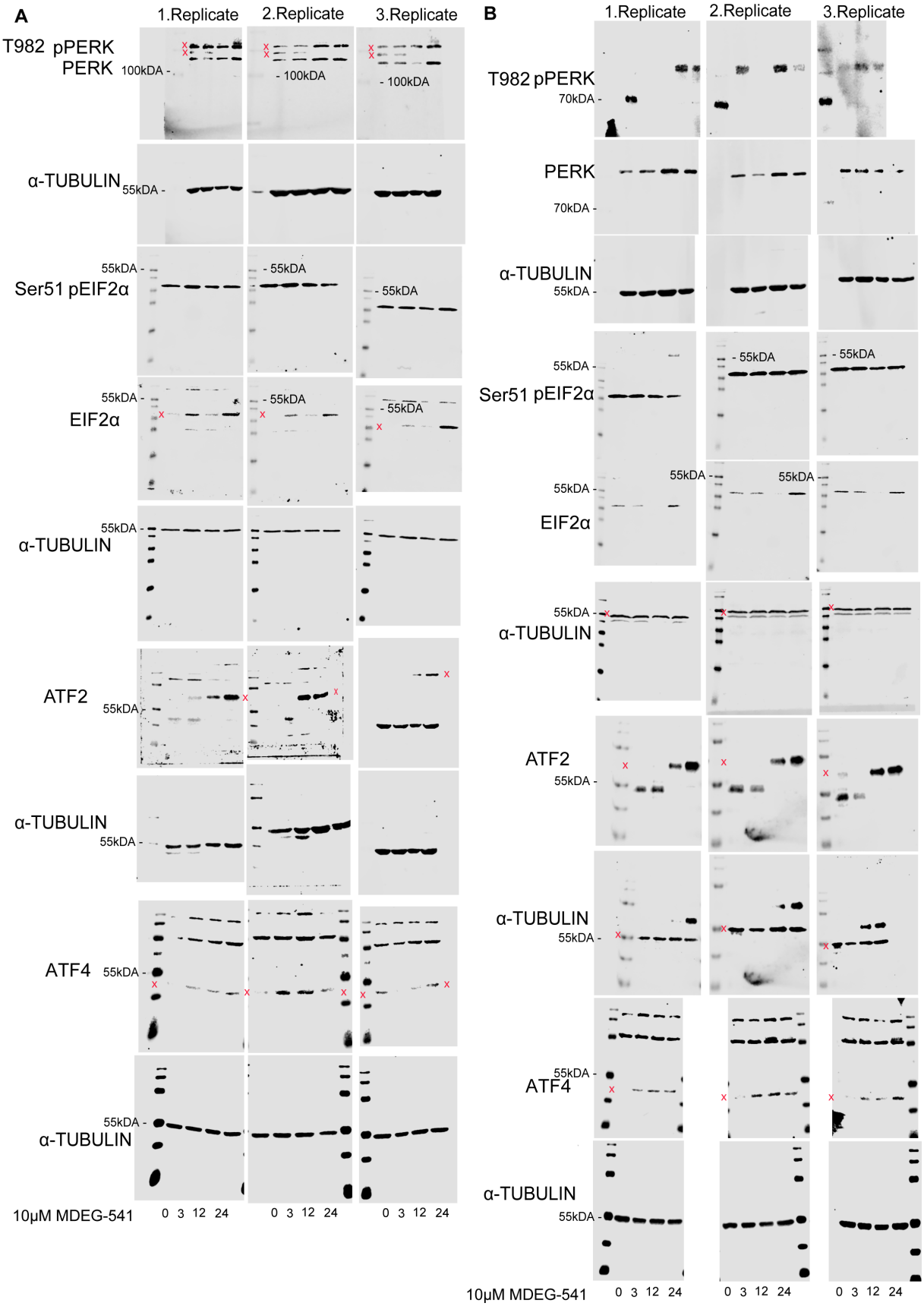

Supplementary Figure 14: Rawdata of western blots according to Figure 21 (A) PSN1 (B) HCT116. The red cross marks the respective protein band. For experimental conditions, quantification and statistics, refer to Figure 21.

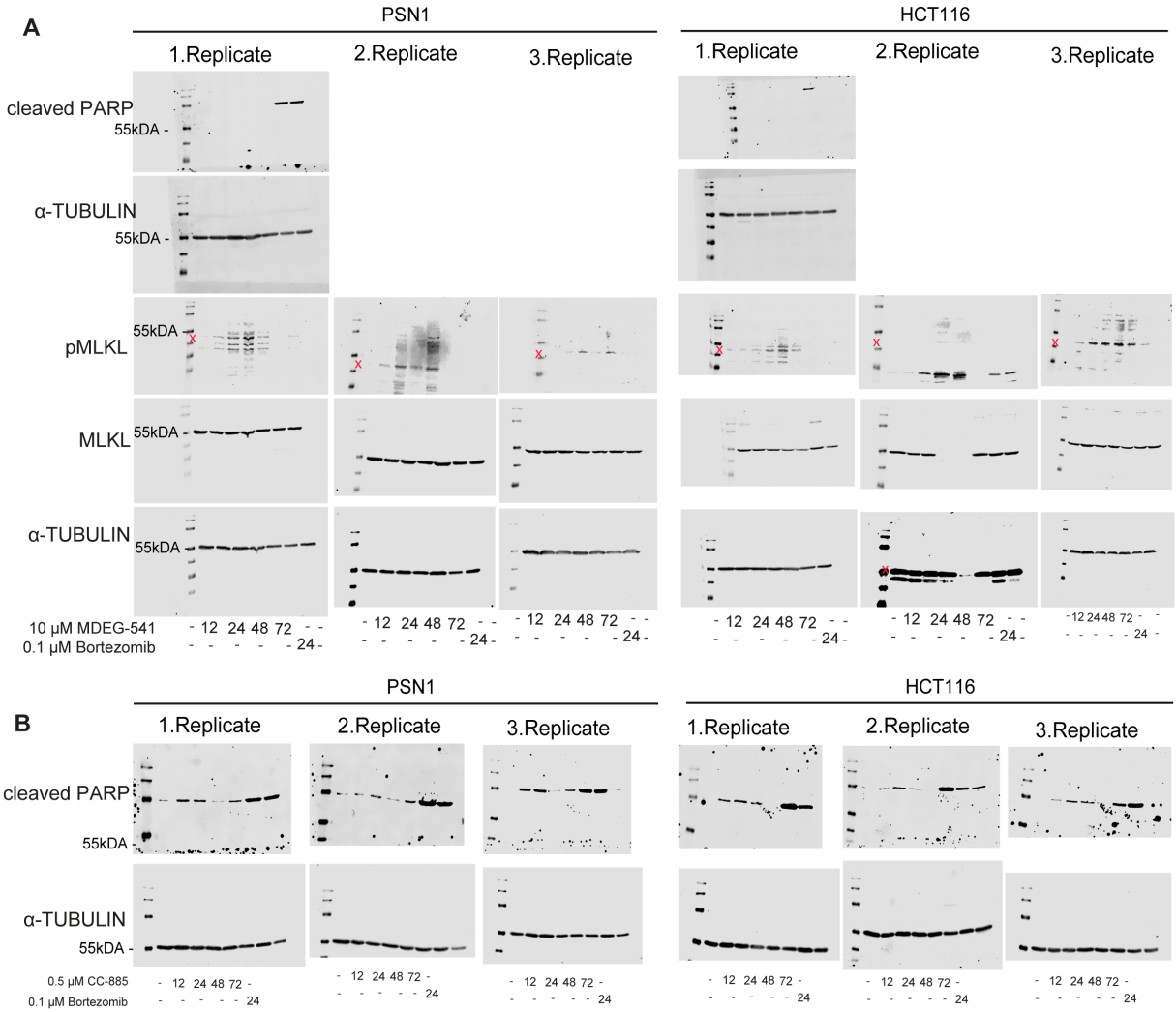

Supplementary Figure 15: Rawdata of western blots according to Figure 23 (A) PSN1 (B) HCT116. The red cross marks the respective protein band. For experimental conditions, quantification and statistics, refer to Figure 23.

Supplementary Table 1: Proteins downregulated in a cluster after 20 h treatment with 10 μM MDEG-541 in proteomics analysis.

Gene names	0 h	1 h	2 h	4 h	6 h	8 h	10 h	12 h	16 h	20 h	24 h
MRFAP1	16.1254	16.0566	16.0671	16.3914	15.6787	15.2876	14.9162	14.3686	14.632	12.2982	14.9271
GSPT2	16.5201	16.0939	15.4084	14.7199	13.758	13.8683	13.3045	13.5181	13.4555	12.8928	12.8433
GSPT1	21.175	21.1158	20.8418	19.94	19.5943	19.2307	18.6694	18.4414	18.2088	17.653	18.2261
LCN2	13.4361	12.4651	13.391	13.6821	13.7565	13.6123	13.7037	12.9395	11.9012	10.2537	NaN
S100A9	14.5911	13.4957	12.8261	12.9467	12.0934	12.5866	12.106	12.297	11.6047	11.4116	11.5604
MID1IP1	16.7205	16.5304	16.8133	16.6734	16.3387	16.0146	15.6053	15.3997	14.9518	13.8653	16.0588
SLMO2	14.7293	15.1141	15.3005	15.0111	14.887	14.2591	13.9565	13.2334	13.7788	11.9636	10.6183
MCM10	12.7406	11.9759	12.8277	13.0985	12.599	12.5364	12.6203	12.1909	12.1085	10.2315	12.9104
BAHD1	12.424	12.4166	12.3423	13.3465	12.5275	12.709	12.3389	10.679	11.2275	10.1063	12.2955
ZNFX1	12.9843	11.6682	12.5471	12.6725	12.1968	12.3398	12.7062	11.3568	12.5103	10.6913	12.7207
PTOV1	14.0534	13.3526	13.8191	13.7821	13.678	13.1383	13.4576	12.8276	13.2549	11.8023	12.8069
APCDD1L	12.4222	11.0576	12.3741	12.1858	12.4864	11.2016	12.4212	11.5579	11.7804	10.3315	NaN
CDCA7	12.1049	12.092	12.2741	12.378	12.0265	12.0334	11.9244	10.5051	10.8275	10.0213	12.1224
IFITM3	16.8337	16.2477	16.2098	15.9623	15.9571	15.9865	15.884	15.3616	15.3553	14.8033	15.1236
ELL2	13.1574	13.6159	13.8805	14.0626	13.1957	13.0905	12.6819	12.4907	12.3899	11.1455	10.6421
KIAA0101	19.0006	19.2867	19.5223	19.8423	19.5581	19.2501	18.5809	18.6302	17.73	17.0488	17.5805
B3GNT7	13.8064	13.1554	13.075	12.6201	13.0082	12.671	12.6783	12.3156	12.9606	11.896	NaN
NARF	13.0137	12.999	13.2418	13.0655	12.4409	12.6109	13.0915	11.9744	12.3201	11.2012	12.6592
MRI	13.5917	13.9202	14.3339	14.3749	13.9206	13.7666	12.7267	13.707	12.7613	11.8136	14.0095
PLD3	12.8467	11.8561	12.3638	12.8824	12.3871	12.317	12.7368	11.8319	12.4094	11.0806	13.9421
URGCP	12.9998	12.8982	13.2004	12.9137	12.6842	12.8772	12.2685	12.4383	13.2503	11.2408	13.3022
MYC	15.4308	15.4357	15.8088	15.423	14.9337	14.9658	14.7243	14.2343	14.9948	13.717	14.0487
PCGF5	11.894	12.1634	NaN	NaN	NaN	12.2094	11.3036	NaN	10.6932	10.1917	NaN
MLPH	16.037	15.884	15.8481	16.2393	15.9975	16.1337	15.5862	15.4815	15.4697	14.3449	14.4919
UBL5	16.8837	16.6183	17.0042	17.0253	16.8798	16.4625	16.2128	15.5865	15.9577	15.231	15.9299
TRIM11	11.8454	11.1509	12.2189	12.1793	12.4944	11.9041	12.118	11.7443	10.922	10.2246	12.3606
FAM60A	15.5361	15.1509	15.7064	15.6517	15.8398	14.9164	15.0382	14.1797	14.8207	13.9286	15.3862
SCAND1	13.6149	12.7377	13.8867	14.0196	14.0947	13.3201	13.0049	12.1242	12.9469	12.0492	13.3091
TFAP4	16.3125	16.3445	15.6203	16.1908	15.7093	16.0506	15.3373	15.6352	15.2635	14.7584	15.0201
ZNF768	11.63	10.983	11.3914	11.3411	11.9061	11.6477	11.619	12.0738	11.6996	10.1479	13.9
EXO1	11.9471	12.0617	12.1695	12.2956	12.2671	10.7805	12.5045	10.7478	11.8195	10.4846	13.2178
REL	12.949	11.9849	12.0625	12.1743	12.6059	12.4363	12.2399	12.5175	11.9276	11.5106	12.0632
CDC25C	12.4259	12.1374	12.0364	12.1695	11.61	11.5725	11.8125	11.8323	11.8557	10.9891	11.4895
AAMP	16.8162	16.4409	16.3973	16.4486	16.2301	16.2377	16.2152	15.8055	16.2883	15.3886	15.4517
C8orf59	18.4692	18.7811	18.998	19.1318	18.9148	18.5054	17.8616	18.0449	17.6027	17.046	17.3196
PTX3	14.557	14.3258	13.986	14.5267	14.2132	14.1447	14.3664	13.8279	13.7217	13.1358	10.5942
MYO10	15.2621	15.2	15.0356	14.6454	15.0402	14.8932	14.8634	14.1932	14.5117	13.8441	12.4975
PIK3CB	11.5097	9.97992	10.8587	NaN	11.1503	10.7771	10.5276	11.2911	11.0486	10.0937	NaN
UBE2C	17.3969	17.6289	17.6064	17.2839	17.1069	17.037	16.7735	16.5706	16.5373	15.9836	15.9608
HSPB1	18.4468	18.1352	18.3797	18.7485	18.8087	18.5538	18.3583	18.382	17.766	17.0601	23.475
APP	18.5947	18.3251	18.2618	18.5079	18.3476	18.2657	18.1465	17.7583	17.7048	17.2311	17.3528
C9orf16	15.2249	15.2306	15.055	15.3889	15.2601	15.2187	14.7374	14.8094	14.4611	13.8641	15.1712
TRPC4AP	13.4637	13.0373	13.663	12.7465	13.4143	13.0844	13.1279	12.5516	12.5116	12.1254	13.6733
FBXO3	11.4804	11.175	11.4474	10.5567	11.8218	11.2224	10.5414	11.6083	NaN	10.1452	11.8476
WWTR1	18.0368	18.0671	18.3419	18.4321	18.2005	17.7931	17.5004	17.3682	17.4994	16.7078	15.514
HLA-A	14.1677	14.1047	14.4667	14.4987	14.2987	13.7868	14.1021	13.8995	13.6065	12.8505	16.4824
RNF149	12.4818	11.6963	12.3546	12.83	11.6905	11.4451	12.6145	11.1493	11.0236	11.18	12.481
C14orf119	15.2325	15.3165	14.9801	15.2084	15.1499	14.7584	14.2918	14.5016	14.0905	13.9314	14.8578
TNS4	19.8938	19.6411	20.0463	19.9615	19.7937	19.5691	19.4807	19.1289	19.2434	18.5955	16.6976
ZFAND5	15.9699	15.8215	15.5029	16.3104	15.8274	16.208	15.6012	15.8262	15.1756	14.681	16.0013
AEBP2	14.1614	13.833	14.098	14.176	14.4196	13.769	13.8211	13.4537	13.299	12.8794	13.9778
STIM2	12.2335	11.6242	12.3652	12.4693	12.122	12.0451	12.0188	12.3305	12.4409	10.9548	13.3788
IVNS1ABP	13.1845	12.9467	13.1973	12.7294	13.2612	12.3012	12.8144	12.2119	12.9113	11.9229	12.5351
CYBA	16.9078	16.6957	17.2202	16.6528	16.5201	16.1063	16.3392	16.0897	15.783	15.6516	15.977
ECD	15.7797	15.8752	16.1373	15.6144	15.7657	15.2516	15.5833	14.8319	15.2458	14.5365	14.1055
TMEM200A	14.3337	14.3508	14.3231	14.2856	14.1247	13.8953	13.7487	13.4795	14.0012	13.0916	NaN
TRAF7	12.4105	12.3452	12.7672	12.5075	12.3003	12.5356	11.8832	11.9505	12.4486	11.1706	12.7591
FBXO38	14.3192	14.059	14.5829	14.4589	14.4689	14.1842	14.5763	14.1729	14.2533	13.0823	14.782
CKS2	16.1369	16.1852	15.8411	15.9673	15.6801	15.4671	15.5458	15.0184	15.3076	14.919	15.6005
KLHL26	12.2524	11.5695	11.8966	10.7774	11.8411	11.9615	10.5827	11.942	11.6536	11.0356	12.0529
GOLM1	18.7641	18.4261	17.7146	18.8001	18.2001	18.864	18.2361	18.3517	18.2062	17.5548	19.0758
NABP1	12.5328	11.5567	12.4715	12.705	11.9831	11.3113	12.1833	11.8504	11.1738	11.3287	NaN
CDC6	11.5853	12.356	12.9979	13.2165	12.3413	11.933	12.2732	12.0776	11.0184	10.3825	12.5072
CHKA	15.8162	15.6148	15.9863	16.1264	16.1425	15.6239	15.6811	15.1055	15.2343	14.6136	15.1347
TFF2	16.4171	15.8035	16.6579	17.2426	17.4952	16.7117	16.3957	16.7107	15.6021	15.215	12.2805
EXT2	13.9809	13.7717	14.0836	13.6774	13.6669	13.4984	13.8671	12.8049	13.7757	12.7804	13.8308
DKK1	12.2395	10.5727	12.4997	12.7254	12.4582	12.3024	11.6345	12.502	12.3361	11.0609	16.1966
MST1R	13.2992	12.3875	12.8475	12.8747	12.8635	12.4594	12.7822	11.8502	12.821	12.1221	14.2141
LGALS3BP	20.1797	19.991	20.0554	19.9201	19.9345	19.8589	19.8858	19.5098	19.7345	19.0063	19.586
CSNK1E	13.0069	12.4684	13.1059	12.7898	12.5095	12.8008	13.3479	11.9381	12.7906	11.8349	13.9251
ITM2C	12.4408	11.6576	11.815	11.9545	11.9269	11.8241	12.0125	10.913	11.6054	11.2837	12.3304
UBE2S	18.3085	18.2487	18.5527	18.4851	18.518	18.394	18.1468	17.968	17.9763	17.1649	18.4658
TNFRSF12A	15.8949	16.2438	15.6487	16.7469	15.8651	16.0665	15.2556	15.4206	15.3041	14.7514	13.7747
SLC20A1	16.064	15.9922	15.5656	15.658	15.7861	15.5618	15.6147	15.0953	15.0924	14.9232	10.8302
FAM199X	12.7542	11.7829	11.9412	12.7985	12.1803	12.5882	13.1445	12.5412	11.8401	11.6146	11.0787
PRSS2	17.4978	17.3532	17.2058	17.5736	17.217	17.1401	16.6892	17.0167	16.2702	16.3624	15.8548
JAG1	19.3241	19.1364	18.9071	19.631	19.469	19.5614	19.0072	19.117	18.3903	18.1896	15.8966
PARP14	15.8466	15.4493	15.5505	15.2948	15.3084	15.3949	15.4426	14.5693	14.983	14.7163	13.892
TIMP1	19.0924	18.9625	18.8498	18.7074	18.4006	18.5656	18.5537	17.9754	18.4878	17.976	15.3926
OTUD5	14.9437	14.6547	14.3812	15.3376	14.5775	14.9521	14.7207	14.5808	14.487	13.8343	13.41
SAPCD2	14.5965	14.2323	14.0873	14.9641	14.6476	14.372	14.4202	14.4935	14.1093	13.493	15.3071
MMACHC	14.8274	14.5856	14.599	14.7471	14.7597	14.296	14.651	14.4231	14.3701	13.7325	13.8644
SNRPN	11.9504	10.8208	11.3963	12.3288	11.1968	11.8371	11.4763	10.5862	9.7514	10.8571	NaN
CDC123	16.6839	16.8536	16.6928	16.5416	16.1532	16.4257	16.0789	15.853	16.0453	15.5969	16.3687
APLP2	15.366	14.8926	15.128	14.6934	15.0272	14.8261	14.6273	14.4743	14.4969	14.2796	13.8437
RLIM	14.2599	14.4859	13.5471	14.9233	14.1989	14.6855	14.1735	13.5024	13.5607	13.174	13.5614
CUEDC2	16.4825	16.6156	16.2732	16.6681	16.1417	16.6153	16.1751	16.0187	15.8151	15.3974	17.239
HLA-C	17.4512	17.1196	16.9503	17.3796	17.1051	17.1242	17.1074	16.7264	16.8757	16.3682	18.0695
MLF2	17.7474	17.3484	17.2193	17.8012	17.6199	17.6292	17.6059	17.2893	17.1677	16.6707	18.3087
UBE2T	18.8627	18.8323	18.891	19.0168	18.7279	18.7448	18.5568	18.4439	18.1473	17.7869	18.7971
NACC2	12.7365	12.7183	12.8951	13.0514	12.7276	12.5586	12.6413	12.2363	12.6635	11.662	13.3408
IGFBP6	14.2586	14.0445	14.5581	14.6504	14.7152	14.273	14.4302	14.1471	14.2045	13.1858	14.5496
TMX2	14.4401	14.7212	14.9558	14.578	14.6577	14.1992	13.839	13.4225	13.8541	13.3711	15.2901
ATXN7L3B	15.3106	14.896	15.4633	15.211	15.1746	15.1226	15.0932	14.846	14.6493	14.2423	14.886
ACD	15.2473	14.9365	15.6445	15.3954	15.3251	15.1685	15.0819	14.8586	14.5834	14.1792	15.469
PLD2	12.9148	12.0307	12.058	12.4763	12.5496	12.1322	12.219	10.8625	12.3034	11.8546	13.8482
LGR4	14.5452	14.1767	14.3635	13.4897	14.3345	14.097	13.9945	13.2256	14.0065	13.4909	11.8239
ARHGAP39	12.3542	11.48	11.5701	11.9177	12.8692	11.672	11.6262	12.1723	11.1491	11.3003	12.1508
RNF181	17.5946	17.6923	17.9317	18.4939	18.2381	17.8809	17.5923	17.5396	17.0095	16.5487	17.4912
ANKMY2	13.4132	13.3302	13.0761	12.5366	12.9006	13.3774	12.6602	13.3156	13.0608	12.3693	14.1863
ZIC2	12.3129	11.9136	12.5269	12.9474	13.4315	12.3058	12.9412	12.1813	12.1263	11.2738	12.9168
TOR1AIP2	15.8657	15.6784	16.2045	16.5693	16.2203	15.6008	15.8005	15.8736	15.623	14.829	15.1257
IPO8	16.2142	15.9104	15.9365	15.7569	15.9459	15.6778	15.9144	15.4214	15.855	15.1824	15.3034
CDKN1B	11.558	10.7046	11.5623	12.3875	12.0229	11.7168	11.3319	11.7742	11.4988	10.5308	11.8933
AMN1	11.7958	10.2114	11.2991	10.5267	11.4549	11.0453	11.4253	10.8758	10.8003	10.7774	10.6956
TSPYL1	17.2883	17.0321	17.4452	17.5345	17.4881	17.0885	17.0677	16.6677	16.84	16.274	17.4828
PRKAR1B	13.7756	13.304	13.5264	13.537	13.402	13.5046	13.7259	13.0786	13.1888	12.7646	12.4222
SERF2	18.7539	19.0046	18.9608	19.3803	19.2589	18.9616	18.2161	18.9976	17.6957	17.7494	17.8944
PAIP2	18.8188	19.0214	19.0431	19.278	19.02	19.127	18.3699	18.8136	17.7171	17.8148	18.7261
FEM1B	14.298	13.9274	14.2727	14.6375	14.4679	13.9317	14.2528	13.8309	14.1712	13.2948	13.6438

Supplementary Table 2: Proteins upregulated in a cluster after 20 h treatment with 10 μM MDEG-541 in proteomics analysis.

Gene names	0 h	1 h	2 h	4 h	6 h	8 h	10 h	12 h	16 h	20 h	24 h
MT1X	11.6814	13.4583	14.6136	16.5925	17.3784	16.8409	16.8149	17.2398	16.4456	16.3146	16.8898
MT2A;MT1G	18.0827	19.4675	19.9202	20.9749	21.5224	21.3709	21.1263	21.9198	21.2141	21.1472	22.3823
FER	14.6279	14.039	17.4314	17.2831	18.0119	15.9121	18.5911	17.2181	18.3138	17.5748	20.2641
FER1L4	11.908	13.1928	14.8906	13.7272	14.7128	13.5549	14.3934	13.444	13.5831	14.4523	14.806
MRPL51	11.5541	11.6561	13.6674	13.8943	14.4946	13.1021	13.7212	13.5664	13.5637	13.9597	15.082
MSLN	14.18	13.9751	16.0742	16.1463	16.8234	15.1348	17.0058	16.1174	16.6569	16.4115	16.4664
RHOC	12.9196	13.3995	15.4782	14.7383	15.203	13.6818	14.7586	14.5397	14.2708	15.1164	14.9451
NR2F1	11.9254	11.4976	11.851	12.2619	12.0844	12.6976	12.3567	13.8196	13.0419	13.9118	13.1007
NFX1	9.60444	9.87896	10.2287	11.1826	11.5818	10.5609	11.3708	10.6641	11.0667	11.4434	NaN
MYEOV2	11.9112	12.3081	13.043	13.9996	13.1667	12.8503	13.0362	13.6893	13.0866	13.7124	13.3875
PPP1R12C	13.9441	13.7631	15.1929	14.7645	14.8345	15.0668	14.3678	15.4216	15.212	15.7363	15.283
ACOT2	12.7369	12.7267	14.4435	14.5077	14.78	13.8105	14.9719	14.4755	14.7001	14.4437	NaN
FAM21C	12.0373	12.9351	13.7136	13.8224	13.4676	13.6359	13.29	14.0594	12.8921	13.6125	13.9914
EIF5A2	10.8483	11.899	12.6125	12.6536	11.04	12.6646	12.6154	12.859	11.8031	12.4199	12.5496
PSTPIP2	10.4403	10.6929	11.4088	11.886	11.9959	11.7546	12.0449	11.8289	11.2701	12.0075	14.1341
COMMD5	10.3125	11.0041	11.3306	10.7812	12.5497	11.154	12.0297	11.4575	12.1485	11.7587	NaN
COL1A2	12.7098	12.9981	13.3982	13.8312	14.026	13.3374	13.0996	13.7876	14.6224	14.1499	13.0722
SEC61G	14.5069	14.4624	15.9565	15.4332	16.0471	14.7425	15.7408	15.6236	15.6236	15.9428	16.2652
GDAP2	10.8594	11.473	9.97814	10.67	10.676	10.8043	11.0061	11.5686	11.7635	12.2733	NaN
NEK11	15.8975	15.7288	18.38	16.9069	18.2936	15.8113	16.9616	17.524	16.5436	17.2536	16.382
RPL36AL	13.9092	13.5428	15.3994	15.1966	15.3	14.4208	15.3749	14.8645	14.9298	15.2396	16.3476
AIF1L	11.2498	12.1349	12.6784	12.5545	12.7049	12.7342	12.5797	12.8468	12.8397	12.5772	14.1321
PLCH1	12.3403	13.2223	13.0068	11.8429	12.5371	13.2766	13.2393	12.3052	13.8251	13.6426	13.004
KIAA1211	11.5786	12.3682	11.723	12.506	12.2376	12.5551	12.997	12.3555	12.1386	12.8468	14.5851
KIAA0930	11.1742	11.1562	12.4041	12.0366	12.5775	11.2275	12.0986	11.5688	12.5736	12.4052	13.5327
NUCKS1	19.6436	20.0709	20.0765	20.5735	20.5681	20.5819	20.3386	21.1168	20.2825	20.818	20.5604
PTGS2	13.5088	14.0462	14.077	14.1548	14.041	14.6287	14.7572	15.0302	14.4401	14.678	NaN
TRMU	10.7383	11.4565	11.8872	11.9197	11.5568	11.4419	12.2361	12.3023	12.2017	11.8898	12.8043
SELH	11.2578	11.0726	11.2709	11.195	12.2087	11.6853	12.6166	11.1223	12.6203	12.4075	NaN
IRS2	11.1853	10.8694	10.4542	11.7831	12.4854	12.1017	12.1755	12.912	12.1301	12.3276	11.1544
GDF15	19.6937	19.0303	19.7554	19.8771	20.3679	19.887	20.1889	20.1287	20.1974	20.8323	21.0366
EPDR1	11.4534	11.9688	11.5911	12.336	12.732	12.2476	12.2135	12.0226	12.0747	12.5917	12.6728
CRIP2	14.6345	15.0436	15.7523	15.929	16.3598	15.8235	15.9261	16.1045	15.6011	15.7505	17.2791
COL1A1	15.2698	15.4717	15.508	16.0586	15.5953	15.5847	15.422	15.8267	16.6533	16.384	15.0714
SSX2IP	17.5959	17.9434	18.4905	18.9406	18.86	18.4653	18.0971	19.1297	18.0788	18.7029	18.815
MTX3	13.0241	13.3063	13.8403	13.5864	13.6715	13.6136	14.005	12.9809	14.0641	14.1054	13.6439
REXO1	12.286	12.2288	13.5425	13.6556	14.4081	12.6719	14.26	13.6718	13.5934	13.3639	14.9829
ITFG3	11.1112	11.541	11.0939	11.3035	10.9956	11.5787	11.0921	11.9999	11.5774	12.1739	NaN
GRK6	10.773	10.8462	12.0499	11.9673	12.3762	11.7577	12.2026	12.2931	11.4051	11.8143	12.4994
RRAS	15.5935	14.0804	15.9766	17.345	17.7356	16.111	17.5213	16.9672	16.758	16.6179	17.7366
BHMT	10.9214	10.8865	12.1586	10.5227	10.84	11.7661	11.7509	11.6717	12.2894	11.9416	11.6612
TOMM7	16.4332	16.189	17.1011	17.3422	17.4235	16.4883	17.5656	17.3657	17.3385	17.4516	18.7914
H1FX	19.4207	19.3806	19.6156	19.6574	19.8252	19.7143	19.9825	20.0665	19.9707	20.4383	21.1725
BPHL	12.707	12.0492	13.3582	12.6964	12.9799	12.5944	13.2935	13.1137	13.3816	13.7239	14.2514
NRIP1	15.8644	15.9926	15.5856	15.6611	15.6463	16.0444	16.4073	15.7529	16.5745	16.8792	15.7459
PIEZO1	11.1753	11.8699	12.1056	11.9749	13.052	12.4885	12.6876	12.1186	12.4528	12.1782	11.881

Supplement Table 3: Top 50 significant genes obtained by a correlation of CCLE mRNA expression dataset with MDEG-541 GI_{50} values from an MTT-based cell viability assay of 16 CRC and PDAC cell lines.

	Gene	p.value	corr.coefficient
1	DGKI	0.00018753	-0.801770567
2	KIF27	0.0002181	-0.797058824
3	ZNF425	0.0003158	-0.78497876
4	BTK	0.00036289	-0.780239383
5	AP3M2	0.00047682	-0.770588235
6	HDAC11	0.00047682	-0.770588235
7	STX17	0.00065403	-0.758823529
8	ABHD8	0.00070589	-0.755882353
9	FXYD7	0.00080847	-0.75055208
10	EPG5	0.00081976	-0.75
11	GPR161	0.00088211	-0.747058824
12	PTGFR	0.00126732	-0.731930397
13	FAM50B	0.00149823	-0.724595778
14	RGS4	0.00151629	-0.724062006
15	HLA.3	0.0017185	-0.718413163
16	LZTS3	0.00176343	-0.717232
17	OBSCN	0.00184169	-0.715231982
18	NBR1	0.00186274	-0.714705882
19	MSR1	0.00192631	-0.713145698
20	BBS2	0.00198404	-0.711764706
21	DLC1	0.00198404	-0.711764706
22	HLCS	0.00198404	-0.711764706
23	ZNF772	0.00202447	-0.710816969
24	CFAP53	0.00215005	-0.707967682
25	PPP1R16B	0.00248683	-0.700942529
26	ESYT3	0.00253509	-0.7
27	MTMR14	0.00269059	-0.697058824
28	LRRC8A	0.00302472	-0.691176471
29	RGS5	0.00302472	-0.691176471
30	OLFML1	0.00355453	-0.682844322
31	NCF1	0.00358549	-0.682389287
32	CTSF	0.00365467	-0.681383555
33	LUC7L3	0.00400825	-0.676470588
34	SEZ6L	0.00401108	-0.676432726
35	RNF165	0.00422351	-0.673647842
36	CRBN	0.00423274	-0.673529412
37	TUB	0.00426528	-0.673113557
38	OSM	0.00438039	-0.671662478
39	SIMC1	0.00446721	-0.670588235
40	ZNF528	0.00454745	-0.669610189

13. REFERENCES

Aarons, C. B., Shanmugan, S., and Bleier, J. I. (2014). Management of malignant colon polyps: current status and controversies. World J Gastroenterol *20*, 16178-16183.

Adamska, A., Domenichini, A., and Falasca, M. (2017). Pancreatic Ductal Adenocarcinoma: Current and Evolving Therapies. Int J Mol Sci *18*.

Alabi, S., and Crews, C. (2021). Major Advances in Targeted Protein Degradation: PROTACs, LYTACs, and MADTACs. J Biol Chem *296*, 100647.

Allevato, M., Bolotin, E., Grossman, M., Mane-Padros, D., Sladek, F. M., and Martinez, E. (2017). Sequence-specific DNA binding by MYC/MAX to low-affinity non-E-box motifs. PLoS One *12*, e0180147.

AlSultan, D., Kavanagh, E., O'Grady, S., Eustace, A. J., Castell, A., Larsson, L. G., Crown, J., Madden, S. F., and Duffy, M. J. (2021). The novel low molecular weight MYC antagonist MYCMI-6 inhibits proliferation and induces apoptosis in breast cancer cells. Invest New Drugs *39*, 587-594.

Amati, B., Brooks, M. W., Levy, N., Littlewood, T. D., Evan, G. I., and Land, H. (1993). Oncogenic activity of the c-Myc protein requires dimerization with Max. Cell *72*, 233-245.

Amati, B., Dalton, S., Brooks, M. W., Littlewood, T. D., Evan, G. I., and Land, H. (1992). Transcriptional activation by the human c-Myc oncoprotein in yeast requires interaction with Max. Nature *359*, 423-426.

Anand, P., Kunnumakkara, A. B., Sundaram, C., Harikumar, K. B., Tharakan, S. T., Lai, O. S., Sung, B., and Aggarwal, B. B. (2008). Cancer is a preventable disease that requires major lifestyle changes. Pharm Res *25*, 2097-2116.

André, T., Meyerhardt, J., Iveson, T., Sobrero, A., Yoshino, T., Souglakos, I., Grothey, A., Niedzwiecki, D., Saunders, M., Labianca, R.*, et al.* (2020). Effect of duration of adjuvant chemotherapy for patients with stage III colon cancer (IDEA collaboration): final results from a prospective, pooled analysis of six randomised, phase 3 trials. Lancet Oncol *21*, 1620-1629.

André, T., Vernerey, D., Mineur, L., Bennouna, J., Desrame, J., Faroux, R., Fratte, S., Hug de Larauze, M., Paget-Bailly, S., Chibaudel, B.*, et al.* (2018). Three Versus 6 Months of Oxaliplatin-Based Adjuvant Chemotherapy for Patients With Stage III Colon Cancer: Disease-Free Survival Results From a Randomized, Open-Label, International Duration Evaluation of Adjuvant (IDEA) France, Phase III Trial. J Clin Oncol *36*, 1469-1477.

Annibali, D., Whitfield, J. R., Favuzzi, E., Jauset, T., Serrano, E., Cuartas, I., Redondo-Campos, S., Folch, G., Gonzàlez-Juncà, A., Sodir, N. M.*, et al.* (2014). Myc inhibition is effective against glioma and reveals a role for Myc in proficient mitosis. Nature Communications *5*, 4632.

Arai, T., Miyoshi, Y., Kim, S. J., Akazawa, K., Maruyama, N., Taguchi, T., Tamaki, Y., and Noguchi, S. (2008). Association of GSTP1 expression with resistance to docetaxel and paclitaxel in human breast cancers. Eur J Surg Oncol *34*, 734-738.

Arvanitis, C., and Felsher, D. W. (2006). Conditional transgenic models define how MYC initiates and maintains tumorigenesis. Semin Cancer Biol *16*, 313-317.

Bagnardi, V., Rota, M., Botteri, E., Tramacere, I., Islami, F., Fedirko, V., Scotti, L., Jenab, M., Turati, F., Pasquali, E.*, et al.* (2015). Alcohol consumption and site-specific cancer risk: a comprehensive dose-response meta-analysis. Br J Cancer *112*, 580-593.

Bailey, P., Chang, D. K., Nones, K., Johns, A. L., Patch, A. M., Gingras, M. C., Miller, D. K., Christ, A. N., Bruxner, T. J., Quinn, M. C.*, et al.* (2016). Genomic analyses identify molecular subtypes of pancreatic cancer. Nature *531*, 47-52.
Barr, F. A., Silljé, H. H., and Nigg, E. A. (2004). Polo-like kinases and the orchestration of cell division. Nat Rev Mol Cell Biol *5*, 429-440.
Beißel, C., Neumann, B., Uhse, S., Hampe, I., Karki, P., and Krebber, H. (2019). Translation termination depends on the sequential ribosomal entry of eRF1 and eRF3. Nucleic Acids Res *47*, 4798-4813.
Beroukhim, R., Mermel, C. H., Porter, D., Wei, G., Raychaudhuri, S., Donovan, J., Barretina, J., Boehm, J. S., Dobson, J., Urashima, M.*, et al.* (2010). The landscape of somatic copy-number alteration across human cancers. Nature *463*, 899-905.
Bhosale, P., Cox, V., Faria, S., Javadi, S., Viswanathan, C., Koay, E., and Tamm, E. (2018). Genetics of pancreatic cancer and implications for therapy. Abdom Radiol (NY) *43*, 404-414.
Blackwood, E. M., and Eisenman, R. N. (1991). Max: a helix-loop-helix zipper protein that forms a sequence-specific DNA-binding complex with Myc. Science *251*, 1211-1217.
Boike, L., Cioffi, A. G., Majewski, F. C., Co, J., Henning, N. J., Jones, M. D., Liu, G., McKenna, J. M., Tallarico, J. A., Schirle, M., and Nomura, D. K. (2021). Discovery of a Functional Covalent Ligand Targeting an Intrinsically Disordered Cysteine within MYC. Cell Chem Biol *28*, 4-13.e17.
Boland, C. R., Thibodeau, S. N., Hamilton, S. R., Sidransky, D., Eshleman, J. R., Burt, R. W., Meltzer, S. J., Rodriguez-Bigas, M. A., Fodde, R., Ranzani, G. N., and Srivastava, S. (1998). A National Cancer Institute Workshop on Microsatellite Instability for cancer detection and familial predisposition: development of international criteria for the determination of microsatellite instability in colorectal cancer. Cancer Res *58*, 5248-5257.
Bonadona, V., Bonaiti, B., Olschwang, S., Grandjouan, S., Huiart, L., Longy, M., Guimbaud, R., Buecher, B., Bignon, Y. J., Caron, O.*, et al.* (2011). Cancer risks associated with germline mutations in MLH1, MSH2, and MSH6 genes in Lynch syndrome. Jama *305*, 2304-2310.
Bondeson, D. P., Mares, A., Smith, I. E., Ko, E., Campos, S., Miah, A. H., Mulholland, K. E., Routly, N., Buckley, D. L., Gustafson, J. L.*, et al.* (2015). Catalytic in vivo protein knockdown by small-molecule PROTACs. Nat Chem Biol *11*, 611-617.
Botteri, E., Iodice, S., Bagnardi, V., Raimondi, S., Lowenfels, A. B., and Maisonneuve, P. (2008). Smoking and colorectal cancer: a meta-analysis. Jama *300*, 2765-2778.
Bray, F., Ferlay, J., Soerjomataram, I., Siegel, R. L., Torre, L. A., and Jemal, A. (2018). Global cancer statistics 2018: GLOBOCAN estimates of incidence and mortality worldwide for 36 cancers in 185 countries. CA Cancer J Clin *68*, 394-424.
Brito, M., Malta-Vacas, J., Carmona, B., Aires, C., Costa, P., Martins, A. P., Ramos, S., Conde, A. R., and Monteiro, C. (2005). Polyglycine expansions in eRF3/GSPT1 are associated with gastric cancer susceptibility. Carcinogenesis *26*, 2046-2049.
Bu, Y., Yang, Z., Li, Q., and Song, F. (2008). Silencing of polo-like kinase (Plk) 1 via siRNA causes inhibition of growth and induction of apoptosis in human esophageal cancer cells. Oncology *74*, 198-206.
Bujanda, L., and Herreros-Villanueva, M. (2017). Pancreatic Cancer in Lynch Syndrome Patients. J Cancer *8*, 3667-3674.
Burslem, G. M., Smith, B. E., Lai, A. C., Jaime-Figueroa, S., McQuaid, D. C., Bondeson, D. P., Toure, M., Dong, H., Qian, Y., Wang, J.*, et al.* (2018). The

Advantages of Targeted Protein Degradation Over Inhibition: An RTK Case Study. Cell Chem Biol *25*, 67-77.e63.
Casey, S. C., Tong, L., Li, Y., Do, R., Walz, S., Fitzgerald, K. N., Gouw, A. M., Baylot, V., Gütgemann, I., Eilers, M., and Felsher, D. W. (2016). MYC regulates the antitumor immune response through CD47 and PD-L1. Science *352*, 227-231.
Castell, A., Yan, Q., Fawkner, K., Hydbring, P., Zhang, F., Verschut, V., Franco, M., Zakaria, S. M., Bazzar, W., Goodwin, J.*, et al.* (2018). A selective high affinity MYC-binding compound inhibits MYC:MAX interaction and MYC-dependent tumor cell proliferation. Sci Rep *8*, 10064.
Cawley, S., Bekiranov, S., Ng, H. H., Kapranov, P., Sekinger, E. A., Kampa, D., Piccolboni, A., Sementchenko, V., Cheng, J., Williams, A. J.*, et al.* (2004). Unbiased mapping of transcription factor binding sites along human chromosomes 21 and 22 points to widespread regulation of noncoding RNAs. Cell *116*, 499-509.
Chan, D. S., Lau, R., Aune, D., Vieira, R., Greenwood, D. C., Kampman, E., and Norat, T. (2011). Red and processed meat and colorectal cancer incidence: meta-analysis of prospective studies. PLoS One *6*, e20456.
Chauvin, C., Salhi, S., and Jean-Jean, O. (2007). Human eukaryotic release factor 3a depletion causes cell cycle arrest at G1 phase through inhibition of the mTOR pathway. Mol Cell Biol *27*, 5619-5629.
Chen, F., Roberts, N. J., and Klein, A. P. (2017). Inherited pancreatic cancer. Chin Clin Oncol *6*, 58.
Chen, H., Liu, H., and Qing, G. (2018). Targeting oncogenic Myc as a strategy for cancer treatment. Signal Transduction and Targeted Therapy *3*, 5.
Chllamma, M. K., Cook, N., Dhani, N. C., Giby, K., Dodd, A., Wang, L., Hedley, D. W., Moore, M. J., and Knox, J. J. (2016). FOLFIRINOX for advanced pancreatic cancer: the Princess Margaret Cancer Centre experience. Br J Cancer *115*, 649-654.
Chuvin, N., Vincent, D. F., Pommier, R. M., Alcaraz, L. B., Gout, J., Caligaris, C., Yacoub, K., Cardot, V., Roger, E., Kaniewski, B.*, et al.* (2017). Acinar-to-Ductal Metaplasia Induced by Transforming Growth Factor Beta Facilitates KRAS(G12D)-driven Pancreatic Tumorigenesis. Cell Mol Gastroenterol Hepatol *4*, 263-282.
Ciriello, G., Miller, M. L., Aksoy, B. A., Senbabaoglu, Y., Schultz, N., and Sander, C. (2013). Emerging landscape of oncogenic signatures across human cancers. Nat Genet *45*, 1127-1133.
Collins, S., and Groudine, M. (1982). Amplification of endogenous myc-related DNA sequences in a human myeloid leukaemia cell line. Nature *298*, 679-681.
Conroy, T., Hammel, P., Hebbar, M., Ben Abdelghani, M., Wei, A. C., Raoul, J. L., Chone, L., Francois, E., Artru, P., Biagi, J. J.*, et al.* (2018). FOLFIRINOX or Gemcitabine as Adjuvant Therapy for Pancreatic Cancer. N Engl J Med *379*, 2395-2406.
Copur, M. S., Talmon, G. A., Wedel, W., Hart, J. D., Merani, S., and Vargasi, L. M. (2020). Hereditary vs Familial Pancreatic Cancer: Associated Genetic Syndromes and Clinical Perspective. Oncology (Williston Park) *34*, 196-201.
Cowling, V. H., Chandriani, S., Whitfield, M. L., and Cole, M. D. (2006). A conserved Myc protein domain, MBIV, regulates DNA binding, apoptosis, transformation, and G2 arrest. Mol Cell Biol *26*, 4226-4239.
Cyrus, K., Wehenkel, M., Choi, E. Y., Han, H. J., Lee, H., Swanson, H., and Kim, K. B. (2011). Impact of linker length on the activity of PROTACs. Mol Biosyst *7*, 359-364.
Dang, C. V. (2013). MYC, metabolism, cell growth, and tumorigenesis. Cold Spring Harb Perspect Med *3*.

Dang, C. V., and Lee, W. M. (1988). Identification of the human c-myc protein nuclear translocation signal. Mol Cell Biol *8*, 4048-4054.
Dang, D. T., Chen, F., Kohli, M., Rago, C., Cummins, J. M., and Dang, L. H. (2005). Glutathione S-transferase pi1 promotes tumorigenicity in HCT116 human colon cancer cells. Cancer Res *65*, 9485-9494.
de Cárcer, G. (2019). The Mitotic Cancer Target Polo-Like Kinase 1: Oncogene or Tumor Suppressor? Genes (Basel) *10*.
de Oliveira, J. C., Brassesco, M. S., Pezuk, J. A., Morales, A. G., Valera, E. T., Montaldi, A. P., Sakamoto-Hojo, E. T., Scrideli, C. A., and Tone, L. G. (2012). In vitro PLK1 inhibition by BI 2536 decreases proliferation and induces cell-cycle arrest in melanoma cells. J Drugs Dermatol *11*, 587-592.
De Rosa, M., Pace, U., Rega, D., Costabile, V., Duraturo, F., Izzo, P., and Delrio, P. (2015). Genetics, diagnosis and management of colorectal cancer (Review). Oncol Rep *34*, 1087-1096.
Deeraksa, A., Pan, J., Sha, Y., Liu, X. D., Eissa, N. T., Lin, S. H., and Yu-Lee, L. y. (2013). Plk1 is upregulated in androgen-insensitive prostate cancer cells and its inhibition leads to necroptosis. Oncogene *32*, 2973-2983.
Deshaies, R. J. (2015a). Protein degradation: Prime time for PROTACs. Nat Chem Biol *11*, 634-635.
Deshaies, R. J. (2015b). Protein degradation. Prime time for PROTACs. Nat Chem Biol *11*, 634-635.
Duesberg, P. H., and Vogt, P. K. (1979). Avian acute leukemia viruses MC29 and MH2 share specific RNA sequences: evidence for a second class of transforming genes. Proc Natl Acad Sci U S A *76*, 1633-1637.
Farrell, A. S., and Sears, R. C. (2014). MYC degradation. Cold Spring Harb Perspect Med *4*.
Fearon, E. R., and Vogelstein, B. (1990). A genetic model for colorectal tumorigenesis. Cell *61*, 759-767.
Fedirko, V., Tramacere, I., Bagnardi, V., Rota, M., Scotti, L., Islami, F., Negri, E., Straif, K., Romieu, I., La Vecchia, C.*, et al.* (2011). Alcohol drinking and colorectal cancer risk: an overall and dose-response meta-analysis of published studies. Ann Oncol *22*, 1958-1972.
Fernandez, P. C., Frank, S. R., Wang, L., Schroeder, M., Liu, S., Greene, J., Cocito, A., and Amati, B. (2003). Genomic targets of the human c-Myc protein. Genes Dev *17*, 1115-1129.
Fieber, W., Schneider, M. L., Matt, T., Krautler, B., Konrat, R., and Bister, K. (2001). Structure, function, and dynamics of the dimerization and DNA-binding domain of oncogenic transcription factor v-Myc. J Mol Biol *307*, 1395-1410.
Filippakopoulos, P., Qi, J., Picaud, S., Shen, Y., Smith, W. B., Fedorov, O., Morse, E. M., Keates, T., Hickman, T. T., Felletar, I.*, et al.* (2010). Selective inhibition of BET bromodomains. Nature *468*, 1067-1073.
Fischer, E. S., Bohm, K., Lydeard, J. R., Yang, H., Stadler, M. B., Cavadini, S., Nagel, J., Serluca, F., Acker, V., Lingaraju, G. M.*, et al.* (2014). Structure of the DDB1-CRBN E3 ubiquitin ligase in complex with thalidomide. Nature *512*, 49-53.
Fleming, M., Ravula, S., Tatishchev, S. F., and Wang, H. L. (2012). Colorectal carcinoma: Pathologic aspects. J Gastrointest Oncol *3*, 153-173.
Fletcher, S., and Prochownik, E. V. (2015). Small-molecule inhibitors of the Myc oncoprotein. Biochim Biophys Acta *1849*, 525-543.
Fodde, R., Kuipers, J., Rosenberg, C., Smits, R., Kielman, M., Gaspar, C., van Es, J. H., Breukel, C., Wiegant, J., Giles, R. H., and Clevers, H. (2001). Mutations in the

APC tumour suppressor gene cause chromosomal instability. Nat Cell Biol *3*, 433-438.
Gao, S., Wang, S., and Song, Y. (2020). Novel immunomodulatory drugs and neo-substrates. Biomarker Research *8*, 2.
García-Gutiérrez, L., Delgado, M. D., and León, J. (2019). MYC Oncogene Contributions to Release of Cell Cycle Brakes. Genes (Basel) *10*.
Girardini, M., Maniaci, C., Hughes, S. J., Testa, A., and Ciulli, A. (2019). Cereblon versus VHL: Hijacking E3 ligases against each other using PROTACs. Bioorg Med Chem *27*, 2466-2479.
Goldberg, R. M., Sargent, D. J., Morton, R. F., Fuchs, C. S., Ramanathan, R. K., Williamson, S. K., Findlay, B. P., Pitot, H. C., and Alberts, S. R. (2004). A randomized controlled trial of fluorouracil plus leucovorin, irinotecan, and oxaliplatin combinations in patients with previously untreated metastatic colorectal cancer. J Clin Oncol *22*, 23-30.
Golsteyn, R. M., Lane, H. A., Mundt, K. E., Arnaud, L., and Nigg, E. A. (1996). The family of polo-like kinases. Prog Cell Cycle Res *2*, 107-114.
Grant, R. C., Selander, I., Connor, A. A., Selvarajah, S., Borgida, A., Briollais, L., Petersen, G. M., Lerner-Ellis, J., Holter, S., and Gallinger, S. (2015). Prevalence of germline mutations in cancer predisposition genes in patients with pancreatic cancer. Gastroenterology *148*, 556-564.
Guo, J., Li, T., Schipper, J., Nilson, K. A., Fordjour, F. K., Cooper, J. J., Gordân, R., and Price, D. H. (2014). Sequence specificity incompletely defines the genome-wide occupancy of Myc. Genome Biol *15*, 482.
Guo, J., Parise, R. A., Joseph, E., Egorin, M. J., Lazo, J. S., Prochownik, E. V., and Eiseman, J. L. (2009). Efficacy, pharmacokinetics, tisssue distribution, and metabolism of the Myc-Max disruptor, 10058-F4 [Z,E]-5-[4-ethylbenzylidine]-2-thioxothiazolidin-4-one, in mice. Cancer Chemother Pharmacol *63*, 615-625.
Guruswamy, S., and Rao, C. V. (2008). Multi-Target Approaches in Colon Cancer Chemoprevention Based on Systems Biology of Tumor Cell-Signaling. Gene Regul Syst Bio *2*, 163-176.
Haeberle, L., and Esposito, I. (2019). Pathology of pancreatic cancer. Transl Gastroenterol Hepatol *4*, 50.
Han, D. P., Zhu, Q. L., Cui, J. T., Wang, P. X., Qu, S., Cao, Q. F., Zong, Y. P., Feng, B., Zheng, M. H., and Lu, A. G. (2012). Polo-like kinase 1 is overexpressed in colorectal cancer and participates in the migration and invasion of colorectal cancer cells. Med Sci Monit *18*, Br237-246.
Hansen, L. L., Jakobsen, C. G., and Justesen, J. (1999). Assignment of the human peptide chain release factor 3 (GSPT2) to Xp11.23-->p11.21 and of the distal marker DXS1039 by radiation hybrid mapping. Cytogenet Cell Genet *86*, 250-251.
Hart, J. R., Garner, A. L., Yu, J., Ito, Y., Sun, M., Ueno, L., Rhee, J. K., Baksh, M. M., Stefan, E., Hartl, M.*, et al.* (2014). Inhibitor of MYC identified in a Kröhnke pyridine library. Proc Natl Acad Sci U S A *111*, 12556-12561.
Hashimoto, Y., Inagaki, H., and Hoshino, S. (2015). Calpain mediates processing of the translation termination factor eRF3 into the IAP-binding isoform p-eRF3. FEBS Lett *589*, 2241-2247.
Hashimoto, Y., Kumagai, N., Hosoda, N., and Hoshino, S. (2014). The processed isoform of the translation termination factor eRF3 localizes to the nucleus to interact with the ARF tumor suppressor. Biochem Biophys Res Commun *445*, 639-644.
Heidelberger, C., Chaudhuri, N. K., Danneberg, P., Mooren, D., Griesbach, L., Duschinsky, R., Schnitzer, R. J., Pleven, E., and Scheiner, J. (1957). Fluorinated pyrimidines, a new class of tumour-inhibitory compounds. Nature *179*, 663-666.

Heitman, S. J., Ronksley, P. E., Hilsden, R. J., Manns, B. J., Rostom, A., and Hemmelgarn, B. R. (2009). Prevalence of adenomas and colorectal cancer in average risk individuals: a systematic review and meta-analysis. Clin Gastroenterol Hepatol *7*, 1272-1278.
Hemminki, K., Li, X., Sundquist, J., and Sundquist, K. (2010). Risk of cancer following hospitalization for type 2 diabetes. Oncologist *15*, 548-555.
Herbst, A., Hemann, M. T., Tworkowski, K. A., Salghetti, S. E., Lowe, S. W., and Tansey, W. P. (2005). A conserved element in Myc that negatively regulates its proapoptotic activity. EMBO Rep *6*, 177-183.
Higgins, J. J., Pucilowska, J., Lombardi, R. Q., and Rooney, J. P. (2004). A mutation in a novel ATP-dependent Lon protease gene in a kindred with mild mental retardation. Neurology *63*, 1927-1931.
Hruban, R. H., Adsay, N. V., Albores-Saavedra, J., Compton, C., Garrett, E. S., Goodman, S. N., Kern, S. E., Klimstra, D. S., Kloppel, G., Longnecker, D. S.*, et al.* (2001). Pancreatic intraepithelial neoplasia: a new nomenclature and classification system for pancreatic duct lesions. Am J Surg Pathol *25*, 579-586.
Hruban, R. H., Petersen, G. M., Ha, P. K., and Kern, S. E. (1998). Genetics of pancreatic cancer. From genes to families. Surg Oncol Clin N Am *7*, 1-23.
Hruban, R. H., Takaori, K., Klimstra, D. S., Adsay, N. V., Albores-Saavedra, J., Biankin, A. V., Biankin, S. A., Compton, C., Fukushima, N., Furukawa, T.*, et al.* (2004). An illustrated consensus on the classification of pancreatic intraepithelial neoplasia and intraductal papillary mucinous neoplasms. Am J Surg Pathol *28*, 977-987.
Hu, S. S., and Vogt, P. K. (1979). Avian oncovirus MH2 is defective in Gag, Pol, and Env. Virology *92*, 278-284.
Hu, X., Fatima, S., Chen, M., Huang, T., Chen, Y. W., Gong, R., Wong, H. L. X., Yu, R., Song, L., Kwan, H. Y., and Bian, Z. (2021). Dihydroartemisinin is potential therapeutics for treating late-stage CRC by targeting the elevated c-Myc level. Cell Death & Disease *12*, 1053.
Hua, J., Shi, S., Liang, D., Liang, C., Meng, Q., Zhang, B., Ni, Q., Xu, J., and Yu, X. (2018). Current status and dilemma of second-line treatment in advanced pancreatic cancer: is there a silver lining? Onco Targets Ther *11*, 4591-4608.
Huang, M. J., Cheng, Y. C., Liu, C. R., Lin, S., and Liu, H. E. (2006). A small-molecule c-Myc inhibitor, 10058-F4, induces cell-cycle arrest, apoptosis, and myeloid differentiation of human acute myeloid leukemia. Exp Hematol *34*, 1480-1489.
Ishino, Y., Shinagawa, H., Makino, K., Amemura, M., and Nakata, A. (1987). Nucleotide sequence of the iap gene, responsible for alkaline phosphatase isozyme conversion in Escherichia coli, and identification of the gene product. J Bacteriol *169*, 5429-5433.
Ishoey, M., Chorn, S., Singh, N., Jaeger, M. G., Brand, M., Paulk, J., Bauer, S., Erb, M. A., Parapatics, K., Müller, A. C.*, et al.* (2018). Translation Termination Factor GSPT1 Is a Phenotypically Relevant Off-Target of Heterobifunctional Phthalimide Degraders. ACS Chemical Biology *13*, 553-560.
Jakobsen, C. G., Segaard, T. M., Jean-Jean, O., Frolova, L., and Justesen, J. (2001). [Identification of a novel termination release factor eRF3b expressing the eRF3 activity in vitro and in vivo]. Mol Biol (Mosk) *35*, 672-681.
Jiang, Y., Ben, Q., Shen, H., Lu, W., Zhang, Y., and Zhu, J. (2011). Diabetes mellitus and incidence and mortality of colorectal cancer: a systematic review and meta-analysis of cohort studies. Eur J Epidemiol *26*, 863-876.
Jung, L. A., Gebhardt, A., Koelmel, W., Ade, C. P., Walz, S., Kuper, J., von Eyss, B., Letschert, S., Redel, C., d'Artista, L.*, et al.* (2017). OmoMYC blunts promoter

invasion by oncogenic MYC to inhibit gene expression characteristic of MYC-dependent tumors. Oncogene *36*, 1911-1924.
Kastrinos, F., Mukherjee, B., Tayob, N., Wang, F., Sparr, J., Raymond, V. M., Bandipalliam, P., Stoffel, E. M., Gruber, S. B., and Syngal, S. (2009). Risk of pancreatic cancer in families with Lynch syndrome. Jama *302*, 1790-1795.
Kato, G. J., Barrett, J., Villa-Garcia, M., and Dang, C. V. (1990). An amino-terminal c-myc domain required for neoplastic transformation activates transcription. Mol Cell Biol *10*, 5914-5920.
Kato, G. J., Lee, W. M., Chen, L. L., and Dang, C. V. (1992). Max: functional domains and interaction with c-Myc. Genes Dev *6*, 81-92.
Kiessling, A., Wiesinger, R., Sperl, B., and Berg, T. (2007). Selective inhibition of c-Myc/Max dimerization by a pyrazolo[1,5-a]pyrimidine. ChemMedChem *2*, 627-630.
Kim, E., Coelho, D., and Blachier, F. (2013). Review of the association between meat consumption and risk of colorectal cancer. Nutr Res *33*, 983-994.
Klein, A. P. (2013). Identifying people at a high risk of developing pancreatic cancer. Nat Rev Cancer *13*, 66-74.
Kujko, A. A., Berki, D. M., Oracz, G., Wejnarska, K., Antoniuk, J., Wertheim-Tysarowska, K., Kołodziejczyk, E., Bal, J., Sahin-Tóth, M., and Rygiel, A. M. (2017). A novel p.Ser282Pro CPA1 variant is associated with autosomal dominant hereditary pancreatitis. Gut *66*, 1728-1730.
Lai, A. C., and Crews, C. M. (2017). Induced protein degradation: an emerging drug discovery paradigm. Nat Rev Drug Discov *16*, 101-114.
Lee, A. Y. L., Dubois, C. L., Sarai, K., Zarei, S., Schaeffer, D. F., Sander, M., and Kopp, J. L. (2018). Cell of origin affects tumour development and phenotype in pancreatic ductal adenocarcinoma. Gut.
Lens, S. M., Voest, E. E., and Medema, R. H. (2010). Shared and separate functions of polo-like kinases and aurora kinases in cancer. Nat Rev Cancer *10*, 825-841.
Li, L., Xue, W., Shen, Z., Liu, J., Hu, M., Cheng, Z., Wang, Y., Chen, Y., Chang, H., Liu, Y.*, et al.* (2020). A Cereblon Modulator CC-885 Induces CRBN- and p97-Dependent PLK1 Degradation and Synergizes with Volasertib to Suppress Lung Cancer. Mol Ther Oncolytics *18*, 215-225.
Li, Z., Van Calcar, S., Qu, C., Cavenee, W. K., Zhang, M. Q., and Ren, B. (2003). A global transcriptional regulatory role for c-Myc in Burkitt's lymphoma cells. Proc Natl Acad Sci U S A *100*, 8164-8169.
Lier, S., Sellmer, A., Orben, F., Heinzlmeir, S., Krauß, L., Schneeweiss, C., Hassan, Z.,Schneider, C., Schäfer, A., Prongratz, H., Engleitner, T., Öllinger, R., Kuisl, A., Bassermann, F., Schlag, C., Kong, B., Dove, S., Küster, B., Rad, R., Reichert, M., Wirth, M., Saur, D., Mahboobi, S., Schneider, G. (2022): A novel Cereblon E3 ligase modulator with antitumor activity in gastrointestinal cancer. Bioorganic Chemistry, Volume 119.
Limsui, D., Vierkant, R. A., Tillmans, L. S., Wang, A. H., Weisenberger, D. J., Laird, P. W., Lynch, C. F., Anderson, K. E., French, A. J., Haile, R. W.*, et al.* (2010). Cigarette smoking and colorectal cancer risk by molecularly defined subtypes. J Natl Cancer Inst *102*, 1012-1022.
Liu, Y., Huang, X., He, X., Zhou, Y., Jiang, X., Chen-Kiang, S., Jaffrey, S. R., and Xu, G. (2015). A novel effect of thalidomide and its analogs: suppression of cereblon ubiquitination enhances ubiquitin ligase function. Faseb j *29*, 4829-4839.
Lopez-Girona, A., Lu, G., Rychak, E., Mendy, D., Lu, C.-C., Rappley, I., Fontanillo, C., Cathers, B. E., Daniel, T. O., and Hansen, J. (2019). CC-90009, a Novel Cereblon E3 Ligase Modulator, Targets GSPT1 for Degradation to Induce Potent

Tumoricidal Activity Against Acute Myeloid Leukemia (AML). In, (American Society of Hematology Washington, DC).
Lorans, M., Dow, E., Macrae, F. A., Winship, I. M., and Buchanan, D. D. (2018). Update on Hereditary Colorectal Cancer: Improving the Clinical Utility of Multigene Panel Testing. Clin Colorectal Cancer *17*, e293-e305.
Lowenfels, A. B., Maisonneuve, P., Cavallini, G., Ammann, R. W., Lankisch, P. G., Andersen, J. R., Dimagno, E. P., Andren-Sandberg, A., and Domellof, L. (1993). Pancreatitis and the risk of pancreatic cancer. International Pancreatitis Study Group. N Engl J Med *328*, 1433-1437.
Macosko, E. Z., Basu, A., Satija, R., Nemesh, J., Shekhar, K., Goldman, M., Tirosh, I., Bialas, A. R., Kamitaki, N., Martersteck, E. M.*, et al.* (2015). Highly Parallel Genome-wide Expression Profiling of Individual Cells Using Nanoliter Droplets. Cell *161*, 1202-1214.
Maisonneuve, P., and Lowenfels, A. B. (2015). Risk factors for pancreatic cancer: a summary review of meta-analytical studies. Int J Epidemiol *44*, 186-198.
Malta-Vacas, J., Aires, C., Costa, P., Conde, A. R., Ramos, S., Martins, A. P., Monteiro, C., and Brito, M. (2005). Differential expression of the eukaryotic release factor 3 (eRF3/GSPT1) according to gastric cancer histological types. J Clin Pathol *58*, 621-625.
Malta-Vacas, J., Chauvin, C., Gonçalves, L., Nazaré, A., Carvalho, C., Monteiro, C., Bagrel, D., Jean-Jean, O., and Brito, M. (2009a). eRF3a/GSPT1 12-GGC allele increases the susceptibility for breast cancer development. Oncol Rep *21*, 1551-1558.
Malta-Vacas, J., Ferreira, P., Monteiro, C., and Brito, M. (2009b). Differential expression of GSPT1 GGCn alleles in cancer. Cancer Genet Cytogenet *195*, 132-142.
Markowitz, S., Wang, J., Myeroff, L., Parsons, R., Sun, L., Lutterbaugh, J., Fan, R. S., Zborowska, E., Kinzler, K. W., Vogelstein, B., and et al. (1995). Inactivation of the type II TGF-beta receptor in colon cancer cells with microsatellite instability. Science *268*, 1336-1338.
Massó-Vallés, D., and Soucek, L. (2020). Blocking Myc to Treat Cancer: Reflecting on Two Decades of Omomyc. Cells *9*.
Matyskiela, M. E., Lu, G., Ito, T., Pagarigan, B., Lu, C.-C., Miller, K., Fang, W., Wang, N.-Y., Nguyen, D., Houston, J.*, et al.* (2016a). A novel cereblon modulator recruits GSPT1 to the CRL4CRBN ubiquitin ligase. Nature *535*, 252-257.
Matyskiela, M. E., Lu, G., Ito, T., Pagarigan, B., Lu, C. C., Miller, K., Fang, W., Wang, N. Y., Nguyen, D., Houston, J.*, et al.* (2016b). A novel cereblon modulator recruits GSPT1 to the CRL4(CRBN) ubiquitin ligase. Nature *535*, 252-257.
McQuade, R. M., Stojanovska, V., Bornstein, J. C., and Nurgali, K. (2017). Colorectal Cancer Chemotherapy: The Evolution of Treatment and New Approaches. Curr Med Chem *24*, 1537-1557.
Michel, J., and Cuchillo, R. (2012). The impact of small molecule binding on the energy landscape of the intrinsically disordered protein C-myc. PLoS One *7*, e41070.
Mini, E., Trave, F., Rustum, Y. M., and Bertino, J. R. (1990). Enhancement of the antitumor effects of 5-fluorouracil by folinic acid. Pharmacol Ther *47*, 1-19.
Mitkevich, V. A., Kononenko, A. V., Petrushanko, I. Y., Yanvarev, D. V., Makarov, A. A., and Kisselev, L. L. (2006). Termination of translation in eukaryotes is mediated by the quaternary eRF1*eRF3*GTP*Mg2+ complex. The biological roles of eRF3 and prokaryotic RF3 are profoundly distinct. Nucleic Acids Res *34*, 3947-3954.
Miyoshi, Y., Ando, H., Nagase, H., Nishisho, I., Horii, A., Miki, Y., Mori, T., Utsunomiya, J., Baba, S., Petersen, G., and et al. (1992). Germ-line mutations of the

APC gene in 53 familial adenomatous polyposis patients. Proc Natl Acad Sci U S A *89*, 4452-4456.
Moreno, T., González-Silva, L., Monterde, B., Betancor-Fernández, I., Revilla, C., Agraz-Doblas, A., Freire, J., Isidro, P., Quevedo, L., Montes-Moreno, S.*, et al.* (2020). ARID2 deficiency promotes tumor progression and is associated with higher sensitivity to PARP inhibition in lung cancer. bioRxiv, 2020.2001.2010.898726.
Mullard, A. (2019). First targeted protein degrader hits the clinic. Nat Rev Drug Discov.
Murugan, R. N., Park, J.-E., Kim, E.-H., Shin, S. Y., Cheong, C., Lee, K. S., and Bang, J. K. (2011). Plk1-targeted small molecule inhibitors: molecular basis for their potency and specificity. Molecules and Cells *32*, 209.
Nazemalhosseini Mojarad, E., Kuppen, P. J., Aghdaei, H. A., and Zali, M. R. (2013). The CpG island methylator phenotype (CIMP) in colorectal cancer. Gastroenterol Hepatol Bed Bench *6*, 120-128.
Nie, Z., Guo, C., Das, S. K., Chow, C. C., Batchelor, E., Simons, S. S. J., and Levens, D. (2020). Dissecting transcriptional amplification by MYC. Elife *9*.
Nie, Z., Hu, G., Wei, G., Cui, K., Yamane, A., Resch, W., Wang, R., Green, D. R., Tessarollo, L., Casellas, R.*, et al.* (2012). c-Myc is a universal amplifier of expressed genes in lymphocytes and embryonic stem cells. Cell *151*, 68-79.
Orth, M., Metzger, P., Gerum, S., Mayerle, J., Schneider, G., Belka, C., Schnurr, M., and Lauber, K. (2019). Pancreatic ductal adenocarcinoma: biological hallmarks, current status, and future perspectives of combined modality treatment approaches. Radiat Oncol *14*, 141.
Otto, C., Schmidt, S., Kastner, C., Denk, S., Kettler, J., Müller, N., Germer, C. T., Wolf, E., Gallant, P., and Wiegering, A. (2019). Targeting bromodomain-containing protein 4 (BRD4) inhibits MYC expression in colorectal cancer cells. Neoplasia *21*, 1110-1120.
Ozawa, K., Murakami, Y., Eki, T., Yokoyama, K., Soeda, E., Hoshino, S., Ui, M., and Hanaoka, F. (1992). Mapping of the human GSPT1 gene, a human homolog of the yeast GST1 gene, to chromosomal band 16p13.1. Somat Cell Mol Genet *18*, 189-194.
Pan, Y., Fei, Q., Xiong, P., Yang, J., Zhang, Z., Lin, X., Pan, M., Lu, F., and Huang, H. (2019). Synergistic inhibition of pancreatic cancer with anti-PD-L1 and c-Myc inhibitor JQ1. OncoImmunology *8*, e1581529.
Parekh, S., Ziegenhain, C., Vieth, B., Enard, W., and Hellmann, I. (2016). The impact of amplification on differential expression analyses by RNA-seq. Sci Rep *6*, 25533.
Park, S., Chung, S., Kim, K. M., Jung, K. C., Park, C., Hahm, E. R., and Yang, C. H. (2004). Determination of binding constant of transcription factor myc-max/max-max and E-box DNA: the effect of inhibitors on the binding. Biochim Biophys Acta *1670*, 217-228.
Payne, G. S., Bishop, J. M., and Varmus, H. E. (1982). Multiple arrangements of viral DNA and an activated host oncogene in bursal lymphomas. Nature *295*, 209-214.
Pelengaris, S., Khan, M., and Evan, G. (2002). c-MYC: more than just a matter of life and death. Nat Rev Cancer *2*, 764-776.
Principe, D. R., DeCant, B., Mascarinas, E., Wayne, E. A., Diaz, A. M., Akagi, N., Hwang, R., Pasche, B., Dawson, D. W., Fang, D.*, et al.* (2016). TGFbeta Signaling in the Pancreatic Tumor Microenvironment Promotes Fibrosis and Immune Evasion to Facilitate Tumorigenesis. Cancer Res *76*, 2525-2539.

Puvvula, P. K., and Moon, A. M. (2021). Novel Cell-Penetrating Peptides Derived From Scaffold-Attachment- Factor A Inhibits Cancer Cell Proliferation and Survival. In Frontiers in oncology, p. 621825.
Raab, M., Sanhaji, M., Matthess, Y., Hörlin, A., Lorenz, I., Dötsch, C., Habbe, N., Waidmann, O., Kurunci-Csacsko, E., Firestein, R.*, et al.* (2018). PLK1 has tumor-suppressive potential in APC-truncated colon cancer cells. Nature Communications *9*, 1106.
Raderer, M., Wrba, F., Kornek, G., Maca, T., Koller, D. Y., Weinlaender, G., Hejna, M., and Scheithauer, W. (1998). Association between Helicobacter pylori infection and pancreatic cancer. Oncology *55*, 16-19.
Ramani, P., Nash, R., Sowa-Avugrah, E., and Rogers, C. (2015). High levels of polo-like kinase 1 and phosphorylated translationally controlled tumor protein indicate poor prognosis in neuroblastomas. J Neurooncol *125*, 103-111.
Rawla, P., Sunkara, T., and Barsouk, A. (2019). Epidemiology of colorectal cancer: incidence, mortality, survival, and risk factors. Prz Gastroenterol *14*, 89-103.
Ren, Y., Bi, C., Zhao, X., Lwin, T., Wang, C., Yuan, J., Silva, A. S., Shah, B. D., Fang, B., Li, T.*, et al.* (2018). PLK1 stabilizes a MYC-dependent kinase network in aggressive B cell lymphomas. J Clin Invest *128*, 5517-5530.
Riihimaki, M., Hemminki, A., Sundquist, J., and Hemminki, K. (2016). Patterns of metastasis in colon and rectal cancer. Sci Rep *6*, 29765.
Robsahm, T. E., Aagnes, B., Hjartaker, A., Langseth, H., Bray, F. I., and Larsen, I. K. (2013). Body mass index, physical activity, and colorectal cancer by anatomical subsites: a systematic review and meta-analysis of cohort studies. Eur J Cancer Prev *22*, 492-505.
Rudolph, D., Steegmaier, M., Hoffmann, M., Grauert, M., Baum, A., Quant, J., Haslinger, C., Garin-Chesa, P., and Adolf, G. R. (2009). BI 6727, a Polo-like kinase inhibitor with improved pharmacokinetic profile and broad antitumor activity. Clin Cancer Res *15*, 3094-3102.
Sabò, A., Kress, T. R., Pelizzola, M., de Pretis, S., Gorski, M. M., Tesi, A., Morelli, M. J., Bora, P., Doni, M., Verrecchia, A.*, et al.* (2014). Selective transcriptional regulation by Myc in cellular growth control and lymphomagenesis. Nature *511*, 488-492.
Safran, M., Dalah, I., Alexander, J., Rosen, N., Iny Stein, T., Shmoish, M., Nativ, N., Bahir, I., Doniger, T., Krug, H.*, et al.* (2010). GeneCards Version 3: the human gene integrator. Database (Oxford) *2010*, baq020.
Sakamoto, K. M., Kim, K. B., Kumagai, A., Mercurio, F., Crews, C. M., and Deshaies, R. J. (2001). Protacs: chimeric molecules that target proteins to the Skp1-Cullin-F box complex for ubiquitination and degradation. Proc Natl Acad Sci U S A *98*, 8554-8559.
Salas-Marco, J., and Bedwell, D. M. (2004). GTP hydrolysis by eRF3 facilitates stop codon decoding during eukaryotic translation termination. Mol Cell Biol *24*, 7769-7778.
Sausen, M., Phallen, J., Adleff, V., Jones, S., Leary, R. J., Barrett, M. T., Anagnostou, V., Parpart-Li, S., Murphy, D., Kay Li, Q.*, et al.* (2015). Clinical implications of genomic alterations in the tumour and circulation of pancreatic cancer patients. Nat Commun *6*, 7686.
Saveljeva, S., Mc Laughlin, S. L., Vandenabeele, P., Samali, A., and Bertrand, M. J. M. (2015). Endoplasmic reticulum stress induces ligand-independent TNFR1-mediated necroptosis in L929 cells. Cell Death & Disease *6*, e1587-e1587.
Schmoll, H. J., Tabernero, J., Maroun, J., de Braud, F., Price, T., Van Cutsem, E., Hill, M., Hoersch, S., Rittweger, K., and Haller, D. G. (2015). Capecitabine Plus Oxaliplatin Compared With Fluorouracil/Folinic Acid As Adjuvant Therapy for Stage

III Colon Cancer: Final Results of the NO16968 Randomized Controlled Phase III Trial. J Clin Oncol *33*, 3733-3740.
Seong, D., Jeong, M., Seo, J., Lee, J.-Y., Hwang, C. H., Shin, H.-C., Shin, J. Y., Nam, Y. W., Jo, J. Y., Lee, H.*, et al.* (2020). Identification of MYC as an antinecroptotic protein that stifles RIPK1–RIPK3 complex formation. Proceedings of the National Academy of Sciences *117*, 19982-19993.
Sheiness, D., and Bishop, J. M. (1979). DNA and RNA from uninfected vertebrate cells contain nucleotide sequences related to the putative transforming gene of avian myelocytomatosis virus. J Virol *31*, 514-521.
Siegel, R. L., Miller, K. D., Fuchs, H. E., and Jemal, A. (2022). Cancer statistics, 2022. CA: A Cancer Journal for Clinicians *72*, 7-33.
Siegel, R. L., Miller, K. D., Goding Sauer, A., Fedewa, S. A., Butterly, L. F., Anderson, J. C., Cercek, A., Smith, R. A., and Jemal, A. (2020). Colorectal cancer statistics, 2020. CA Cancer J Clin.
Simon, K. (2016). Colorectal cancer development and advances in screening. Clin Interv Aging *11*, 967-976.
Singh, M. P., Rai, S., Pandey, A., Singh, N. K., and Srivastava, S. (2021). Molecular subtypes of colorectal cancer: An emerging therapeutic opportunity for personalized medicine. Genes & Diseases *8*, 133-145.
Sodir, N. M., Kortlever, R. M., Barthet, V. J. A., Campos, T., Pellegrinet, L., Kupczak, S., Anastasiou, P., Swigart, L. B., Soucek, L., Arends, M. J.*, et al.* (2020). MYC Instructs and Maintains Pancreatic Adenocarcinoma Phenotype. Cancer Discov *10*, 588-607.
Sodir, N. M., Swigart, L. B., Karnezis, A. N., Hanahan, D., Evan, G. I., and Soucek, L. (2011). Endogenous Myc maintains the tumor microenvironment. Genes Dev *25*, 907-916.
Sohal, D. P. S., Duong, M., Ahmad, S. A., Gandhi, N. S., Beg, M. S., Wang-Gillam, A., Wade, J. L., 3rd, Chiorean, E. G., Guthrie, K. A., Lowy, A. M.*, et al.* (2021). Efficacy of Perioperative Chemotherapy for Resectable Pancreatic Adenocarcinoma: A Phase 2 Randomized Clinical Trial. JAMA Oncol *7*, 421-427.
Song, X., Lu, Z., and Xu, J. (2020). Targeting cluster of differentiation 47 improves the efficacy of anti-cytotoxic T-lymphocyte associated protein 4 treatment via antigen presentation enhancement in pancreatic ductal adenocarcinoma. Exp Ther Med *20*, 3301-3309.
Soucek, L., Jucker, R., Panacchia, L., Ricordy, R., Tatò, F., and Nasi, S. (2002). Omomyc, a potential Myc dominant negative, enhances Myc-induced apoptosis. Cancer Res *62*, 3507-3510.
Soucek, L., Whitfield, J., Martins, C. P., Finch, A. J., Murphy, D. J., Sodir, N. M., Karnezis, A. N., Swigart, L. B., Nasi, S., and Evan, G. I. (2008). Modelling Myc inhibition as a cancer therapy. Nature *455*, 679-683.
Sperling, A. S., Burgess, M., Keshishian, H., Gasser, J. A., Bhatt, S., Jan, M., Słabicki, M., Sellar, R. S., Fink, E. C., Miller, P. G.*, et al.* (2019). Patterns of substrate affinity, competition, and degradation kinetics underlie biological activity of thalidomide analogs. Blood *134*, 160-170.
Stefan, E., and Bister, K. (2017). MYC and RAF: Key Effectors in Cellular Signaling and Major Drivers in Human Cancer. Curr Top Microbiol Immunol *407*, 117-151.
Stellas, D., Szabolcs, M., Koul, S., Li, Z., Polyzos, A., Anagnostopoulos, C., Cournia, Z., Tamvakopoulos, C., Klinakis, A., and Efstratiadis, A. (2014). Therapeutic effects of an anti-Myc drug on mouse pancreatic cancer. J Natl Cancer Inst *106*.
Strippoli, A., Cocomazzi, A., Basso, M., Cenci, T., Ricci, R., Pierconti, F., Cassano, A., Fiorentino, V., Barone, C., Bria, E.*, et al.* (2020). c-MYC Expression Is a Possible

Keystone in the Colorectal Cancer Resistance to EGFR Inhibitors. Cancers (Basel) *12*.
Sun, X., Lee, J., Navas, T., Baldwin, D. T., Stewart, T. A., and Dixit, V. M. (1999). RIP3, a novel apoptosis-inducing kinase. J Biol Chem *274*, 16871-16875.
Tan, J., Li, Z., Lee, P. L., Guan, P., Aau, M. Y., Lee, S. T., Feng, M., Lim, C. Z., Lee, E. Y., Wee, Z. N.*, et al.* (2013). PDK1 signaling toward PLK1-MYC activation confers oncogenic transformation, tumor-initiating cell activation, and resistance to mTOR-targeted therapy. Cancer Discov *3*, 1156-1171.
Tejpar, S., and Van Cutsem, E. (2002). Molecular and genetic defects in colorectal tumorigenesis. Best Pract Res Clin Gastroenterol *16*, 171-185.
Thoma, C. (2018). Inherited pancreatic cancer risk. Nature Reviews Gastroenterology & Hepatology *15*, 454-454.
Tsalic, M., Bar-Sela, G., Beny, A., Visel, B., and Haim, N. (2003). Severe toxicity related to the 5-fluorouracil/leucovorin combination (the Mayo Clinic regimen): a prospective study in colorectal cancer patients. Am J Clin Oncol *26*, 103-106.
Tsilidis, K. K., Kasimis, J. C., Lopez, D. S., Ntzani, E. E., and Ioannidis, J. P. (2015). Type 2 diabetes and cancer: umbrella review of meta-analyses of observational studies. Bmj *350*, g7607.
Tut, T. G., Lim, S. H., Dissanayake, I. U., Descallar, J., Chua, W., Ng, W., de Souza, P., Shin, J. S., and Lee, C. S. (2015). Upregulated Polo-Like Kinase 1 Expression Correlates with Inferior Survival Outcomes in Rectal Cancer. PLoS One *10*, e0129313.
Uemura, N., Okamoto, S., Yamamoto, S., Matsumura, N., Yamaguchi, S., Yamakido, M., Taniyama, K., Sasaki, N., and Schlemper, R. J. (2001). Helicobacter pylori infection and the development of gastric cancer. N Engl J Med *345*, 784-789.
Ullman, B., Lee, M., Martin, D. W., Jr., and Santi, D. V. (1978). Cytotoxicity of 5-fluoro-2'-deoxyuridine: requirement for reduced folate cofactors and antagonism by methotrexate. Proc Natl Acad Sci U S A *75*, 980-983.
Vega, E. A., Kutlu, O. C., Salehi, O., James, D., Alarcon, S. V., Herrick, B., Krishnan, S., Kozyreva, O., and Conrad, C. (2020). Preoperative Chemotherapy for Pancreatic Cancer Improves Survival and R0 Rate Even in Early Stage I. J Gastrointest Surg *24*, 2409-2415.
Vennstrom, B., Sheiness, D., Zabielski, J., and Bishop, J. M. (1982). Isolation and characterization of c-myc, a cellular homolog of the oncogene (v-myc) of avian myelocytomatosis virus strain 29. J Virol *42*, 773-779.
Vincent, A., Herman, J., Schulick, R., Hruban, R. H., and Goggins, M. (2011). Pancreatic cancer. Lancet *378*, 607-620.
Von Hoff, D. D., Ervin, T., Arena, F. P., Chiorean, E. G., Infante, J., Moore, M., Seay, T., Tjulandin, S. A., Ma, W. W., Saleh, M. N.*, et al.* (2013). Increased survival in pancreatic cancer with nab-paclitaxel plus gemcitabine. N Engl J Med *369*, 1691-1703.
Wang, D., Pierce, A., Veo, B., Fosmire, S., Danis, E., Donson, A., Venkataraman, S., and Vibhakar, R. (2021). A Regulatory Loop of FBXW7-MYC-PLK1 Controls Tumorigenesis of MYC-Driven Medulloblastoma. Cancers (Basel) *13*.
Wang, X., Li, X., Wei, X., Jiang, H., Lan, C., Yang, S., Wang, H., Yang, Y., Tian, C., Xu, Z.*, et al.* (2020a). PD-L1 is a direct target of cancer-FOXP3 in pancreatic ductal adenocarcinoma (PDAC), and combined immunotherapy with antibodies against PD-L1 and CCL5 is effective in the treatment of PDAC. Signal Transduction and Targeted Therapy *5*, 38.
Wang, Y., Jiang, X., Feng, F., Liu, W., and Sun, H. (2020b). Degradation of proteins by PROTACs and other strategies. Acta Pharm Sin B *10*, 207-238.

Weichert, W., Schmidt, M., Jacob, J., Gekeler, V., Langrehr, J., Neuhaus, P., Bahra, M., Denkert, C., Dietel, M., and Kristiansen, G. (2005). Overexpression of Polo-like kinase 1 is a common and early event in pancreatic cancer. Pancreatology *5*, 259-265.
Winawer, S. J., Zauber, A. G., Ho, M. N., O'Brien, M. J., Gottlieb, L. S., Sternberg, S. S., Waye, J. D., Schapiro, M., Bond, J. H., Panish, J. F., and et al. (1993). Prevention of colorectal cancer by colonoscopic polypectomy. The National Polyp Study Workgroup. N Engl J Med *329*, 1977-1981.
Winter, G. E., Buckley, D. L., Paulk, J., Roberts, J. M., Souza, A., Dhe-Paganon, S., and Bradner, J. E. (2015). DRUG DEVELOPMENT. Phthalimide conjugation as a strategy for in vivo target protein degradation. Science *348*, 1376-1381.
Wirth, M., Mahboobi, S., Kramer, O. H., and Schneider, G. (2016). Concepts to Target MYC in Pancreatic Cancer. Mol Cancer Ther *15*, 1792-1798.
Witkiewicz, A. K., McMillan, E. A., Balaji, U., Baek, G., Lin, W. C., Mansour, J., Mollaee, M., Wagner, K. U., Koduru, P., Yopp, A.*, et al.* (2015). Whole-exome sequencing of pancreatic cancer defines genetic diversity and therapeutic targets. Nat Commun *6*, 6744.
Witt, H., Beer, S., Rosendahl, J., Chen, J. M., Chandak, G. R., Masamune, A., Bence, M., Szmola, R., Oracz, G., Macek, M., Jr.*, et al.* (2013). Variants in CPA1 are strongly associated with early onset chronic pancreatitis. Nat Genet *45*, 1216-1220.
Wolfer, A., and Ramaswamy, S. (2011). MYC and metastasis. Cancer Res *71*, 2034-2037.
Wolfer, A., Wittner, B. S., Irimia, D., Flavin, R. J., Lupien, M., Gunawardane, R. N., Meyer, C. A., Lightcap, E. S., Tamayo, P., Mesirov, J. P.*, et al.* (2010). MYC regulation of a "poor-prognosis" metastatic cancer cell state. Proc Natl Acad Sci U S A *107*, 3698-3703.
Xi, Q., Chen, Y., Yang, G.-Z., Zhang, J.-Y., Zhang, L.-J., Guo, X.-D., Zhao, J.-Y., Xue, Z.-Y., Li, Y., and Zhang, R. (2020). miR-128 Regulates Tumor Cell CD47 Expression and Promotes Anti-tumor Immunity in Pancreatic Cancer. Frontiers in Immunology *11*.
Xiao, D., Yue, M., Su, H., Ren, P., Jiang, J., Li, F., Hu, Y., Du, H., Liu, H., and Qing, G. (2016). Polo-like Kinase-1 Regulates Myc Stabilization and Activates a Feedforward Circuit Promoting Tumor Cell Survival. Mol Cell *64*, 493-506.
Xie, Y.-H., Chen, Y.-X., and Fang, J.-Y. (2020). Comprehensive review of targeted therapy for colorectal cancer. Signal Transduction and Targeted Therapy *5*, 22.
Xin, W., Xiaohua, N., Peilin, C., Xin, C., Yaqiong, S., and Qihan, W. (2008). Primary function analysis of human mental retardation related gene CRBN. Mol Biol Rep *35*, 251-256.
Xu, D., Popov, N., Hou, M., Wang, Q., Bjorkholm, M., Gruber, A., Menkel, A. R., and Henriksson, M. (2001). Switch from Myc/Max to Mad1/Max binding and decrease in histone acetylation at the telomerase reverse transcriptase promoter during differentiation of HL60 cells. Proc Natl Acad Sci U S A *98*, 3826-3831.
Yamamoto, J., Suwa, T., Murase, Y., Tateno, S., Mizutome, H., Asatsuma-Okumura, T., Shimizu, N., Kishi, T., Momose, S., Kizaki, M.*, et al.* (2020). ARID2 is a pomalidomide-dependent CRL4(CRBN) substrate in multiple myeloma cells. Nat Chem Biol.
Yang, J., Li, Y., Aguilar, A., Liu, Z., Yang, C. Y., and Wang, S. (2019). Simple Structural Modifications Converting a Bona fide MDM2 PROTAC Degrader into a Molecular Glue Molecule: A Cautionary Tale in the Design of PROTAC Degraders. J Med Chem *62*, 9471-9487.

Zack, T. I., Schumacher, S. E., Carter, S. L., Cherniack, A. D., Saksena, G., Tabak, B., Lawrence, M. S., Zhsng, C. Z., Wala, J., Mermel, C. H., *et al.* (2013). Pan-cancer patterns of somatic copy number alteration. Nat Genet *45*, 1134-1140.
Zauber, A. G., Winawer, S. J., O'Brien, M. J., Lansdorp-Vogelaar, I., van Ballegooijen, M., Hankey, B. F., Shi, W., Bond, J. H., Schapiro, M., Panish, J. F., *et al.* (2012). Colonoscopic polypectomy and long-term prevention of colorectal-cancer deaths. N Engl J Med *366*, 687-696.
Zeller, K. I., Zhao, X., Lee, C. W., Chiu, K. P., Yao, F., Yustein, J. T., Ooi, H. S., Orlov, Y. L., Shahab, A., Yong, H. C., *et al.* (2006). Global mapping of c-Myc binding sites and target gene networks in human B cells. Proc Natl Acad Sci U S A *103*, 17834-17839.
Zhang, M., Fan, H. Y., and Li, S. C. (2015a). Inhibition of c-Myc by 10058-F4 induces growth arrest and chemosensitivity in pancreatic ductal adenocarcinoma. Biomed Pharmacother *73*, 123-128.
Zhang, R., Shi, H., Ren, F., Liu, H., Zhang, M., Deng, Y., and Li, X. (2015b). Misregulation of polo-like protein kinase 1, P53 and P21WAF1 in epithelial ovarian cancer suggests poor prognosis. Oncol Rep *33*, 1235-1242.
Zhao, Z., Feng, Q., Yin, Z., Shuang, J., Bai, B., Yu, P., Guo, M., and Zhao, Q. (2017). Red and processed meat consumption and colorectal cancer risk: a systematic review and meta-analysis. Oncotarget *8*, 83306-83314.
Zheng, N., and Shabek, N. (2017). Ubiquitin Ligases: Structure, Function, and Regulation. Annu Rev Biochem *86*, 129-157.
Zhouravleva, G., Frolova, L., Le Goff, X., Le Guellec, R., Inge-Vechtomov, S., Kisselev, L., and Philippe, M. (1995). Termination of translation in eukaryotes is governed by two interacting polypeptide chain release factors, eRF1 and eRF3. Embo j *14*, 4065-4072.
Zuber, J., Shi, J., Wang, E., Rappaport, A. R., Herrmann, H., Sison, E. A., Magoon, D., Qi, J., Blatt, K., Wunderlich, M., *et al.* (2011). RNAi screen identifies Brd4 as a therapeutic target in acute myeloid leukaemia. Nature *478*, 524-528.

Homepages:

American Cancer Society (McQuade et al., 2017, https://www.cancer.org/cancer/colon-rectal-cancer/treating/by-stage-colon.html, Accessed 27 April 2020
Bosman FT, Carneiro F, Hruban RH, et al. WHO Classification of Tumours of the Digestive System. 4th ed. WHO/IARC Classification of Tumours. Lyon: IARC Press, 2010:211-2, Accessed 23 June 2021.
Ferlay J EM, Lam F, Colombet M, Mery L, Pineros M, Znaor A, Soerjomataram I, Global Cancer Observatory: Cancer Tomorrow. Lyon, France: International Agency for Research on Cancer; Accessed 23 June 2021. Available from: http://gco.iarc.fr/tomorrow/graphic-isotype?type=1&population=900&mode=population&sex=0&cancer=39&age_group=value&apc_male=0&apc_female=0
United States National Cancer Institute. Pancreatic cancer: statistics 2018, May. Available from: https://www.cancer.net/cancer-types/pancreatic-cancer/statistics Accessed 23 June 2021.

Note: At the date of submission (29.01.2022) of this work, the related paper (Lier et al., 2022) is in the process of being published.

14. Acknowledgements

First of all, I want to thank my doctor father PD Dr. Günter Schneider, for giving me the opportunity to perform my PhD in his lab contributing to this promising and exiting project with great benefits for cancer research. Throughout the duration of this dissertation he provided a great deal of support and assistance resulting in a successful outcome of my thesis.

I would like to acknowledge my second supervisor Prof. Dr. Thomas Floss and my mentor Prof. Dr. Gisela Keller for their valuable guidance throughout my studies. You offered me the support I needed to choose the right direction and successfully complete my dissertation.

Furthermore, I would like to thank my collaborators in AG Saur, AG Rad, AG Reichert and AG Küster at the TUM for all their interdisciplinary expertise. I also, wouldn´t miss to thank Prof. Dr. Peter Vogt and his team members in San Diego for offering me a position as research intern in his laboratory.

In addition, I would like to acknowledge my coworkers for providing an inspiring working environment. Specifically, I want to thank Christian Schneeweiß for his support in generating genetic cell models, Lukas Krauß for his support in scientific analyzation of my data, Zonera Hassan for supervising in all the miner and major challenges and Bettina Urban and Matthias Wirt for proof reading my thesis.

I could not have completed this dissertation without my friends. Specifically, Meike Kohlruß and Sandra Romero, you were always listening and gave wise counsel and not to forget all the happy distractions to rest my mind outside of research.

From my heart, I want to thank Jannik Fahlisch for his patience, stimulating discussions and his point of view as a non-scientist.

Finally, I want to thank my parents, sister and grandparents for their sympathetic ear and support.